

**An unbiased infrared H<sub>2</sub> search  
for embedded flows  
from young stars  
in Orion A**

Dissertation  
zur Erlangung des akademischen Grades  
Doktor der Naturwissenschaften (Dr. rer. nat.)  
in der Wissenschaftsdisziplin Astrophysik

eingereicht an der  
Mathematisch-Naturwissenschaftlichen Fakultät  
der Universität Potsdam

von  
**Thomas Stanke**

(geboren am 29. August 1970 in Bad Kissingen)

Potsdam, im Juli 2000



**An unbiased infrared H<sub>2</sub> search  
for embedded flows  
from young stars  
in Orion A**

Dissertation  
zur Erlangung des akademischen Grades  
Doktor der Naturwissenschaften (Dr. rer. nat.)  
in der Wissenschaftsdisziplin Astrophysik

eingereicht an der  
Mathematisch-Naturwissenschaftlichen Fakultät  
der Universität Potsdam

von  
**Thomas Stanke**  
(geboren am 29. August 1970 in Bad Kissingen)

Potsdam, im Juli 2000



*In the space of one hundred and seventy-six years the Mississippi has shortened itself two hundred and forty-two miles. Therefore . . . in the Old Silurian Period the Mississippi River was upward of one million three hundred thousand miles long . . . seven hundred and forty-two years from now the Mississippi will be only a mile and three-quarters long. . . . There is something fascinating about science. One gets such wholesale returns of conjecture out of such a trifling investment of fact.*

Mark Twain



## Zusammenfassung

Gasausströmungen, oft in der Form hoch kollimierter Jets, sind ein allgegenwärtiges Phänomen bei der Geburt neuer Sterne. Emission von stoßangeregtem molekularem Wasserstoff bei Wellenlängen im nahen Infrarotbereich ist ein Merkmal ihrer Existenz und auch in eingebetteten, im Optischen obskurierten Ausströmungen generell gut zu beobachten. In dieser Arbeit werden die Resultate einer von Auswahleffekten freien, empfindlichen, großflächigen Suche nach solchen Ausströmungen von Protosternen in der  $v=1-0$  S(1) Linie molekularen Wasserstoffs bei einer Wellenlänge von  $2.12\ \mu\text{m}$  vorgestellt. Die Durchmusterung umfasst eine Fläche von etwa einem Quadratgrad in der Orion A Riesenmolekülwolke. Weitere Daten aus einem großen Wellenlängenbereich werden benutzt, um die Quellen der Ausströmungen zu identifizieren. Das Ziel dieser Arbeit ist es, eine Stichprobe von Ausströmungen zu bekommen, die so weit wie möglich frei von Auswahleffekten ist, um die typischen Eigenschaften protostellarer Ausströmungen und deren Entwicklung festzustellen, sowie um die Rückwirkung der Ausströmungen auf die umgebende Wolke zu untersuchen.

Das erste Ergebnis ist, daß Ausströmungen in Sternentstehungsgebieten tatsächlich sehr häufig sind: mehr als 70 Jet-Kandidaten werden identifiziert. Die meisten zeigen eine sehr irreguläre Morphologie anstelle regulärer oder symmetrischer Strukturen. Dies ist auf das turbulente, klumpige Medium zurückzuführen, in das sich die Jets hineinbewegen. Die Ausrichtung der Jets ist zufällig verteilt. Insbesondere gibt es keine bevorzugte Ausrichtung der Jets parallel zum großräumigen Magnetfeld in der Wolke. Das legt nahe, daß die Rotations- und Symmetrieachse in einem protostellaren System durch zufällige, turbulente Bewegung in der Wolke bestimmt wird.

Mögliche Ausströmungsquellen werden für 49 Jets identifiziert; für diese wird der Entwicklungsstand und die bolometrische Leuchtkraft abgeschätzt. Die Jetlänge und die  $\text{H}_2$  Leuchtkraft entwickeln sich gemeinsam mit der Ausströmungsquelle. Von null startend, dehnen sich die Jets schnell bis auf eine Länge von einigen Parsec aus und werden dann langsam wieder kürzer. Sie sind zuerst sehr leuchtkräftig, die  $\text{H}_2$  Helligkeit nimmt aber im Lauf der protostellaren Entwicklung ab. Die Längen- und  $\text{H}_2$  Leuchtkraftentwicklung läßt sich im Wesentlichen durch eine zuerst sehr hohe, dann niedriger werdende Massenausflußrate erklären, die auf eine zuerst sehr hohe, dann niedriger werdende Gasakkretionsrate auf den Protostern schließen läßt (Akkretion und Ejektion sind eng verknüpft!). Die Längenabnahme der Jets erfordert eine ständig wirkende Abbremsung der Jets. Ein einfaches Modell einer simultanen Entwicklung eines Protosterns, seiner zirkumstellaren Umgebung und seiner Ausströmung (Smith 2000) kann die gemessenen  $\text{H}_2$ - und bolometrischen Leuchtkräfte der Jets und ihrer Quellen reproduzieren, unter der Annahme, daß die starke Akkretionsaktivität zu Beginn der protostellaren Entwicklung mit einer überproportional hohen Massenausflußrate verbunden ist.

Im Durchmusterungsgebiet sind 125 dichte Molekülwolkenkerne bekannt (Tatematsu et al. 1993). Jets (bzw. Sterne) entstehen in ruhigen Wolkenkernen, d.h. solchen mit einem niedrigen Verhältnis von interner kinetischer Energie zu gravitativer potentieller Energie; dies sind die Wolkenkerne höherer Masse. Die Wolkenkerne mit Jets haben im Mittel größere Linienbreiten als die ohne Jets. Dies ist darauf zurückzuführen, daß sie bevorzugt in den massereicheren Wolkenkernen zu finden sind, welche generell eine größere Linienbreite haben. Es gibt *keinen* Hinweis auf stärkere interne Bewegungen in Wolkenkernen mit Jets, die durch eine Wechselwirkung der Jets mit den Wolkenkernen erzeugt sein könnte. Es gibt, wie von der Theorie vorausgesagt, eine Beziehung zwischen der Linienbreite der Wolkenkerne und der  $\text{H}_2$  Leuchtkraft der Jets, wenn Jets von Klasse 0 und Klasse I Protosternen separat betrachtet werden; dabei sind Klasse 0 Jets leuchtkräftiger als Klasse I Jets, was ebenfalls auf

eine zeitabhängige Akkretionsrate mit einer frühzeitigen Spitze und einem darauffolgenden Abklingen hinweist.

Schließlich wird die Rückwirkung der Jetpopulation auf eine Molekülwolke unter der Annahme strikter Vorwärtsimpulserhaltung betrachtet. Die Jets können auf der Skala einer ganzen Riesemolekülwolke und auf den Skalen von Molekülwolkenkernen nicht genügend Impuls liefern, um die abklingende Turbulenz wieder anzuregen. Auf der mittleren Skala von molekularen Klumpen, mit einer Größe von einigen parsec und Massen von einigen hundert Sonnenmassen liefern die Jets jedoch genügend Impuls in hinreichend kurzer Zeit, um die Turbulenz “am Leben zu erhalten” und können damit helfen, einen Klumpen gegen seinen Kollaps zu stabilisieren.



## Abstract

The presence of outflows, often in the form of well-collimated jets, is a phenomenon commonly associated with the birth of young stars. Emission from shock-excited molecular hydrogen at near-infrared wavelengths is one of the signposts of the presence of such an outflow, and generally can be observed even if the flow is obscured at optical wavelengths. In this thesis, I present the results of an unbiased, sensitive, wide-field search for flows from protostellar objects in the  $\text{H}_2$   $v=1-0$  S(1) line at a wavelength of  $2.12\ \mu\text{m}$ , covering a 1 square degree area of the Orion A giant molecular cloud. Further data covering a wide wavelength range are used to search for the driving sources of the flows. The aim of this work is to obtain a sample of outflows which is free from biases as far as possible, to derive the typical properties of the outflows, to search for evolutionary trends, and to examine the impact of outflows on the ambient cloud.

The first result from this survey is that outflows are indeed common in star forming regions: more than 70 candidate jets are identified. Most of them have a fairly ill-defined morphology rather than a regular or symmetric structure, which is interpreted to be due to the turbulent, clumpy ambient medium into which the jets are propagating. The jets are randomly oriented. In particular, no alignment of the jets with the large scale ambient magnetic field is found, suggesting that the spin and symmetry axis in a protostellar object is determined by random, turbulent motions in the cloud.

Candidate driving sources are identified for 49 jets, and their evolutionary stage and bolometric luminosity is estimated. The jet lengths and  $\text{H}_2$  luminosities evolve as a function of the age of the driving source: the jets grow quickly from zero length to a size of a few parsec and then slowly shorten again. The jets are very luminous early on and fade during the protostellar evolution. The evolution in length and  $\text{H}_2$  luminosity is attributed to an early phase of strong accretion, which subsequently decreases. The shortening of the jets with time requires the presence of a continuous deceleration of the jets. A simple model of the simultaneous evolution of a protostar, its circumstellar environment, and its outflow (Smith 2000) can reproduce the measured values of  $\text{H}_2$  luminosity and driving source luminosity under the assumption of a strong accretion plus high ejection efficiency phase early in the protostellar evolution.

Tatematsu et al. (1993) found 125 dense cloud cores in the survey area. The jet driving sources are found to have formed predominantly in quiet cores with a low ratio of internal kinetic energy to gravitational potential energy; these are the cores with higher masses. The cores which are associated with jets have on average larger linewidths than cores without jets. This is due to the preferred presence of jets in more massive cores, which generally have larger linewidths. There is *no* evidence for additional internal motions excited by the interaction of the jets with the cores. The jet  $\text{H}_2$  luminosity and the core linewidth (as predicted by theory) are related, if Class 0 and Class I jets are considered separately; the relation lies at higher values of the  $\text{H}_2$  luminosity for the Class 0 jets than for Class I jets. This also suggests a time evolution of the accretion rate, with a strong peak early on and a subsequent decay.

Finally, the impact of a protostellar jet population on a molecular cloud is considered. Under the conservative assumption of strict forward momentum conservation, the jets appear to fail to provide sufficient momentum to replenish decaying turbulence on the scales of a giant molecular cloud and on the scales of molecular cloud cores. At the intermediate scales of molecular clumps with sizes of a few parsec and masses of a few hundred solar masses, the jets provide enough momentum in a short enough time to potentially replenish turbulence and thus might help to stabilize the clump against further collapse.



# Contents

<b>1</b>	<b>Flows from young stellar objects</b>	<b>1</b>
1.1	The need for an unbiased survey . . . . .	1
1.2	Some prototypes . . . . .	2
1.3	Some key questions . . . . .	6
1.4	Flows from young stellar objects: the aim of this thesis . . . . .	9
<b>2</b>	<b>Star formation and outflows: an overview</b>	<b>11</b>
2.1	The current picture of low-mass star formation . . . . .	11
	A glimpse at theory . . . . .	11
	The observational picture . . . . .	12
	The four stages of protostellar evolution . . . . .	13
	Observational evidence for circumstellar disks . . . . .	13
2.2	Observational evidence for flows from young stars . . . . .	14
	Optical Herbig-Haro objects . . . . .	14
	Molecular outflows . . . . .	16
2.3	Molecular hydrogen jets . . . . .	17
	The H <sub>2</sub> molecule . . . . .	17
	Observations of interstellar H <sub>2</sub> : Milestones . . . . .	18
	Origin of the H <sub>2</sub> emission: excitation mechanisms . . . . .	20
	Origin of the H <sub>2</sub> emission: (molecular) shocks . . . . .	21
	Origin of the H <sub>2</sub> emission: Constraints from observations . . . . .	22
2.4	The jet-disk connection . . . . .	24
2.5	Models of outflow activity . . . . .	25
	Jet acceleration & collimation . . . . .	25
	Jet structure . . . . .	27
	Molecular outflows . . . . .	28
	The X-wind . . . . .	29
2.6	Star formation in Orion . . . . .	30
<b>3</b>	<b>Observations</b>	<b>36</b>
3.1	The near-infrared H <sub>2</sub> S(1) line survey . . . . .	36
	Observing strategy . . . . .	37

Data reduction . . . . .	39
Calibration . . . . .	41
3.2 The optical continuum survey . . . . .	41
3.3 1.3 mm maps . . . . .	43
3.4 IRAS data . . . . .	44
<b>4 Data analysis</b>	<b>45</b>
4.1 The near-infrared H <sub>2</sub> survey . . . . .	45
Method of data extraction . . . . .	45
Results in summary . . . . .	46
4.2 The outflow driving sources . . . . .	46
Results in summary . . . . .	48
4.3 Limitations and errors . . . . .	48
The H <sub>2</sub> jet survey . . . . .	48
The driving sources . . . . .	51
<b>5 The H<sub>2</sub> jet sample</b>	<b>53</b>
5.1 The number of H <sub>2</sub> jets . . . . .	53
5.2 The distribution of jets in the survey area . . . . .	53
5.3 Flow morphology . . . . .	54
Symmetry . . . . .	55
H <sub>2</sub> jet beams . . . . .	56
H <sub>2</sub> bow shocks and multiple working surfaces . . . . .	58
A few words about binaries . . . . .	60
5.4 Flow lengths . . . . .	61
5.5 H <sub>2</sub> luminosities . . . . .	67
5.6 H <sub>2</sub> jets and molecular (CO) outflows . . . . .	70
5.7 Orientation of the jets with respect to the large scale magnetic field . . . . .	73
<b>6 H<sub>2</sub> Jets and CS cores</b>	<b>80</b>
6.1 Association of jets with CS cores . . . . .	80
6.2 Properties of cores with and without H <sub>2</sub> jets . . . . .	84
Core masses . . . . .	84
Virial parameters . . . . .	86
Linewidths . . . . .	88
6.3 Jet- vs. core properties . . . . .	93
Core mass & jet H <sub>2</sub> luminosity . . . . .	93
Core linewidth & jet H <sub>2</sub> luminosity . . . . .	94
<b>7 Discussion</b>	<b>96</b>

7.1	Jet & protostar statistics in Orion A . . . . .	96
7.2	$L_{\text{H}_2}$ vs. $L_{\text{bol}}$ : Testing the toy model of protostar/outflow evolution . . . . .	102
7.3	Estimated impact of the jets on the Orion A molecular cloud . . . . .	107
<b>8</b>	<b>Conclusions and future prospects</b>	<b>113</b>
8.1	Conclusions . . . . .	113
8.2	What next? . . . . .	114
	<b>References</b>	<b>117</b>
<b>A</b>	<b>The H<sub>2</sub> features</b>	<b>132</b>
A.1	Field 1 . . . . .	133
	H <sub>2</sub> features: Overview . . . . .	133
	H <sub>2</sub> features: Details . . . . .	134
A.2	Field 2 . . . . .	144
	H <sub>2</sub> features: Overview . . . . .	144
	H <sub>2</sub> features: Details . . . . .	145
A.3	Field 3 . . . . .	147
	H <sub>2</sub> features: Overview . . . . .	147
	H <sub>2</sub> features: Details . . . . .	148
A.4	Field 4 . . . . .	151
	H <sub>2</sub> features: Overview . . . . .	151
	H <sub>2</sub> features: Details . . . . .	152
A.5	Field 5 . . . . .	154
	H <sub>2</sub> features: Overview . . . . .	154
	H <sub>2</sub> features: Details . . . . .	155
A.6	Field 6 . . . . .	163
	H <sub>2</sub> features: Overview . . . . .	163
	H <sub>2</sub> features: Details . . . . .	164
A.7	Field 7 . . . . .	168
	H <sub>2</sub> features: Overview . . . . .	168
	H <sub>2</sub> features: Details . . . . .	169
A.8	Field 8 . . . . .	172
	H <sub>2</sub> features: Overview . . . . .	172
	H <sub>2</sub> features: Details . . . . .	173
A.9	Field 9 . . . . .	175
	H <sub>2</sub> features: Overview . . . . .	175
	H <sub>2</sub> features: Details . . . . .	176
<b>B</b>	<b>The H<sub>2</sub> flows</b>	<b>180</b>

---

B.1	Overview maps . . . . .	181
B.2	List of H <sub>2</sub> flows . . . . .	190
B.3	Notes on individual flows . . . . .	192
<b>C</b>	<b>The outflow driving sources</b>	<b>197</b>
C.1	Candidate driving sources . . . . .	198
C.2	Notes on individual objects . . . . .	202
C.3	Spectral energy distributions . . . . .	208
<b>D</b>	<b>H<sub>2</sub> jets and molecular (CO) outflows: Details</b>	<b>212</b>
	<b>Acknowledgements/Danksagung</b>	<b>223</b>

## List of Figures

1	The HH 46/47 giant Herbig-Haro flow . . . . .	2
2	The HH 211 infrared jet . . . . .	3
3	The HH 212 infrared jet . . . . .	4
4	The L1551 bipolar molecular outflow . . . . .	5
5	Cha IRN . . . . .	6
6	Potential energy curves of molecular hydrogen . . . . .	17
7	Schematic drawing of a jet bow shock . . . . .	23
8	HH 30 . . . . .	24
9	Schematic drawing of the jet driving and collimating mechanism . . . . .	26
10	Molecular clouds in Orion/Monoceros: an overview . . . . .	31
11	Star formation sites in Orion A: an overview . . . . .	33
12	The mosaicing pattern . . . . .	37
13	Overview of the survey area . . . . .	38
14	1.3 mm-map of south-eastern survey part . . . . .	42
15	1.3 mm-maps of L1641-N, HH 34 IRS, and V 380 Ori NE . . . . .	43
16	Symmetric jets . . . . .	55
17	H <sub>2</sub> jet beams . . . . .	57
18	H <sub>2</sub> bow shocks . . . . .	59
19	Distribution of flow lengths: all flows . . . . .	63
20	Distribution of flow lengths: from Class 0 to Class II . . . . .	64
21	Flow length vs. $L_{\text{bol}}$ : all flows . . . . .	65
22	Flow length vs. $L_{\text{bol}}$ : from Class 0 to Class II . . . . .	66
23	Distribution of flow $L_{\text{H}_2}$ : all flows . . . . .	68
24	Distribution of flow $L_{\text{H}_2}$ : from Class 0 to Class II . . . . .	69
25	$L_{\text{H}_2}$ vs. $L_{\text{bol}}$ : all flows . . . . .	70
26	$L_{\text{H}_2}$ vs. $L_{\text{bol}}$ : from Class 0 to Class II . . . . .	71
27	$L_{\text{H}_2}$ for jets with/without associated CO outflow . . . . .	72
28	Distribution of flow position angles . . . . .	75
29	The fraction of flows “parallel” to an arbitrary position angle . . . . .	75
30	Flow orientations in OMC-2/3 . . . . .	76
31	Flow orientations in L1641 . . . . .	76
32	Flow orientations vs. position . . . . .	77

33	Flow length/ $L_{\text{H}_2}/L_{\text{bol}}$ vs. flow orientation . . . . .	78
34	Jets and CS cores . . . . .	81
35	Location of jets within the cores . . . . .	83
36	Masses of cores with/without jets . . . . .	85
37	Masses of cores with/without jets sorted by survey subregions . . . . .	85
38	Virial parameter $\alpha_{\text{vir}}$ of cores with/without jets . . . . .	87
39	Virial parameter $\alpha_{\text{vir}}$ of cores with/without jets sorted by survey subregions . . . . .	87
40	Core mass – virial parameter $\alpha_{\text{vir}}$ relation . . . . .	88
41	Velocity dispersion in cores with/without jets (entire area) . . . . .	89
42	Velocity dispersion in cores with/without jets (north, middle, and southern survey part) . . . . .	90
43	Core mass – linewidth relation . . . . .	91
44	$\text{H}_2$ luminosity vs. core mass . . . . .	93
45	$\text{H}_2$ luminosity vs. CS linewidth . . . . .	94
46	The unification scheme data . . . . .	104
47	$L_{\text{H}_2}$ vs. $L_{\text{bol}}$ : Model evolutionary tracks . . . . .	105
48	$\text{H}_2$ features in Field 1 . . . . .	133
49	$\text{H}_2$ features in Field 2 . . . . .	144
50	$\text{H}_2$ features in Field 3 . . . . .	147
51	$\text{H}_2$ features in Field 4 . . . . .	151
52	$\text{H}_2$ features in Field 5 . . . . .	154
53	$\text{H}_2$ features in Field 6 . . . . .	163
54	$\text{H}_2$ features in Field 7 . . . . .	168
55	$\text{H}_2$ features in Field 8 . . . . .	172
56	$\text{H}_2$ features in Field 9 . . . . .	175
57	Jets in Field 1 . . . . .	181
58	Jets in Field 2 . . . . .	182
59	Jets in Field 3 . . . . .	183
60	Jets in Field 4 . . . . .	184
61	Jets in Field 5 . . . . .	185
62	Jets in Field 6 . . . . .	186
63	Jets in Field 7 . . . . .	187
64	Jets in Field 8 . . . . .	188
65	Jets in Field 9 . . . . .	189
66	SEDs of outflow driving sources . . . . .	208
67	SEDs of outflow driving sources (continued) . . . . .	209
68	SEDs of outflow driving sources (continued) . . . . .	210
69	SEDs of outflow driving sources (continued) . . . . .	211
70	$\text{H}_2$ and molecular outflows: OMC-2/3 . . . . .	213
71	$\text{H}_2$ and molecular outflows: OMC-1S . . . . .	214



---

72	H <sub>2</sub> and molecular outflows: L1641-N . . . . .	215
73	H <sub>2</sub> and molecular outflows: L1641-N (wide field) . . . . .	216
74	H <sub>2</sub> and molecular outflows: HH 34 . . . . .	217
75	H <sub>2</sub> and molecular outflows: the HH 1/2 area (wide field) . . . . .	218
76	H <sub>2</sub> and molecular outflows: V 380 Ori NE and HH 1/2 . . . . .	219
77	H <sub>2</sub> and molecular outflows: Haro 4-255 . . . . .	220
78	H <sub>2</sub> and molecular outflows in L1641-S/S3 . . . . .	221



---

## List of Tables

1	List of observations . . . . .	39
2	Jets with multiple working surfaces . . . . .	60
3	Cores with outflows . . . . .	82
4	The evolution of a protostellar jet. . . . .	102
5	List of H <sub>2</sub> flows . . . . .	190
6	List of H <sub>2</sub> flows (continued) . . . . .	191
7	Outflow driving sources . . . . .	198
8	Outflow driving sources (continued) . . . . .	199
9	Outflow driving sources (continued) . . . . .	200
10	Outflow driving sources (continued) . . . . .	201



---

# 1 Flows from young stellar objects

## 1.1 The need for an unbiased survey

A star in its earliest evolutionary phases closely resembles a human being during its earliest “evolutionary stages”. Both have to be fed in order to grow, and both “expel” a certain fraction of the stuff which is supposed to make them grow, sometimes seriously affecting their respective surroundings. Moreover, in both cases feeding as well as expelling seems to be episodic, meals (typical period about 3 hours, more often during night time...) and “burps” in the case of little babies, and episodic accretion and outflow activity (FU Orionis outbursts, typical period about 1000 years) in young stars. The difference is that this behaviour has presumably been known to mankind since quite a long time for the babies, whereas the recognition of outflow activity from young stellar objects came as a surprise only some 25 years ago.

A number of observed features in star forming regions are nowadays known to have their origin in the energetic outflow activity of young stars. Small optical emission line nebulae (Herbig-Haro objects, HH-objects) with shock specific spectral properties indicate the places where fast moving gas in the flow hits quiescent material in the ambient gas or parts of the outflow which move more slowly. At near-infrared wavelengths, emission from ro-vibrational transitions of molecular hydrogen traces these shocks. Very often, the molecular hydrogen shocks and optical HH-objects delineate narrow, well collimated beams of gas (jets) moving with velocities of typically a few hundred km/s. Millimetre-line spectroscopy revealed the presence of molecular outflows, i.e., large amounts of gas moving with moderate (several km/s) to high velocities (few hundred km/s), often in a bipolar configuration with blue- and redshifted gas moving away from a source at the centre. Small centimetre wavelength radio jets and masers are often found at the base of these flows. A more indirect indicator of outflow action are conical, often bipolar, reflection nebulae associated with young stars. These are frequently explained as empty cavities in the star forming cloud core, being illuminated from the inside by the young star at their base. An important feature is common to virtually all sources exhibiting these signs of outflow activity: they are surrounded by large amounts of circumstellar material, most likely in the form of circumstellar disks (and envelopes), through which the protostar accretes its mass. Together, these observations suggest that jets are fed, driven, and collimated by the young star and its surrounding accretion disk (most likely due to the action of the rotating magnetosphere of the star and the disk), and that they entrain more material as they move through the cloud core from which the star is forming. They thereby create the massive molecular outflows and the gas and dust cavities around the young stars.

Although the outflow phenomenon seems to be understood well enough to be summarized in two sentences, there are still many uncertainties and open questions in the field, some of them quite fundamental. Furthermore, much of the above picture is based on observations of a few well known, prototypical examples. Thus we do not yet know to what extent this picture is representative for all protostellar objects, or biased by observations of only a few, possibly exceptional cases. In order to improve on this situation, a jet sample largely free from biases is wanted: I will present such a sample and a first analysis of its properties in this thesis. This sample will show how the jets from young stars *typically* are, how they evolve, and how they affect their environment.

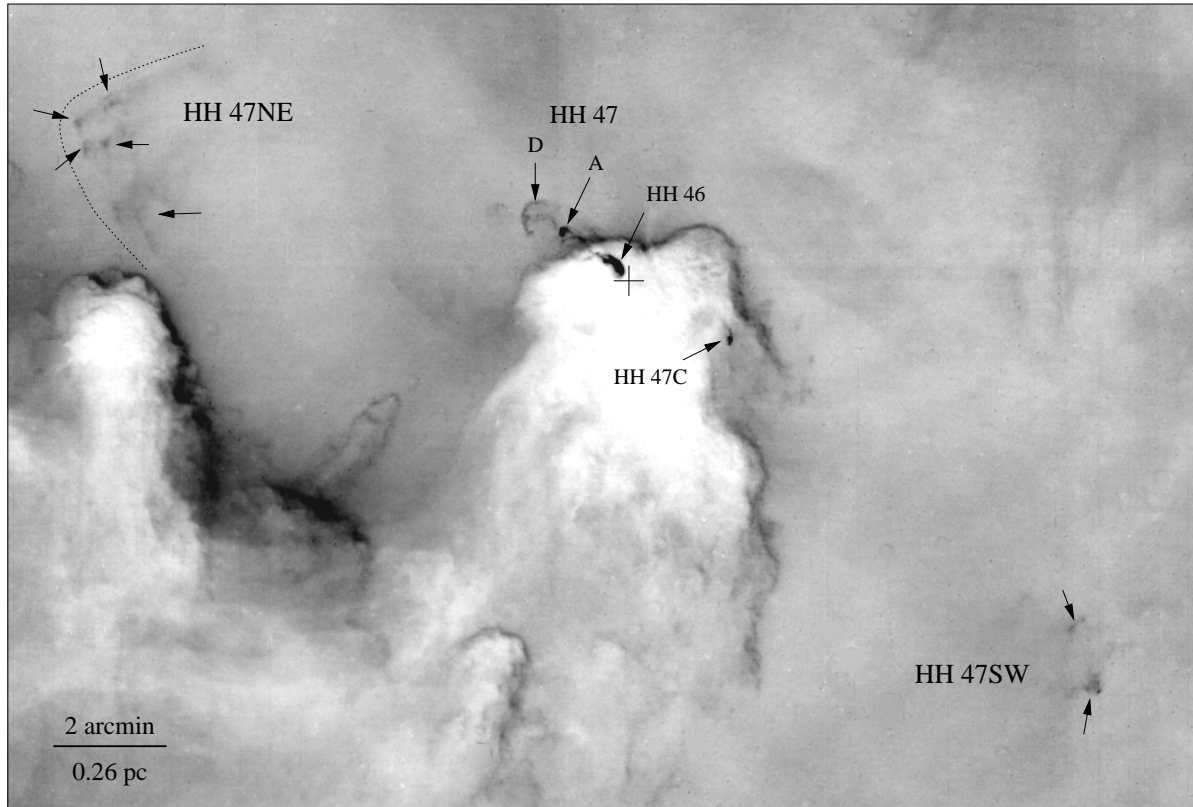


Figure 1: A continuum-subtracted  $H\alpha$  image of the HH 46/47 giant Herbig-Haro flow (from Stanke et al. 1999). The flow is driven by a young star (position marked by the cross), which is embedded in a bright-rimmed dark globule in the Gum nebula H II region. The inner section of this flow, from the driving source out to HH 47 C and HH 47 D, was among the first recognized bipolar jets from young stars. The new wide field image shown here demonstrated that this flow, as many other well-known Herbig-Haro flows, extends over a total length of much more than a parsec.

## 1.2 Some prototypes

Below I will show some prototypical examples of observations of protostellar outflows and related phenomena. These will serve to raise a number of the still open questions, which will be explored (and answered) in this thesis.

Fig. 1 shows an optical emission line image of the HH 46/47 system (Schwartz 1977a; Dopita 1978), one of the first HH objects recognized to form a well-collimated bipolar jet from a young low-mass star (Dopita et al. 1982), embedded in a dark globule in the Gum nebula H II region. The innermost part of this system (HH 46 and the knots between HH 46 and HH 47 A) is delineated by a well-collimated, apparently wiggling jet, which terminates in bow-shaped working surfaces (HH 47 A, HH 47 D, HH 47 C), commonly referred to as bow-shocks. Further out, another recently discovered pair of HH-type features (HH 47 NE, HH 47 SW) indicates that this flow, as many others, extends over a total length of much more than a parsec (Stanke et al. 1999). This represents an impressive illustration of power of even such a low-mass, low- $L_{\text{bol}}$  protostellar driving engine.

The parsec-scale extent found not only for the “prototypical” HH 46/47 system naturally brings up a number of questions: *Is such a “giant jet” really prototypical? Do all protostars drive such a giant outflow or even longer ones? For how long can such a giant outflow be maintained? At which point in the protostellar evolution do we see it? Early on, in a “main outflow phase”, or later on, as the time to reach parsec scale sizes must be very long?* These questions may be hard to answer from the study of

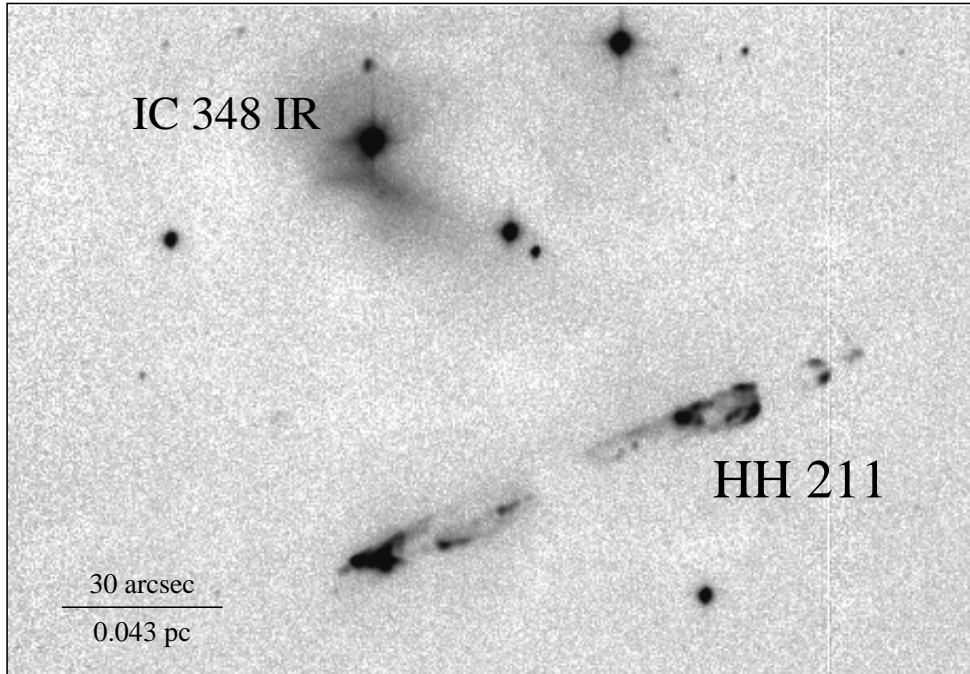


Figure 2: The HH 211 H<sub>2</sub> jet (see McCaughrean et al. 1994), located near the young IC 348 stellar cluster in the Perseus molecular cloud complex at a distance of  $\sim 300$  pc. This is the first protostellar jet which was discovered by near-infrared H<sub>2</sub> imaging. Subsequent CO observations at millimetre wavelengths revealed an associated molecular outflow, with a remarkable highly collimated high velocity molecular jet seen in interferometric observations (Gueth & Guilloteau 1999). The driving source is a deeply embedded Class 0 protostar located exactly in the middle between the two jet lobes. The apparent shortness of the jet (it extends over  $\sim 1.75''$ , corresponding to  $\sim 0.15$  pc) implies a kinematical timescale of only  $\sim 1000$  years, making HH 211 one of the youngest protostellar outflows known.

a few examples. Instead, I will analyze a large sample of jets in this thesis, and suggest an evolutionary scenario for the length of a protostellar jet parallel to the evolution of the driving source.

Figs. 2 and 3 show the prototypical infrared jets HH 211 (McCaughrean et al. 1994) and HH 212 (Zinnecker et al. 1998). Both are driven by very young protostellar objects still deeply embedded in their natal cloud. The driving source of HH 212 is detected only at wavelengths greater than  $25 \mu\text{m}$ , and the driving source of HH 211 is not even detected at the longest IRAS wavelengths ( $60 \mu\text{m}$  and  $100 \mu\text{m}$ ). However, the jets driven by these protostars, although completely obscured at optical wavelengths, are shining bright at near infrared wavelengths. Here one can see them in emission lines of molecular hydrogen, particularly the  $v = 1-0S(1)$  line at  $2.12 \mu\text{m}$ . Thus, the jets betray the presence of their hidden driving sources.

HH 211 was the first protostellar jet which was found through infrared imaging. Its shortness suggests a kinematical timescale of only about 1000 years, making it one of the youngest known protostellar outflows. Another remarkable feature of HH 211 is the highly collimated high velocity molecular (CO) jet revealed by millimetre interferometry (Gueth & Guilloteau 1999). HH 212, also discovered through infrared imaging, deserves particular attention because of its great symmetry and the apparently largely undisturbed structure: here we can hope to observe a jet “as it is”, largely free from any disturbing effects. Particularly intriguing is the quasi-periodic occurrence of knots and bow shocks. These knots and bow shocks appear at equal distances from the central protostar in both outflow lobes, thus generating the symmetry. This behaviour strongly suggests that they are caused by some events at the protostellar source itself (periodic outburst, with different timescales associated with different outburst amplitudes), and not by instabilities in the flow or interaction with an inhomogeneous environment.

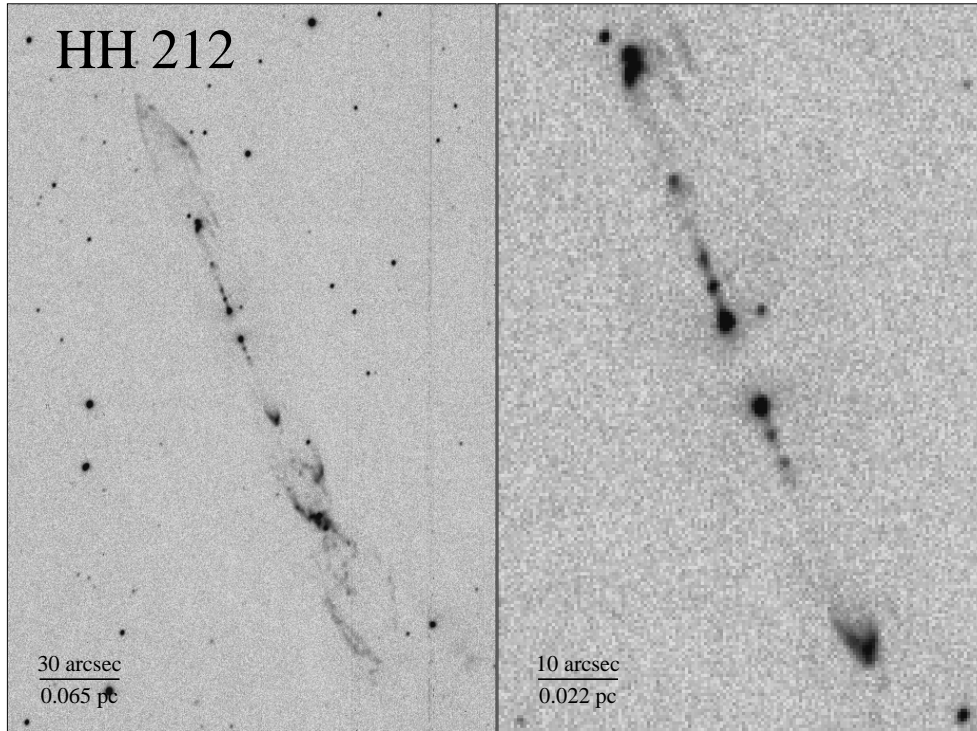


Figure 3: The HH 212  $H_2$  jet (see Zinnecker et al. 1998), located in the Orion B giant molecular cloud at a distance of  $\sim 450$  pc. The left panel shows the entire jet, the right panel shows a closeup of the central part. The driving source (which is invisible in this near infrared image) is located right between the two brightest knots in the center of the image on the right side. The innermost part of the jet is marked by a series of compact knots in both jet lobes, which fade with increasing distance from the driving source. Then, after a gap with only faint features of emission, in the lower and upper part of the right panel a pair of clearly resolved bow shocks is seen, again symmetric about the driving source. Going back to the left panel, another much larger pair of bow shocks is seen to bracket the inner part of the jet, again located symmetrically about the driving source, with the southern feature being brighter than the northern bow. Going further out, the symmetry breaks, with another large, fragmented bow shock structure seen only in the southern outflow lobe. HH 212 extends over  $\sim 4'$ , corresponding to about 0.5 pc.

It was the discovery of HH 211 and HH 212 through infrared imaging which motivated the idea to search larger areas for embedded molecular hydrogen jets, which eventually resulted in this thesis. Besides the discovery of more very young jets in its own right, the other promise from such a survey was to use the jets as pointers to the deeply embedded, thus otherwise hard-to-find, youngest protostars: these are obviously key objects for an understanding of the star formation process.

Having introduced HH 211 and HH 212 as prototypes, some new questions arise, which again call for a study of a large sample of jets rather than just a few examples: *Does each protostar go through an “infrared jet phase”?* *Why is the infrared emission so bright in some flows, but fainter in others?* *Is there an evolution in jet ( $H_2$ ) luminosity, and what is its cause?* *Do all jets have a symmetric structure similar to HH 212?* *What is the reason for the presence or absence of symmetry?* I will propose an evolutionary scenario for jets, which includes the presence of infrared jets and the evolution of their luminosity as a consequence of the evolution of the protostellar driving source, based on a large jet sample. In fact, the jet sample will provide valuable information not only on the evolution of the jets themselves, but also on the evolution of the underlying protostars. The jets trace the accretion activity onto the protostar, and thus will allow us to constrain protostellar evolution models.

Fig. 4 shows the prototypical molecular CO outflow L1551 in the Taurus star forming region (Snell et al. 1980; see also the review by Staude & Elsässer 1993). The intensity of emission from high velocity CO is shown as a contour plot, with dashed contours for the redshifted, and solid contours for



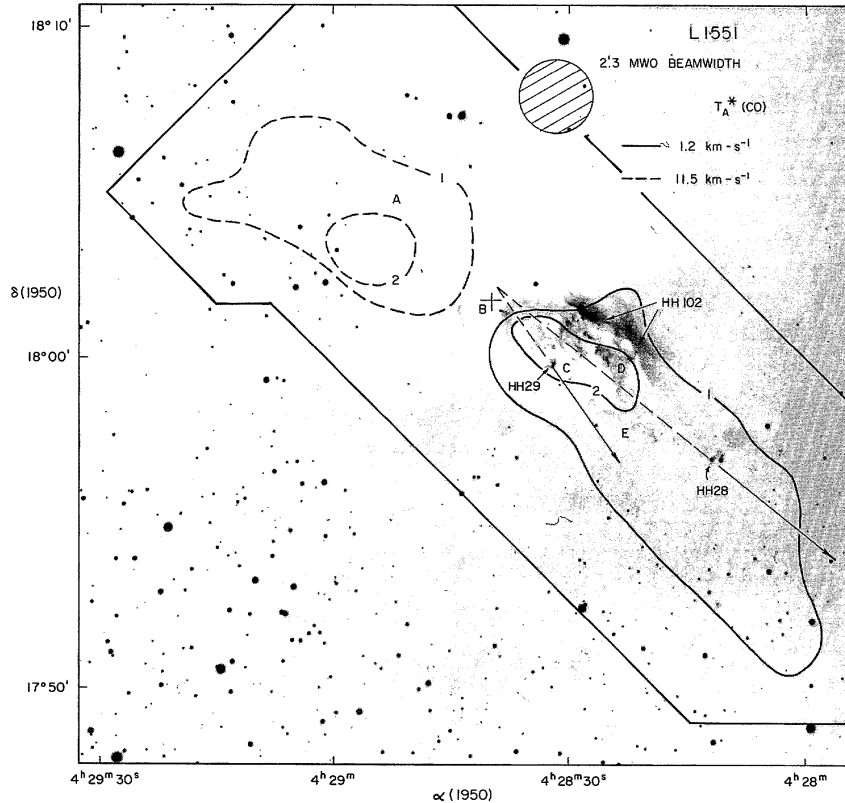


Figure 4: The L1551 bipolar molecular outflow (taken from Snell et al. 1980). The contours show the distribution of high velocity molecular gas, with the solid contours indicating blue-shifted gas, and dashed contours indicating red-shifted gas. The blue- and red-shifted gas is found in two distinct lobes in a bipolar configuration around a deeply embedded young stellar object (L1551-IRS5), indicating (moderately) collimated mass outflow from this star. The CO map is superposed on an optical photo of the region, on which some Herbig-Haro objects are marked. HH 28 and HH 29 move at a high velocity in a direction away from the embedded source, as can be seen from the proper motion vectors drawn in the above image. (Cudworth & Herbig 1979; but see Devine et al. 1999b). Closer to the driving source, a short optical Herbig-Haro jet is found (e.g., Mundt & Fried 1983; Fridlund & Liseau 1998), and on even smaller scales, a well collimated free-free emission radio jet (Cohen et al. 1982) is found to originate in the embedded source.

the blueshifted gas. The young stellar object driving the flow (L1551-IRS5) is located between the red- and blueshifted lobe. It is found to drive a rather small, well collimated optical HH-jet (e.g., Mundt & Fried 1983; Fridlund & Liseau 1998), which is presumably responsible for driving the much wider, but still collimated molecular outflow. At even smaller spatial scales, Cohen et al. (1982) found a collimated free-free emission radio jet, apparently at the base of the Herbig-Haro and molecular flow system. This radio jet was among the first radio jets detected from young stellar objects (see Rodríguez 1997 for a recent review).

For the study of molecular (CO) outflows the jet survey presented here so far is of limited use. Jets presumably play a major role in driving the massive, only moderately collimated molecular outflows (see Cabrit et al. 1997 for a review). A detailed comparison of jets and associated molecular outflows could help to explore this issue, once appropriate molecular outflow data are available for the jet sample presented in this thesis.

Finally, Fig. 5 shows a deep near-infrared image of the young stellar object called the Chameleon Infrared Nebula (Cha IRN), recently obtained with the infrared camera ISAAC at the ESO-VLT UT1 (Zinnecker et al. 1999). This instrument shows the huge bipolar, fan-shaped reflection nebula in unprecedented detail. It extends out to a distance of about 0.1 pc from the embedded young star, i.e., out to

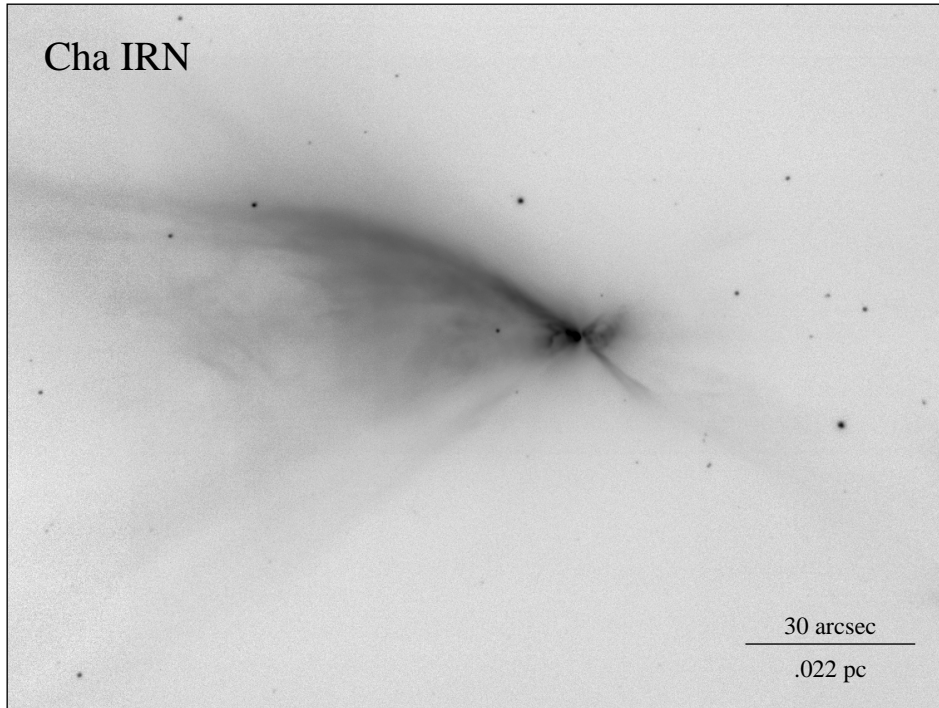


Figure 5: This image shows a deep near-infrared exposure of the Chameleon infrared nebula (Cha IRN), taken with the ISAAC infrared camera at the VLT (Zinnecker et al. 1999). The image is a black and white rendering of a composite colour image, which is a combination of a J-, H-, and K-band image. A large, east-west oriented biconical reflection nebula is seen. The brightest part of the nebula at the center is intersected by a narrow, north-south running dark lane, presumably an edge-on circumstellar disk around the central illuminating source, which itself is not directly seen. The bipolar reflection nebula presumably outlines the walls of a cavity which has been evacuated by an outflow from the embedded young star.

the edges of the cloud core from which the star has formed. The most commonly advocated explanation for this type of nebulosities (see, e.g., the review by Staude & Elsässer 1993) is a conical cavity in the cloud core, which has been excavated by a flow from the young star (although it should be noted that at least in the case of the Cha IRN no other sign for outflow activity has so far been found).

In view of this huge cavity several questions come to mind: *Do outflows “only” dig out cavities, or do they disrupt the entire cloud core? Do they stir up the core inducing turbulent motions, thus preventing further infall and determining the stellar mass? Are jets powerful enough to have a significant impact on the entire star forming (giant) molecular cloud?* These are fundamental questions, as they might hold clues on the final outcome of the star formation process and thus the initial distribution of stellar masses (initial mass function, IMF), and the star formation efficiency. The comparison of the jet survey with the known population of dense cloud cores (Tatematsu et al. 1993) in the survey area will allow a reexamination of these questions.

### 1.3 Some key questions

Observationally it becomes more and more evident that virtually all young stellar objects are driving outflows during their early evolution (e.g., Parker et al. 1991; Bontemps et al. 1996a). Even more, the very youngest protostars appear to drive the most energetic outflows. A number of questions exist in addition to those raised above. They may be subdivided into two categories. First, there are problems connected with the mechanisms involved to explain the existence and the properties of the jets and outflows themselves. Second, there is the question whether the jets and flows from young stars are just

an ornamental accessory to the star formation process, or whether they have a significant impact on the star formation process. Not all of these questions can be answered in this thesis. The jet sample compiled in this work may however help in future to investigate these questions in a more statistical way. Let me describe the first complex first.

**Jets are high velocity, well-collimated beams of gas: how are jets accelerated and collimated?**

It is now widely accepted that the main ingredients in the formation and collimation of astrophysical jets are accretion disks and magnetic fields: a poloidal field anchored in the rotating disk centrifugally accelerates the jet gas; toroidal field components, generated by the winding up of the poloidal field lines, are responsible for the collimation of the flow (Blandford & Payne 1982). The details of these models are, however, not yet clear. In addition, it is very hard to directly test these models observationally, since the acceleration and collimation regions close to the driving sources are very small even for the most nearby star forming regions and hard or even impossible to resolve with currently feasible observations (e.g., Eisloffel et al. 2000a). Furthermore, these regions usually are either deeply embedded and thus obscured at optical or near-infrared wavelengths, or the emission from the star itself is too strong to sort out the contribution of the jet. It also proves very difficult to derive useful information about the strength, origin, and morphology of the magnetic fields around young stellar objects and in their associated flows (but see Guenther et al. 1999; Ray et al. 1997). Theory thus has to rely largely on the properties of the jets far from the source (such as the degree of collimation of the jet, the width of the jet, and the velocity of the jet gas) in order to constrain the models, which is not very satisfactory. High resolution imaging at infrared and millimetre wavelengths (VLTI, NGST, ALMA) might be used in future to investigate these regions in the jet sample presented in this thesis.

**What causes the observed structure of the jets, and what is the composition of the jet gas?**

Further out along the jet beam, one has to explain the generally found knotty structure of the jet beams and the nature of the more extensive Herbig-Haro objects, as well as the composition of the jet material. The knots in the jet beams as well as the larger Herbig-Haro type shocks are usually explained as working surfaces, where faster moving material hits slower moving jet material (internal working surfaces, e.g., Raga et al. 1990) or the quiescent ambient material (e.g., Mundt 1985); note, however, that a number of other possible explanations exist. The periodicity and symmetry of such features may give important information on their formation mechanism and, in turn, on the processes responsible for driving the jets.

The composition of the jet gas, whether mainly atomic, ionized, or molecular, may also hold clues to processes close to the driving sources, where the material is injected into the jet. For example, molecular jets might point to disk material which has been ejected. Therefore it would be important to see how frequent molecular jets like HH 211 and HH 212 are, and whether the molecular emission in these jets arises from molecular material in the jet itself or from material entrained by the jet during its passage through the molecular cloud cores.

**Are the jet orientation and magnetic field orientation related?**

Having accepted that jets are accelerated and collimated through magnetic fields, it is worthwhile to ask to what extent magnetic fields in the ambient molecular cloud affect the propagation of the jet far from its driving source. It is a long standing proposal that jets and outflows are preferentially oriented parallel to ambient magnetic fields. There are two possible reasons, namely a preferred orientation of the symmetry and rotation axis of the driving source parallel to the ambient field, or a preferred propagation of outflows along the field lines. This proposal will be tested in Orion A using the new jet sample presented in this thesis. Connected to this is the question to what extent magnetic fields are responsible for the often observed bends, wiggles,

and misalignments of jet beams (e.g., Fendt & Zinnecker 1998).

Secondly, besides understanding the outflow phenomenon itself, it is also mandatory to ask to what extent outflows might have an impact on the star formation process itself. Below I will sketch some ideas why and how this could be the case.

**Can jets solve the angular momentum problem?** One of the long standing problems in star formation is to understand how the collapsing cloud core gets rid of excess angular momentum, allowing material to accrete onto the protostar without spinning it up to breakup (e.g., Pringle 1989). Magnetocentrifugally driven jets may provide an efficient way of removing angular momentum from the disk (Blandford & Payne 1982). There is clear evidence from observations that outflow activity is tightly correlated to the presence of disks and accretion activity (e.g., Strom et al. 1988a; Königl & Pudritz 2000; references therein). It may be possible that accretion is not only responsible for driving jets by providing the material and the energy, but that jets may also be *necessary* for accretion to take place at all (e.g., Königl 1989). Jets and outflows may thus indeed be an integral part of the star formation process, without which star formation could not proceed as it does. An exciting new perspective on this issue may just open up, as possibly evidence for a spin motion in the HH 212 jet beam has been found recently (Davis et al. 2000a), with the jet spinning in the same direction as the flattened molecular core from which the HH 212 driving source is forming (Wiseman et al. 2000).

**What is the role of outflows in determining the stellar masses?** Another (unsolved) key problem in star formation is to understand how the mass of the forming star is determined and how the stellar mass function is produced in a star forming cloud. Recently, some evidence has been found that the mass function may be determined prior to the actual star forming process by the fragmentation of the cloud into smaller subclumps (Motte et al. 1998). It is still unknown, however, which fraction of such a clump ends up in a star. Large amounts of energy and momentum are observed in the outflows from young stars, and apparently they have the capability to dig out large cavities in the star forming cloud cores. It is obviously a possibility that these flows may have a profound impact on the cloud cores and on the star formation process inside the cloud core. There is, e.g., a long standing idea that outflow opening angles widen with time (see, e.g., Shu et al. 1993), eventually reaching a  $180^\circ$  opening angle and shutting off accretion. Observational evidence for this picture has recently been claimed by Velusamy & Langer (1998) for the B5 outflow. In a scenario proposed by Nakano et al. (1995), outflows directly blow away parts of the cloud core. As a consequence, the outer parts of the cloud core become gravitationally unbound and are no longer available for accretion onto the star. Thus the outflow action will terminate accretion at some time and limit the stellar mass. This model, applied to a sample of 125 cloud cores in Orion A found by Tatematsu et al. (1993), yields an initial mass function which is in good agreement with the field star initial mass function. Nakano et al. take this as evidence that outflows from young stars may indeed have a significant impact on the mass of the forming stars.

**Do jets have a significant feedback on the star forming cloud?** Outflow activity from young stars may help to solve yet another problem connected to star formation: the lifetimes of the giant molecular clouds in which stars form, and the low star formation efficiency observed in the clouds demonstrate that the clouds cannot be in free fall collapse. Instead, there must be mechanisms which support the cloud against the action of its self-gravity. The most likely of these are magnetic fields and (supersonic) turbulence (see, e.g., Shu et al. 1987). The problem with supersonic turbulence is, however, that it is strongly dissipative, with decay time scales of the order of or less than the free fall time scale (e.g., MacLow 1999). In order to be able to support the cloud, turbulence would have to be replenished. One

possible mechanism (admittedly not the only mechanism one could think of) is the action of outflows (e.g., Solomon et al. 1981). This mechanism could have another appealing consequence: as soon as star formation sets in in a collapsing cloud, jets form and stir up the cloud, thus counteracting the collapse and holding up further star formation activity. Star formation may thus be a self-regulating process. An understanding of this issue may be the key to an understanding of the star formation efficiency of a cloud.

Finally, it should be noted that many of the items noted above also have their implications in other fields of astrophysics. Collimated outflows are generally found to be connected to processes involving accretion through disks. This includes accreting binary systems as well as black holes at the centers of galaxies (e.g., Burgarella et al. 1993).

#### 1.4 Flows from young stellar objects: the aim of this thesis

Many of the above mentioned jet-related problems have already been tackled either by studying single prototypical outflows or groups of objects selected in a certain way. One of the major deficiencies in the field is, however, that to date no representative sample of protostellar flows exists, which is on the one hand numerous enough to allow statistical investigations and which is on the other hand free from selection effects. *It is the main aim of the work presented in this thesis to provide such a sample and to perform a first analysis of this sample.* To do so, a substantial part (roughly one square degree) of the Orion A giant molecular cloud was imaged in the near infrared at a wavelength of  $2.12\ \mu\text{m}$  in order to reveal the population of protostellar  $\text{H}_2$  jets. The observed part of Orion A offered itself as survey area, since it was previously surveyed for dense cloud cores by Tatematsu et al. (1993). These authors found 125 cloud cores in that area, and as these cloud cores are the suspected sites of ongoing or future star formation, there was also a good chance to find a substantial number of outflows. Initially, it was the idea to search for  $\text{H}_2$  emission only towards the centres of these cloud cores; however, with the advent of the wide field near-infrared camera Omega Prime on Calar Alto, it became possible to search the entire region uniformly in a reasonable amount of observing time, resulting in a truly unbiased survey.

Besides providing a representative sample of flows from young stellar objects, in which many of the above questions could subsequently be studied, such a survey seemed promising also in other respects. As already noted above, the HH 211 and HH 212 jets were discovered through infrared imaging, and signal the presence of their embedded driving sources<sup>1</sup>. Loosely speaking, deeply embedded protostars, which are themselves not visible at near infrared wavelengths, may still be “found” at near infrared wavelengths by finding their jets! Thus it may be possible to detect the youngest protostars through near infrared imaging (which is relatively easy to do) instead of (costly) wide field (sub)millimetre searches: *the jets will serve as pointers to the locations of the protostars.*

The unbiased, area-covering  $\text{H}_2$  survey will reveal flows in various evolutionary stages. Additional photometric data will be used to constrain the bolometric luminosities and evolutionary stages of the jet driving sources. *Thus it will be possible to search for evolutionary trends in outflow properties and to establish an evolutionary sequence for protostellar outflows parallel to the driving source evolution.* This may include evolutions in flow lengths, morphology (e.g., degree of collimation, presence of collimated  $\text{H}_2$  jet beams, presence and morphology of bow shocks, etc.), and flow  $\text{H}_2$  luminosity. The latter would point to an evolution in the flow energetics and, given the tight correlation between accretion and outflow activity, to an evolution of the driving source, particularly its accretion activity. Moreover, outflows may provide a fossil record of the accretion history of their driving sources (e.g., Frank 1998), since at a given location in a jet we see material that has been ejected at a certain time in the

<sup>1</sup>In the case of HH 212 the driving source was known before as a cold IRAS source (Zinnecker et al. 1992), but the infrared jet alone would give a precise location of the source, also allowing a subsequent discovery.

past. Protostellar outflows thus carry important information on the accretion activity of the driving protostar, which is hard to get otherwise. *The study of protostellar outflows can thus be used to reconstruct the accretion history of protostars and to constrain cloud collapse and protostellar evolution models.*

Another flow property which is easy to derive is the orientation (projected onto the plane of the sky). It has often been claimed that outflows are preferentially oriented parallel to the ambient interstellar magnetic field (e.g., Strom et al. 1986, see Section 5.7). *Given a large outflow sample in a single molecular cloud and the known field orientation, it will be possible to reveal such a preferred orientation, if present.*

The jets will mark the currently star forming cloud cores. *The jet survey combined with the CS survey of Tatematsu et al. can thus be used to search for differences between star forming and non star forming cloud cores, and to search for an impact of cloud core properties on the star formation process, which will be reflected in the jet properties.*

Finally, the survey will provide a census of the jets in Orion A, and information about their momentum and kinetic energy from their H<sub>2</sub> brightness. *This will allow us to reexamine the question whether protostellar jets could play a significant role in providing kinetic energy and momentum to the host cloud, possibly at a sufficient rate to stabilize the cloud against collapse.*

Thus the H<sub>2</sub> jet survey as presented in this thesis may help to find new answers to some of the above questions and problems. For many of them, however, additional observations will be necessary.

The structure of this thesis is as follows:

- In Chapter 2, I will give an overview over previous work on protostellar evolution and protostellar outflows, and I will give a short introduction to the survey area, the Orion A giant molecular cloud.
- In Chapter 3, I will describe the observations that have been carried out in the course of the jet survey. Besides the 2.12  $\mu\text{m}$  jet survey itself, this includes observations made in order to identify and characterize the jet driving sources.
- Chapter 4 describes which kind of information I have extracted from the data and gives a short resume of the results of the observations (the details are presented in Appendices A, B, and C).

The following parts describe a first go at the investigation of the newly acquired flow sample.

- In Chapter 5, a detailed analysis of the sample is performed. This includes a discussion of morphological features, the lengths of the flows, their H<sub>2</sub> luminosities, a comparison of the H<sub>2</sub> flows with molecular CO outflows as found in the literature, and a detailed analysis of the orientations of the flows with respect to the ambient, large scale magnetic field.
- In Chapter 6, I will compare the properties of the jet sample to the properties of the CS cloud cores, in order to search for a possible disrupting impact of the outflows on the cloud cores, in order to search for differences between star forming and non star forming cloud cores, and in order to search for an influence of the cloud core properties (particularly the sound speed) on the outflow properties.
- In Chapter 7, the implications of the observations will be discussed and evolutionary trends will be identified and discussed. The survey data will be used to test a scheme of simultaneous protostar and outflow evolution. Furthermore, the possible impact of the protostellar jets on the evolution of a molecular cloud will be discussed.
- Finally, in Chapter 8, I will give a summary and an outlook on what has to be done in the future.

## 2 Star formation and outflows: an overview

### 2.1 The current picture of low-mass star formation

#### A glimpse at theory

Stars form through collapse of cloud cores, the densest parts of molecular clouds (e.g., Lada et al. 1993). The theoretical framework for the current picture of star formation has been outlined by Larson (1969). His calculations, starting from a uniform density distribution, showed that the collapse of cloud cores is a nonhomologous process. The cloud evolves dynamically towards a centrally condensed configuration, the center of which then starts a rapid “runaway” collapse. It leads to the subsequent formation of (two) hydrostatic protostellar cores at the cloud center, onto which the contracting rest of the cloud core accumulates through accretion.

What is often referred to as the “standard picture of isolated star formation” has been set up by Shu and coworkers (Shu 1977; Shu et al. 1987; 1993). In this picture, the collapse starts from a static singular isothermal sphere with a density distribution  $\rho \sim c_{\text{eff}}^2/2\pi Gr^2$  ( $c_{\text{eff}}$  is the effective sound speed in the core). Since the free-fall time  $t_{\text{ff}} \propto 1/\sqrt{\rho}$ , the collapse starts from inside out: the innermost, densest part collapses very quickly, while the outermost parts of the core are still at rest. The collapse proceeds in a rarefaction wave expanding outwards at the sound speed  $c_{\text{eff}}$ . The mass accretion rate is predicted to be *constant in time* and determined by the conditions in the cloud core via its dependence on the effective sound speed:  $\dot{M}_{\text{acc}} \sim c_{\text{eff}}^3/G$ . Other initial collapse conditions (density distributions, boundary conditions, etc.) generally result in time-dependent mass accretion rates  $\dot{M}_{\text{acc}} \sim c_{\text{eff}}^3/G \cdot f(t)$  (e.g., Larson 1969; Zinnecker & Tscharnuter 1984; Foster & Chevalier 1993; André et al. 2000 and references therein).  $f(t)$  typically has a sharp rise and a first rather quick, then more gradual decay.

The slow (but practically inevitable) rotation of cloud cores (with sizes of some 10000 AU) implies the presence of substantial angular momentum, which prevents a direct collapse onto a stellar sized (0.01 AU) object for a significant part of the core. Instead, part of the material forms a flattened structure around the protostellar core (circumstellar disk, see e.g., Cassen et al. 1986; Yorke et al. 1993; Bate 1998). The angular momentum is then redistributed within the disk or extracted through mechanisms whose nature is not yet really known. Once the disk matter has lost most of its angular momentum, it is accreted onto the protostar (e.g., Lynden-Bell & Pringle 1974; Blandford & Payne 1982; Pringle 1989). The presence of disk-like structures was postulated long ago (nebular hypothesis of Kant and Laplace; “Urnebel”) and recognized as a possibility to store and redistribute angular momentum early on. In contrast, the need for the presence of *mass-ejection* during the mass build-up-phase of a protostar came as a complete surprise from observations, only  $\sim 25$  years ago.

The temperature in the centre of a (low mass,  $m \lesssim 8M_{\odot}$ ) star is not yet high enough for hydrogen fusion at the time when accretion dies out. The main source of energy is still gravitational energy. Thus the star contracts during its “pre-main-sequence” evolution on the Kelvin-Helmholtz time scale given by the ratio of its gravitational energy and its surface luminosity ( $\tau_{\text{PMS}} \sim GM_*^2/R_*L_*$ ,  $\sim 10^7$  years for a  $1 M_{\odot}$  star). Once the central temperature is high enough for hydrogen fusion, the star

joins the main sequence (e.g., Hayashi 1961; Larson 1969; Stahler & Walter 1993).

### The observational picture

Observations of the star formation process have for a long time been hindered by the strong obscuration of the young stars by the dusty cloud cores that surround them and from which they accumulate their mass. Thus early observations, limited to optical wavelengths, only revealed the population of rather evolved young stars, the (classical) T Tauri stars (Joy 1942; 1945; Cohen & Kuhn 1979; Appenzeller & Mundt 1989; Bertout 1989). Dark clouds, absorbing the light of background stars and with sizes ranging from small globules to huge dark cloud complexes (e.g., in Taurus Auriga), were identified as the birth places of stars. Classical T Tauri stars show a rich emission line spectrum and excess continuum emission at ultraviolet, optical, and infrared wavelengths. The emission lines are believed to be produced by the combination of accretion shocks, magnetospheric accretion funnel flows (e.g., Camenzind 1990; Königl 1991; see Fig. 9), and simultaneous mass loss through winds (e.g., Najita et al. 2000). Excess continuum emission at UV and optical wavelengths (causing the often observed veiling of photospheric absorption lines) is thought to be produced mainly in the accretion shocks. Further signatures of mass loss in the form of winds from T Tauri stars are P Cygni line profiles and preferentially blueshifted forbidden emission lines. Excess emission at infrared and (sub)millimetre wavelengths indicates the presence of circumstellar gas and dust (e.g., Mendoza 1966, 1968; Beckwith et al. 1990).

Weak-line or naked T Tauri stars are of similar mass and age (some of them older) as classical T Tauri stars. However, they lack the indications of accretion noted for the classical T Tauri stars such as UV and (in most cases) infrared/(sub)millimetre excess as well as the strong emission line spectrum (hence weak-line). Simultaneously, they lack evidence for outflow activity like forbidden line emission and P Cygni line profiles. It is suggested that these stars have already finished the accretion process. Most of the circumstellar dust and gas has been dispersed or processed to larger grains, rocks, and ultimately planets (e.g. Brandner et al. 2000). Characteristic of these stars is their strong X-ray emission (one of the main tools to search for them), caused by strong coronal activity (e.g., Appenzeller & Mundt 1989; Bertout 1989; Neuhäuser 1997).

Major advances in the field were tightly related to advances in detector technology, which opened the infrared to millimetre wavelength range. Large scale millimetre surveys in the  $J=1-0$   $^{12}\text{CO}$  line revealed the true extent and the masses of the dark clouds (e.g., Kutner et al. 1977; Maddalena et al. 1986). Surveys in optically thin lines (e.g.,  $J=1-0$   $^{13}\text{CO}$ , Bally et al. 1987; Nagahama et al. 1998; CS lines, e.g., Lada et al. 1991; Tatematsu et al. 1993, 1998) revealed the clumpy and filamentary nature of the molecular clouds. Infrared observations led to the discovery of a population of optically obscured sources. A breakthrough came with the IRAS satellite, which observed the entire sky at 12, 25, 60, and 100  $\mu\text{m}$ . Based on these IRAS observations, a classification scheme for young stellar objects was introduced (Lada & Wilking 1984; Lada 1987; Wilking et al. 1989), which used the shape of the near-to mid-infrared spectral energy distribution (SED in the following) as a criterion for the subdivision of sources into three classes. Class III sources have SEDs basically resembling those of normal stellar photospheres, decreasing strongly towards longer wavelengths. Class II sources are optically visible, but show infrared excess emission if compared to normal stellar photospheres. Their spectral energy distribution declines more slowly towards longer wavelengths than that of Class III sources or is even flat. Class I sources finally are often obscured at optical wavelengths, become visible at near-infrared wavelengths, and their SED rises strongly towards longer wavelengths. This sequence was interpreted to be due to decreasing amounts of circumstellar material when going from Class I to Class III, reflecting the evolution of a star and its environment.

Later on, a small population of even more deeply embedded objects was found through



(sub)millimetre continuum observations (e.g., Mezger et al. 1992a, 1992b; André et al. 1993; Chini et al. 1993). These sources are not visible at near-infrared or even IRAS wavelengths. They emit the bulk of their luminosity at far-infrared wavelengths and are strong (sub)millimetre sources. This implies the presence of still more circumstellar material and thus an evolutionary stage prior to Class I, thus these objects were labelled Class 0 (André et al. 1993).

### The four stages of protostellar evolution

It is currently believed that these four classes trace the complete evolution of a young stellar object from the onset of accretion onto a protostellar core up to the main sequence (e.g., André & Montmerle 1994; André et al. 2000; Mundy et al. 2000). Class 0 sources are the youngest stage, here the protostar rapidly accretes the bulk of its mass (main accretion phase) and is surrounded by a massive envelope and a disk. Class I sources are slowly accreting the rest of the final stellar mass (late accretion phase). The young stellar object is still surrounded by a remnant envelope and a massive circumstellar disk. Class II sources no longer have an envelope, but still have an accretion disk producing the observed excess infrared emission. Most T Tauri stars (classical as well as some weak-line) belong to this class. At the Class III stage finally, the star is basically free from circumstellar material, evolving towards the main sequence. Most weak-line, but none of the classical T Tauri stars belong to this class.

### Observational evidence for circumstellar disks

Our own planetary system provides a wealth of observations which strongly suggest its formation out of a flattened, rotating cloud: the planet orbits all lie within the ecliptic plane (except Pluto), revolve around the sun in the same direction, and most of them rotate in the same sense. This “Urnebel” idea dates back to the times of Kant (1755) and Laplace (1796).

Unambiguous evidence for circumstellar disks in *other* forming stellar systems proved hard to find. The first arguments were indirect. The predominantly blueshifted forbidden emission lines often found in T Tauri star spectra were interpreted to arise in a bipolar wind, whose redshifted part is obscured by a flattened dust distribution in the equatorial plane of the star (e.g., Appenzeller et al. 1984). Further evidence for flattened structures around young stars came from polarization measurements (e.g., Elsässer & Staude 1978). Last, but not least, the presence of collimated jets from young stellar objects called for an axially symmetric, flattened structure of circumstellar matter.

The presence of circumstellar material in general was suggested by the excess emission at infrared wavelengths (Mendoza 1966, 1968; Appenzeller & Mundt 1989). The infrared SEDs were quite successfully modeled as (accretion) disks (e.g., Lynden-Bell & Pringle 1974; Adams et al. 1987, 1988; Kenyon & Hartmann 1987; Myers et al. 1987; Bertout et al. 1988). Improving millimetre wavelength observing techniques permitted the constraint of circumstellar masses through dust continuum measurements. These dust masses were found to be too high to be distributed in a spherical envelope around the star without completely obscuring it. A disk-like configuration is needed to store the mass, but leave free view to the central star for most lines of sight (e.g., Beckwith et al. 1990). Particularly large dust masses were found around the driving sources of Herbig-Haro objects (Reipurth et al. 1993a). Millimetre interferometry revealed elongated gas distributions around young low mass stars with velocity structures consistent with rotating circumstellar disks (Sargent & Beckwith 1987; Dutrey et al. 1996; reviews by Beckwith & Sargent 1993; Guilloteau et al. 1997; Mundy et al. 2000; Wilner & Lay 2000, and references therein).

Finally, recent high angular resolution optical and near-infrared observations were able to trace narrow dark lanes crossing the centres of a number of reflection nebulosities associated with young

stars (e.g., Padgett et al. 1999; Zinnecker et al. 1999 (see Fig. 5); see McCaughrean et al. 2000 for a review). These dark lanes presumably are circumstellar disks seen edge on, thus blocking the light from the innermost part of the disk and the central star. Particularly intriguing is the HST picture of HH 30 (Burrows et al. 1996; Ray et al. 1996; see Section 2.4), which shows a bipolar conical reflection nebula, with the lobes separated by a dark lane. The biconical reflection nebula is readily explained by scattering of light of the central star in a flared disk. The most interesting aspect of this system is that a highly collimated optical Herbig-Haro jet is seen to originate from this disk, with the jet axis apparently exactly perpendicular to the disk plane. Maybe the most spectacular and direct proof for disk-like distributions of circumstellar material has been found in HST pictures taken towards the Orion Nebula (e.g., McCaughrean & O'Dell 1996; Bally et al. 2000). Here disks around young stars appear as dark silhouettes as they block out the light of the background nebula. Of the 6 examples analyzed by McCaughrean & O'Dell, 5 were seen as round or elliptical silhouettes with a star at their centres. The sixth one had an elongated, cigar-like morphology, and no star was seen at the centre (however, small, faint reflection nebulosities above and below the middle of the silhouette indicated the presence of a star). In this latter case, the disk is seen edge-on, and the emission from the star is obscured. In all other cases, the disks are seen more or less pole-on, allowing direct light from the star to be seen.

One particular aspect of accretion disks around young stellar objects with possible implications for the jet and outflow phenomenon are the FU Orionis outbursts (FUOr's; for reviews see Hartmann et al. 1993; Hartmann & Kenyon 1996). FUOr's are young stars (still surrounded by an envelope) which undergo a sudden increase in brightness by several (5-6) magnitudes over months to years, followed by a slow decline over many decades. The SED and other observed features of FUOr's can be reproduced by accretion disk models with high accretion rates ( $\dot{M}_{\text{acc}} \sim 10^{-4} M_{\odot}/\text{yr}$ , to be compared to  $10^{-7}$  to  $10^{-6} M_{\odot}/\text{yr}$  observed for typical young stellar objects), leading to the suggestion that one observes states of highly enhanced disk accretion activity. Accompanying the accretion activity is strong mass loss through winds, with mass loss rates  $\dot{M}_{\text{wind}} \sim 0.1 \cdot \dot{M}_{\text{acc}}$ . Statistics on observed outbursts suggest that FUOr events repeat several times during the evolution of a young stellar object with a period of less than  $10^4$  years. The mechanism responsible for the outbursts is most likely thermal ionization instabilities (theoretical models of such instabilities yield timescales between FUOr outbursts of order  $10^3$  years, see, e.g., Bell & Lin 1994). As an alternative triggering mechanism for FUOr's interactions of the disks in binary or multiple systems have been proposed (Bonnell & Bastien 1992; Reipurth 2000).

## 2.2 Observational evidence for flows from young stars

A large amount of observational facts led to the recognition that star formation is usually accompanied by strong outflow activity. Below, I try to collect some of the key observations which mark the way towards this discovery and its understanding, sorted by wavelength ranges and with a special emphasis on infrared observations of molecular hydrogen emission in flows from young stars. This collection is certainly very incomplete. As a starting point for a review of the literature in the field, the reader is referred to the articles by Lada (1985), Mundt (1985), Edwards et al. (1993), Fukui et al. (1993), Bachiller (1996), and Richer et al. (2000), and the proceedings of the IAU symposium No. 182 held in 1997 in Chamonix.

### Optical Herbig-Haro objects

Herbig-Haro objects are defined as optically visible, "small-scale shock regions intimately associated with star formation" (Reipurth 1999; for reviews see, e.g., Schwartz 1983; Mundt 1985; Dyson 1987; Mundt 1988; Reipurth 1989a; Edwards et al. 1993; Reipurth & Heathcote 1997). The first object of this

class (Burnham's Nebula, now known as HH 255: Burnham 1890, 1894) was observed close to the prototype T Tauri star T Tau itself. In the late forties, George Herbig (1950, 1951, 1952) and Guillermo Haro (1952, 1953) independently discovered three semi-stellar objects close to the variable star V 380 Ori with peculiar emission line spectra resembling that of Burnham's Nebula. The objects, now known as HH 1, HH 2, and HH 3, show strong hydrogen recombination lines and a variety of atomic forbidden lines, in particular [S II] and [O II], and no detectable optical continuum emission. Their discovery by Herbig and Haro eventually led to the designation of this kind of objects as Herbig-Haro objects (HH-objects; Ambartsumian 1954). Their nature and origin remained a puzzle over quite some time, although it was clear from the beginning that they were somehow connected to star formation. In the years that followed, further HH-objects were found and studied. Herbig (1974) gives a compilation of HH-objects (more than 40) found up to that year; nowadays, several hundred HH-objects are known and catalogued by Reipurth (1999; see <http://casa.colorado.edu/hhcat>).

A major step towards an understanding of Herbig-Haro objects came with the suggestion that their spectral properties might arise in gas that is shock excited by supersonic winds from the young stars (Schwartz 1975). Several different possibilities of how a wind could produce shocks resembling Herbig-Haro objects were considered: small cloudlets exposed to the wind (Schwartz 1978), moving shock fronts (Böhm 1978), fragmentation of a stellar wind bubble into a number of fragments, "bullets" (Norman & Silk 1979), or refocussing shocks at the tip of ovoidal cavities created by initially spherical winds collimated by a density stratified ambient medium (Cantó 1980; Cantó & Rodríguez 1980).

The next crucial step was the discovery of the high proper motions in Herbig-Haro objects indicative of space motions of several hundred km/s (Cudworth & Herbig 1979; see Fig. 4). A particularly insightful finding was provided by the prototype Herbig-Haro objects HH 1 and HH 2: these two objects appeared to move in opposite directions, apparently away from a common source <sup>2</sup> (Herbig & Jones 1981; Eislöffel et al. 1994b).

Another observation finally led to the still widely accepted basic picture of what the majority of Herbig-Haro objects are: Dopita et al. (1982) concluded that the HH 46/47 system is caused by a bipolar, very well-collimated flow, a "jet", from a young, embedded star. Just one year later, Mundt & Fried (1983) presented images of the areas around some young stars in the Taurus star forming region taken with new sensitive CCD array detectors. These images showed clear evidence for very well-collimated, very narrow jets from the T Tauri stars under study (see also Mundt et al. 1990, 1991). Based on this kind of observations, it was suggested that most Herbig-Haro objects were not independent entities (like bullets), but shock fronts in continuous, well collimated jets driven by young stellar objects (e.g., Mundt 1985; Mundt et al. 1987). The jet beams appear to be rather broad (of the order of 100 AU) even very close to the source. This suggests that there must be an initially wide angle wind, which is collimated into the jet beam not too far from the disk plane (Mundt et al. 1991; Ray et al. 1996).

One puzzle, however, remained: the apparent terminating working surfaces of some jets (with typical lengths of order a few tenths of a parsec) were found to run into gas which apparently was already moving away from the driving sources at high velocities (e.g., HH 34: Heathcote & Reipurth 1992; Morse et al. 1992; HH 46/47: e.g., Dopita 1978; Morse et al. 1994; HH 111: Morse et al. 1993a). Thus one had to assume that the flows were much longer than was known at that time. Indeed it is now known that many Herbig-Haro flows extend over distances of several parsecs, among them some of the finest, prototypical examples like HH 34 (Bally & Devine 1994; Devine et al. 1997; Eislöffel & Mundt 1997), HH 111 (Reipurth et al. 1997), and also the HH 46/47 system (Stanke et al. 1999). Many of the working surfaces initially thought to be the terminating working surfaces of the jets are now known to

<sup>2</sup>At that time the Cohen-Schwartz star (Cohen & Schwartz 1979), a T Tauri star on the connecting line through both objects, was thought to be the exciting source; now it is known that the driving source is the more deeply embedded infrared, millimetre, and radio-continuum source HH 1/2 VLA1 located precisely between both objects (Pravdo et al. 1985)

be only one of a series of internal working surfaces in a larger flow. This points to another important jet property: the ejection of matter into the jets has to be nonsteady, like a sequence of eruptions, thus creating internal working surfaces. The timescales of the periods between the ejection events of order 1000 to 2000 years are similar to those found for the FUOr outbursts. Thus it was suggested that the ejection events might have their cause in the episodic strong accretion phases of FUOr outbursts (e.g., Dopita 1978; Reipurth 1985b; 1989a; 1989b; Reipurth & Heathcote 1992).

### Molecular outflows

Kwan and Scoville (1976) pointed out for the first time that the high velocity line wings observed in CO towards OMC-1 could have their origin in outflow motion rather than rotation or infall (see also Zuckerman et al. 1976; Solomon et al. 1981; Erickson et al. 1982). A crucial discovery was the bipolar nature of CO outflows, first recognized in the L1551 outflow (Snell et al. 1980; see Fig. 4). Since then, a large number of bipolar molecular outflows have been found: Lada (1985) lists 63, Fukui (1989) 144, Fukui et al. (1993) 163, and Wu et al. (1996) 264 of them.

Given the large body of observations, only the main general findings will be noted here. A number of review articles may provide a deeper insight (Lada 1985; Fukui 1989; Bachiller & Gómez-González 1992; Fukui et al. 1993, Bachiller 1996; Padman et al. 1997; Richer et al. 2000).

- Flow extents are of the order of  $<0.1$  to  $\sim 5$  pc (e.g., Fukui et al. 1993).
- The lifetimes of molecular outflows are statistically estimated to be of the order of  $10^5$  years (Fukui et al. 1993; Fukui 1989; Parker et al. 1991). Dynamical lifetimes, estimated from the flow extent and a characteristic CO velocity, are generally shorter.
- The molecular outflows are moderately collimated, with younger objects tending to be better collimated and jet-like, older flows being more poorly collimated and of shell-like appearance (e.g. Padman et al. 1997; Richer et al. 2000).
- Typical flow velocities are of the order of a few to a few tens of km/s. Some flows have high velocity components ( $v \gtrsim 100$  km/s), typically in collimated jet-like beams or as chains of small blobs of gas (“bullets”, e.g., HH 111: Cernicharo & Reipurth 1996; Cernicharo et al. 1997)
- The masses of the outflows ( $0.1$ - $100 M_{\odot}$ ; Fukui 1989) are of the same order or greater than the masses of the driving sources, implying that the bulk of the gas is swept up cloud material rather than material provided directly by the protostars themselves (e.g., Lada 1985; Fukui et al. 1993).
- The average kinetic energy input rates (mechanical luminosities)  $L_{\text{mech}} = E_{\text{kin}}/t_{\text{dyn}}$  of molecular outflows range from  $\sim 0.001$ - $2600 L_{\odot}$ . The range in outflow momentum is  $0.1$  to  $1000 M_{\odot}$  km/s (e.g., Fukui et al. 1993). The radiation pressure from the driving sources is far too low to drive the outflows by radiation pressure (e.g., Bally & Lada 1983).

There is a well established correlation between the bolometric luminosity  $L_{\text{bol}}$  of the driving sources and the flow energetics expressed in  $L_{\text{mech}}$  and the average momentum input rate  $F_{\text{CO}}$  (e.g., Bally & Lada 1983; Lada 1985; Richer et al. 2000). Bontemps et al. (1996a) find that, for low mass young stellar objects, the youngest sources (Class 0) lie above the  $L_{\text{bol}}$  vs.  $L_{\text{mech}}$  and  $F_{\text{CO}}$  relation marked by the older Class I sources. A relation between flow kinematics and the circumstellar mass is found, which holds throughout the entire evolution: the more circumstellar mass there is, the stronger the outflow is (see also Cabrit & André 1991). Furthermore, molecular outflows are more frequent in

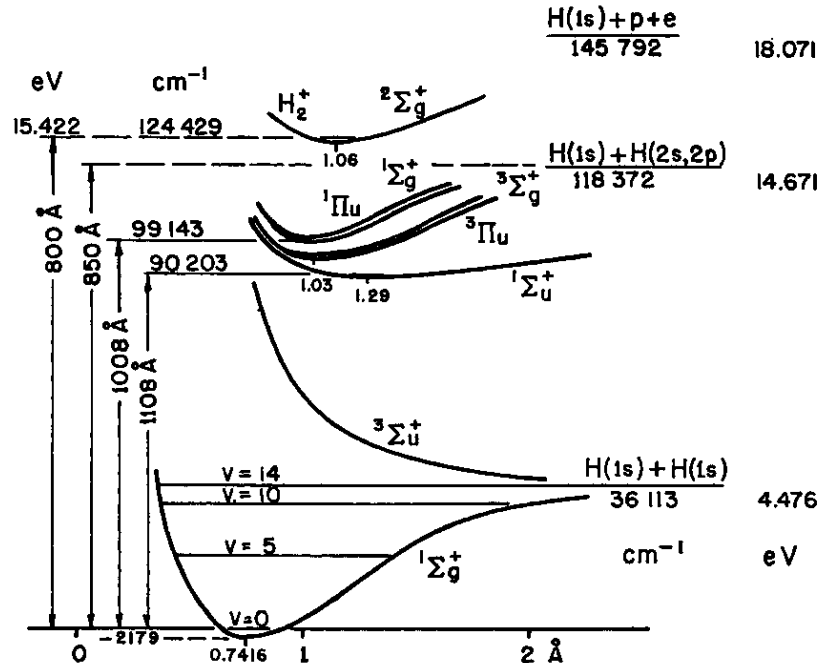


Figure 6: Potential energy curves of the ground state and the lowest excited states of molecular hydrogen (taken from Field et al. 1966). The total energy is plotted as a function of the separation of the two hydrogen nuclei. Excitation, dissociation, and ionization energies are given relative to the  $v = 0$  level of the ground state.

embedded sources than in visible stars (Lada 1985; Fukui 1989). Together, this suggests that outflow activity is particularly frequent and energetic in younger sources.

Finally, it should be noted that throughout this thesis the term “molecular outflow” will be reserved for flows in which the bulk of the gas is traced by emission from high velocity CO (or other molecules); although the jets which are the subject of this thesis are also traced by molecular ( $\text{H}_2$ ) emission, this is emission from shock heated, hot gas, which only traces interaction regions of the jets.

## 2.3 Molecular hydrogen jets

### The $\text{H}_2$ molecule

The large majority of this thesis deals with observations of infrared emission lines from hydrogen molecules. Before giving an overview of the observational work done on  $\text{H}_2$  emission in flows from young stars and discussing the relevant excitation mechanisms (and the tools to discriminate between these and to constrain the nature of the emitting gas), it seems mandatory to sketch some of the properties of hydrogen molecules relevant for an understanding of molecular hydrogen near-infrared emission lines (for more detailed information see Field et al. 1966; Shull & Beckwith 1982).

The  $\text{H}_2$  molecule is the simplest (neutral) molecule one could think of. It consists of two protons plus two electrons. In Figure 6 the potential energy of the  $\text{H}_2$  molecule is plotted as a function of the separation of the hydrogen nuclei for the ground state and a number of excited states (taken from Field et al. 1966; see this paper for an explanation of the level notation). Each electronic state possesses a set of rotation-vibration levels, usually characterized by a vibrational quantum number  $v$  and a rotational quantum number  $J$ . The electronic ground state possesses 14 bound vibrational levels (as is indicated in Fig. 6), each of which is split into a number of rotational levels. The dissociation energy of the  $\text{H}_2$  molecule is 4.48 eV, corresponding to a kinetic velocity of an  $\text{H}_2$  molecule of  $\sim 20$  km/s.

The first allowed electronic dipole transitions from the ground state  $X^1\Sigma_g^+$  are to the  $B^1\Sigma_u^+$  and  $C^1\Pi_u$  states. They occur at energies between 11 and 14 eV (i.e., at UV wavelengths,  $\lambda \sim 0.1 \mu\text{m}$ ) and are known as the  $\text{H}_2$  Lyman and Werner bands.

More important for this work are the rotation-vibrational transitions (ro-vibrational transitions in the following) in the electronic ground state. Since the homonuclear  $\text{H}_2$  molecule does not possess a permanent dipole moment, dipole transitions between levels of different  $v$  and  $J$  within the electronic ground state are forbidden. Electric quadrupole transitions, however, may occur. For those, no selection rules exist for transitions between various  $v$  states. For the rotational quantum number, transitions between ro-vibrational levels must satisfy  $\Delta J = 0, \pm 2$ , with  $J = 0 \rightarrow 0$  also forbidden. Ro-vibrational transitions are usually named giving the vibrational transition, the difference in  $J$  (with the letters O, Q, and S indicating  $\Delta J = +2, 0$ , and  $-2$ , respectively), and the rotational quantum number  $J$  of the final state. For example, the  $2.12 \mu\text{m}$  line used in the present work is the  $v = 1-0 \text{ S}(1)$  line, i.e., the transition from  $v = 1$  to  $v = 0$  and from  $J = 3$  to  $J = 1$ .

The pure rotational transitions of the vibrational ground state of  $\text{H}_2$  are located at wavelengths in the mid-infrared (e.g.,  $J = 2-0$ :  $28.22 \mu\text{m}$ ;  $J = 3-1$ :  $17.04 \mu\text{m}$ ; ...;  $J = 10-8$ :  $5.05 \mu\text{m}$ ). Ro-vibrational transitions with  $\Delta v$  of 1 or 2 occur at near infrared wavelengths (J-, H-, K-bands), transitions with higher  $\Delta v$  are also found at optical wavelengths shortward of  $1 \mu\text{m}$  (see, e.g., Black & Dalgarno 1976; Black & van Dishoeck 1987; Wolfire & Königl 1991; Smith 1995).

### Observations of interstellar $\text{H}_2$ : Milestones

It was suggested for quite a long time that hydrogen in its molecular form might well exist in some parts of the interstellar space, most likely in dense interstellar clouds which shield their interior from energetic,  $\text{H}_2$  dissociating radiation (e.g., Eddington 1937; Gould & Salpeter 1963; Gould et al. 1963; Hollenbach et al. 1971; but see Strömgren 1939). Up to the late 1960s however,  $\text{H}_2$  was only observed in the atmospheres of planets and some stars (see reviews by Field et al. 1966; Shull & Beckwith 1982). The first signatures of interstellar  $\text{H}_2$  were found through rocket and satellite observations as UV absorption features (due to electronic transitions) in the spectra of some bright stars (Carruthers 1970; Smith 1973; Spitzer et al. 1973), and had their origin in thin interstellar clouds in the line of sight to the stars. The detection of electronic transitions at UV wavelengths and of pure rotational transitions at mid-infrared wavelengths both require air-based or space-borne observatories. In contrast, many ro-vibrational transitions occur in atmospheric windows at far-red and near-infrared wavelengths and are thus observable with comparatively low technical efforts. A search for those lines was suggested as an interesting alternative (Gould & Harwit 1963; see also Osterbrock 1962). However, the first attempts to detect these lines at far-red optical wavelengths in dark clouds near hot stars proved difficult (Werner & Harwit 1968; Gull & Harwit 1971). Finally, a number of ro-vibrational  $\text{H}_2$  emission lines were found in K-band spectra of the planetary nebula NGC 7027 (Treffers et al. 1976) and towards the BN and KL regions in Orion (Gautier et al. 1976; Grasdalen & Joyce 1976; Beckwith et al. 1978a; 1979). It became clear very soon that the observed lines in Orion (characteristic of a  $\sim 2000 \text{ K}$  warm gas, apparently coming from only a rather small mass of  $\text{H}_2$  gas) could not represent the bulk of the  $\text{H}_2$  gas in the region. Instead, heating of the gas in a shock wave was proposed (e.g., Hollenbach & Shull 1977; Kwan 1977; London et al. 1977; Draine & Roberge 1982; Chernoff et al. 1982).

The following years brought a number of other detections of ro-vibrational  $\text{H}_2$  sources, many of them in star forming dark clouds (see compilation in Shull & Beckwith 1982). These included  $\text{H}_2$  emission from (or from around) the prototype T Tauri star T Tau (Beckwith et al. 1978b), a number of intermediate to high mass star forming regions (DR 21, OMC-2: Fischer et al. 1980a; NGC 7538: Fischer et al. 1980b; NGC 2071, Cep A, GL 961: Bally & Lane 1982; W51: Beckwith & Zuckerman

1982; NGC 6334: Fischer et al. 1982), and a number of Herbig-Haro objects (HH 1 & 2, HH 46, HH 53, HH 54: Elias 1980; see also Fischer et al. 1980a). The generally observed coexistence of H<sub>2</sub> emission regions with high velocity molecular CO outflows (e.g., Fischer et al. 1985; Bally & Lane 1982; Simon & Joyce 1983; Burton et al. 1989b), the spectral properties, and the detection of H<sub>2</sub> emission in Herbig-Haro objects suggested that the H<sub>2</sub> emitting regions trace shock heated gas in outflows from young stellar objects, similar or equivalent to the optically visible Herbig-Haro objects.

This suggestion was supported by further observations (e.g., Taylor et al. 1984; Zealey et al. 1984, 1986; Lane & Bally 1986; Garden et al. 1986; Sandell et al. 1987; Schwartz et al. 1987; Zinnecker et al. 1989; Wilking et al. 1990a) with increasing sensitivity and spatial as well as spectral resolution (particularly after the installation of infrared array cameras; e.g., Schwartz et al. 1988; Hartigan et al. 1989; Lane 1989; Garden et al. 1990). However, it also became clear that the H<sub>2</sub> shocks in some cases had to originate in different parts of the shock fronts than optical Herbig-Haro objects. These sometimes have shock velocities of order 200 km/s (e.g., HH 1/2, Hartigan et al. 1987), whereas H<sub>2</sub> molecules should only survive in shocks with a velocity up to  $\sim 50$  km/s (see below). The solution to this problem is that H<sub>2</sub> molecules can survive in parts of fast moving shock waves, where the shock front is not parallel to the direction of propagation of the shock wave, e.g., in the wings of bow shocks (see Fig. 7). There the velocity component of the shock front along the direction of propagation is much smaller. Besides emission from bow shock like working surfaces (whether internal or at the leading working surface), in some cases turbulent mixing or shear layers along the jet beam or outflow cavity walls may be responsible for H<sub>2</sub> emission (e.g., HH 26A, HH 40: Chrysostomou et al. 2000; Davis et al. 2000a; Zinnecker et al. 1989; HH 46/47: Eislöffel et al. 1994a; see also Noriega-Crespo 1997). In a few cases, H<sub>2</sub> emission may also originate in “shocked cloudlets” immersed in the flow (e.g., HH 11: Davis et al. 2000a, see also Hartigan et al. 1987).

In the following, only a few selected observations will be highlighted, but a much larger body of examples of H<sub>2</sub> emission in flows from young stars exists (see Eislöffel 1997 for an overview of recent H<sub>2</sub> observations in flows from young stars).

- The H<sub>2</sub> emission in the BN-KL area in Orion was resolved into a system of fingerlike jets through higher resolution images (Taylor et al. 1984; Allen & Burton 1993; McCaughrean & MacLow 1997; Schultz et al. 1999). The tips of some of these fingers are not visible in the low-excitation H<sub>2</sub> lines, but only in higher excitation lines (as optical Herbig-Haro objects or in the near infrared [Fe II] 1.644  $\mu$ m line; e.g., Axon & Taylor 1984; O’Dell et al. 1997; Allen & Burton 1993; Tedds et al. 1999; Lee & Burton 2000).
- High spectral resolution (velocity resolved) observations of H<sub>2</sub> emission in Herbig-Haro objects (e.g., Zinnecker et al. 1989; Carr 1993; Davis et al. 1996, 2000a) and similar H<sub>2</sub> shocks in flows from young stars (e.g., Nadeau & Geballe 1979; Garden et al. 1986; Davis & Smith 1996) showed general agreement with theories explaining H<sub>2</sub> shocks as arising in bow shock like working surfaces, similar to the optical Herbig-Haro objects. Also detailed comparisons of high resolution H<sub>2</sub> images show agreement with bow shock models (e.g., Davis et al. 1996, 1999; Hartigan et al. 1996; Chrysostomou et al. 2000)

Comparison of H<sub>2</sub> imagery with molecular (CO) outflow maps demonstrated that “prompt entrainment” at the leading working surface of a flow is likely a major contributor to the formation of the CO outflows (e.g., Eislöffel et al. 1994a; Davis & Eislöffel 1995; Davis et al. 1997a, 1997b, 1998a, 1998b, 2000b; Gueth & Guilloteau 1999; see also Bence et al. 1996).

- The H<sub>2</sub> infrared jets HH 211 (McCaughrean et al. 1994) and HH 212 (Zinnecker et al. 1998) have both been found more or less by chance (HH 211 in a search for embedded clusters, HH 212 in

a search for a binary system in the deeply embedded IRAS 05413–0104 source (Zinnecker et al. 1992)). No other sign for outflow activity was known in these areas before, and the driving sources are both in the youngest known protostellar evolutionary phase, the Class 0 stage. The discovery of HH 211 and HH 212 demonstrated the power of infrared H<sub>2</sub> imaging in revealing new, particularly very young, deeply embedded flows, and strongly suggested a more systematic search, resulting eventually in the work presented in this thesis.

- The availability of infrared array cameras with high angular resolution, sufficient field-of-view, and high sensitivity recently led to the first publications of near-infrared H<sub>2</sub> proper motion measurements (Noriega-Crespo et al. 1997; Coppin et al. 1998; Micono et al. 1998a; Hodapp 1999; Chrysostomou et al. 2000; Lee & Burton 2000). The proper motions inferred from these studies are surprisingly high, some exceeding 400 km/s. This is much larger than the H<sub>2</sub> dissociation speed in shocks, suggesting that the shocks either form in internal working surfaces in the jets or in oblique portions of bow-shocks.
- Recent high spatial and spectral resolution long slit H<sub>2</sub> spectra of the inner knots of HH 212 show for the first time evidence for a spin motion of the jet around the outflow axis (Davis et al. 2000a); moreover, the flattened molecular core surrounding the HH 212 driving source spins in the same direction as the jet (Wiseman et al. 2000). It has been a long standing suggestion that jets and outflows may play a crucial role in extracting angular momentum from the accretion disk material, thus allowing accretion onto the star to occur. The detection of the spin motion in HH 212 may be the first evidence that this is indeed the case.

### Origin of the H<sub>2</sub> emission: excitation mechanisms

There are several mechanisms which could contribute to the population of the ro-vibrational levels of the electronic ground state and thus give rise to emission of near infrared ro-vibrational H<sub>2</sub> lines. First it has to be noted that generally the gas in the molecular clouds is much too cold to substantially populate even the lowest ro-vibrational levels (a few times 10 K, compared to level energies corresponding to temperatures of more than 6000 K even for the lowest ro-vibrational levels). A detailed discussion of the various possible H<sub>2</sub> excitation mechanisms in HH-objects is given by Wolfire & Königl (1991), along with possible means of distinguishing between them.

The most relevant excitation mechanism for the present work is without doubt collisional excitation of the H<sub>2</sub> molecules in the hot post-shock gas in the protostellar flows. There, the ro-vibrational levels are populated by collisions with other H<sub>2</sub> molecules, atoms, or electrons. The temperature of the gas is typically of order 2000-3000 K, thus only the lower  $v$  levels will be populated (H<sub>2</sub> would be dissociated in hotter gas). The signatures of shock-excited H<sub>2</sub> emission are the absence of transitions from high- $v$  levels and a high ratio ( $\sim 10:1$ ) of fluxes in the 2.12  $\mu\text{m}$  1–0 S(1) and the 2.24  $\mu\text{m}$  2–1 S(1) lines (see, e.g., Wolfire & Königl 1991; Smith 1995).

As a second excitation mechanism UV fluorescence must be kept in mind. In this case, the H<sub>2</sub> molecule is lifted into an electronic excited state through absorption of UV photons in the Lyman and Werner bands. Subsequent decay either leads to dissociation of the molecule (in about 10 % of all transitions) or to decay into bound ro-vibrational levels of the ground state. From there, the H<sub>2</sub> molecule decays through a cascade of ro-vibrational transitions (e.g., Black & Dalgarno 1976; Black & van Dishoeck 1987). UV-fluorescence leads to population of both, high- and low- $v$  states. Consequently, transitions from higher  $v$  states can be observed; another often used first discriminant against collisional excitation is the usually comparably low ratio (2:1) of fluxes in the 2.12  $\mu\text{m}$  1–0 S(1) and the 2.24  $\mu\text{m}$  2–1 S(1) lines (e.g., Black & Dalgarno 1976; Black & van Dishoeck 1987; Wolfire & Königl 1991).



Similar to UV continuum pumping,  $\text{H}_2$  molecules in vibrationally excited levels of the ground state might absorb Lyman- $\alpha$  photons from atomic hydrogen and thus be pumped to the first excited electronic state.

Collisional excitation is the dominant  $\text{H}_2$  excitation mechanism in outflows from young stellar objects (see below). However, the possibility of  $\text{H}_2$  excitation through UV fluorescence has to be kept in mind, particularly if  $\text{H}_2$  features near hot stars are to be explained.

### Origin of the $\text{H}_2$ emission: (molecular) shocks

The theoretical explanation of optical emission from Herbig-Haro objects and  $\text{H}_2$  emission in flows from young stars are both based on the presence of shocks as heating and excitation mechanism. Shocks are introduced by McKee & Hollenbach (1980) as follows: “Shock waves occur in compressible media when pressure gradients are large enough to generate supersonic compressive motions. Because the shock propagates faster than the characteristic signal velocity, the medium ahead of the shock cannot dynamically respond to the shock until the shock strikes. The shock then compresses, heats, and accelerates the medium.” In short, shocks are sometimes described as a “hydrodynamic surprise”. Besides the density, pressure, temperature, and velocity, a number of other quantities change in a gas subject to a shock. This includes the entropy (kinetic energy of ordered motion is converted into heat), magnitude and direction of magnetic fields, the elemental abundances in the gas (through grain sputtering) as well as the chemical composition (for reviews of astrophysical shocks see McKee & Hollenbach 1980; Shull & Draine 1987; McKee & Draine 1991; Draine & McKee 1993; an overview with the focus on shocks in outflows from young stars is given by Hollenbach 1997). Shocks in which the just noted quantities indeed undergo a “discontinuous” change within a very thin layer (with a thickness of order the mean free path of the particles) are referred to as “J-shocks” (jump-shocks). Behind the shock, the gas cools in a cooling zone and its density further increases.

**C-shocks:** The dense molecular gas through which the outflows from young stars propagate can give rise to a different type of shocks. If the magnetic field is strong enough and if the ionization fraction is low enough, so-called “C-shocks” (continuous-shocks) can form (e.g., Draine 1980; Draine et al. 1983; Smith & Brand 1990; Smith et al. 1991b; Smith & MacLow 1997). Low ionization is expected for the interior of molecular clouds, which is shielded against ionizing radiation. If the ionization fraction is low enough, the ions are not well coupled (through collisions) to the neutrals any more; the gas then has to be treated as a two-component fluid. The speed of signal propagation in the ion fluid (which is of the order of the ion Alfvén velocity  $v_{A,i} = B_0/(4\pi\rho_{i0})^{1/2}$ ) can be much larger than the sound speed of the neutrals. If the ion Alfvén velocity is greater than the shock velocity, compressive magnetic waves can reach the pre-shock gas *before* the actual (neutral) shock arrives. As the magnetic waves are damped, the ion fluid is continuously accelerated and compressed before the neutral shock arrives. Friction between the ion and neutral fluids, which now move at different velocities in the preshock gas, leads to acceleration and heating of the neutral fluid (“magnetic precursor”), before the neutral jump arrives. Depending on the field strength and cooling efficiency, the magnetic precursor may eventually lead to a continuous compression of the neutral gas to its post-shock properties *without the presence of a jump*. Such a shock is then called a “C-shock”.

C-shocks are interesting in the context of this thesis (and observations of  $\text{H}_2$  shocks in general) since the kinetic energy dissipation is a much more gradual process and is spread over a much larger volume. This leads to a much lower temperature in the shocked gas for a given shock velocity.  $\text{H}_2$  molecules can thus survive much faster shocks, with shock velocities up to 50 km/s (e.g., Draine et al. 1983; Smith & Brand 1990) or even higher velocities for shocks propagating into a region with a large

bulk Alfvén velocity (Smith et al. 1991b). In contrast, the temperature in the post-shock gas in a J-shock reaches a value too high to allow for H<sub>2</sub> molecule survival at shock velocities of about 20-25 km/s (e.g., Kwan 1977); somewhat higher shock velocities without H<sub>2</sub> dissociation may be possible in lower density gas (Smith 1994b). Another difference of C-shocks with respect to J-shocks is that there is no clear-cut difference between shock region and cooling zone; instead the gas already radiates and cools within the continuous acceleration region.

**Working surfaces:** The interaction region (working surface) of a (collimated) stellar wind with the ambient medium contains more than one shock. On the one hand, there has to be a shock which accelerates the ambient medium to the propagation speed of the working surface (ambient shock). On the other hand, the material in the flow has to be decelerated to the propagation speed of the working surface (inner shock; wind or jet shock); in the case of a collimated jet-like outflow, this shock is called the “Mach disk”. Located between the inner shock and the ambient shock is a shell or layer of dense gas (e.g., Hollenbach 1997).

**Bow shocks** are a frequently discussed special case of such working surfaces (see Fig. 7; e.g., Blandford & Rees 1974; Norman et al. 1982; Blondin et al. 1989; Hollenbach 1997; Wilkin et al. 1997; Raga et al. 1998). In this case, the gas which went through the jet-decelerating shock and the shock accelerating the ambient medium ahead of the jet squirts out sideways of the region between leading shock and Mach disk. This material then forms another working surface with the ambient gas, which surrounds the head of the jet in a shell-like envelope with a shape similar to a rotation paraboloid. Numerical simulations show that such a shell is likely to fragment into clumps and filaments, thus providing an explanation of the generally observed knotty structure of HH-objects and H<sub>2</sub> shocks (e.g., Blondin et al. 1989; de Gouveia dal Pino & Benz 1993; Stone & Norman 1994a; Suttner et al. 1997; O’Sullivan & Ray 2000).

Bow shock models have been very successful in explaining many observed features of optical HH-objects (as well as H<sub>2</sub> shocks, as already noted). This includes the width and shapes of emission lines, position velocity diagrams, as well as the spatial distribution of emission in various lines (e.g., Raga & Böhm 1985; Hartigan et al. 1987; Raga et al. 1997 and references therein).

### Origin of the H<sub>2</sub> emission: Constraints from observations

As already noted above, the flux ratios of the  $v = 1-0 S(1)$  and the  $v = 2-1 S(1)$  lines can be used as a first test of collisional excitation in a hot gas versus excitation through UV fluorescence. These line ratios can be obtained by imaging through narrow band filters centred at the respective lines, or by low- to intermediate resolution spectroscopy. More detailed information about the excitation mechanism may be obtained through measuring the intensities of a number of H<sub>2</sub> ro-vibrational lines by low- to intermediate resolution spectroscopy. From the line intensities, column densities of H<sub>2</sub> in the upper energy level of the respective transition can be derived. Plots of the H<sub>2</sub> column density versus upper level excitation energy (excitation diagrams) are frequently used to constrain the properties of the H<sub>2</sub> emitting gas and the details of the shock mechanism at work (e.g., Smith et al. 1991a; Smith 1994b). In many cases the column density distributions are well modeled as arising from gas at a single temperature (2000-3000 K; e.g., Gredel et al. 1992; Gredel 1994; 1996). Other studies, mostly based on a larger range in upper level energies, showed that a single temperature could not give a satisfying fit to the measured column densities. Instead, a gas with a range of temperatures (as expected for a gas cooling after being heated by specific types of (bow)-shocks) had to be assumed (e.g., Brand et al. 1988; Burton et al. 1989a; Burton & Haas 1997; Smith et al. 1998; Eisloffel et al. 2000b).

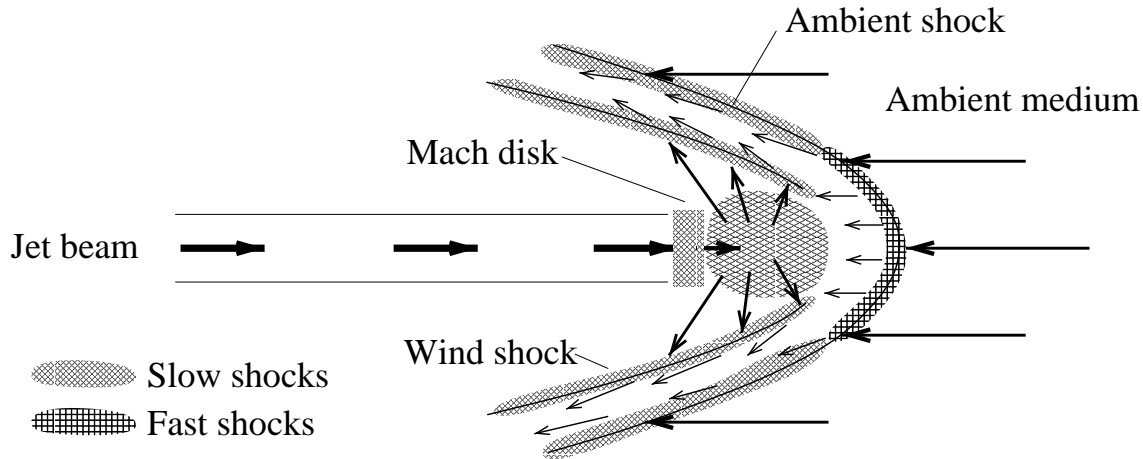


Figure 7: Schematic drawing of a bow shock working surface (in the bow shock rest frame; not to scale; for more details see, e.g., Raga et al. 1998; Wilkin et al. 1997; Hollenbach 1997). The jet comes in from the left and is decelerated in the Mach disk shock (in the case of an overdense jet, the bow shock propagates through the ambient medium at a large fraction of the jet velocity, and the jet only has to be decelerated by a small amount in a slow shock). The ambient medium, streaming in from the right in the bow rest frame, is decelerated in the ambient shock. Between the leading cap of the bow shock and the Mach disk, a layer or clump of dense gas forms, from which gas squirts out sideways. This is equivalent to a wide angle wind, which then interacts with the ambient medium to form the entire bow shaped working surface (e.g., Wilkin et al. 1997). The layer between ambient shock and wind shock is usually assumed to be infinitely thin; note that numerical simulations predict that this layer is unstable to fragmentation into clumps and filaments, thus providing an explanation for the generally knotty structure of Herbig-Haro objects. The ambient shock is fastest at the leading cap of the bow, possibly  $\text{H}_2$  dissociating and of J-type. In the flanks of the bow, the shock front is oblique with respect to the velocity vector of the incoming ambient medium; since only the velocity component perpendicular to the shock front determines the shock speed, the shocks in the bow shock flanks are slow. There,  $\text{H}_2$  molecules can survive, even if the propagation speed of the bow is much larger than the  $\text{H}_2$  dissociation speed.

High resolution (velocity resolved) spectroscopy offers another way to study the origin of the  $\text{H}_2$  emission. By resolving the  $\text{H}_2$  line profiles, detailed information can be obtained about the kinematics of the  $\text{H}_2$  emitting gas, particularly if simultaneously a high spatial resolution can be achieved (e.g., through long slit spectroscopy or Fabry-Perot imaging). Depending on the spatial resolution and sampling, line profiles can be analyzed for a shock-front as an entity (e.g., a bow shock) or dependent on the location within a shock front or in the form of position-velocity diagrams (see, e.g., Carr 1993; Davis & Smith 1996; Davis et al. 1996). This information can then be compared to theoretical predictions of line profiles, e.g., from bow shock modelling or from simulations of entire outflows (e.g., Suttner et al. 1997; Völker et al. 1999).

Bow-shock models or simulations of entire flows can also be used to synthesize  $\text{H}_2$  emission maps (e.g., Smith 1991; Suttner et al. 1997b; Völker et al. 1999) and predict proper motions for  $\text{H}_2$  features. Comparison with images at sufficient angular resolution then allows one to constrain the gas properties and the conditions in the shock front.

Although there is a well equipped tool box available, examination of various  $\text{H}_2$  flows does not yield a typical or unique type of shock. Instead, each object seems to call for an individual explanation (e.g. Eisloffel et al. 2000b). In some cases, C-shock or C-type bow shock models provide a good fit to the data (e.g., L1448: Davis & Smith 1996; HH 99 & HH 313: Davis et al. 1999). In other cases, J-type shocks seem the better choice (e.g., HH 90/91: Smith 1994a), sometimes requiring the presence of magnetic precursors (e.g., HH 7: Hartigan et al. 1989; Carr 1993). The common feature of all the studies cited in this section is that *virtually all observations of  $\text{H}_2$  emission associated with flows from young stars can be explained as arising from collisionally excited  $\text{H}_2$  molecules in gas heated by the passage of shock fronts; no other excitation mechanism is required.*

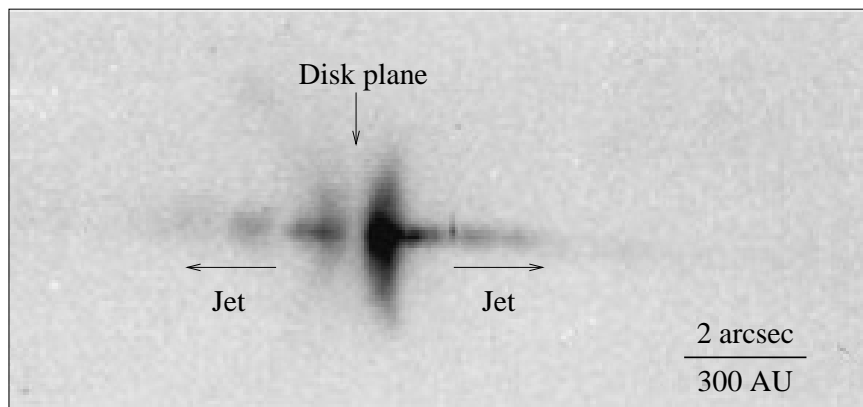


Figure 8: HST  $H\alpha$  image of the HH 30 jet-disk system (taken from Ray et al. 1996; see also Burrows et al. 1996). The jet is seen to be perpendicular to the circumstellar disk, which is indicated by the vertical dark lane bisecting the biconical reflection nebula indicative of a flared disk illuminated from the inside by the central, obscured star.

## 2.4 The jet-disk connection

Before moving on to an introduction to the theoretical concepts which have been invoked in order to explain the various phenomena related to protostellar outflow activity, there is another crucial observation: the strong link between the presence of disks and accretion on the one side, and the presence of outflows on the other side, commonly referred to as the “jet–disk” or the “accretion–outflow” connection (see Königl & Pudritz 2000 for a recent review). A multitude of observations have contributed in establishing this paradigm. First of all, it is interesting to note that the first observational evidence of disklike structures around young stars was based on observations of apparently partially obscured winds (e.g., Appenzeller et al. 1984).

It has been noted that jets and outflows as well as circumstellar material, in the form of disks and envelopes, are commonly found in protostellar objects. The youngest objects, having the largest reservoir of circumstellar material, are associated with the most powerful molecular CO outflows (e.g., Cabrit & André 1991; Bontemps et al. 1996a); similarly, the driving sources of Herbig-Haro objects are known to be associated with particularly large circumstellar dust masses (Reipurth et al. 1993a). Furthermore, the outflow mechanical luminosity is known to be correlated with the driving source bolometric luminosity (which is dominated by the accretion luminosity at these early stages) since a long time (Bally & Lada 1983; Lada 1985; Richer et al. 2000).

In addition to the pure coexistence of disks, accretion activity, and outflows, even tighter relations are known. Strom et al. (1988a; see also Strom et al. 1988b) present a comprehensive compilation of observations indicative of the coexistence and strong correlation between accretion activity and outflow activity for a variety of young stellar objects. Particularly well established correlations between accretion indicators (such as infrared excess emission, UV excess emission, and continuum veiling) and outflow indicators (such as the strength of specific emission lines as, e.g., the [O I]  $\lambda 6300$  line) are known for T Tauri stars (e.g., Cohen et al. 1989; Cabrit et al. 1990) and suggest a proportionality between mass accretion rate and mass outflow rate. Hartigan et al. (1995) provide evidence for a tight relation between mass accretion and outflow in T Tauri stars, with a mass ejection rate of about 1 % of the mass accretion rate; Corcoran & Ray (1998) find a similar behaviour for the more massive Herbig Ae/Be stars. Similarly, the mass ejection rate in FUOr systems is known to be of the order of 10 % of the mass accretion rate (e.g., Hartmann et al. 1993; Hartmann & Kenyon 1996).

Besides these relations between the strengths of accretion and outflow activity, there is another, geometrical relation: jet and outflow axes are generally found to be perpendicular to the disk planes. Polarization measurements towards molecular outflow sources indicated the presence of flattened cir-

cumstellar dust structures oriented perpendicular to the outflows (e.g., Hodapp 1984; Sato et al. 1985). High resolution, interferometric imaging at millimetre wavelengths offers another possibility to probe the geometry of outflow-disk systems. Again, elongated, flattened distributions of circumstellar material are frequently seen to be oriented perpendicular to the outflow axes (e.g., Guilloteau et al. 1997; Gueth & Guilloteau 1999; Wiseman et al. 2000). Maybe the most impressive illustration of the jet-disk connection has been delivered by the HST images of the HH 30 system as shown in Fig. 8 (taken from Ray et al. 1996; see also Burrows et al. 1996; Stapelfeldt et al. 1997). The disk in this case is seen as a biconical reflection nebula bisected by a dark lane. The reflection nebula is caused by the illumination of the surfaces of a flaring disk by the central star. The dark lane is caused by the obscuration by the midplane of the edge-on disk, through which the central star itself is obscured. The jet is seen to be perpendicular to the disk plane.

Taken together, these observations strongly suggest that jets and outflows are powered by accretion, and that accretion disks play a major role in accelerating and collimating the outflows into jets. Magnetically driven and collimated disk winds therefore provide the most natural explanation of the jet and outflow phenomenon in young stellar objects (see below).

## 2.5 Models of outflow activity

A number of observed phenomena related to protostellar outflow activity have to be explained by theory. In the following, I will give an overview of theoretical proposals to explain the various phenomena in flows from young stars. It has to be noted in advance that there is still much discussion going on, and for many problems strongly differing possible explanations exist. The literature on these issues is extensive, thus I will only try to sketch some of the basic ideas, with some emphasis on currently apparently more popular models (for reviews see, e.g., Königl & Ruden 1993; Camenzind 1997; Cabrit et al. 1997; Königl & Pudritz 2000).

### Jet acceleration & collimation

Jets are highly collimated gas beams, seen as optical and infrared jets in emission lines apparently arising from shocks, as radio continuum jets at the base of the optical jets, and sometimes also as well-collimated beams of molecular (CO) gas. This calls for an explanation of the origin of the jet gas, and the acceleration and collimation mechanism.

For the origin of the material forming the jet, three possibilities exist: winds from the stellar surface (e.g., Hartmann & MacGregor 1982; Kwan & Tademaru 1988; Camenzind 1997), winds from the interaction zone between the star and its accretion disk (e.g., the X-wind: e.g., Shu & Shang 1997; see below), and disk winds (e.g., Blandford & Payne 1982; Pudritz & Norman 1983; 1986; Pudritz & Ouyed 1997; Fendt & Elstner 1999). Certainly, more than one of these possibilities may be present in a given protostar/outflow system.

As already noted in section 1.3, the high velocity, highly collimated gas streams – jets – raise two major problems, namely how the jet material is accelerated, and how it is collimated. Radiation pressure from the central protostar was regarded as insufficient to drive the protostellar outflows early on (e.g., Kwan & Scoville 1976; Bally & Lada 1983). In addition to radiation, gravitation and rotation are yielding energy sources in a protostar/disk/core system. Most models invoke magnetohydrodynamic (MHD) processes in order to explain both acceleration and collimation of gas into jet beams. The seminal contribution in this context has been given by Blandford & Payne (1982) in order to explain galactic radio jets. In their model, as is shown in Fig. 9, a poloidal magnetic field is frozen into a rotating accretion disk. It is shown that if the field lines are inclined with respect to the rotation axis

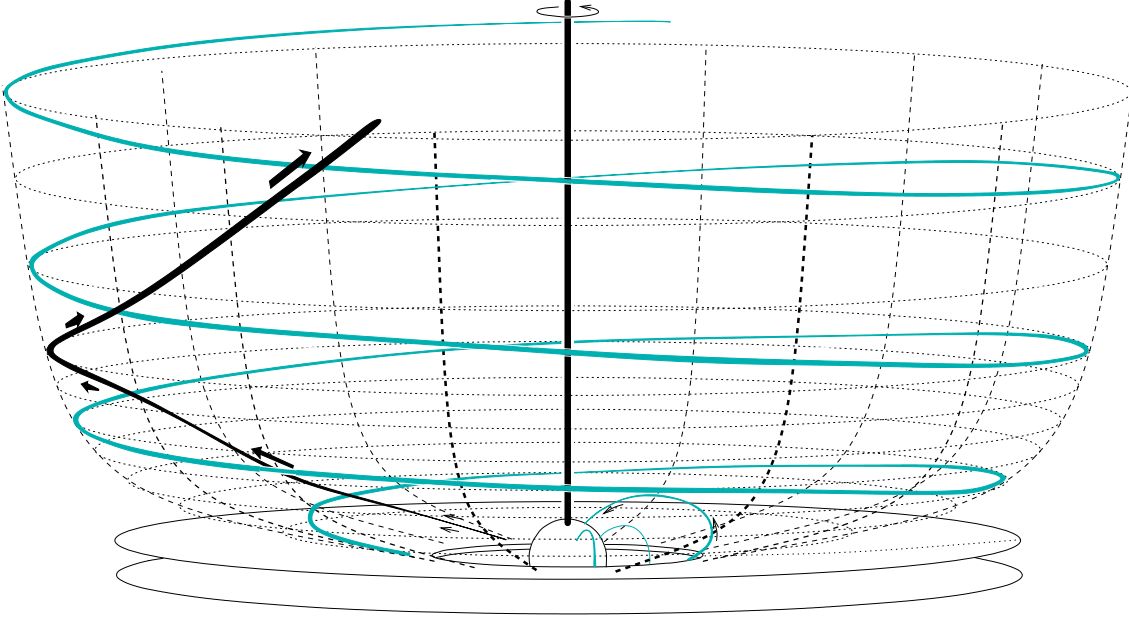


Figure 9: Schematic drawing (not to scale) of the driving and collimation zone of a jet from a young stellar object. Representative magnetic field lines are drawn as grey lines, and a representative trajectory of a jet gas parcel is drawn as a black line. The central star is surrounded by an accretion disk, which is truncated at the corotation radius (the point at which the angular velocity in the disk equals the angular velocity of the star). The magnetic field within the gap between the star and the disk is the largely undisturbed field of the protostar (here assumed to be dipolar). The protostar is coupled to the inner edge of the accretion disk via the magnetic field. Matter is accreted along the field lines connecting the star and the disk in accretion funnels (indicated by the small arrows). Field lines which are anchored in the disk slightly further out first extend out radially away from the central region and are then wound up by the inertia of the material frozen in the magnetic field, as the entire configuration rotates. Material on these field lines is flung out and centrifugally accelerated (the trajectory marks the path of a gas parcel along a field line, as the field line takes part in the overall rotation; the field line drawn in the figure is a snapshot only). Field lines originating from the same radius of the disk form a rotation surface (flux tube, indicated by the dotted lines), along which the (partly ionized) material from above the disk surface can flow. The toroidal field created by winding up of the field lines eventually collimates the flow in a direction parallel to the polar axis of the star/disk system (Blandford & Payne 1982).

by a sufficiently large angle ( $> 30^\circ$ ), it is energetically favorable for material to leave the disk plane and to slide outwards along the field lines. The field lines rotate at a constant angular velocity, and as the gas moves outwards along the field lines, it is accelerated by an increasing centrifugal force (magnetocentrifugal acceleration). At some point, when the rotation velocity is about the same as the Alfvén velocity in the gas, the field lines get increasingly wound up by the inertia of the attached gas and a strong toroidal field component is generated. The toroidal component is the main agent in collimating the flow into a direction along the rotation axis.

The acceleration of the wind along the radial, rigidly rotating field lines also leads to a large acceleration of the gas in the azimuthal direction (until the wind reaches the Alfvén point at the radius  $r_A$ ). This implies the action of a forward torque on the wind, and consequently a backward torque on the disk, whereby angular momentum is removed from the disk. The length of the lever arm torquing down the disk is given by the wind injection radius  $r_0$  and  $r_A$ . Assuming that the entire disk angular momentum at  $r_0$  is extracted from the disk, angular momentum conservation yields a relation between  $\dot{M}_{\text{out}}$  and  $\dot{M}_{\text{acc}}$ :  $\dot{M}_{\text{out}} = (r_0/r_A)^2 \cdot \dot{M}_{\text{acc}}$ . This is an important feature of magnetocentrifugally driven winds from accretion disks: the mass outflow rate  $\dot{M}_{\text{out}}$  is a certain, fixed fraction  $\epsilon = (r_0/r_A)^2$  of the mass accretion rate  $\dot{M}_{\text{acc}}$ :

$$\dot{M}_{\text{out}} = \epsilon \cdot \dot{M}_{\text{acc}}$$

The value of  $\epsilon$  is usually taken to be of the order of 0.1 (corresponding to  $r_A$  a few times  $r_0$ ; e.g., Ouyed & Pudritz 1997a:  $\epsilon \sim 1/6$ ; Shu & Shang 1997:  $\epsilon = 0.25 \dots 0.33$  for the X-wind; Hartmann et al. 1993:  $\epsilon \sim 0.1$  for FUOr's; Hartigan et al. 1995:  $\epsilon \sim 0.01$  for classical T Tauri stars). The terminal wind velocity is of the order of the azimuthal velocity  $\Omega_0 \cdot r_A$  of the wind as it reaches the Alfvén radius  $r_A$ , i.e., of the order of a few times the Keplerian velocity  $\Omega_0 \cdot r_0$  of the disk in the wind injection region (see Königl & Ruden 1993).

During recent years the study of MHD disk winds has become a domain of numerical simulations. It seems that a full, self consistent picture of the MHD processes in and around the protostar, in the interaction region of protostar and disk, in the accretion disk and above the surface of the disk, in the acceleration and collimation region of a jet, and in the jet far from the source is still not at hand. However, numerical simulations show that jet formation by magnetocentrifugal acceleration and self-collimation corresponding to the Blandford & Payne model seems to be a natural consequence of the presence of rotating magnetic fields in an accretion disk plus star system (e.g., Ouyed & Pudritz 1997a, 1997b; Kudoh et al. 1998; Fendt & Elstner 1999; Vlahakis et al. 2000; see reviews by Camenzind 1997; Pudritz & Ouyed 1997; Königl & Pudritz 2000, and references therein). Other authors point out a possible importance of magnetic pressure gradients as accelerating agents (e.g., Draine 1983; Uchida & Shibata 1985; Stone & Norman 1994b; Kudoh & Shibata 1997). Finally, it should be noted that there are also models which explain the collimation of jets as a purely hydrodynamic phenomenon (e.g., Königl 1982; Smith et al. 1983; Smith 1986; Cantó et al. 1988; Raga & Cantó 1989; see Frank & Mellema 1997 and references therein).

One of the astonishing properties of astrophysical jets is that they remain collimated over quite large distances. Again, MHD processes seem to be most likely responsible for this behaviour: the same pinch mechanism, which forced the gas into a beam directed along the polar axis of the driving source, is also collimating the jet further out. The idea of magnetic collimation of jets in the asymptotic regime (i.e., far from the driving sources) has been proposed first for galactic radio jets (e.g., Chan & Henriksen 1980). Heyvaerts & Norman (1989; see also Heyvaerts & Norman 1997) showed that any axisymmetric (nonrelativistic) magnetized wind will approach a cylindrically collimated structure, if the electric current carried by the flow is non-zero (the collimation mechanism is straightforward to understand for a current carrying flow: the current creates a magnetic field wrapping around the current via Ampère's law ( $\nabla \times \mathbf{B} \propto \mathbf{j}$ ); the action of this (toroidal) field then pinches the current back to the flow axis via the Lorentz force ( $\mathbf{F} \propto \mathbf{j} \times \mathbf{B}$ )). In case of a vanishing current, the flow would still be paraboloidally collimated. The importance of (particularly, but not only, toroidal) magnetic fields for jet collimation is also seen in many MHD jet simulations (e.g., Clarke et al. 1986; Ouyed & Pudritz 1997a; O'Sullivan & Ray 2000).

### Jet structure

One observed characteristic of the optical and infrared jets is that in most cases a series of (sometimes roughly equally spaced) emission knots is seen (e.g., Mundt et al. 1987) rather than a continuous beam. Proper motion studies have shown that the knots move at velocities comparable to the inferred velocity of the jet gas (e.g., Eislöffel & Mundt 1992). This rules out the models which interpreted the knots as steady features, like reconfinement shocks as a consequence of the density structure in the ambient medium (e.g., Falle et al. 1987; Cantó et al. 1989). Other models explain the knots as series of shocks due to Kelvin-Helmholtz instabilities in the shear layer between the jet and the ambient medium (e.g., Norman et al. 1982; Bührke et al. 1988; Blondin et al. 1990; Micono et al. 1998b and companion papers), or as being due to comoving, refocussing magnetic pinch modes (e.g., Camenzind 1997).

Besides these models, which rely on a steadily injected jet, there is another group of models

which explain the knots as internal working surfaces in a jet with a variable jet source (an idea which was also proposed first in the context of galactic radio jets: Rees 1978). Working surfaces occur where faster moving material catches up to slower moving material (e.g., Raga et al. 1990; Hartigan & Raymond 1993; Stone & Norman 1993; de Gouveia dal Pino & Benz 1994; Suttner et al. 1997; Smith et al. 1997a; Völker et al. 1999; Cantó et al. 2000). This approach seems to be rather promising since it can explain a wide variety of observations (kinematical as well as morphological) in a rather straightforward way by simply changing the time behaviour of the driving source (mainly injection velocity; other possibilities exist and lead to a large variety in knot shapes and properties: Völker et al. 1999).

As noted above, outflow is tightly connected to accretion. The driving sources of jets (T Tauri stars and presumably their more embedded predecessors) are known to exhibit photometric as well as spectrometric variability (e.g., Appenzeller & Mundt 1989), which strongly points to variable accretion and wind activity. In fact, variability is one of the classification criteria for T Tauri stars (Joy 1945). More dramatic evidence for variable accretion is given by the FU Orionis outbursts (e.g., Hartmann et al. 1993). It is reasonable to assume that the nonsteady accretion also implies nonsteady ejection. Furthermore, numerical simulations of magnetic accretion disks also tend to produce unsteady disks and magnetospheres, and consequently unsteady magnetically driven winds (e.g., Uchida & Shibata 1985; Stone & Norman 1994b; Goodson et al. 1997; Kudoh et al. 1998; see also Fendt & Elstner 1999). Ouyed & Pudritz (1997b, 1999) found intrinsically episodic MHD jets even from steady disks.

The smaller, barely resolved knots can then be easily attributed to smaller variations, whereas the larger, well developed internal bow shock working surfaces correspond to major outbursts, like possibly FU Ori events. Zinnecker et al. (1998) suggest a self-similar, chaotic behaviour of these outbursts to explain the features of the HH 212 jet, with major outbursts occurring at longer periods, smaller outbursts at somewhat smaller periods, even smaller outbursts at even smaller periods, and so on. The high symmetry observed in HH 212 also supports the model of internal working surfaces being due to variations at the source: the symmetry would be hard to understand in terms of instabilities along the jet beam.

Recent high angular resolution observations of a number of jets with the HST (e.g., Ray et al. 1996; see Reipurth & Heathcote 1997 for a summary) resolved many of the knots into small (partial) bow shock like structures. This also seems to be in support of the internal working surface models caused by variations in ejection at the source.

## **Molecular outflows**

Models explaining the presence of the massive CO outflows can roughly be subdivided in two classes. On the one hand there are models trying to explain the CO outflows as a standalone phenomenon. On the other hand, the currently more popular models explain molecular outflows as a consequence of the presence of the collimated jets. A recent review of molecular outflow models has been given by Cabrit et al. (1997).

The first group comprises the so-called wind driven shell models. There, an initially spherical or wide-angle wind expands into a density stratified medium (as is, e.g., found for circumstellar disks or toroidal cores) and sweeps up a shell-like CO outflow. The flow can easily expand into the polar low density regions, whereas expansion is inhibited in the equatorial plane, naturally leading to a collimation (e.g., Snell et al. 1980; Shu et al. 1991; but see Masson & Chernin 1992). The assumption of adiabatic winds may also lead to the formation of de Laval like nozzles (e.g., Königl 1982). Draine (1983) replaced the cavity creating wind by magnetic pressure, which builds up when a rotating protostar winds up frozen-in field lines. Thus an expanding magnetic bubble is created, which then sweeps up ambient material.



Magnetohydrodynamic mechanisms similar to the Blandford & Payne model have also been invoked to accelerate a stellar wind (e.g., Hartmann & MacGregor 1982) to a molecular outflow. Pudritz & Norman (1983, 1986) propose models in which massive ( $\sim 100 M_{\odot}$ ) molecular disks drive massive outflows from the outer disk regions through centrifugal acceleration. The high disk masses required in both models (and the presence of a young early type star at the disk centre in the first model) make them poorly suited to explain particularly the outflows from low mass protostars discussed here. An interesting feature of the second model is that the outflow has a core-envelope structure. The envelope is formed by molecular material from the outer, cool parts of the disk and moving rather slowly (50 km/s). The core consists of ionized material, launched from the innermost, hot part of the disk at high velocity (250 km/s), providing a possible explanation for the optical Herbig-Haro objects and jets.

The discovery of coexisting collimated (optical or infrared) jets and molecular CO outflows (e.g., Mundt & Fried 1983 (L1551 and others); HH 1/2: Correia et al. 1997; Moro-Martín et al. 1999; HH 34: Chernin & Masson 1995; HH 46/47: Olberg et al. 1991; HH 111: Reipurth & Olberg 1991; HH 211: Gueth & Guilloteau 1999; HH 212: Sargent & McCaughrean, in prep.) strongly suggests a connection between these phenomena. Earlier observations of jets suggested too low a momentum supply rate by jets to explain the massive, energetic molecular outflows (e.g., Mundt et al. 1987). The interpretation of these observations however relied on a more or less complete ionization of the jet material, an assumption which is probably not valid: Hartigan et al. (1994) found ionization fractions of only a few percent in the HH 34, HH 47, and HH 111 jets (see also Bacciotti 1997; Bacciotti & Eisloffel 1999). Thus the jets might indeed provide enough momentum to drive molecular outflows.

There may be two distinct ways through which a jet could accelerate quiescent ambient material to velocities as observed in CO outflows: steady entrainment in a (turbulent) shear layer along the jet beam, and prompt entrainment at the head of the jet (bow-shock entrainment).

In the case of “steady entrainment” a jet accelerates the material in a tube along the jet beam eventually to a velocity close to that of the jet gas. This tube then accelerates the next outer tube to some lower velocity, and so on (e.g., Stahler 1994). The friction necessary to accelerate the next outer layer is provided by turbulence, e.g., caused by Kelvin-Helmholtz instabilities. As the jet loses momentum to the surrounding gas, it is also decelerated “tube by tube”, until finally the jet beam is also entirely turbulent. Raga et al. (1993) invoke bow shock like internal working surfaces, which eject jet material sideways out of the beam, thus creating a turbulent shear layer, which then accelerates the material along the jet beam. However, jets with high Mach number such as protostellar jets tend to produce a low density, atomic or ionized cavity or cocoon around the jet beam (e.g., Stone & Norman 1993; Chernin et al. 1994; Suttner et al. 1997; Völker et al. 1999), thus steady entrainment of molecular material along the jet beam is not efficient.

Currently more popular models invoke prompt or bow shock entrainment. Observational support for this idea comes from regularly observed shock emission closely correlated to local maxima in high velocity CO maps (see above). Raga & Cabrit (1993) proposed a simple analytic model for a bow shock entraining ambient molecular material and sweeping up a cavity. The model yields many of the observed features of CO outflows and has very successfully been used to explain high resolution molecular outflow maps (e.g., Gueth & Guilloteau 1999; Bachiller et al. 1995; Gueth et al. 1996). Further models, mostly numerical simulations, also tend to support bow shock entrainment scenarios (e.g., Masson & Chernin 1993; Chernin et al. 1994; Smith et al. 1997b; Downes & Ray 1999).

### The X-wind

Including many aspects in one is the X-wind model for protostellar outflows, promoted mainly by Shu and coworkers (Shu et al. 1994 and companion papers; see Shu et al. 1988 for an earlier version, and

Shu & Shang 1997 and Shu et al. 2000 for recent reviews).

In this picture (some features of which are included in Fig. 9), the central star is surrounded by a conducting disk with an inner hole (with a radius  $R_X$  determined by the magnetic field at the inner disk edge and the mass accretion rate through the outer disk). Shielding currents prevent the threading of the disk by field lines, thus an initially dipolar stellar magnetic field (connecting the polar regions by field lines crossing the equatorial plane at a large distance from the star) has to squeeze through the disk's inner hole and is strongly compressed in the equatorial plane. In case of a nonideal disk, with some magnetic diffusivity and in the presence of accretion, the field will penetrate the innermost ring of the disk. This field threaded ring is termed the X-region. Since the disk material close to the star will be well ionized and coupled to any magnetic field, the (entire) ring of the disk threaded by the field (in steady state) has to corotate with the star in order to prevent a winding up of the field lines (i.e., the star has to adjust to the angular velocity of the inner disk edge:  $\Omega_* = \Omega_X = \sqrt{GM_*/R_X^3}$ ). The radial extent of the part of the disk which is threaded by the magnetic field is of the order of the thickness of the disk.

Material in the innermost part of the X-region rotates at sub-Keplerian velocities and is thus ready to move further in. The magnetic field (which is similar to the undisturbed dipole very close to the star) channels this material in an accretion funnel flow towards some region close to the stellar pole. As the gas moves in, it would like to spin up due to angular momentum conservation. It is, however, attached to the rigidly rotating field lines and thus exerts a forward torque on the star and, more important, on the disk. The angular momentum of the accreting gas is thus stored in the X-region of the disk, which would thus be spun up. At the same time, the field lines threading the outer part of the X-region are inclined to the disk plane by only a very small angle (they have been squeezed through the disk in the equatorial plane from large distances). This part of the disk, rotating at super-Keplerian velocity, can thus launch a magnetocentrifugally driven disk wind: the X-wind. It is powerful enough to open the initially closed stellar field lines (which trace the weak field of the outermost parts of the stellar dipole), allowing the wind to expand. The X-wind efficiently removes angular momentum from the X-region which has been deposited there by the accretion flow.

The density as well as the velocity of the X-wind increase strongly but smoothly towards the polar axis: the X-wind has a core-envelope structure. The degree of concentration towards the polar axis (i.e., the collimation of the flow) increases logarithmically slow with distance from the star. In the X-wind picture, the well collimated jets seen as Herbig-Haro or infrared jets are only the densest axial parts of a more extensive structure. The lower density, slower envelope might explain often observed wide-angle winds (e.g. Kwan & Tademaru 1988) and is supposed to be responsible for the widening of molecular outflow lobes (which are driven by the entire wind/jet). The X-wind driven molecular outflow may thus be regarded as a hybrid of a jet driven outflow and a cavity swept out by a wide angle wind.

It is not yet clear whether the X-wind model really describes the processes at work in a protostellar outflow driving source. Its strength is that it is able to account for many observations in one, fairly self-consistent model (optical observations of time variable accretion/wind phenomena in T Tauri stars, the slow rotation rates of T Tauri stars, a number of the features of jets and molecular outflows, protostellar X-ray activity).

## 2.6 Star formation in Orion

One of the most active nearby sites of recent, ongoing, and future star formation is located in the direction towards the Orion constellation. It consists of several components, spanning an age range of  $\sim 12 \cdot 10^6$  years for the oldest group of the Orion OB1 association (e.g., Brown et al. 1994), to  $\sim 1 \cdot 10^6$  years for the presumably youngest Orion OB1 subgroup, the Trapezium cluster in the Orion

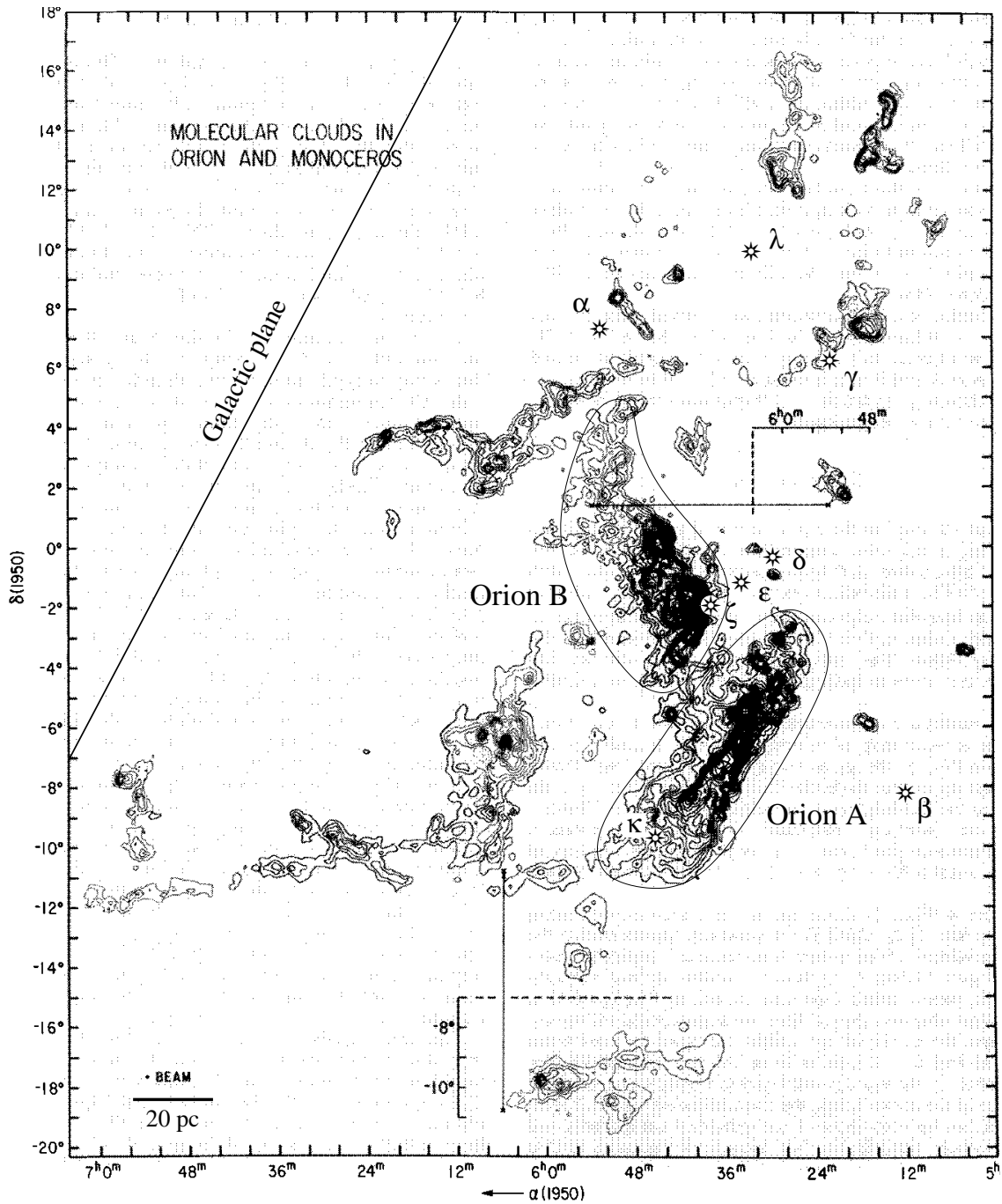


Figure 10: Large scale distribution of molecular gas in Orion and Monoceros (adopted from Maddalena et al. 1986). For orientation, the main stars of the Orion constellation are also shown. The Orion B giant molecular cloud extends in a north-south direction to the east of  $\zeta$  Ori. Orion A extends from the area just south of the belt stars down to  $\kappa$  Ori.

Nebula H II region (Brown et al. 1994; Hillenbrand 1997), and even younger protostellar objects. Among them is the most nearby high-mass protostellar object Irc2-I, located in the BN-KL area in the OMC-1 molecular core behind the Orion Nebula (e.g., Genzel & Stutzki 1989; Menten & Reid 1995). Distance estimates towards the Orion star forming regions typically range from 400 to 500 pc (e.g., Genzel & Stutzki 1989; Brown et al. 1994). In the following I will use a canonical distance of 450 pc.

The proximity of the Orion complex as well as the high mass protostar(s) in the BN-KL region make Orion one of the prime target areas for observational work on star formation. Also very helpful is the fact that it is located in a direction towards the outer region of the galaxy and below the galactic plane. No other star forming regions are known on the line of sight towards Orion, neither in the foreground nor in the background. Confusion with other star forming regions is thus largely excluded. In the following I will try to give a rough overview of the area under study in this thesis, focusing on low to intermediate mass star formation, and leaving aside the certainly extremely interesting BN-KL area, the Orion Nebula and the Trapezium cluster. A comprehensive up to date view on various aspects of star formation research in Orion will be published in the proceedings of the Ringberg conference “The Orion complex revisited” (McCaughrean 2000).

The current generation of star formation takes place in a large complex of molecular clouds. The full extent of the molecular gas has been revealed in extensive  $^{12}\text{CO}$  maps (Kutner et al. 1977; Madalena et al. 1986, see Figure 10). The most prominent clouds in the area are the Orion A and Orion B giant molecular clouds, both with a mass of about  $10^5 M_{\odot}$ . Since then, a large body of observations has been accumulated on the molecular gas in Orion. Observations in the optically thin  $^{13}\text{CO}$  line at higher spatial resolution revealed the clumpy and filamentary nature of the moderate density ( $\sim 10^3 \text{cm}^{-3}$ ) gas (Bally et al. 1987; Nagahama et al. 1998). These filaments have typical lengths of several parsec, widths of order 1 to 2 parsec, masses of several hundred  $M_{\odot}$ , and velocity dispersions of a few (1-3) km/s. Perhaps the most eye-catching feature in these maps is a bright, narrow, winding filament in the northernmost part of the cloud. It is commonly termed the “integral shaped filament” (marked in Fig. 11) and extends over  $\sim 1^{\circ}$  ( $\sim 8$  pc) roughly north-south behind the Orion Nebula H II region.

A major survey for dense ( $10^5 \text{cm}^{-3}$ ) molecular gas has been carried out by Tatematsu et al. (1993 (T93), 1998; see also Wilson et al. 1999), covering  $\sim 1$  square degree in the CS  $J=1-0$  line. The data collected by T93 are shown in Fig. 11 to the upper left. From these data, 125 dense cloud cores were identified. This survey was used to define the area for the present  $\text{H}_2$  survey: the final outcome of this survey, a large  $2.12 \mu\text{m}$  narrow band mosaic, is shown in direct comparison to the CS data in Fig. 11 to the lower right.

The northern half of the integral shaped filament is one of the most active nearby sites of star formation. For one thing, it harbours the BN-KL area with its luminous IR sources and the OMC-1 outflow.  $2'$  to the south, another energetic, well-collimated molecular outflow (OMC-1S, Schmid-Burgk et al. 1990; see also Ziurys & Friberg 1987; Ziurys et al. 1990) is found emanating from a luminous ( $8 \cdot 10^3 L_{\odot}$ ) FIR/mm-source. North of the OMC-1/BN-KL area, the dense molecular clouds OMC-2 and OMC-3 (Gatley et al. 1974; Kutner et al. 1976; Batrla et al. 1983; Cesaroni & Wilson 1994; Castets & Langer 1995; Aso et al. 2000) form the northern part of the integral shaped filament. Various signs of active star formation are found in OMC-2/3. Millimetre and submillimetre continuum observations revealed a chain of compact dust condensations (Mezger et al. 1990; Chini et al. 1997b; Lis et al. 1998; Johnstone & Bally 1999), some of them associated with centimetre continuum emission (Reipurth et al. 1999). Most of them presumably represent low- to intermediate mass young stellar objects. OMC-3 and its embedded sources seem to be in an earlier evolutionary stage than OMC-2 and its embedded sources (Castets & Langer 1995; Chini et al. 1997b). At near-infrared wavelengths, a small cluster of red, nebulous sources is found at the center of the OMC-2 core (e.g., Gatley et al. 1974; Pendleton et al. 1986; Rayner et al. 1989; Johnson et al. 1990; Jones et al. 1994). Further north, the bipolar reflection nebula Haro 5a/6a is found (e.g., Wolstencroft et al. 1986). Various signs for outflow activity have been found in OMC-2/3. First evidence for outflow activity was found in infrared  $\text{H}_2$  observations of OMC-2 by Fischer et al. (1980a), a corresponding CO outflow was found by Fischer et al. (1985). Indications for additional molecular outflows further north in the OMC-2/3 region are reported by Castets & Langer (1995), Chini et al. (1997b), Aso et al. (2000), and Yu (2000). A number of Herbig-Haro objects are

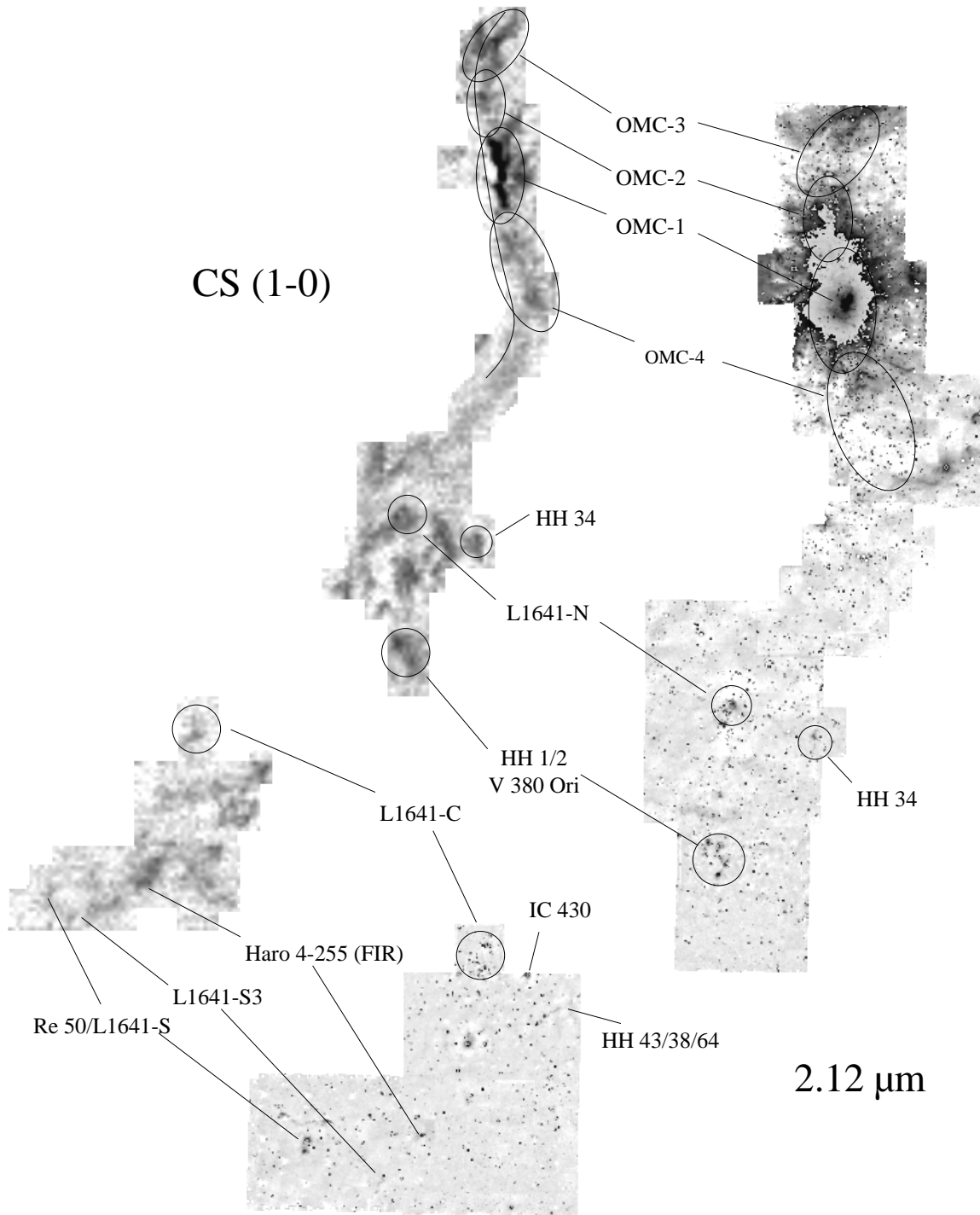


Figure 11: Locations of various star formation sites in Orion A. Both maps show approximately the same area. The left-hand map is the CS(1–0) map taken by Tatematsu et al. (1993), and shows the distribution of dense molecular gas. The right-hand map is a heavily scaled down version of the 2.12 μm mosaic taken for this thesis. At this angular resolution, only very few features are visible. The area around the Orion Nebula has been scaled down in intensity, in order to show at least some structure in this area. The region shown in the maps extends over about 2.5° north-south.

known in the OMC-2/3 area (e.g., Schwartz 1977b; Reipurth 1985a; Reipurth et al. 1997). The most convincing evidence so far for a multitude of active flows in this area has been delivered by the H<sub>2</sub> imaging survey by Yu et al. (1997), who found evidence for about a dozen collimated flows in OMC-2/3.

The area south of the Orion Nebula is much less active. The 450/850  $\mu$ m maps by Johnstone & Bally (1999) only revealed two knotty filaments of relatively faint submillimetre condensations forming a V-shaped structure which they termed OMC-4. These structures presumably are not yet protostellar objects.

Further south one reaches the area of the L1641 (Lynds 1962) dark cloud. This dark cloud has been the subject of many studies, and contains some prototypical examples for the phenomena associated with star formation. Strom et al. (1989b) and Chen et al. (1993a) compiled lists of infrared sources from the IRAS co-added data, which were the base for many subsequent studies (e.g., Strom et al. 1989a; Morgan & Bally 1991; Chen et al. 1993b; Chen & Tokunaga 1994). Wide field near infrared surveys of parts of L1641 have been carried out by Strom et al. (1993) and Allen (1996), and by Ali & Depoy (1993) in the northern portion of the Orion A cloud. The study of the embedded stellar population in Orion A, particularly the L1641 dark cloud, revealed the presence of a substantial population of stars formed or forming in the “isolated” mode rather than in the “clustered” mode (Allen 1996). This is in contrast to the results for the Orion B/L1630 cloud, where virtually all stars seem to form in the clustered mode (Li et al. 1996; see also the reviews by Lada et al. 1993; Zinnecker et al. 1993).

In the northern part of the L1641 dark cloud, Fukui and coworkers (Fukui et al. 1986, 1988; Fukui 1989; see also Wilking et al. 1990b) found a bipolar outflow (termed the L1641-N outflow) associated with the rather luminous IRAS 05338–0624 source in the course of their unbiased search for outflows in several clouds. Near infrared imaging revealed the presence of a small, dense cluster of embedded sources associated with this IRAS source (Strom et al. 1989a; Chen et al. 1993b; Hodapp & Deane 1993). The L1641-N molecular outflow is also seen in infrared H<sub>2</sub> emission (Davis & Eislöffel 1995). It is only the innermost part of the much larger L1641-N giant outflow, which is traced by a 6 pc long chain of Herbig-Haro objects in its northern lobe (Reipurth et al. 1998; Mader et al. 1999), and by a 4 pc long chain of infrared H<sub>2</sub> features in its southern lobe (Stanke et al. 1998, 2000). It is one of the longest protostellar outflows known. A number of other Herbig-Haro jets apparently have their origin in or near the L1641-N cluster (Reipurth et al. 1998; Mader et al. 1999).

12' to the west and 5' south of L1641-N there is a small group of partly nebulous infrared sources (e.g., Strom et al. 1993; Chen & Tokunaga 1994). Among them is the driving source of the highly collimated HH 34 jet and bowshock (Reipurth et al. 1986; Mundt et al. 1987; Bührke et al. 1988). More recent observations showed that this jet system is in fact much larger: it is the prototypical giant Herbig-Haro jet (Bally & Devine 1994; Devine et al. 1997; Eislöffel & Mundt 1997).

About 23' due south of the L1641-N cluster, one encounters the prototypical Herbig-Haro objects HH 1, HH 2, and HH 3 (Herbig 1950, 1951, 1952; Haro 1952, 1953). This area is home to a number of other phenomena indicating active star formation. A few more emission line stars, among them the Herbig Ae/Be star V 380 Ori, are found, and some more, fainter Herbig-Haro objects (e.g., Corcoran & Ray 1995). HH 1 and HH 2 are part of a bipolar flow system driven by a VLA source (HH 1/2 VLA1, Pravdo et al. 1985) located between them. HH 1/2 VLA1 drives a faint, well collimated Herbig-Haro jet (Bohigas et al. 1985; Strom et al. 1985; Mundt et al. 1987; Davis et al. 1994; Eislöffel et al. 1994b; Noriega-Crespo & Garnavich 1994; Hester et al. 1998; Reipurth et al. 2000a) and a radio jet (Rodríguez et al. 1990, 2000). Repeated attempts finally revealed the presence of a weak molecular CO flow driven by the HH 1/2 jet system (Moro-Martín et al. 1999). The HH 1/2 system seems also to be a giant outflow (Ogura 1995). A second, nearby VLA source, HH 1/2 VLA2, may be a binary companion

to HH 1/2 VLA1 and also drives a faint Herbig-Haro jet (Reipurth et al. 1993b), with the axes of this jet and the HH 1/2 jet making a large angle to one another. Finally, a number of millimetre continuum sources, a H<sub>2</sub>O maser, and high velocity CO lobes complete the zoo of observations of star formation activity in this area (e.g., Edwards & Snell 1984; Levreault 1988a; Chernin & Masson 1995; Chini et al. 1997a).

Finally, the southernmost part of the survey area harbours a small aggregate of embedded stars (the L1641-C cluster, see Strom et al. 1993). The area is dominated by a few, partly fairly luminous IRAS sources: the FUOr IC 430 = IRAS 05358–0704 (Strom & Strom 1993); IRAS 05357–0710 and IRAS 05355–0709C (Cohen 1990; see also Stanke et al. 2000) in the HH 43/38 region; Haro 4-255 FIR = IRAS 05369–0728 driving a molecular outflow (Levreault 1988a; Morgan et al. 1991; Davis & Eisloffel 1995; an optical jet is seen to be driven by the Haro 4-255 T Tauri star itself: Aspin & Reipurth 2000); the Re50 reflection nebulosity and its illuminating source IRAS 05380–0728 (Reipurth & Bally 1986; Strom & Strom 1993) driving the L1641-S/MB 40 molecular outflow (Reipurth & Bally 1986; Fukui et al. 1986; Morgan & Bally 1991; but see Stanke et al. 2000); and finally IRAS 05375–0731, driving the L1641-S3/MB41 molecular outflow (Fukui et al. 1989; Morgan & Bally 1991).

Several searches for signs of outflow activity have been undertaken towards Orion A, and many of the prototypical objects are found here (e.g., the OMC-1 molecular outflow, the Herbig-Haro objects HH 1-3 (see Bally 1982 for an early review), the giant outflow HH 34). Fukui and coworkers (Fukui et al. 1986, 1988; Fukui 1989) performed an unbiased search for molecular outflows in the entire giant molecular cloud. Various other groups have undertaken more biased systematic searches for molecular outflows towards various types of young stellar objects (e.g., Edwards & Snell 1984; Levreault 1988a, 1988b; Morgan & Bally 1991; Morgan et al. 1991, to cite only a few). As already noted, the northern part of the cloud (OMC-2/3) has repeatedly been searched for high velocity gas (e.g., Fischer et al. 1985; Castets & Langer 1995; Chini et al. 1997b), most recently by Yu (2000) and Aso et al. (2000), and a multitude of outflows are now known there. Most impressive is probably the H<sub>2</sub> survey in the OMC-2/3 area by Yu et al. (1997; see also Yu 2000), who found more than a dozen collimated H<sub>2</sub> flows. Systematic searches for Herbig-Haro objects in the survey area have been performed by Schwartz (1977b), Reipurth (1985a, 1989c; Reipurth & Graham 1988) and Ogura & Walsh (1991).

## 3 Observations

In the following section I will describe the various data that were used to search for the outflows and their driving sources in Orion A. The main part of the work is a wide field near-infrared survey for H<sub>2</sub> emission line features forming parts of protostellar outflows. The survey covers a total area of about 1.2 square degrees. To identify H<sub>2</sub> emission line features, images were taken through a narrow band filter centered at a wavelength of 2.12  $\mu\text{m}$ , the wavelength of the  $v = 1-0 S(1)$  line of molecular hydrogen. In order to discriminate H<sub>2</sub> emission features from continuum features, the same area was also imaged through a broad band K' filter. These data were taken during several observing runs with the near-infrared wide field camera Omega Prime on the 3.5 m telescope on Calar Alto. The K'-band survey was also used to search for the driving sources of the outflows (embedded near-infrared sources). Additional data covering a fairly large wavelength range were also used to search for the outflow sources, including data from own observations and publicly available data or data taken from the literature:

- At optical wavelengths, the new Wide Field Imager on the ESO/MPG 2.2 m telescope on La Silla was used to perform a CCD imaging survey in a red continuum filter to identify (together with the K'-band survey) the more evolved, optically visible outflow sources (T Tauri stars).
- The IRAS database was used to search for mid- to far-infrared sources revealing younger objects still obscured at optical or even near-infrared wavelengths, but bright in the far-infrared.
- For a few objects, 10  $\mu\text{m}$  observations with the thermal infrared camera TIMMI at the ESO 3.6 m telescope were also available.
- Area-covering 1.3 mm continuum maps were obtained of the southernmost part of the survey area; for some sources smaller maps were available. Finally, the 450 and 850  $\mu\text{m}$  submillimetre maps taken by Johnstone & Bally (1999, data kindly provided by Doug Johnstone as FITS files), the 350  $\mu\text{m}$  data by Lis et al. (1998), and the 1.3 mm data from Chini et al. (1997b) as available in the literature were used to search for emission from cold dust revealing even the youngest objects, which may be hard to find even in the IRAS data.

Whereas the optical survey and the IRAS data cover the complete area of the near-infrared survey, at (sub)millimetre wavelengths only part of the area has been mapped so far (the OMC-1/2/3/4 area in the north, some patches in the L 1641-N area, and the southernmost part of the survey area). In the following, the individual data sets will be described in more detail.

### 3.1 The near-infrared H<sub>2</sub> S(1) line survey

To search for H<sub>2</sub> emission features indicative of shocked gas in flows from young stellar objects, a near infrared imaging survey was performed. It included exposures through a narrow band filter centred at 2.12  $\mu\text{m}$ , the wavelength of the  $v = 1-0 S(1)$  transition of molecular hydrogen, and exposures through a K' filter to discriminate line emission from continuum emission.



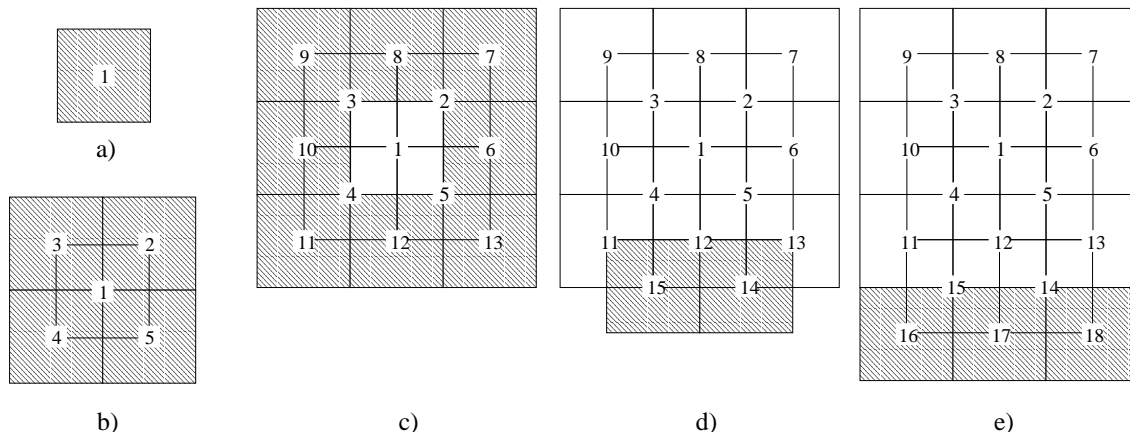


Figure 12: Schematic representation of a typical mosaicing pattern. For each survey field, this pattern was observed once going forward, once going backward, with a small spatial offset between the forward and backward sequence.

The observations were done using the near-infrared wide field camera Omega Prime (<http://www.mpia-hd.mpg.de/IRCAM/OPRIME/>; Bizenberger et al. 1998; McCaughrean et al., in prep.) on the 3.5 m telescope on Calar Alto/Spain. The camera uses a 1024 pixel  $\times$  1024 pixel HgCdTe array as detector, which yields, at a pixel scale of  $0''.4$ , a field of view of about  $6'.7 \times 6'.7$ . The narrow band H<sub>2</sub> filter used was a 1% passband filter centred at a wavelength of  $2.125 \mu\text{m}$ , while the K' continuum filter transmits from  $1.944$  to  $2.292 \mu\text{m}$ . Typical integration times through the narrow band filter were 10 minutes, and 2 minutes through the K' filter. This yielded a surface brightness sensitivity for extended H<sub>2</sub> emission line features of order  $10^{-19} \text{ W}/(\text{m}^2 \text{ arcsec}^2)$  ( $3\sigma$ ) and a limiting magnitude of about  $K' = 17$  ( $5\sigma$  in peak pixel) for continuum point sources. This is of the same order (or even more sensitive) as many targeted H<sub>2</sub> observations of individual sources found in the literature.

To complete the near-infrared survey, a number of observing runs were necessary, mostly due to bad weather. Observations were made on the following dates: December 24–26 1996, September 11–14 1997, January 10–13 1998, October 23–26 1998, and December 5 1998.

### Observing strategy

The extent of the survey area is given by the CS (1–0) map by Tatematsu et al. (1993; see Fig. 11). The original plan was to image all 125 cloud cores one by one. However, with the advent of the wide field camera Omega Prime it became possible (and more efficient) to image the complete area covered by the CS survey, including also the regions between the dense cores, which guarantees a truly unbiased survey. In addition, during the survey it became apparent that wide field images covering the whole area are needed to reveal the full extent of some very long flows. The total survey area was subdivided into 9 partly overlapping fields (Fig. 13), labeled as Field 1 to 9 in the following, with the field number increasing from north to south, and in the case of Fields 8 and 9 from west to east. The typical size of the fields is  $\sim 20' \times 27'$  corresponding to  $\sim 3 \times 4$  times the field of view of Omega Prime, with the only exception of field 5 which covers about  $27' \times 33'$ .

Following McCaughrean (1988), the mosaicing pattern (see Fig. 12) was designed such that, for the central part of the mosaic, each position on the sky was imaged four times on different parts of the detector array in order to allow for a correction of pixel defects. Starting with an exposure at a position at the center of a field (step a in Fig. 12), the next four exposures were taken with the array centered on the corners of the first frame (step b). Then another sequence of 8 exposures was done around this central part (step c), and so on, until the entire field was observed. The same pattern was then done backwards,

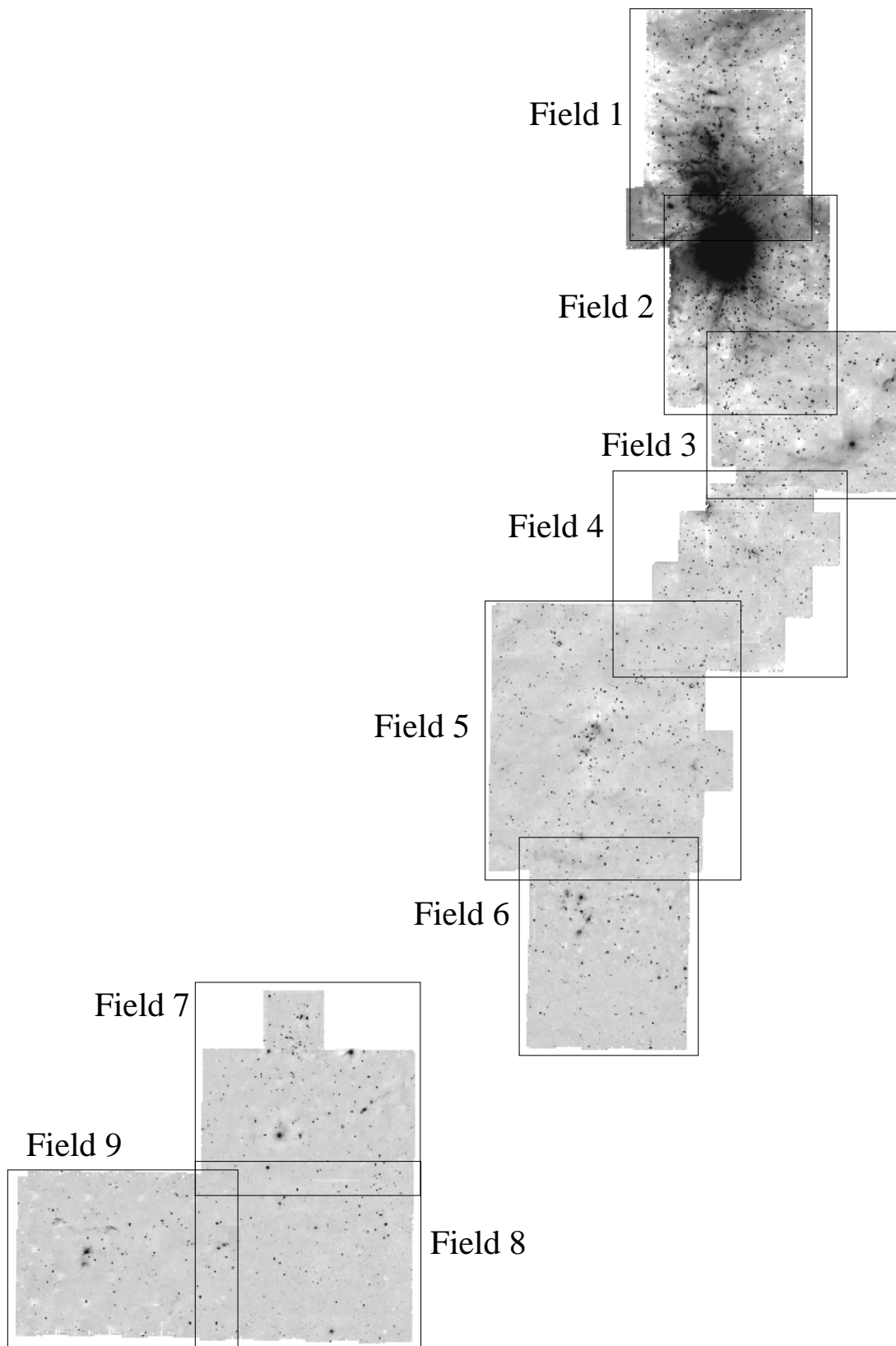


Figure 13: Overview of the entire survey area, showing a strongly compressed version of the  $2.12\ \mu\text{m}$  narrow band mosaic. The bounds of the individual survey fields are indicated by the rectangles.

Date	Observatory	Telescope	Instrument	What has been observed
26.12.1996	Calar Alto	3.5 m	Omega Prime	Field 5: 2.12 $\mu\text{m}$ , K' HH 212: 2.12 $\mu\text{m}$
11.9.1997	Calar Alto	3.5 m	Omega Prime	Field 4: 2.12 $\mu\text{m}$ , K' HH 211: 2.12 $\mu\text{m}$
12.9.1997	Calar Alto	3.5 m	Omega Prime	Field 2: 2.12 $\mu\text{m}$ , K' (50 %)
13.9.1997	Calar Alto	3.5 m	Omega Prime	Field 1: 2.12 $\mu\text{m}$ , K' (70 %)
10.1.1998	Calar Alto	3.5 m	Omega Prime	Field 9: 2.12 $\mu\text{m}$ (50 %), K' Field 3: 2.12 $\mu\text{m}$ , K'
11.1.1998	Calar Alto	3.5 m	Omega Prime	Field 1: K' (np) Field 6: 2.12 $\mu\text{m}$ (np)
23.10.1998	Calar Alto	3.5 m	Omega Prime	Field 6: K' (np) Field 2: K'
24.10.1998	Calar Alto	3.5 m	Omega Prime	Field 8: 2.12 $\mu\text{m}$ (np), K' (50 %, np) Field 7: 2.12 $\mu\text{m}$ (np), K' (np) Field 8: K' (bad)
26.10.1998	Calar Alto	3.5 m	Omega Prime	Field 7: 2.12 $\mu\text{m}$ (50 %, np) Field 9: 2.12 $\mu\text{m}$ (50 %), K' (50 %) Field 8: K' (50 %) single 5: 2.12 $\mu\text{m}$ , K' single 2: 2.12 $\mu\text{m}$ , K' single 1: 2.12 $\mu\text{m}$ , K'
5.12.1998	Calar Alto	3.5 m	Omega Prime	Field 7: 2.12 $\mu\text{m}$ , K'(50 %) Field 6: K' (50 %)
20.1.1999	ESO La Silla	2.2 m	WFI	Entire area: 0.816 $\mu\text{m}$ (I-band)
Feb. 1999	Pico Veleta	30 m	MAMBO	Field 7, 8, 9: 1.3 mm

Table 1: List of observations done in the course of the Orion A jet survey. “np” marks observations taken under apparently nonphotometric conditions.

with a small shift relative to the first coverage. The inner part of such a mosaic has a uniform coverage, with a margin of the width of half the field of view of Omega Prime with only half the integration time.

### Data reduction

**Array defects.** The data reduction followed standard procedures. The first step was to identify (for each observing run) the defects of the Omega Prime detector array. To identify hot pixels, short exposures were taken with a cold blank inserted as filter, thus blocking out the thermal background. A hot-pixel mask was constructed from the pixels with signals exceeding a certain level. Well-illuminated flat field exposures were used to identify cold pixels showing no signal, and a corresponding cold-pixel mask was constructed. Then, a final bad-pixel mask was constructed from the cold- and hot-pixel mask. Bad pixels were flagged and excluded from processing during the following steps of the data reduction. Since the Omega Prime detector shows quite a few dead rows and columns, which are frequently adjacent to each other, it was generally not useful to interpolate over neighbouring pixels, hence the mosaics were done in a way ensuring that each location on the sky was imaged four times on different parts of the detector (twice at the edges of the mosaics), thus allowing me to fill in the bad pixels.

**Flatfield construction.** Next, for each night and each filter, flatfields were constructed, to correct for sensitivity variations of the array. Exposures of the inside of the telescope dome were taken, once illuminated by a tungsten lamp, once without illumination. The difference between two such exposures should reflect the sensitivity of the detector for a 2000-3000 K spectrum, well suited for observations of

cool and/or reddened astronomical objects, as are found in star forming regions. A number of lamp-on and lamp-off exposures were averaged, and the average lamp-off frame subtracted from the average lamp-on frame. The intensity of the resulting difference frame was normalized to 1; bad pixels were set to exactly 1. Later on, the science frames were divided by these normalized flatfields, thus correcting for the spatially varying sensitivity of the array. It should be noted that it was indeed necessary to take new flatfields from run to run, since significant differences were apparent when comparing flatfields taken during different runs.

**Sky subtraction.** The next steps concern the reduction of the individual science exposures. Near infrared observations are generally strongly affected by thermal background radiation from the sky and the telescope, with strongly increasing background when going to longer wavelengths. This background emission has to be removed from the science images, otherwise only very strong sources are visible. To do so, images containing only the background emission (sky frames) have to be constructed. The easiest way would be to image nearby areas on the sky without any sources in them, but given the large extent of the Omega Prime field of view, this is impossible. Instead, sky frames have to be constructed by combining images taken at different positions on the sky and rejecting the signals from any sources. Instead of observing extra sky positions, the science frames themselves were used for this purpose. For each science exposure, a number (typically five or six) of adjacent (in observing time and location on the sky, mostly the three images taken immediately before and after the respective image) science frames were median combined, thus efficiently rejecting all astronomical sources and also cosmic ray signatures. This provides useful sky frames in not too crowded areas or areas not too strongly affected by extended nebulosity, and worked well for most of the survey area. A more careful selection of exposures suited for sky frame construction had to be done only in the area around and to the north of the Orion Nebula. The sky frames were then subtracted from the respective science frames. Usually the result of this procedure was very good, with only very faint negative features from incomplete source rejection in the sky frames visible.

**Readout voltage variations.** An apparent, at the moment of this writing still persistent, problem with Omega Prime are instabilities in the readout voltage of the array, ranging from smooth drifts over the time of an individual readout to short spikes (leading to single narrow vertical stripes in the images) to rapid changes throughout the entire readout (leading to a multitude of vertical stripes), with these patterns changing from readout to readout. Since these stripes are at a significant intensity level, they also had to be removed. To do so, a frame only containing the stripes had to be constructed. This was done by first replacing all image values above a certain limit (in most cases  $3 \times$  the standard deviation of a frame) by the mean value of the frame, thus removing most of the stars. Then the frame was averaged along the columns, leaving a single row containing the profile of the stripe pattern. A frame with the full array size was then reconstructed, containing 1024 times this averaged profile. This frame was then subtracted from the science frame, usually leading to a very good removal of the stripe patterns.

**Flatfielding.** Finally, the frames were divided by the corresponding normalized flatfield, to correct for sensitivity variations of the detector array. Note that the stripe removal procedure also removes any remaining offsets from variations of the sky background, and that the sky subtraction also removes the bias level, which has to be separately removed in optical CCD data reduction.

**Construction of the mosaics.** Then the individual frames had to be combined into the final mosaics. This was done by registering the positions of stars in regions of overlap between frames taken at different

positions. Since the field of view of Omega Prime is very large and since the mosaicing pattern was designed such that large overlaps between neighbouring positions were present, there were enough stars in the overlapping parts to do this throughout the entire survey area. As can be seen in Table 1, some observations were done under nonphotometric conditions (a rough check of the photometry was done by comparing the fluxes of moderately bright stars as derived from individual exposures). For each survey field there is at least one sequence of observations taken under good conditions. These data were used to correct the data taken under nonphotometric conditions by multiplicatively scaling them to consistent flux levels. Then the individual frames were median averaged into the final mosaics.

### Calibration

For the final mosaics an astrometric calibration was performed using stars from the Hubble Space Telescope guide star catalog (GSC 1.0) which were identified on the infrared mosaics. Comparison of the positions of several sources obtained with this method with positions given in the literature indicates that the positional accuracy is of the order  $1''$ ; this is about the accuracy which is given for the GSC (e.g., on the GSC web pages: <http://www-gsss.stsci.edu/gsc/GSC.HTML>).

A number of standard stars from the UKIRT list of faint infrared standards (FS 12, FS 15, FS 29, FS 30; Casali 1992) was observed during the several observing runs through both the  $H_2$  narrow-band filter and the  $K'$  broad-band filter to allow for a photometric calibration of the data. The  $K'$  data were calibrated using the interpolated  $K'$  magnitudes for the UKIRT faint standards as given on the Calar Alto web pages ([http://www.mpia-hd.mpg.de/IRCAM/FAINTSTD/faintstd\\_kprime.html](http://www.mpia-hd.mpg.de/IRCAM/FAINTSTD/faintstd_kprime.html)).

The  $H_2$  fluxes were calibrated by calculating a 0 magnitude flux for the  $H_2$  filter (0 magnitude flux density  $F_{0,\lambda=2.12\mu\text{m}}$  times  $H_2$  filter width of  $0.0206\mu\text{m}$ ). From the exposures of the standard stars a conversion factor between counts (per second and pixel) to flux was determined: 1 count/(second pixel) corresponds to a flux of  $4.3 \times 10^{-20} \text{ W m}^{-2}\text{arcsec}^{-2}$ . This conversion factor was the same to within a few percent for different nights and observing runs, so one value was used for all the data. For the  $H_2$  features in the L1641-N cluster, this flux calibration yielded flux measurements in reasonable agreement ( $\sim 10$ – $20\%$ ) with those published by Davis & Eisloffel (1995).

### 3.2 The optical continuum survey

In order to help find and characterize the sources of the outflows found during the  $H_2$  jet survey, part of an observing run during January 20 1999 at the ESO/MPG 2.2 m telescope on La Silla/Chile was used to obtain images of the survey area through a medium passband filter centred at 816 nm using the new optical Wide Field Imager. This camera uses a mosaic of 8 CCDs, each a  $2\text{K} \times 4\text{K}$  chip. With a pixel scale of  $0.''25$  per pixel, the field of view is about  $34' \times 33'$  (see WFI web-page at ESO: <http://www.ls.eso.org/lasilla/Telescopes/2p2T/E2p2M/WFI/>). Seven positions were observed, and a set of 5 dithered exposures was taken for each position to be able to correct for the gaps between the individual CCDs, for bad pixels, and for cosmic ray events. The integration time for each individual exposure was 120 seconds, yielding a total exposure time for each position of 10 minutes. The limiting magnitude for the final images corresponds to about  $I = 21.5$  ( $3\sigma$ ).

Data reduction included the standard steps. First, a bias frame constructed from a series of short dark exposures was subtracted from the raw data, then the data were divided by a normalized flat field constructed from a series of dome flats and sky flats. The data of each of the 8 CCD chips were first reduced individually, and then a mosaic was constructed in the following way: First, a ‘‘positional reference frame’’ was constructed from the dithered exposures at each of the seven positions by accurately registering and combining the data for each chip separately, resulting in one average image for each chip.

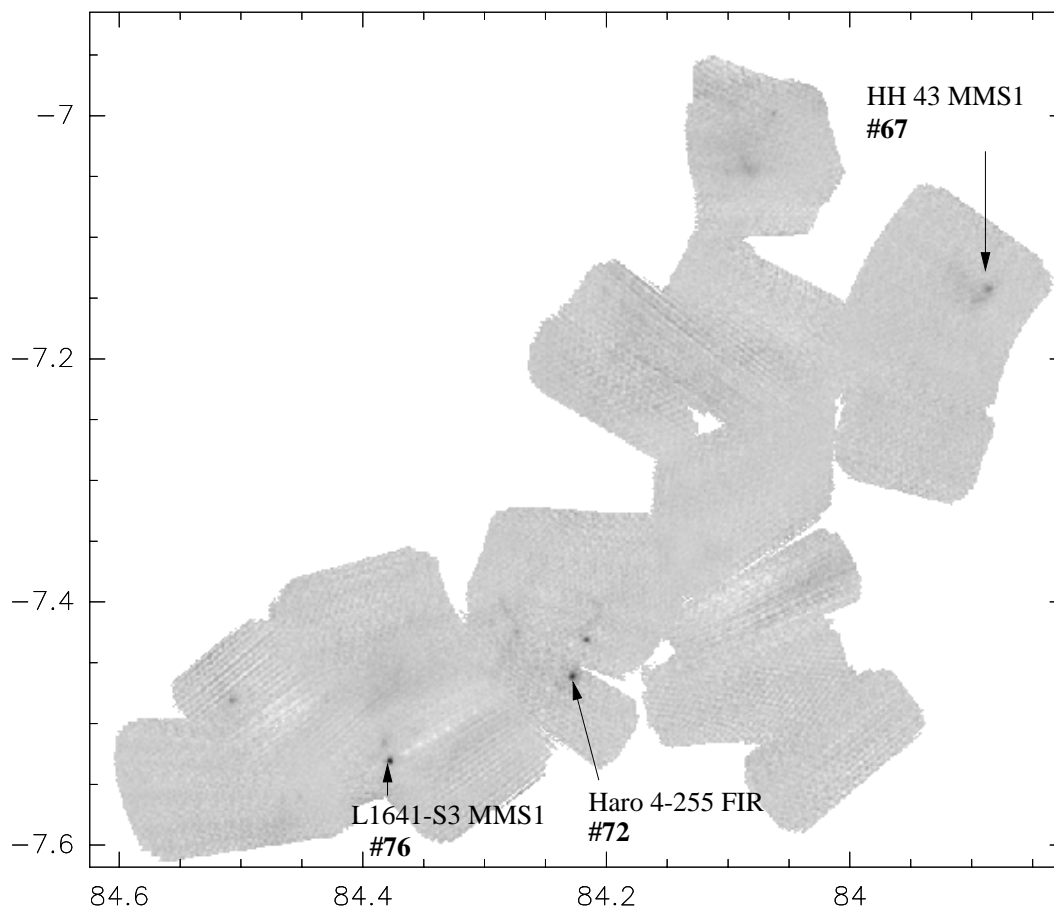


Figure 14: 1.3 mm continuum map of the south-eastern portion of the survey area. Outflow driving sources are marked, with the associated outflow number noted. The angular resolution is about  $12''$ . Positions are given in degrees (B1950).

Large enough dithering steps had been chosen such that these images overlapped, allowing an accurate determination of the position of each chip with respect to the others. The averaged images for each of the 8 chips were then registered, rotated, shifted, and finally averaged into one large master image which served as positional reference frame. After registering the individual exposures (chip by chip) to this positional reference frame, the final mosaics were constructed by taking the median of the rotated and shifted single exposures to reject cosmic ray events. Finally, the images were rebinned to the pixel scale and orientation of the infrared data to ease comparison between these datasets.

It was not possible in that night to take standard star images due to technical problems, but an approximate flux calibration of the 816 nm medium passband data was obtained by comparing the count rates of a number of stars in the Trapezium cluster to published I-band photometry taken from Prosser et al. (1994; source identification was done using the images and cross identifications given by McCaughrean & Stauffer 1994). Although the filter passbands are different and the accuracy certainly is very limited ( $\sim 0.^m1$ ), it is good enough for the purpose of this work, namely to get an impression on whether the candidate outflow driving sources are already visible at optical wavelengths and whether a substantial fraction of the source luminosity may be radiated at optical wavelengths.

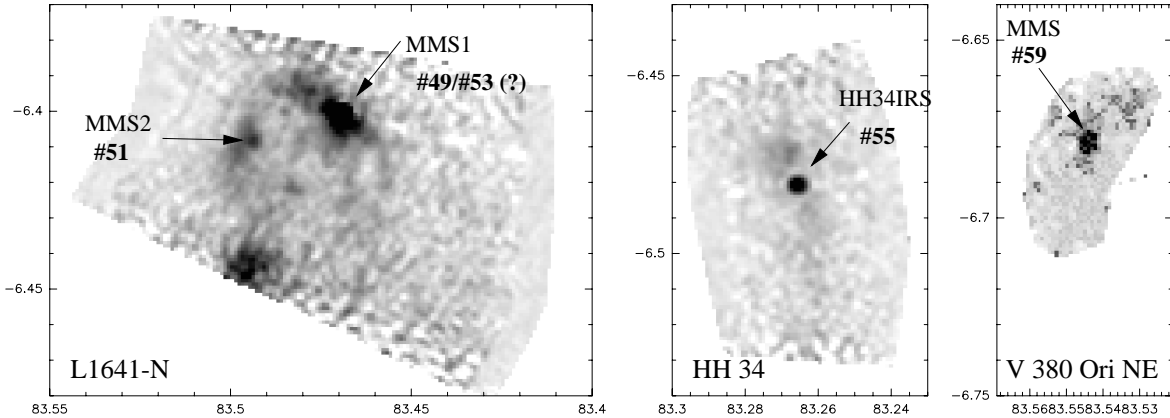


Figure 15: 1.3 mm continuum maps of the L1641-N cluster, HH 34 IRS, and V 380 Ori NE (data taken by Karl Menten). Outflow driving sources are marked, with the associated outflow number noted. The angular resolution is about  $12''$ . Positions are given in degrees (B1950).

### 3.3 1.3 mm maps

The south-eastern part of the  $H_2$  survey region was mapped in 1.3 mm continuum emission during an observing run in late February/early March 1999 at the IRAM 30 m millimetre telescope on Pico Veleta using the MPIfR 37 channel bolometer array (MAMBO; Kreysa et al. 1998). These observations form the first part of an ongoing project, in which the entire  $H_2$  survey region will be mapped at millimetre wavelengths.

The observations consist of a number of “on the fly” scan maps, in which the telescope repeatedly scans across the observed field in azimuth, with offsets in elevation between the subscans. Individual maps typically extended over about  $5'$  to  $10'$  in azimuth, and several arcminutes in elevation. The scan velocity usually was  $8''/\text{sec}$ , with offsets between individual subscans of  $6''$ .

The NIC software package was used for data reduction. The data were corrected for different receiver gains (“flat fielding”) using array parameters derived from observations of bright planets. The data were corrected for atmospheric absorption using regularly determined sky opacities. A flux calibration was done using maps of bright planets. Linear (in some cases higher order polynomial) baselines were subtracted and the data despiked. A sky noise filter was applied in order to reduce the (correlated) sky variations. Then, from the chopped raw data the unchopped image was restored. Finally, the data were converted from the azimuth-elevation map coordinates to a RA-DEC coordinate system, and the individual maps combined into a mosaic. The data analysis is so far only preliminary, a more sophisticated analysis will presumably lead to better maps (higher sensitivity), but will be the subject of later work. Here I will use this map only as a help in driving source identification and to get approximate 1.3 mm fluxes of the sources.

The resulting map is shown in Fig. 14. The noise level is about 15 mJy per beam. The positional accuracy of the map is presumably of order  $1''$  to  $2''$ , the pointing of the telescope was checked regularly and found to be stable.

In addition to this wide field survey some smaller 1.3 mm maps were obtained by Karl Menten of the L1641-N cluster, the HH 34 source region, and the V 380 Ori NE jet. These maps are presented in Fig. 15.

### 3.4 IRAS data

Two sets of data were used to obtain photometric information at mid- to far-infrared wavelengths, namely the IRAS point source catalog (PSC) and the coadded and HIRES processed IRAS maps. For each outflow identified from the H<sub>2</sub> survey (see Section 4.1) it was checked if there was a nearby IRAS point source possibly associated. In most cases there was not, so the coadded maps and the HIRES processed maps were examined to search for sources which were not recognized when the PSC was compiled. In the cases where sources were found on the coadded or HIRES processed maps, a rough estimate of their brightness was obtained by subtracting a point spread function template (obtained from images of bright isolated sources) at the desired position. The flux of the template point spread function was varied until the source vanished. To derive upper limits for sources which were seen at other wavelengths, but not in the respective IRAS map, these point spread function templates with varying flux were added to the maps, then it was checked by eye, whether the artificial source was visible or not. This procedure was done both for the HIRES processed and not HIRES processed maps, and significant differences to the original maps had to be visible in both cases, which probably gives very robust values for the upper limits.

It should be noted that in certain parts of the survey area, namely in the area around and to the north of the Orion Nebula (OMC-1/2/3/4, and in other densely populated regions like the L 1641-N cluster), the IRAS maps are not very helpful, since there are presumably many sources which are not resolved by IRAS, and since there also is presumably bright extended emission. OMC-1 itself appears saturated on the IRAS maps. Generally, fluxes and other quantities derived for sources in that area (e.g., luminosities) should be taken with great care, since they are probably strongly overestimated; similarly, the upper limits for IRAS fluxes in that area are much less stringent than in other parts of the cloud.



## 4 Data analysis

### 4.1 The near-infrared H<sub>2</sub> survey

#### Method of data extraction

H<sub>2</sub> emission line objects can be identified by comparison of images taken through a narrow-band filter transmitting at the wavelength of the emission line and a continuum filter. This can either be a narrow-band filter centred on a nearby emission line free wavelength interval, or a broad-band filter. In the case of the H<sub>2</sub> 2.12  $\mu\text{m}$  emission line this will be a K-band filter; for the present thesis a K' filter (1.944–2.292  $\mu\text{m}$ ) was used (a filter with about the same width as a standard K-band filter ( $\sim 2.01$ – $2.43 \mu\text{m}$ ), but shifted towards shorter wavelengths in order to reduce the thermal background emission, which is coming up at the long wavelength part of the standard K filter). The K' filter includes the 2.12  $\mu\text{m}$  emission line (and others), but transmits more continuum than the narrow-band line filter: the K' filter is  $\sim 10$  times broader than the 2.12  $\mu\text{m}$  narrow band filter, thus 10 times more continuum light will pass the K' filter than the narrow-band filter. Since the line flux from the 2.12  $\mu\text{m}$  line remains the same, continuum features will appear 10 times brighter in the broad-band filter than through the narrow-band filter (for the same integration time). In contrast, emission line features will appear at the same brightness as through the narrow-band filter (in fact, contributions of other emission lines increase the brightness of shock excited emission line features by about a factor of two in the broad-band filter; see, e.g., Smith 1995). Although the use of a narrow-band continuum filter is more efficient in separating line emission objects particularly from nebulous continuum sources, the use of a broad-band K' filter was preferred in order to save telescope time (in order to achieve a similar signal-to-noise ratio for continuum features through the 10 times broader filter, a 10 times shorter integration time is sufficient).

Besides shock excitation of hydrogen molecules a second excitation mechanism must be kept in mind: UV fluorescence (see Section 2.3). Given the lack of spectral information, I had to rely on morphological information in discriminating between shock excited features and UV excited H<sub>2</sub> emission. The cooling time for shocked molecular hydrogen gas in flows from young stars is of the order of a few years. For a shock front moving with a velocity of the order of 100 km/s, this converts to a cooling length of the order of 100 AU, i.e., hardly resolvable by the present, seeing limited observations (angular resolution  $\sim 1''$ , corresponding to 450 AU in Orion). Thus the shocks will have a rather compact morphology, either compact knots or narrow filaments. UV excited H<sub>2</sub> emission arises from cloud surfaces which are exposed to strong UV radiation. In this case, the emission features will be large and diffuse, easily distinguishable from the compact shocks.

H<sub>2</sub> features were identified in the reduced data by blinking the 2.12  $\mu\text{m}$  narrow-band images against the K'-band continuum images. The cut values for the image display were chosen such that stars and continuum nebulae appeared at about the same brightness in both images: then, H<sub>2</sub> emission line features appear much fainter (by roughly a factor of 5) in the broader K' filter. A list of all identified H<sub>2</sub> features was compiled (presented in Appendix A), containing an identification number, the position, the H<sub>2</sub> 2.12  $\mu\text{m}$  line flux, and some comments on the morphology of the feature. Some of the H<sub>2</sub> features are listed on a knot by knot basis, in other cases groups of apparently related features are listed as one

entity, with some more detailed astrometric and photometric information on the individual or the most prominent parts of the respective feature.

The features are labeled by the number of the survey field they are located in, followed by a running number, which usually increases from north to south. The acronym SMZ stands for Stanke, McCaughrean, and Zinnecker (see Stanke et al. 1998, 2000), according to the recommendations of the IAU for the naming of new astronomical sources. As an example, a feature labeled SMZ 3-11 is feature No. 11 in survey field 3.

A second list was then compiled, containing information about the candidate protostellar H<sub>2</sub> flows identified in this work (presented in Appendix B). It includes a list of H<sub>2</sub> features thought to be associated with the respective flow, a representative position, the angular extent of the flow, the (projected) spatial extent based on an assumed distance to the Orion A cloud of 450 pc, and the position angle of the flow (measured in degrees east of north). As a representative flow position, I give the position of the suggested outflow driving source if there is one. Otherwise a position is given which is regarded to be possibly close to a driving source, e.g., the geometric center of a apparently bipolar H<sub>2</sub> configuration, a position being possibly close to the driving source as suggested by other morphological hints, or just the position of a prominent part of the candidate H<sub>2</sub> flow.

## Results in summary

A total of 76 candidate flows are identified. Since the bright nebulosity of the Orion Nebula makes it possible to see only the brightest flows in that area and thus introduces a bias towards brighter flows, the flows found in the Orion Nebula area (flows #26, #27, and #28) will not be included in the statistical analysis, except where noted. This leaves us with 73 flows, which will be subdivided into two groups:

- **the “certain” group:** flow identifications regarded as quite certain; this group contains 44 out of the 73 (60%) flows under discussion (the Orion Nebula flows #26, #27, and #28 would also belong to this group). Flow numbers of flows from this group will be printed in bold letters in the following.
- **the “uncertain” group:** flow identifications which look like flows, but may be not true, or flows where only poorly constraining H<sub>2</sub> features were found, or flows which are real, but not necessarily recognizable based on the H<sub>2</sub> data alone. As an example for the latter group the flow from the T Tauri star Haro 4-255 may be cited (flow #73), which is a well collimated Herbig-Haro jet terminating in a bow shock (Aspin & Reipurth 2000); in H<sub>2</sub>, only a faint whisp of the bow shock is visible, from which alone it would be impossible to identify the flow. This group comprises 29 out of the 73 flows (40%); flow numbers of flows from this group will be printed in normal letters in the following.

## 4.2 The outflow driving sources

For each of the flows, the available optical, near-infrared, mid- to far-infrared, and submillimetre/millimetre data were searched for candidate outflow driving sources. The following pieces of information were used to identify the driving source candidates:

- **Flow morphology:** Obvious centres of symmetry, positions along obvious flow axes, or positions suggested by other morphological hints (like the orientation of bow shock like structures) were preferentially checked.

- **Spectral information:** Since it is known that outflows are driven by very young objects, driving source candidates were selected by their spectral energy distribution: optically obscured sources, sources with strong infrared excess, or sources obscured even at near- or mid-infrared wavelengths, but being bright at far-infrared or submillimetre/millimetre wavelengths were preferentially regarded as outflow driving sources.
- **Source morphology:** Young stars are often associated with reflection nebulosities. The presence of optical or near-infrared continuum nebulosities was thus used as an additional indicator of youth. Particularly interesting are sources associated with fan shaped nebulosities opening towards H<sub>2</sub> features, indicating outflow cavities. Bipolar reflection nebulae, bisected by dark dust lanes with the dust lanes oriented perpendicular to the suggested outflow direction, are likely indicative of disklike structures around the respective central sources, which may be responsible for driving and collimating the flow.

The use of the flow morphology returns to the original idea to use the jets as pointers to the youngest, most deeply embedded protostars. This idea was motivated by the discoveries of HH 211 and HH 212, which both display a very clear morphology, precisely indicating the positions of their driving sources at their centres of symmetry. However, it turned out that this was more difficult than anticipated, since not a single flow was found which rivals HH 212 regarding its high degree of symmetry. Only rather few flows were found whose morphology indicated the position of the driving source in a similarly stringent way as it is the case for HH 211 and HH 212.

A list of outflow source candidates is presented in Appendix C. It contains the position of the suggested outflow source, photometric information covering the wavelength range from 0.8  $\mu\text{m}$  to 2000  $\mu\text{m}$ , an estimate of the bolometric luminosity of the source derived from model fits to the photometric data, and an estimate of the infrared class the source belongs to, which allows a crude estimate of its evolutionary stage. Finally, for each source a short note containing additional information (e.g., about the morphology and how the photometric information has been obtained) is included.

Driving source bolometric luminosities and the infrared spectral classes were estimated by adjusting simple model spectral energy distributions to match the photometry. The long wavelength range was modeled using greybody curves (see, e.g., Dent et al. 1998). The shorter wavelength data were approximated using star + (flared) disk models according to Kenyon & Hartmann (1987) and Adams et al. (1988). Photometric upper limits generally were treated as true measurements, which in many cases certainly leads to very unrealistic SED shapes and overestimates of the bolometric luminosities. The bolometric luminosities were estimated by integrating over the model SEDs. To get an estimate of the evolutionary stage of each source, the near-infrared spectral index  $\alpha_{\text{IR}}$  from 2.2 to 12/25  $\mu\text{m}$  was determined from the model curve. I also derived the ratio  $L_{\text{bol}}/L_{\text{submm}}$  (with  $L_{\text{submm}}$  measured from 2000  $\mu\text{m}$  to 300  $\mu\text{m}$ ), which serves to classify the youngest protostars.

Based on the derived near-infrared spectral index and/or the  $L_{\text{bol}}/L_{\text{submm}}$  ratio the sources were classified according to the classification scheme of Lada (1987) and André et al. (1993; see also André & Montmerle 1994; André et al. 2000). Sources with a spectral index  $\alpha_{\text{IR}} > 0$  are classified as Class I, and sources with a spectral index  $-2 < \alpha_{\text{IR}} < 0$  as Class II (sources with  $\alpha_{\text{IR}} < -2$  would be Class III sources, but no jet driving source was found in this class). Sources with  $L_{\text{bol}}/L_{\text{submm}} < 200$  are candidate Class 0 sources (no near-infrared spectral index can be given for these sources, since they are not visible at near-infrared wavelengths).

## Results in summary

A total of 49 candidate outflow driving sources could be identified (for 36 of the “certain” flows, and for 13 of the “uncertain” flows).

- 8 of them are Class 0 sources (7 “certain”, 1 “uncertain”)
- 31 are Class I sources (25 “certain”, 6 “uncertain”)
- 10 are Class II sources (4 “certain”, 6 “uncertain”)

## 4.3 Limitations and errors

### The H<sub>2</sub> jet survey

**The jet sample** The H<sub>2</sub> survey covers a large area of a molecular cloud with a uniform sensitivity and with comparable angular resolution. This ensures that similar features (with respect to brightness and morphology) can be detected with the same likelihood throughout the entire survey field, with the exception of the areas affected by strong nebulosity, in particular the Orion Nebula area. This area will thus be excluded from statistical investigations, as already noted above.

The large variety in the morphology of the H<sub>2</sub> features, ranging from large, extended, filamentary features to compact or even unresolved knots, makes it impossible to give a certain detection threshold in surface brightness or total H<sub>2</sub> flux for the H<sub>2</sub> features. This not only affects individual H<sub>2</sub> features, but also entire flows. The detection of flows thus depends on the brightness or H<sub>2</sub> luminosity and for a given brightness on the flow morphology. This is different from samples of (e.g.) certain types of galaxies or stars, which for a given data set are either detected or not, depending on their brightness alone.

Due to the variety in flow morphologies the identification of flows is not a truly objective process. Some basic rules were followed as far as possible (e.g., just two knots next to each other alone are not regarded as a flow, although they might form one), but the flow identification often involved case by case reasonings, which are impossible to quantify in a reasonable way. The subdivision of the identified flows in a “certain” and an “uncertain” group reflects this difficulty. Some of the flows identified in this work later on might well turn out not to form a flow as suggested here, but belong to other systems. However, this is a problem generally found in the field, as might be seen in the example of the HH 43/38/64 flow, for which the new data obtained during the present H<sub>2</sub> survey suggested a greatly revised picture (Stanke et al. 2000).

Thus I cannot derive a sample of jets from the survey data which is selected according to well defined criteria, such as, e.g., a flux limited sample, although the survey is unbiased and covers the survey area completely and uniformly. This limitation has to be kept in mind if statistical statements about the jet sample are made.

For the jet sample, a number of quantities are derived (the location of the jet, its position angle, its length, and its H<sub>2</sub> brightness or luminosity), each of which is subject to errors and uncertainties.

**The location of the jets.** For a reasonable fraction of the jets a candidate driving source is suggested. The positions of these will generally be accurate to a few arcseconds, possibly less accurate, if only IRAS positions are known. For the jets without a driving source identification, a characteristic position is given. This position might be wrong by as much as the given flow length for some jets. Generally, however, the jets without driving source identification are among the shorter jets, such that the errors in jet location will not be much larger than about a few arcminutes at most.

The jet locations are discussed in Section 5.2, 5.7, and 6. Sections 5.2 and 5.7 only deal with the general location of the jets within the molecular cloud. The uncertainties in the determination of the driving source position will thus not affect the conclusions drawn there at all. Section 6 discusses the possible association of the jets with the molecular cloud cores in the survey area. The cloud cores are typically of a size of the order of one to a few arcminutes, and the positional accuracy for the location of the cores is of the order of  $\sim 10''$ . Thus for the jets with a driving source identification the positional uncertainties of the jets will not be a major problem. For a few of the jets without driving source identification, the positional uncertainty might be big enough to lead to an error in stating the association or non-association of a jet with a cloud core. This will be the case for at most a few jets, and very likely also not affect the conclusions of Section 6.

**The position angle of the jets.** This is a fairly easy to derive quantity and reasonably well constrained (to a few degrees) even for the more poorly defined flows. In only one flow (#76) there is evidence for a major (i.e., more than  $10^\circ$ ) change of flow direction, making it difficult to give an accurate flow position angle. The flow position angles are discussed in Section 5.7. Here only the general, approximate alignment or misalignment with a given orientation is tested, and uncertainties in the jet position angle of a few degrees will not affect the result of this section.

**The length of the jets.** The jet length is also an observable which is relatively easy to derive. Pure measurement errors will be at most of the order of a few arcseconds, due to possible errors in the pixel scale or the positional registration of the individual exposures going into a mosaic. Given the extent of the jets of the order of an arcminute or more, this measurement errors will be negligible.

However, a number of other uncertainties exist, which will lead to a systematic underestimate of jet lengths. First, the inclination of the jets with respect to the line of sight is not known. Second, it is not necessarily the case that the full extent of the flow is observed, either because extinction hides parts of the flow, or because the jet is not visible over some part of its extent in  $H_2$  emission, or because it extends beyond the observed area. For example, the HH 34 giant flow ( $H_2$  flow #55) is known to extend over a total length of  $\sim 3$  pc, but only part of its northern lobe lies within the area covered by the  $H_2$  survey. Thus its length is given here as 2.3 pc only. Similarly, the L1641-N giant flow ( $H_2$  flow #49) is listed with a length of 4.4 pc. However, only a small part of its northern lobe is seen in the  $H_2$  survey; the rest is too faint, or again out of the survey area. Including the chain of Herbig-Haro objects which outline the northern lobe, the total flow length would be at least 10 pc. Another example is the  $H_2$  flow #51, of which also only one lobe is seen. Presumably, this outflow has a counterlobe located within the survey area, thus its length, here given as 0.9 pc, presumably is twice as much as is given here, of the order of 2 pc.

The jet length will be discussed in Sections 5.4 and 7.1. The conclusions drawn in these sections rely on the statements of general trends seen in comparison of various groups of jets rather than an interpretation of the actual value of the jet lengths. The uncertainties which have been noted here should affect these groups to a similar extent and will not greatly affect the conclusions of Sections 5.4 and 7.1.

**The  $H_2$  brightness/luminosity of the jets.** The determination of the  $H_2$  brightness of the jets and its interpretation is subject to various sources of uncertainty. First, photometric measurement errors have to be regarded. As it is stated above, the photometric calibration yields results which are in reasonable agreement with other work. However, parts of the observations have been made under apparently not-photometric conditions. For each survey field, at least one coverage of the field was taken under likely photometric conditions, and the not-photometric data were scaled in intensity to match the data taken in

photometric conditions before constructing the final mosaics (observations which were obviously heavily affected by clouds were rejected). This procedure will certainly introduce some errors in parts of the survey area, which may be of the order of 10%. A second source of uncertainty in obtaining the photometry lies in the generally extended morphology of the H<sub>2</sub> features. Using apertures of different sizes might well lead to significant variations of the measured fluxes caused by faint emission surrounding the features or by intensity variations in the background. For the more compact features, this may also be of the order of 10%, for some low surface brightness, very extended features this may be much more. Generally, the errors in H<sub>2</sub> photometry may be of the order of 10–30% for most of the H<sub>2</sub> features.

Besides these pure measurement errors, extinction will be the major problem in the interpretation of the H<sub>2</sub> fluxes. The quantity of interest in obtaining the H<sub>2</sub> photometry is the intrinsic H<sub>2</sub> luminosity of the jets. Differing extinction is not only a problem from flow to flow, extinction might also vary greatly along the length of each flow, as it breaks out of a dense cloud core, ploughs through the interclump medium and possibly through other clumps. For example, in HH 212 extinctions ranging from  $A_V \sim 20$  mag for the innermost knots down to  $A_V \sim 2$  mag for the outer bow shocks are estimated (Zinnecker et al. 1998), altering the measured 2.12  $\mu\text{m}$  luminosity of  $0.0053 L_\odot$  to an intrinsic 2.12  $\mu\text{m}$  luminosity of  $0.018 L_\odot$  by a factor of more than 3. As an additional example, Bontemps et al. (1996b) derive a H<sub>2</sub> luminosity for the infrared jet apparently originating in the Class 0 protostar HH 24 MMS, assuming a K-band extinction of  $A_K \sim 5$  mag (corresponding to  $A_V \sim 50$  mag, Rieke & Lebofsky 1985). They also point out that this estimate is very uncertain due to the unknown extinction. On the other hand there are certainly some H<sub>2</sub> shocks which suffer only little extinction, as they are seen as HH objects at optical wavelengths.

As a rule of thumb I will assume a K-band extinction of  $A_K \sim 1$  mag towards the H<sub>2</sub> flows wherever possible effects of extinction are included in the discussion. The extinction through dark clouds is typically a few magnitudes at optical wavelengths. Lynds (1962) subdivides the dark clouds in opacity classes, ranging from 1 to 6, where the opacity class very roughly corresponds to the optical extinction. The L1641 dark cloud belongs to opacity class 4. The present H<sub>2</sub> survey is targeted towards the densest parts of this dark cloud and the even denser integral shaped filament. Thus the extinction will on average be larger than 4 mag, presumably of the order of 10 mag, corresponding to  $A_K \sim 1$  mag. The jets are not all located behind the cloud, but at arbitrary depths within the cloud, thus generally not suffering the full amount of extinction. On the other hand, the jet driving sources, and therefore parts of the jets, are embedded in the densest molecular clumps, from which they form, systematically leading to a somewhat higher average extinction. Since these two effects counteract, I will assume that they cancel out, and take the average extinction through the cloud of  $A_K \sim 1$  mag as a good value for the extinction towards the embedded flows. Finally, there may be a systematically higher extinction towards the flows from the youngest protostars, particularly the shortest ones, since in those cases also the amount of circumstellar material is highest, probably causing higher extinction.

However, as in the case of the jet length, the results drawn from the measured H<sub>2</sub> luminosities of the jets in Sections 5.5 and 7.1 at first rely on the interpretation of general trends rather than an interpretation of the actual value of the jet H<sub>2</sub> luminosities. The uncertainties which have been noted here should affect these groups to a similar extent and will not greatly affect the conclusions of the respective Sections.

Further on, the jet H<sub>2</sub> luminosities will be used to get an estimate of the kinetic energy input rate of the jets, the mass outflow rate, and the underlying mass accretion rate of the protostellar system. These estimates (or rather educated guesses) are based on additional assumptions, and the uncertainties introduced by these assumptions very likely by far dominate the uncertainties (rather than the above noted measurement errors). But again, most conclusions of the respective Sections (6.3 and 7) rely on the interpretation of general trends in the data.

### The driving sources

Regarding the driving sources, it should be kept in mind that their identification relies only in part on unbiased data sets. The IRAS data (with its deficiencies: confusion, sensitivity) as well as the optical and  $K'$  data covered the survey area uniformly. Higher spatial resolution, targeted  $10\mu\text{m}$  data were available only for a few sources. Only some parts of the survey area (OMC-1/2/3 and the southernmost part) were uniformly covered at (sub)millimetre wavelengths so far. Some more targeted observations exist. However, a 1.3 mm continuum survey has meanwhile been completed at the IRAM 30 m telescope which will be the subject of future work.

The photometric data often were upper limits only, thus in many cases the derived luminosity is also an upper limit only. Mainly due to the very limited angular resolution of the IRAS data, constraining the SEDs turned out to be particularly difficult and unreliable in crowded areas like the OMC-1/2/3 region, the areas around the L 1641-N cluster, and the V 380 Ori and HH 1/2 area, which also contains several young stellar objects. But also in less crowded regions many sources were not detected at IRAS wavelengths, and, since the sensitivity of IRAS compared to, e.g., the near infrared measurements is comparably low, in many cases the derived limits on the source luminosities only reflect the sensitivity limit of IRAS. For a number of driving sources the measurements appear to resemble reasonably well usually found SED shapes. In these cases, the estimated bolometric luminosities may be well constrained and accurate to better than a factor of two. Some sources have very poorly constrained SEDs, and the luminosity estimates may be wrong by more than an order of magnitude. For the cases in which the SED is constrained by at least a few reasonably good measurements, the estimated luminosity may be wrong by a factor of a few.

Virtually the only section in which the driving source luminosity is the subject of discussion is Section 7.2. Here only the general location of the jets and their driving sources in a  $L_{\text{H}_2}$  vs.  $L_{\text{bol}}$  plot is compared to the Smith (2000) unification scheme, rather than an interpretation of the actual  $L_{\text{bol}}$  values. The conclusion from this section will not change if the bolometric luminosities of the driving sources are not systematically wrong by more than an order of magnitude.

The estimate of the evolutionary stage of the sources should be comparably safe for most objects. This is because at the near- to mid-infrared wavelength range (which is used to discriminate Class I and Class II sources) the angular resolution of IRAS is comparably good (and of course also the angular resolution of the near-infrared and optical wavelength observations). Class 0 sources are identified based on the large millimetre flux compared to the bolometric luminosity of the sources and on not-detection at near- to mid-infrared wavelengths; in case of poorly determined far-infrared measurements (IRAS 60 and  $100\mu\text{m}$ ), an overestimate of the bolometric luminosity will rather lead to a rejection of a source as Class 0 than a misidentification of a Class I source as Class 0, and the general brightness of Class I sources at mid-infrared wavelengths will generally allow a good discrimination of Class I from Class 0 sources.

Mid- to far-infrared observations at higher angular resolution and better sensitivity are highly desirable in order to better constrain the SEDs of the outflow driving sources, and to derive more meaningful source properties. It also has to be noted that no attempt was made to derive any other source properties (mass/luminosity/temperature of embedded sources, circumstellar disk parameters, disk or envelope masses, dust properties, etc.) from the available data due to the large uncertainties present in the photometry. This will be a task of future work.

**Summary.** The conclusions drawn throughout this work generally do not rely on a precise interpretation of measured values, but rather on obvious trends in the data. In the following I will not perform detailed analysis of measurement errors, and also no plot will contain error bars. In most cases, other

uncertainties than pure measurement errors will limit the exactness to which conclusions can be drawn from the data (e.g., the unknown, but possibly substantial and varying extinction, unknown jet inclination to the line of sight, unknown jet velocities, etc.). Clearly, the uncertainties noted in this section should be kept in mind.



## 5 The H<sub>2</sub> jet sample

In this chapter, the properties of the jet sample will be presented in detail. The focus will be on the properties of the sample as such, not so much on properties of individual objects. This keeps with the intention of this thesis, namely to perform a statistical study of protostellar jets. The above noted limitations of the sample should, however, be kept in mind throughout the following parts.

### 5.1 The number of H<sub>2</sub> jets

The first outcome of the Orion A jet survey is the large number of active jets. Evidence for more than 70 jets has been found, of which 44 are regarded as rather reliable identifications (termed the “certain” group), whereas 29 are regarded as either doubtful or only recognizable with additional information (the “uncertain” group). Of the latter group, some will presumably turn out to be real misidentifications. Then one still has to explain the origin of the remaining H<sub>2</sub> shocks, and the most likely explanation is that they originate in flows that are simply not recognized as such due to (e.g.) unfavourable morphology. Note also that there are still a number of H<sub>2</sub> features listed in Appendix A for which no obvious flow association was seen. Furthermore, the present H<sub>2</sub> survey is shown in Section 5.6 to be effectively more sensitive than previous searches for high velocity CO outflows, which revealed ~15–20 flows in the survey area. Taking these arguments together, the number of more than 70 flows seems reasonable regarding the sensitivity of the survey. Although no separate comparison of Herbig-Haro object searches with the H<sub>2</sub> survey is presented here, I would like to note that the H<sub>2</sub> survey was able to recover most (but not all) Herbig-Haro objects known in the survey area.

Comparing the H<sub>2</sub> outflow searches (this work, Yu et al. 1997) with existing molecular (CO) outflow searches clearly indicates that H<sub>2</sub> searches are in fact more successful. The (now possible) sensitive and wide field search for H<sub>2</sub> features is much more efficient in revealing less energetic flows driven by low luminosity, low mass protostellar objects. Another great benefit is the naturally achieved arcsecond angular resolution, which is of great importance in clustered and crowded regions like the OMC-2/3 area and the L1641-N cluster.

### 5.2 The distribution of jets in the survey area

The jets are signposts of *currently* occurring star formation. They allow one to examine the properties of the spatial distribution of the star formation activity in the cloud, without the ambiguities introduced by the possible separation of the more evolved young stars from their birth places. In particular, this allows one to check to what extent star formation in Orion A occurs in the “clustered” or “aggregated” mode or in the “isolated” mode (e.g., Lada et al. 1993), the latter also including the formation of binary/multiple stellar systems. For the Orion B/L1630 giant molecular cloud, the clustered mode seems to be clearly dominant, with only very few stars forming or formed in isolation (Li et al. 1996). For Orion A/L1641, the situation seems to be less clear-cut, with a larger population of “isolated” stars (e.g., Allen 1996; Lada et al. 1993; Zinnecker et al. 1993).

The Orion A jet survey is in line with the suggestion of the presence of a substantial population of “isolated” protostars. Clear evidence for the “clustered” mode is found in the northernmost part of the survey area, in OMC-2/3. This area had already been identified by Yu et al. (1997) as an extremely active site of outflow (hence star formation) activity, and the chain of bright (sub)millimetre condensations tracing the integral shaped filament (Mezger et al. 1990; Chini et al. 1997b; Johnstone & Bally 1999; Lis et al. 1998; Reipurth et al. 1999a) also suggested this. The present survey confirms the conclusions obtained by Yu et al., although the interpretation of some individual features differs. The OMC-2/3 area is an extremely active site of star formation: 1/3 of the flows identified in the full Orion A survey area are located in the OMC-2/3 field (H<sub>2</sub> jets # 1 through # 25), i.e., within only ~10 % of the entire survey area, and 45 % of the total H<sub>2</sub> luminosity is emitted in this area.

A second site of clustered active star formation is the L1641-N cluster. A number of flows have their origin in the cluster or its immediate surroundings (H<sub>2</sub> jets # 48 through # 54). The three Orion Nebula jets # 26, # 27, and # 28 presumably belong to the jets driven by protostars in clustered environments as well. The V 380 Ori/HH 1/2 area seems to be a small, loose cluster or group. Furthermore, there are a few more small groups, which may not really deserve the label “cluster” (e.g., the HH 34 area, containing the H<sub>2</sub> jets # 55 and # 56, plus some more nebulous sources).

One can regard as being isolated jets whose driving sources are separated from any others by more than a typical cloud core radius, i.e., by more than ~0.1 pc, or roughly 1 arcminute. This would include the H<sub>2</sub> jets # 29 through # 47, # 57, # 58, # 59, # 66 through # 71, # 74, # 75, and # 76.

In total it seems that a bit more than half of the jets detected in the present survey are driven by protostars in clusters or groups, and a bit less than half by isolated protostars. However, it also has to be assumed that the effective sensitivity of the survey (i.e., the ability to recognize faint flows) is lower particularly in the crowded, confused OMC-1/2/3 area, such that very likely a number of fainter flows have been overlooked there. But even taking this into account, there seems to be clear evidence for a substantial population (maybe 1/4 to 1/3 of all) of protostellar objects which form in the “isolated” mode in Orion A. Regarding the L1641 area alone, about 2/3 of the jets appear to originate in “isolated” protostars, well in agreement with the result of Allen (1996), who found that 1/2 to 3/4 of the (more evolved) stars in L1641 formed in isolation. In contrast, for Orion B/L1630 it is claimed that probably more than 90 % of all stars there formed in clusters.

### 5.3 Flow morphology

Generally, when talking about “jets” from young stars, one thinks about narrow (width of the order of 100 AU) beams (e.g., Mundt et al. 1990, 1991), which will hardly be resolved at the seeing limited angular resolution of the present observations. The great majority of the flows identified here consist of comparatively broad (transverse to the inferred flow direction) features or groups of knots, which together delineate a rather broad, but still well collimated path. In only a few cases very narrow jet beams are directly seen (see below). Usually, there are also gaps between these groups of knots, the flows are not continuous. Such a morphology is generally explained by the presence of wide, fragmented, bow shock-like working surfaces caused by an underlying, much narrower jet. The occurrence of distinct working surfaces with emissionless gaps in between points to episodic outflow behaviour. Thus, although only a few jet beams are directly seen, I will assume that in the most identified flows intrinsically highly collimated jets are present. Keeping this in mind, I will widely use the terms “jet” and “flow” or “outflow” synonymously.

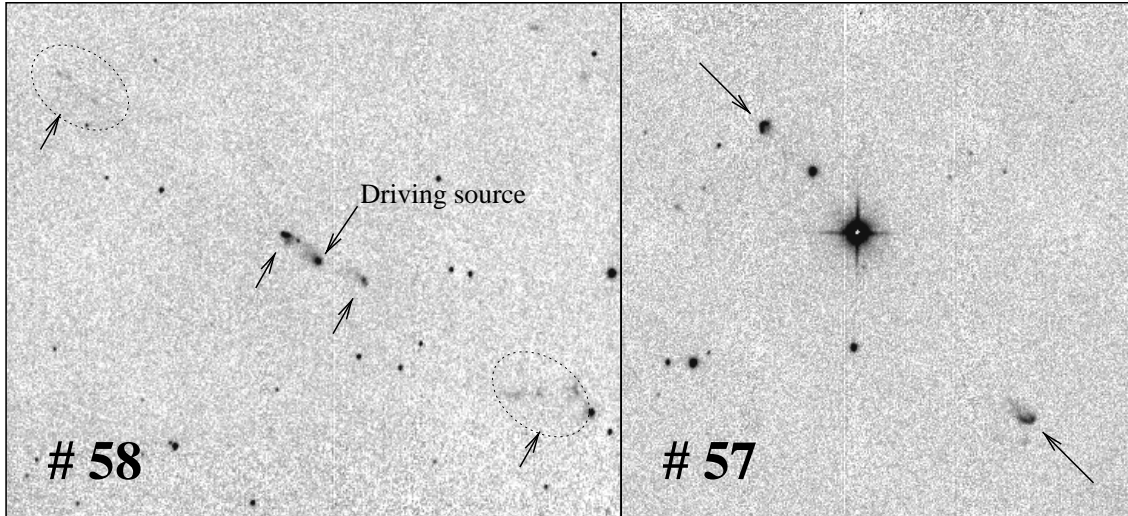


Figure 16: Two jets showing relatively clear signs of symmetry (image size is  $\sim 4' \times 3'3$  (left panel) and  $2'3 \times 2'3$  (right panel)).

### Symmetry

It has already been noted that no single jet has been found in the survey which shows a degree of symmetry similar to HH 212 or a similarly suggestive morphology. However, a number of H<sub>2</sub> jets show at least *some* degree of symmetry. The nicest example is the faint H<sub>2</sub> jet #58 (Fig. 16, left panel). It consists of two pairs of H<sub>2</sub> features bracketing the driving source. The nearby H<sub>2</sub> jet #57 (Fig. 16, right panel) also shows some symmetry, created by two oppositely directed, very compact, bright bow-shock like features. The HH 1/2 jet (H<sub>2</sub> jet #64) certainly also belongs to the jets showing symmetry, created by the two working surfaces HH 1 and HH 2 bracketing the driving source, although the structure of the working surfaces is very different. Some degree of symmetry seems to be present in the HH 43 giant flow (H<sub>2</sub> jet #67). In addition, some bipolar, though not necessarily symmetric features are found in many other flows.

The lack of symmetry in the H<sub>2</sub> jets found in the present survey has some implications. First, it limits the applicability of the original idea, to use the (supposed) symmetry of the jets to get a precise indication of the location of the driving sources. Second, one has to find a reason for the less pronounced symmetry and morphological clarity of the H<sub>2</sub> survey jets.

In the case of HH 212, the symmetry suggests that the structure of the jet and its morphological appearance is largely imposed on the flow at the driving source (Zinnecker et al. 1998). The absence of symmetry in the Orion survey jets could then have two different reasons: either the behaviour of the driving sources of the Orion survey jets is not the same as in HH 212, or it is the same, and the symmetry is erased as the flows propagate through the cloud. One particular property of the cloud core harbouring the driving source of HH 212 is its unusually small linewidth (Wouterloot et al. 1989), indicating a unusually quiet, unturbulent environment.

First, it is reasonable to assume that such a quiet environment favours an undisturbed propagation of the jet, whereas a turbulent environment might perturb an initially more systematic jet structure, thus erasing the initial symmetry. In that respect it may be interesting to note that the few jets showing a relatively high degree of symmetry are driven by rather isolated protostars, and are not located in the regions of clustered star formation such as the L1641-N cluster or the systematically more turbulent northern part of the cloud (e.g., Tatematsu et al. 1993), the OMC-1/2/3 area. Similarly, HH 212 originates from an exceptional, rather isolated protostar in Orion B (where the majority of stars are known to

form in clusters; see, e.g., Lada et al. 1993).

Second, a quiet environment might imply a particularly smooth and undisturbed accretion from the cloud core onto the protostellar disk and subsequently the star, thus favouring a very regular and uniform occurrence of periodic accretion outbursts. However, the ejection of the compact knots in HH 212 implies fairly short timescales (of order 50 years). Furthermore, the ejection of jets is thought to take place rather close to the central star (a few stellar radii), deep inside the stars potential well. Thus it seems unlikely that disturbances of the cloud core far away from the jet launching region have a major impact on the processes in the innermost part of the jet launching accretion disk. Therefore it seems reasonable to assume that similar processes govern the jet ejection and the intrinsic jet properties independent of the turbulence in the cloud cores. The deficiency of symmetry and morphological clarity in the Orion survey jets, if compared to HH 212, are thus more likely a result of disturbances as the jets propagate through the more turbulent, possibly more clumpy, environment in Orion A.

### H<sub>2</sub> jet beams

Well collimated, continuous jet beams which are virtually unresolved perpendicular to the flow direction are only seen in very few jets. These are the well known HH 1/2 jet (**#64**; see Strom et al. 1985; Mundt et al. 1987; Davis et al. 1994, 2000c; Noriega-Crespo & Garnavich 1994; Reipurth et al. 2000a), the equally well known HH 34 jet (**#55**), and the newly discovered jet **#42**. Furthermore, the H<sub>2</sub> jet **#5** consists of a narrow chain of very closely spaced, bright knots. Less clear evidence for a possibly well-collimated jet beam is found in the H<sub>2</sub> flow **#37**. Images of these jet beams are shown in Fig. 17. With the exception of jet **#5**, all these beams are very faint, sometimes hardly visible.

Interestingly, all of the beams shown in Fig. 17 are of similar length, of order 30'' or 0.06 pc. On the other hand, the sources creating these beams do not have many other features in common. The sources cover a range in luminosity spanning more than an order of magnitude (HH 1/2 VLA1:  $\sim 44 L_{\odot}$ ; HH 34:  $21 L_{\odot}$ ; **#42**:  $\leq 3 L_{\odot}$ ; **#5**:  $< 53 L_{\odot}$ ; no conclusive source is identified for **#37**). The driving sources of HH 34 and **#42** are Class I sources, the driving source of **#5** is a likely Class 0 source, and HH 1/2 VLA1 may either be a Class 0 or Class I source. The jets driven by these sources also differ greatly on larger scales. The beam in HH 34 is only the innermost part of the prototypical HH 34 giant jet (Bally & Devine 1994; Devine et al. 1997; Eislöffel & Mundt 1997), and HH 1/2 is presumably also the innermost part of a much greater flow (Ogura 1995). The length of the H<sub>2</sub> jet **#42** seems to be of order 0.7 pc, whereas the H<sub>2</sub> jet **#5** is seen to extend only over the 0.05 pc shown in Fig. 17. Thus there seems to be no particular property which favours the formation of a well-collimated beam, at least none can be seen from the small sample seen here.

The handful of H<sub>2</sub> jet beams may hold important clues on the origin of the jet material and the processes at work close to the driving source. A still poorly understood issue is the composition of the jet beams. Initially, it was suggested that the jet beams consisted mainly of ionized material (e.g., Mundt et al. 1987). Later on, it was shown that the ionization fraction is in fact fairly low, of the order of a few percent (e.g., Hartigan et al. 1994; Bacciotti & Eislöffel 1999). Finally, a highly collimated *molecular* CO jet was found in HH 211 (Gueth & Guilloteau 1999). The problem with the molecular (CO) gas is that it is not clear whether it is original jet material or gas which has been entrained in a shear layer along the jet beam. For the molecules radiating in the H<sub>2</sub> shocks, it is even more suggestive that these are molecules which are just entrained in a turbulent shear layer or through bow shocks created by internal working surfaces (e.g., Raga et al. 1993). Assuming that the CO and/or H<sub>2</sub> molecules are indeed original jet material, it is not clear whether the gas had to be molecular as it was injected into the jet or whether the molecules could have formed later on in the jet.

At least in the case of the HH 34 system (H<sub>2</sub> flow **#55**), there may be some arguments that the

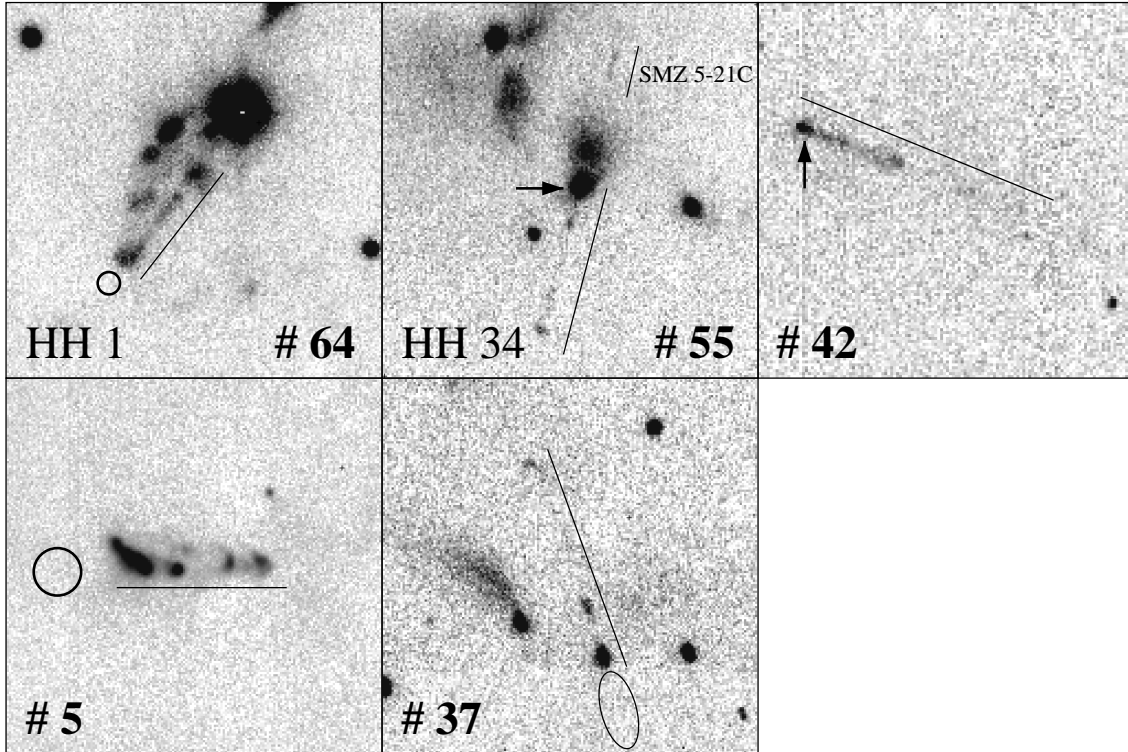


Figure 17: A collection of  $H_2$  jet beam images. The image section is  $1'.1 \times 1'.1$  in each panel, corresponding to  $\sim 0.15$  pc. The circles/arrows mark the positions of the suspected driving sources; no conclusive source position is known for  $H_2$  jet #37.

$H_2$  emission is due to molecular material in the jet beam rather than material currently being entrained. HH 34 (Reipurth et al. 1986; Mundt et al. 1987; Bührke et al. 1988) is one of the finest examples of an optical Herbig-Haro jet. Its blueshifted southern lobe consists of a knotty jet which points towards the apex of the original HH 34S Herbig-Haro object, which shows a very nice bow-shaped appearance and is located about  $100''$  away from the driving source. The jet is not seen to reach the bow shock, but vanishes at a distance of  $\sim 30''$  from the star. Between the jet end and HH 34S a smaller bow shock is located. In the redshifted counterlobe, only the main bow shock HH 34S has a counterpart (HH 34N). As noted above, the system of HH objects extending from HH 34S to HH 34N is only the innermost part of the prototypical HH 34 giant Herbig-Haro flow. Chernin & Masson (1995) found an extremely weak bipolar molecular CO outflow associated with HH 34 (see Fig. 74). Its redshifted, northern lobe was seen to be more massive than the blueshifted, southern lobe. This suggests that the HH 34 jet encounters more molecular material in its northern lobe, whereas almost no molecular gas is entrained by the southern lobe. The absence of the northern, redshifted lobe at optical wavelengths is then readily explained by higher extinction, caused by molecular cloud material in front of and around the northern jet beam.

The  $H_2$  images obtained for this thesis revealed for the first time direct evidence for a counterjet to the HH 34 jet (in fact, the images revealed for the first time  $H_2$  emission in the HH 34 jet beam itself; cf. Stapelfeldt et al. 1991; Zealey et al. 1993). A faint, linear  $H_2$  feature (SMZ 5-21C) extends along the jet axis (as defined by the southern optical beam) over a length of  $\sim 6''$  from  $\sim 19''$  to  $\sim 25''$  from the driving source. It seems that the  $H_2$  emission in the HH 34 jet and counterjet are at about the same intrinsic brightness (extinction hides the portion of the counterjet close to the source). This suggests that the jet and counterjet have similar properties, in particular similar amounts of molecular  $H_2$  emission. As it was noted above, the molecular outflow is much stronger in the northern lobe, whereas only little blueshifted CO is found in the southern lobe close to the driving source. If the jet  $H_2$  emission was due

to steady entrainment along the beam, one could expect stronger H<sub>2</sub> emission in the northern lobe, and weaker emission in the southern jet lobe. It thus seems to be more likely that the H<sub>2</sub> emission from the HH 34 jet beam represents emission from molecules within the jet rather than emission from molecules which are entrained. It is also interesting to note that the H<sub>2</sub> emission in the blueshifted lobe is seen over a similar part of the jet as is the emission from the optical jet knots. The optical knots are most likely explained as internal working surfaces in the jet caused by variable ejection at the source (e.g., Morse et al. 1993b). Morse et al. determined shock velocities of order 20 km/s, low enough to allow the survival of H<sub>2</sub> molecules.

The evidence for molecular gas in the HH 34 jet presented above is at most indirect and based on very faint H<sub>2</sub> features. It would be desirable to study the connections between optical shock emission and H<sub>2</sub> emission in more detail (higher resolution and sensitivity) in HH 34 and also the other beams presented above. A further test could be made by high resolution spectroscopy: if the H<sub>2</sub> emission was due to the same shocks causing the optical knots, then the velocity of the H<sub>2</sub> gas should be the same as the velocity of the optically emitting gas, and the line widths should be rather narrow, of order the inferred shock velocities of about 20 km/s. It may be encouraging that recently Davis et al. (2000c) found the H<sub>2</sub> emission in the HH 1 jet beam to be confined to the core of the jet and apparently enveloped by higher excitation [Fe II] emission. This is interpreted as evidence that the H<sub>2</sub> emission indeed arises from molecular gas in the jet beam itself rather than in the jet-ambient interface. Unfortunately, this still does not give an answer to the question whether the gas was already molecular as it was injected (disk wind?) or formed later on inside the jet beam.

### H<sub>2</sub> bow shocks and multiple working surfaces

The working surfaces of protostellar jets in general are well explained as bow-shock-like structures. Theoretical bow-shock models are fairly successful in reproducing many observed features of Herbig-Haro and H<sub>2</sub> bow shocks (see Section 2.3 and references therein). The H<sub>2</sub> jet survey presented here provides a great hunting ground for further, possibly nearly ideal bow shocks (e.g., bow shocks which are not (yet) fragmented). A more detailed examination of those might then reveal important information on the physics governing the propagation of the jet. For example, bow shock models can be used to probe the conditions (density, ionisation fraction, magnetic fields) in the pre-shock medium. Besides the bow shock propagation velocity, the cooling mechanisms of the jet gas as well as the magnetic fields of the jet can be expected to have an influence on the appearance of the bow shock (e.g., Blondin et al. 1989, 1990; Smith 1991; Stone & Norman 1993, 1994a; Cerqueira et al. 1997; Frank et al. 1998; O’Sullivan & Ray 2000). Needless to say, any information about the structure and strength of magnetic fields in and around the jet would be highly welcome, since magnetic fields are supposed to have a major role in driving and collimating the jets. In Fig. 18, a gallery of rather undisturbed bow shock structures identified from the survey data is presented.

Besides these rather fine examples of bow shocks, there are a large number of more disordered groups of knots presumably indicating fragmented bow shock type working surfaces. Most of the jets found here consist of several of such fragmented working surfaces with emission-free sections separating the individual working surfaces. Table 5.3 lists a number of flows showing rather clear evidence for major multiple working surfaces. The H<sub>2</sub> jet #5 consists of a chain of rather compact, but resolved knots. The spacings between the knots as well as their brightness are reminiscent of the knots in HH 212. The knot separations in this jet correspond to timescales of the order of 60 to 100 years. Leaving the H<sub>2</sub> jet #5 aside, the typical separations between working surfaces are of the order of  $2_{-1}^{+2}$  arcminutes. This corresponds to projected separations of the order of  $0.26_{-0.13}^{+0.26}$  pc, or timescales of order  $1300_{-650}^{+1300}$  years (assuming a typical jet speed of 200 km/s). This confirms the usual notion (see Section 2.2) that multiple

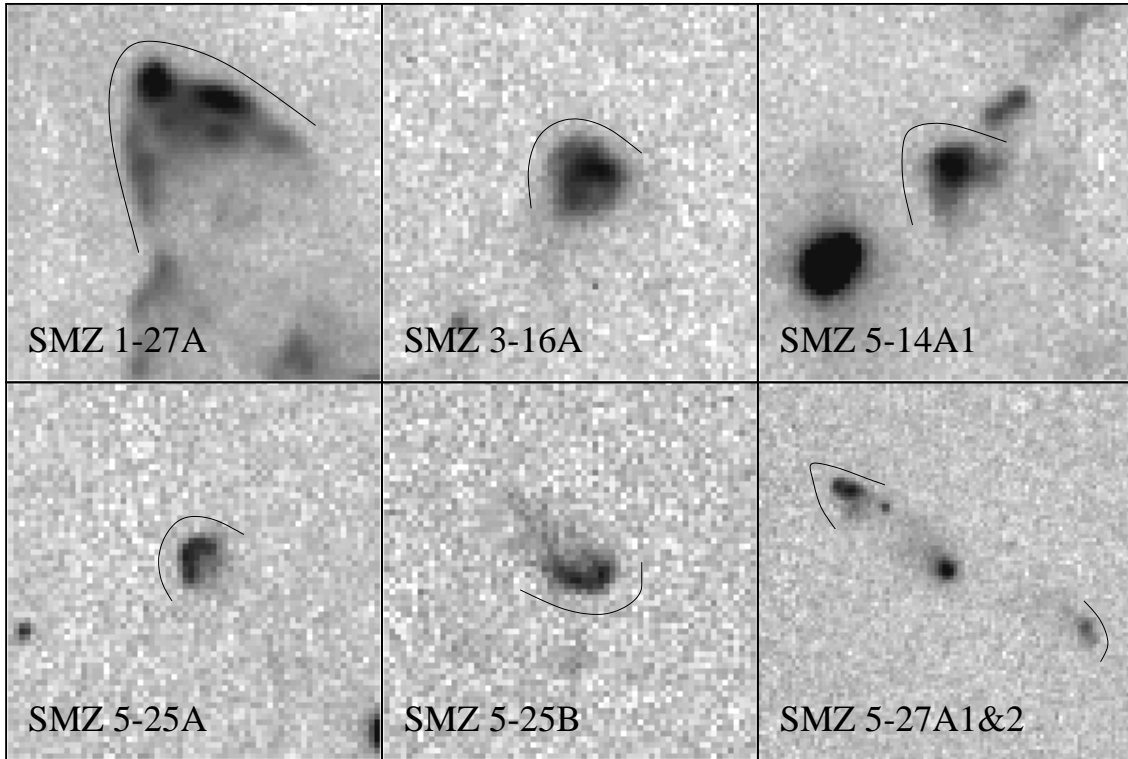


Figure 18: A gallery of largely undisturbed bow-shock-like working surfaces (the image sizes are  $26'' \times 26''$  ( $0.''4/\text{pix}$ ) except for the last panel; there it is  $48'' \times 48''$ ).

working surfaces might correspond to ejection events occurring on timescales of the order of a few thousand years.

The L1641-N giant flow ( $\text{H}_2$  jet #49) might be particularly interesting. It is one of the longest jets known. Its southern lobe extends over 4 pc and is traced in  $\text{H}_2$ , whereas its northern lobe is seen as a chain of Herbig-Haro objects extending over 6 pc from the source (Reipurth et al. 1998; Mader et al. 1999). A multitude of working surfaces traces its path. Since it is so long, it offers an opportunity to explore the time behaviour of its driving source over a very long time scale: the dynamical time scale of the southern jet lobe corresponds to 20000 years (at an assumed propagation velocity of 200 km/s). The first part of this lobe, well south of the L1641-N cluster, is traced by the group of  $\text{H}_2$  features comprising SMZ 5-23. SMZ 5-23 consists of a series of filamentary features, the most prominent being SMZ 5-23E, and a group of bright knots (SMZ 5-23G) at its southern end. The filaments SMZ 5-23B and SMZ 5-23D north of the bright SMZ 5-23E, and the filament SMZ 5-23F (between SMZ 5-23E and SMZ 5-23G) may form additional, fainter working surfaces. Then a rather long section of the jet lobe is free from emission (between SMZ 5-23G and SMZ 6-2), followed by a series of 3 more features (SMZ 6-2, SMZ 6-4A, SMZ 6-4B, and possibly SMZ 6-4C). Then again a large gap follows, until the flow terminates in SMZ 6-16. Taking each of these features as a working surface of the same level of a hierarchy, there seem to be strong deviations from a strict periodicity. However, the features may trace two levels: a periodicity of order  $2'$  (1300 years), modulated by a larger cycle (traced roughly by SMZ 5-23G, SMZ 6-4, and SMZ 6-16) with a period of order  $8'$  (5300 years). This would be consistent with other observations (e.g., of HH 212, Zinnecker et al. 1998), which suggest a hierarchical system of ejection events, with larger amplitude outbursts occurring at larger periods, smaller amplitude outbursts at shorter periods. However, apparently it is necessary to study more than just one outflow lobe to give more weight to this suggestion (or to disprove it): additional “10-parsec scale” flows have to be found, in order to be able to follow the ejection history over timescales of a few ten thousand years, rather than

Jet	S1	d1	S2	d2	S3	d3	S4	d4	S5	d5	S6
#3	1-4	1'1	1-5	1'5	1-6						
#5	1-8A	0'11	1-8B	0'15	1-8C	0'10	1-8D				
#31	3-9	2'2	3-7	2'0	3-6						
#49	5-23E	5'3	5-23G	4'6	6-2	2'5	6-4A	1'8	6-4B	9'2	6-16
#51	5-16	3'4	5-12	2'9	5-11						
#55	5-26A	2'1	5-26B								
#58	5-27A1	1'7	5-27C								
#58	5-27A2	1'4	5-27B								
#67	7-6	1'5	7-5								
#67	7-7A	1'3	7-9	1'9	7-10	3'3	7-14				

Table 2: Jets with multiple working surfaces.  $S_x$  gives the H<sub>2</sub> feature forming a working surface, and  $d_x$  gives the angular separation between  $S_x$  and  $S_{x+1}$ . In the cases of the H<sub>2</sub> jets #58 and #67 both lobes are shown separately.

a few thousand years.

### A few words about binaries

One important aspect of low mass star formation has so far been completely ignored: most stars do not form as single objects, but in binary or multiple systems (e.g., Mathieu 1994; Reipurth & Zinnecker 1993; Brandner & Köhler 1998; Zinnecker & Mathieu 2000). One could expect that this is somehow reflected in the jet survey. Even more, it has been proposed recently that multiplicity, particularly the decay of nonhierarchical triples, might play a crucial role in determining the protostellar evolution and the presence and structure of jets and outflows (Reipurth 2000).

A binary could signal its presence in two ways in the jet survey. The more direct way is the presence of two jets originating in the same protostellar system. This presupposes that the “double jet” is separable through the observations, and that both binary components have accretion disks capable of driving a jet. The second condition is presumably fulfilled: e.g., in a mid-infrared ( $\lambda = 10 \mu\text{m}$ ) study of a sample of young binaries, Stanke & Zinnecker (2000) found  $10 \mu\text{m}$  emission generally from both components, indicating the presence of (inner, AU sized) accretion disks in both binary components. For the first condition, it would be helpful if the jets from the binary were not parallel (even if the separation of two parallel jets was larger than the angular resolution of the observations, it would be questionable whether the morphology of the flows, which might wind around each other, would allow a conclusive identification of two flows instead of one). This would imply that the disks driving the jets were not coplanar. Although a number of young binaries are known with apparently misaligned disks and jets (e.g., HK Tau: Stapelfeldt et al. 1998; HH 1/2/HH 144: Reipurth et al. 1993b; HH 111/HH 121: Gredel & Reipurth 1993; Reipurth et al. 1999b), it is not known whether these are exceptions or more the rule (e.g., Jensen et al. 2000).

Besides the previously known HH 1/2/HH 144 binary jets (H<sub>2</sub> flows #64 and #65), no other clear candidates for such a configuration of two misaligned jets from a binary source have been found in the present survey. The far-infrared source driving the Haro 4-255 molecular outflow might be an exception. It has been argued by Davis & Eisloffel (1995) and Aspin & Reipurth (2000) that this molecular outflow is in fact a superposition of two outflows. In fact, a  $450 \mu\text{m}$  map (not shown here) taken recently with SCUBA at the JCMT reveals this source to be a wide double with a projected separation of order  $10''$  (4500 AU). Besides the H<sub>2</sub> outflow #72 from this (double) source, some more H<sub>2</sub> knots (SMZ 8-3; SMZ 8-5) are found in its surrounding, possibly forming another, independent, misaligned flow.

Wiggles and bends in the outflow path may be another, more indirect indicator of the binarity of a jet driving source. They might be due to shifts in the position of the driving source (Fendt & Zinnecker



1998), or due to wobbling and precession of the accretion disk driving the jet induced by the gravitational pull of the companion (e.g., Terquem et al. 1999; Bate et al. 2000). It is, however, not clear whether this mechanism works. One object in which it *might* be at work could be the prototypical HH 46/47 jet. This jet shows wiggles and bends over various length- and timescales, from short-period wiggles best seen in the HST images (Heathcote et al. 1996) to a gradual change in the overall outflow direction of  $20^\circ$  over a timescale of 9000 years (Stanke et al. 1999; Reipurth & Heathcote 1991). Recently, the driving source of HH 46/47 was indeed found to be a binary (Reipurth et al. 2000b). Besides HH 46/47, many other jets show bends and wiggles along their beams, often with S-shaped point symmetry (e.g., HH 34: Bally & Devine 1994; Devine et al. 1997; Eislöffel & Mundt 1997; RNO 43: Bence et al. 1996).

Besides the previously known S-shaped HH 34 giant flow ( $H_2$  flow #55, which is however not very clearly traced in  $H_2$  emission), the L1641-N giant flow ( $H_2$  flow #49) shows some evidence for a gradual change in flow direction. Since its driving source is located in the L1641-N cluster, it is hard to tell whether the change in flow direction is due to a binary companion or due to interaction with other cluster members. The HH 43 giant flow ( $H_2$  flow #67) might also show some (not very pronounced) S-shaped bend. The clearest example revealed by the  $H_2$  survey for a (possibly periodic) bending outflow is the north-eastern lobe of the L1641-S3 giant outflow ( $H_2$  flow #76, see Fig. 78; see Stanke et al. 2000). Close to the source, it is oriented at a position angle of  $\sim 60^\circ$ , then it turns north to a position angle of  $\sim 30^\circ$ , then at the position of the bright  $H_2$  filament SMZ 9-6A it bends to an eastward flow direction (outlined by  $H_2$  feature SMZ 9-5), before finally turning back north to roughly its original position angle of  $60^\circ$ . Since the direction of the flow at its end is about the same as at its beginning, the outflow lobe might just delineate one period of precession. The timescale for the precession period in this system is then  $\sim 9000$  years, assuming a flow propagation velocity of 200 km/s. Following the arguments given by Terquem et al. (1999), this implies a binary separation (very roughly) on the order 10 to 100 AU, corresponding to angular separations of the order  $0''.1$  in Orion. It should be possible to resolve separations of order a few tenths of an arcsecond with existing or future instruments in the mid-infrared and millimetre wavelength ranges (e.g., the diffraction limit at  $10\ \mu\text{m}$  at Keck/VLT/LBT is of the order of  $0''.3$ , at  $5\ \mu\text{m}$   $0''.15$ ; much higher resolution will be possible once the interferometric modes are available; the upcoming ALMA (sub)millimetre interferometer will also have an angular resolution of better than  $0''.1$ ). Thus the driving source of the L1641-S3 outflow might be a further test case for companion-induced jet precession.

## 5.4 Flow lengths

One observable of a protostellar jet which is relatively easy to obtain is its length (the term “length” will be taken to measure the full extent of a flow including both lobes). This, however, presupposes that one can observe the flow over its entire length. Besides extinction possibly hiding parts of the flow, this is not at last a technical issue. Early observations of Herbig-Haro jets from young stars made use of the new, sensitive, but initially small CCD arrays. The jet lengths which were found at these times were typically of order a few arcminutes or a few tenths of a parsec (e.g., Dopita et al. 1982; Mundt & Fried 1983; Mundt et al. 1987; Reipurth et al. 1986; Reipurth 1989a, 1989b). The situation changed with the advent of large field of view cameras equipped with large format CCD detectors: it is now well known that many Herbig-Haro jets extend over several parsecs (parsec-scale or giant Herbig-Haro jets), among them some of the prototypical examples (e.g., Bally & Devine 1994, 1997; Bally et al. 1995; Devine et al. 1997, 1999a; Eislöffel & Mundt 1997; Ogura 1995; Reipurth et al. 1997, 1998; Mader et al. 1999; Stanke et al. 1999). A similar evolution can right now be followed at infrared wavelengths, as infrared array detectors get bigger (Stanke et al. 1998, 2000; Eislöffel 2000). A few jets may even extend over more than 10 parsecs (e.g., the L1641-N giant flow).

The situation is somewhat different for the molecular CO outflows. Here, the first examples were preferentially very massive flows from high mass star forming regions, which were at the beginning observed with large beams (i.e., poor angular resolution, but comparably large area coverage). This, and their generally large distances demonstrated early on that molecular outflows could extend over several parsecs (e.g., Mon R2: 4 pc; see, e.g., Bally & Lada 1983). However, the full extent of the molecular outflows associated with low mass protostars in nearby star forming regions was often underestimated, since time constraints generally did not allow one to search very large areas at sufficient sensitivity. However, increasing sensitivity of millimetre detectors and the use of scan mapping techniques (On-the-Fly mapping) now also allows mapping of large areas in low mass star forming regions with high sensitivity, which now also reveals the parsec-scale extent of molecular CO outflows from low mass protostars (e.g., VLA 1623: Dent et al. 1995; RNO 43: Bence et al. 1996; Barnard 5: Bally et al. 1996a; Yu et al. 1999; L1448: Wolf-Chase et al. 2000; see also Padman et al. 1997).

Finally, the spectra of classical T Tauri stars often show a multitude of forbidden emission lines, often with broad or multiply peaked line profiles, generally explained as arising in anisotropic winds originating from the stars (e.g., Appenzeller et al. 1984; Appenzeller & Mundt 1989). The line profiles indicate gas motions up to several hundred km/s. The spatial structure of these winds on sub-arcsecond scales has been constrained using long-slit spectroscopy (e.g., Solf 1989; 1997; Hirth et al. 1997; Bacciotti et al. 2000). It is apparent that the line emission regions are displaced from the stellar position. The displacement is usually greatest along a particular position angle, and less pronounced or absent along other position angles. This suggest an anisotropic flow preferably along one direction: a collimated jet. Since this phenomenon usually shows emission regions (jets) confined to within a few arcseconds from the star (corresponding to few hundred AU at the distance to the most nearby star forming regions), these objects have been termed “microjets”. Some of the objects recently have been imaged at 0.1 arcsec resolution, indeed showing evidence for short, well collimated jets (Dougados et al. 2000). It should be noted, however, that the short jet lengths inferred from these observations might be an underestimate of the true jet length: in some cases, Herbig-Haro objects can be seen at larger distances from the stars, indicating a much greater jet length (e.g., Mundt & Eisloffel 1998).

What determines the apparent flow lengths? Are the currently discovered giant Herbig-Haro jets (sometimes called superjets) still the inner parts of “hyperjets” which extend still further out? If so, why don’t we see them? Are the fields-of-view still too small, or do the jets fade from view as they leave the cloud and there is no more material which they could run into and produce shocks (e.g., Eisloffel 2000)? An unbiased sample of flows, as provided by the H<sub>2</sub> survey, should allow one to determine the typical extent of protostellar flows, the number of parsec-scale flows among all flows, and to study the possible evolution of the flow length with time.

Throughout this section it should be kept in mind that the flow lengths under discussion certainly are lower limits in most cases for several reasons (see Section 4.3). Furthermore, in the following discussion of parsec-scale flows among the H<sub>2</sub> jets I will use the term “parsec-scale” jet to mark those jets, which are visible over a total projected length of more than one parsec (e.g., Eisloffel & Mundt 1997 and Eisloffel 2000 use the term “parsec-scale” jet also for slightly shorter jets).

Fig. 19 shows the distribution of the flow lengths for all flows (except for the flows #26, #27, and #28 in the Orion Nebula area). The solid histogram represents flows from the “certain” group only, whereas the dotted histogram includes both the “certain” and “uncertain” flows (both distributions seem to be very similar). The thin lines represent gaussian fits to the histograms, the solid (dotted) line stands for the “certain” (“certain” plus “uncertain”) flows. It is seen that most flows indeed extend over some tenths of a parsec: the mean flow length is 0.54 pc, if only “certain” flows are considered (0.46 pc for both “certain” and “uncertain” flows), and the median flow length is 0.25 pc (0.22 pc) for the “certain” (“certain” plus “uncertain”) flows. The drop in flow numbers for flows shorter than the

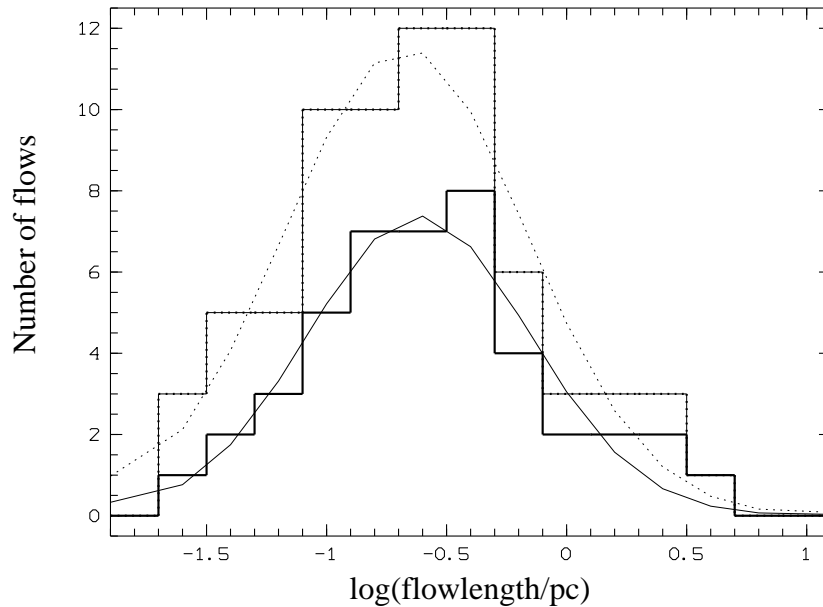


Figure 19: The distribution of flow lengths, including flows from the entire survey field, except for the flows in the Orion Nebula area (flows # 26, # 27, and # 28). The solid histogram shows the distribution for flows from the “certain” group only, the dotted histogram represents all flows (“certain” and “uncertain” group). The thin lines represent gaussian fits to the histograms.

median flow length is presumably real, since flows much shorter than this length should be easily seen (0.1 pc corresponds to about  $40''$  in Orion).

From the “certain” group, 5 flows (11 %) extend over more than one parsec; including the “uncertain” flows, 7 (10 %) extend over more than a parsec. Thus the fraction of parsec-scale flows as found here is about 10 %. Eislöffel (2000) reports a parsec-scale flow frequency of  $\sim 25\%$ . At first glance, the parsec-scale flow fraction of 10 % found here seems to be lower. However, since the flow lengths measured here are certainly a lower limit for many flows, the fraction of parsec-scale flows (among the  $H_2$  detectable flows at least) may well be as high as 20 to 25 %. It should also be noted that the observations done by Eislöffel (2000) were not really unbiased, but targeted towards some regions of known highly active star formation activity, containing a number of very young, very active (Class 0) sources.

To search for evolutionary trends in the flow length, in Fig. 20 the distribution of flow lengths is plotted for the individual infrared classes of the driving sources. For the Class 0 sources, the mean flow length is 0.73 pc, the median is 0.28 pc for the “certain” flows (0.85 pc and 0.32 pc respectively, if both “certain” and “uncertain” flows are taken into account). For the Class I sources, the mean flow length is 0.66 pc, the median is 0.42 pc (0.58 pc and 0.37 pc) for the “certain” (“certain” plus “uncertain”) group. For the Class II sources finally, the mean length is 0.26 pc, the median is 0.24 pc (0.21 pc and 0.24 pc) for the “certain” (“certain” plus “uncertain”) group. These results seem to indicate a decrease in typical flow length, at least when going from Class I to Class II. The situation is not so clear when going from Class 0 to Class I. It seems that there is no typical or characteristic flow length for the Class 0 sources, with very short flows, medium sized flows, and very long flows showing up with the same likelihood.

On the other hand, a clear trend appears to be present in the fraction of parsec-scale flows, when going from Class 0 to Class II: 2 out of 7 (29 %) “certain” flows (3 out of 8 (38 %) of the “certain” plus “uncertain” flows) from Class 0 objects extend over more than a parsec, which is about three times the parsec-scale flow fraction of the entire sample. For the Class I driven flows, 3 out of 25 (12 %) of the “certain” flows (3 out of 31 (10 %) of the “certain” plus “uncertain” flows) extend over more than a

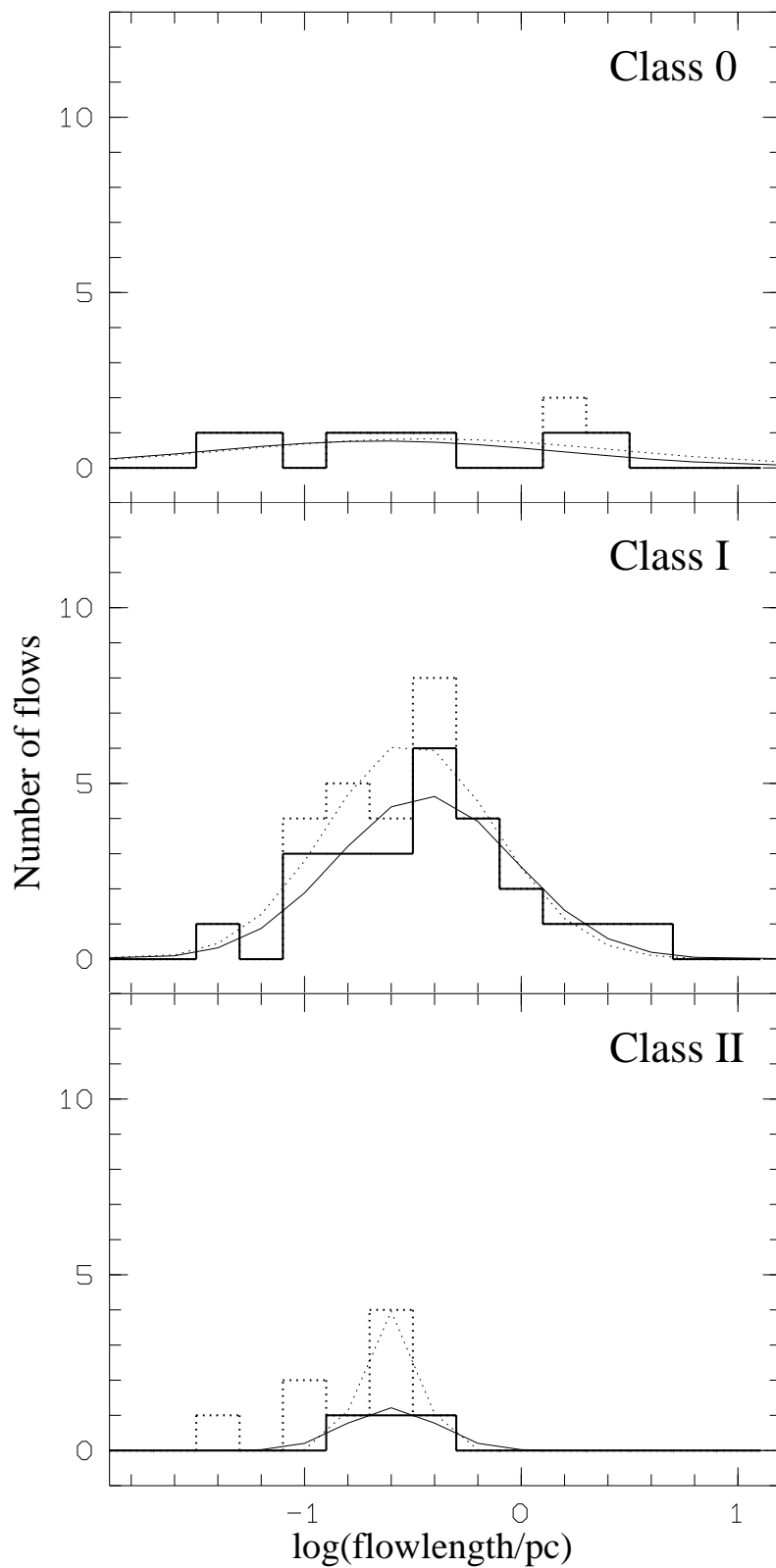


Figure 20: The distribution of flow lengths, sorted by the infrared class of the driving sources. The solid lined histogram shows the distributions for flows from the “certain” group only, the dotted histogram represents all flows (“certain” and “uncertain” group). The thin curves represent gaussian fits to the histograms.

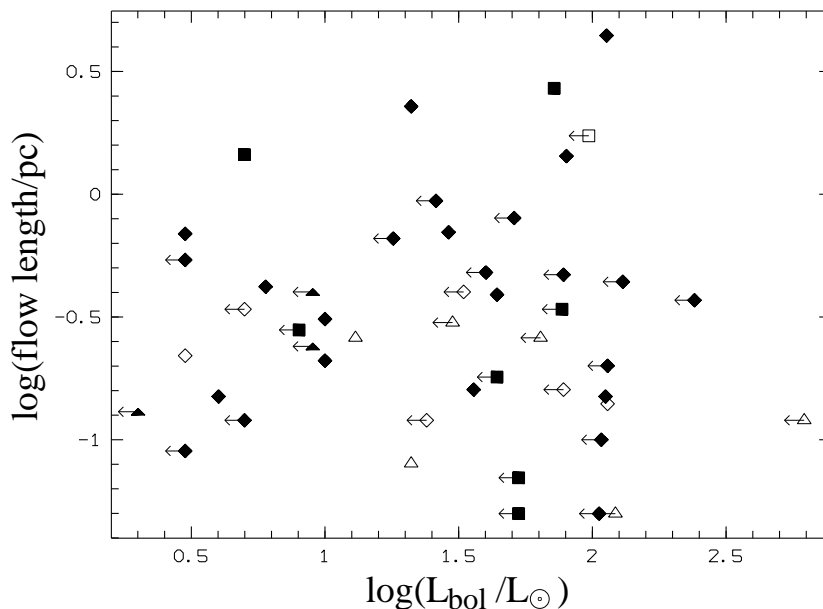


Figure 21: Flow lengths as a function of the bolometric luminosities of their driving sources. Filled symbols mark objects from the “certain” group, whereas open symbols mark objects from the “uncertain” group. Class 0 sources are plotted as squares, Class I sources as diamonds, and Class II sources as triangles.

parsec, whereas none of the flows driven by a Class II source is longer than a parsec.

The difference in the parsec-scale flow fractions found from group to group are presumably real, not induced by some observing effects. There is no reason, why a parsec-scale flow from a Class 0 protostar should be seen more easily than one from a Class I source. It is not likely that Class I parsec-scale flows break out of the parent molecular cloud more frequently, then being invisible in  $H_2$ , since Class I sources are likely to be distributed in the same manner in the cloud as are Class 0 sources. Also the cloud cores, from which stars form and which may be more massive and denser around the younger Class 0 sources, are much smaller than a parsec. Thus, once a flow has reached parsec-scale extent it should run, on average, into the same kind of medium, namely the normal average cloud environment, or alternatively with the same likelihood for all kinds of sources break out of the cloud and disappear in the intercloud medium. Thus the likelihood to recognize a parsec-scale flow as such should be the same for all kinds of driving sources. Consequently, the difference in the fraction of detected parsec-scale flows from group to group must have its reason in a true difference in the frequency of parsec-scale flows within these groups.

In Fig. 21 the flow lengths are plotted as a function of the bolometric luminosity  $L_{\text{bol}}$  of their driving sources. There is no clear evidence for a correlation between these observables. High luminosity sources do drive very long flows as well as very short flows, and the same is true for low luminosity sources (the different flow lengths cannot be a consequence of projection only; for a sample of jets with similar, parsec-scale lengths, but different, random orientations, projection would yield much fewer jets with a short apparent length than are seen in Fig. 21; note that the scaling in the plot is logarithmic). There may be a trend for the longest flows to be driven by more luminous sources. For example, the two longest flows #49 (the L1641-N giant flow) and #76 (the L1641-S3 giant flow) are both driven by sources with bolometric luminosities of order  $100 L_{\odot}$ . On the other hand, the flow #67 (the HH 43/38/64 giant flow) is driven by a source with a bolometric luminosity of only  $\sim 4 L_{\odot}$ .

To search for possible trends with evolutionary stage, in Fig. 22 the flow lengths are plotted as a function of the bolometric luminosities of their driving sources, sorted by the infrared class of the

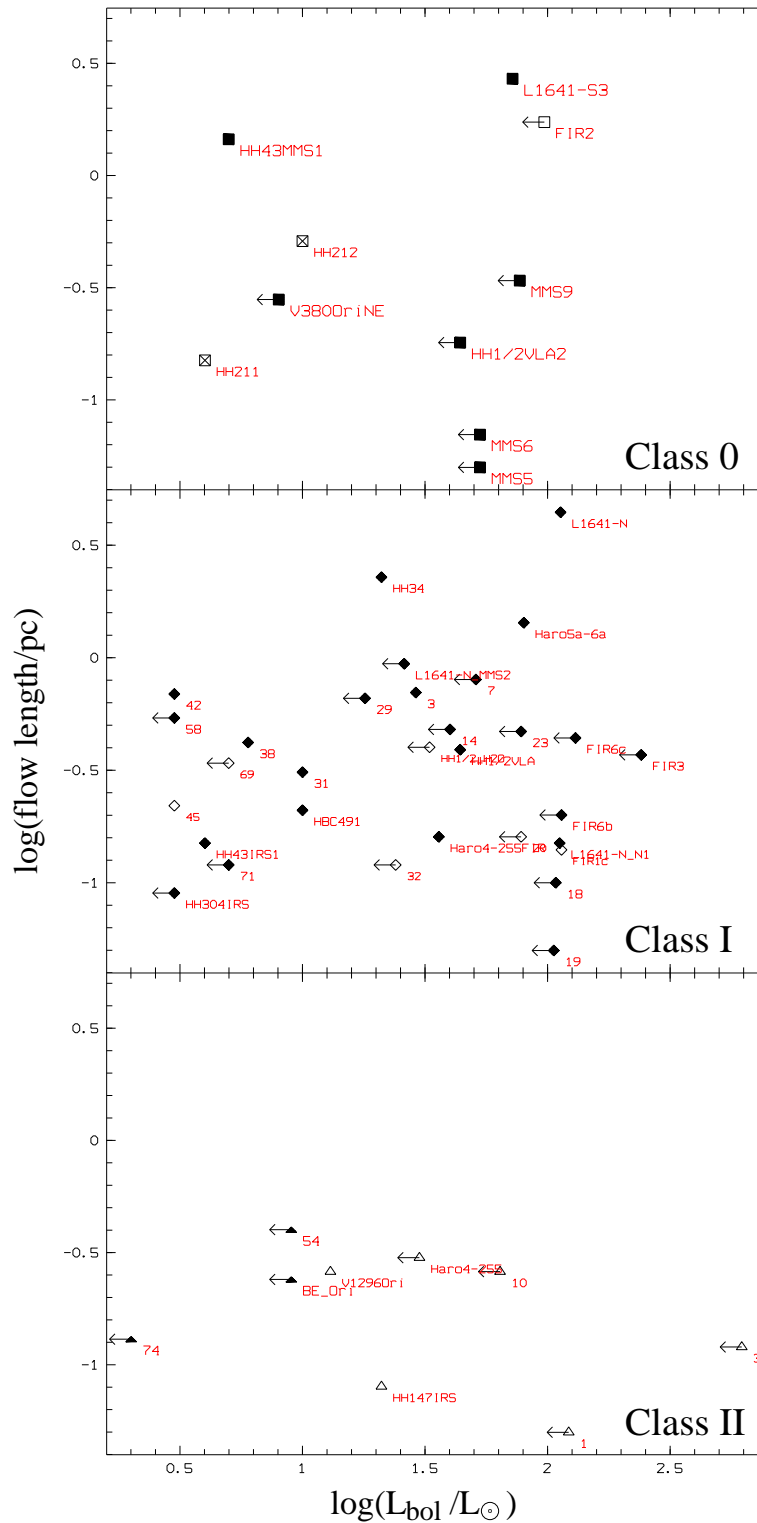


Figure 22: Flow lengths as a function of the bolometric luminosities of their driving sources, sorted by the infrared class of the driving source. Filled symbols mark objects from the “certain” group, whereas open symbols mark objects from the “uncertain” group. Class 0 sources are plotted as squares, Class I sources as diamonds, and Class II sources as triangles. The locations of the Class 0 driven prototype H<sub>2</sub> flows HH 211 and HH 212 are also shown in the upper panel.

driving source. Again, no clear correlations are visible between flow length and  $L_{\text{bol}}$  of the driving source.

The data analyzed in this section suggest that the driving source luminosity is not the main ingredient in determining the outflow length. Instead, there appears to be a strong dependency on the evolutionary stage of the driving source, particularly if the likelihood of producing parsec-scale jets is considered: about 1/3 of the Class 0 source flows, only 1/10 of the Class I flows, and none of the Class II source flows is found to be longer than a parsec. Note also that the Class I parsec-scale flow driving sources tend to appear as rather early Class I sources, being very faint in the K-band, but rather bright at millimetre wavelengths. Particularly, the driving source of the longest flow in the sample (#49, the L1641-N flow) is detected at near-infrared wavelengths as a small, faint reflection nebulosity only, it is also only moderately bright at 10  $\mu\text{m}$ , but has a high far-infrared luminosity.

## 5.5 H<sub>2</sub> luminosities

The measurement of the total shock luminosity in a flow gives information about the instantaneous energy supply for the flow. This is complementary to the common measurements of the kinetic energy (or kinetic luminosity) or the momentum (or momentum supply rates) of molecular outflows, which measure the energy/momentum supply averaged over the entire outflow life time. For example, a young flow will presumably be associated with a rather small amount of molecular outflow gas, but produce strong shocks, whereas an old outflow may consist of a large reservoir of moving gas, which has been accelerated over the lifetime of the flow, but the driving jet may already have been faded, not producing strong shocks anymore (e.g., Smith 2000). Such a comparison of the shock luminosity of a flow with the energetics of the associated molecular outflow may give important clues about the evolutionary stage of an outflow.

So far, comparisons of H<sub>2</sub> luminosities with molecular outflow properties have been limited to rather few objects (e.g., Davis & Eislöffel 1995). The survey for H<sub>2</sub> jets presented here will allow us in future a much more constraining investigation of this issue with corresponding observations of associated molecular outflows. But also the H<sub>2</sub> survey alone (together with the identification of the flow driving source and the determination of their evolutionary stage) will already give some clues about the evolution of shock activity and the instantaneous energy supply throughout the evolution of a protostar.

In the following the total H<sub>2</sub> luminosities of the flows in the sample will be analyzed. The total H<sub>2</sub> luminosity has been assumed to be 10 times the luminosity emitted in the 2.12  $\mu\text{m}$   $v = 1-0$  S(1) line. This is a value typical for molecular shocks expected in flows from young stars (Smith 1995).

Throughout the following section, there is one big caveat which should be kept in mind: no correction for extinction was applied to the H<sub>2</sub> photometry, since no measure for the extinction is available (see Section 4.3).

Figure 23 shows the distribution of the H<sub>2</sub> luminosities of all flows (except for the flows #26, #27, and #28 in the Orion Nebula area). The solid histogram represents flows from the “certain” group only, whereas the dotted histogram includes both the “certain” and “uncertain” flows. Both distributions appear to be fairly similar, possibly with a tendency towards more fainter flows in the “uncertain” group. This is easily understood, since fainter flows are certainly harder to identify as such.

Compared to the distribution of flow lengths (Fig. 19), the distribution of the H<sub>2</sub> luminosities is apparently much broader, less well peaked, and the gaussian fits to the histograms (indicated by the thin lines in Fig. 19) seem to be less satisfactory. But in contrast to the flow lengths, in the case of the H<sub>2</sub> luminosities the faint end is determined by the sensitivity of the observations (a combination of surface brightness sensitivity, morphology of the features making up the flow, and the willingness/ability of the

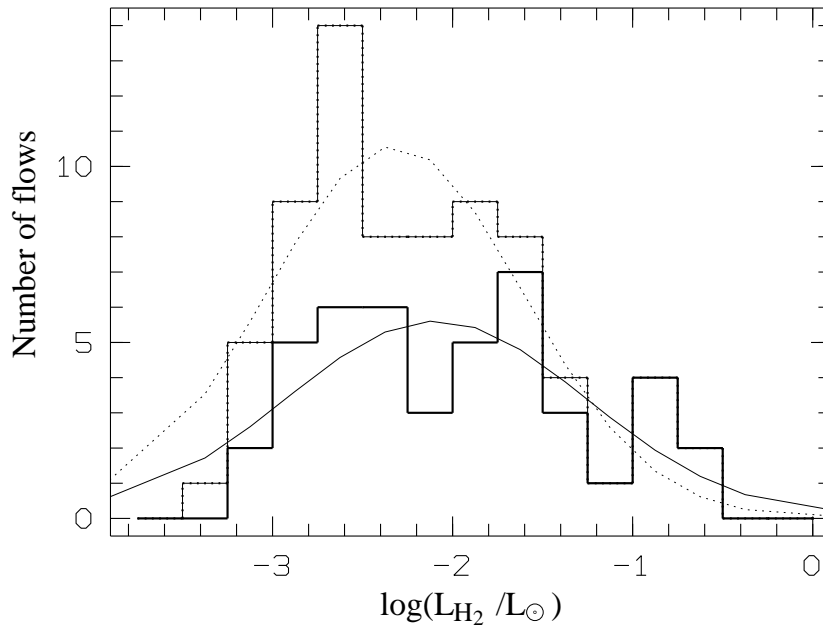


Figure 23: The distribution of flow H<sub>2</sub> luminosities, including flows from the entire survey field, except for the flows in the Orion Nebula area (flows #26, #27, and #28). The solid histogram shows the distribution for flows from the “certain” group only, the dotted histogram represents all flows (“certain” and “uncertain” group). The thin lines represent gaussian fits to the histograms.

observer to recognize a number of features as parts of a flow). More sensitive observations will certainly reveal more fainter flows. In fact, the distribution of H<sub>2</sub> luminosities between  $\log(L_{\text{H}_2}/L_{\odot}) \sim -3$  and  $-1.5$  may well be represented by a straight horizontal line, which may easily continue towards even fainter flows.

To search for evolutionary trends in the flow H<sub>2</sub> luminosities, in Fig. 24 the distributions of  $L_{\text{H}_2}$  are plotted for the individual infrared classes of the driving sources, together with gaussian fits to these distributions. Generally it is seen that the gaussians do not provide compelling fits to the histograms. The Class 0 outflows cover the entire observed luminosity range, apparently with some tendency towards high luminosity flows. The luminosity distribution of Class I sources resembles that of the entire flow sample, showing a very broad, poorly defined peak or plateau. Although there are some high luminosity flows from Class I sources, the typical Class I outflow seems to be of intermediate to low H<sub>2</sub> luminosity. Finally, at the Class II stage, only low H<sub>2</sub> luminosity flows are found.

In Fig. 25 the H<sub>2</sub> luminosities of the flows are plotted as a function of the bolometric luminosities of their driving sources. There is apparently some correlation between these parameters, with some objects falling off this correlation at very high and very low H<sub>2</sub> luminosities. The situation becomes clearer when  $L_{\text{H}_2}$  is plotted versus  $L_{\text{bol}}$ , with the objects sorted by infrared classes: now for the Class I sources a very clear correlation is seen, with  $L_{\text{H}_2}$  increasing with  $L_{\text{bol}}$ , although there appears to be quite some scatter around this correlation. In contrast, the Class 0 sources form a very inhomogenous group with no correlation, but populating mainly the upper part of the plot area, while the Class II sources all are found in the lower part of the plot, covering only a small interval in  $L_{\text{H}_2}$ , but the entire range of observed  $L_{\text{bol}}$ .

The scatter of the Class 0 sources over the  $L_{\text{H}_2}$  vs.  $L_{\text{bol}}$  plot as well as the fact that almost all of their bolometric luminosities represent upper limits only suggests a case by case view on this plot. The only two Class 0 sources with a rather reliably determined bolometric luminosity are HH 43 MMS1 and L1641-S3 MMS1, with the latter one presumably being at the transition between Class 0 and Class I.



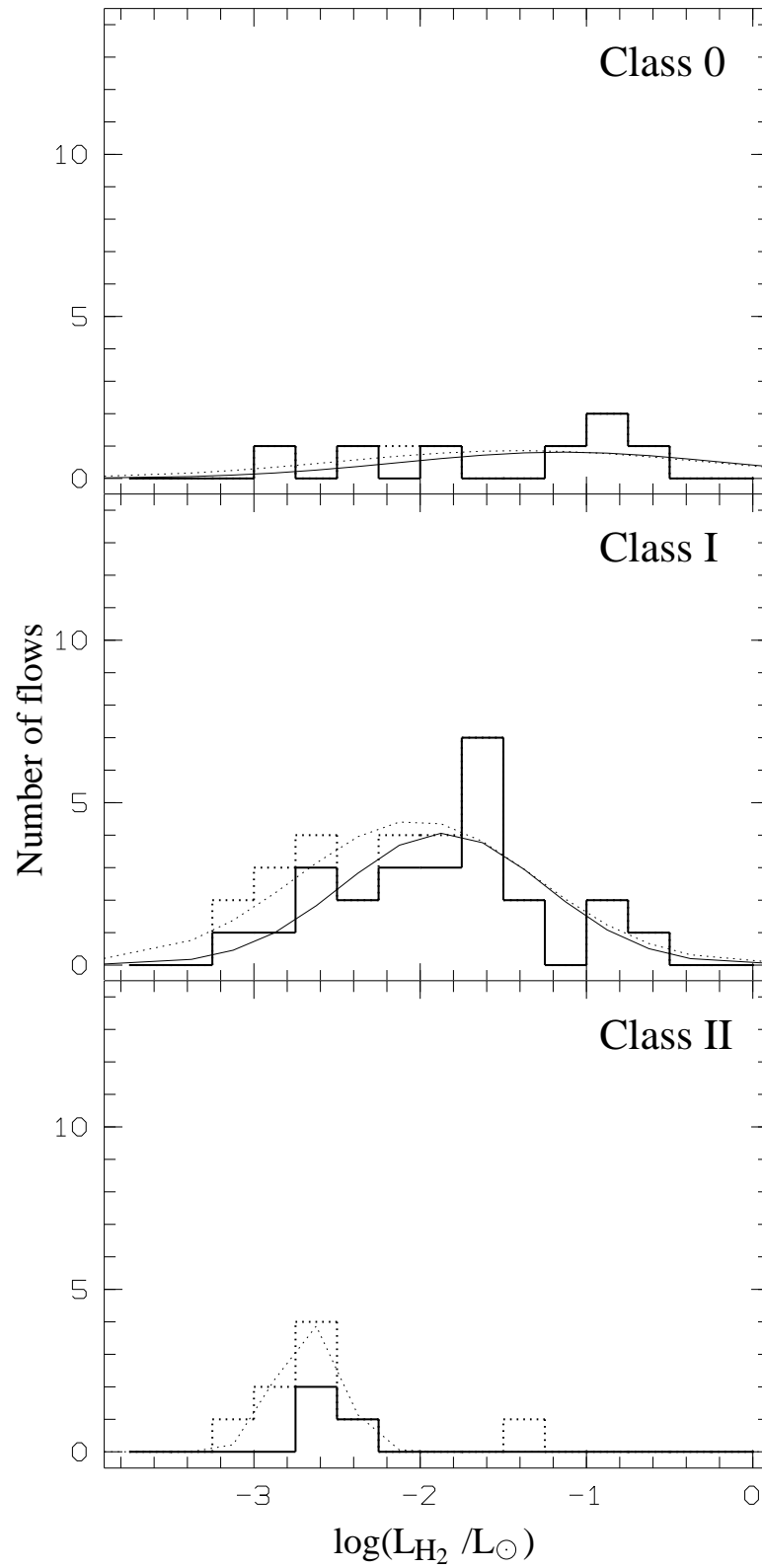


Figure 24: The distribution of flow H<sub>2</sub> luminosities, sorted by the infrared class of the driving sources. The solid lined histogram shows the distributions for flows from the “certain” group only, the dotted histogram represents all flows (“certain” and “uncertain” group). The thin curves represent gaussian fits to the histograms.

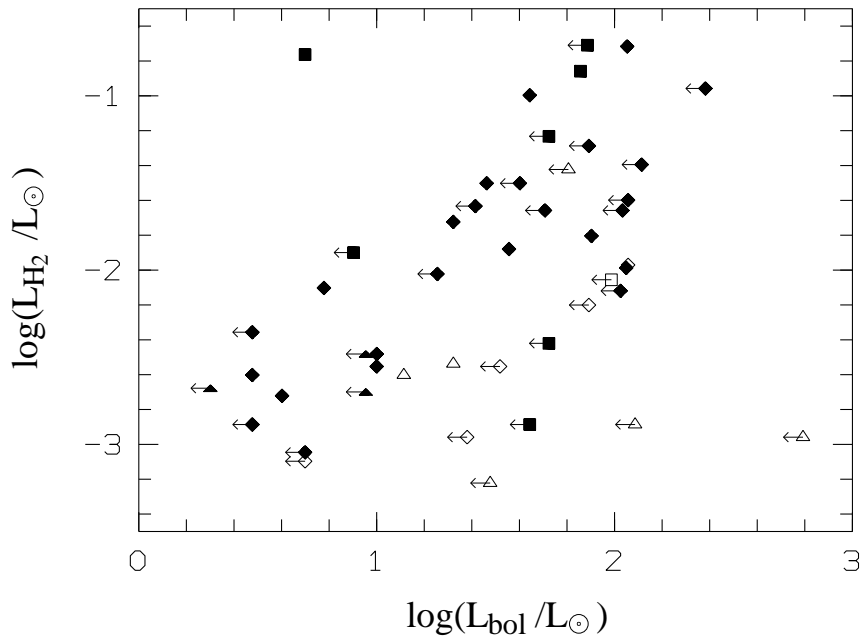


Figure 25: Flow H<sub>2</sub> luminosities as a function of the bolometric luminosities of their driving sources. Filled symbols mark objects from the “certain” group, whereas open symbols mark objects from the “uncertain” group. Class 0 sources are plotted as squares, Class I sources as diamonds, and Class II sources as triangles.

The bolometric luminosity of V 380 Ori NE is also given as an upper limit, which might however be rather close to the true value. All the other sources are located in regions with strong confusion at IRAS wavelengths, presumably leading to heavy overestimates of their bolometric luminosities (MMS 5, 6, and 9, as well as FIR 2 are located in OMC-2/3, and HH 1/2 VLA2 only a few arcseconds from HH 1/2 VLA1; also the assignment of the Class 0 stage to this source is very doubtful; see also discussion of the individual sources in the Appendix C). For all these sources, the bolometric luminosities should be taken with great care, and additional mid- to far-infrared photometry is highly desirable. Finally, in addition to the Class 0 flows identified in the Orion A survey, the locations of the two prototype H<sub>2</sub> jets HH 211 and HH 212 (which are also driven by Class 0 sources) are plotted.

Now, regarding the uncertain bolometric luminosity sources with great care (particularly HH 1/2 VLA2, FIR 2, and MMS 6), it appears that the typical Class 0 source location in the  $L_{\text{H}_2}$  vs.  $L_{\text{bol}}$  plot is to the left and above the Class I location, i.e., at lower bolometric luminosities and higher H<sub>2</sub> luminosities. Although this is a not very well established finding, this might suggest a more efficient conversion of accretion energy into outflow H<sub>2</sub> luminosity than for Class I sources. A more in-depth discussion of this issue is deferred to Chapter 7.

In summary, the analysis of the flow H<sub>2</sub> luminosities in this section shows that there may be a trend for more H<sub>2</sub> luminous flows to occur at earlier evolutionary stages.

## 5.6 H<sub>2</sub> jets and molecular (CO) outflows

About 15-20 molecular outflows are known in the survey area (the exact number depends on the detailed interpretation of various CO features). As noted in Section 2.2 the term “molecular outflow” will be reserved for the CO outflows, in which the bulk of the material is seen in CO, rather than for the H<sub>2</sub> jets, in which only shock heated molecular gas is seen. A detailed comparison of molecular outflow data from the literature with the H<sub>2</sub> jet data of the present survey is performed in Appendix D.

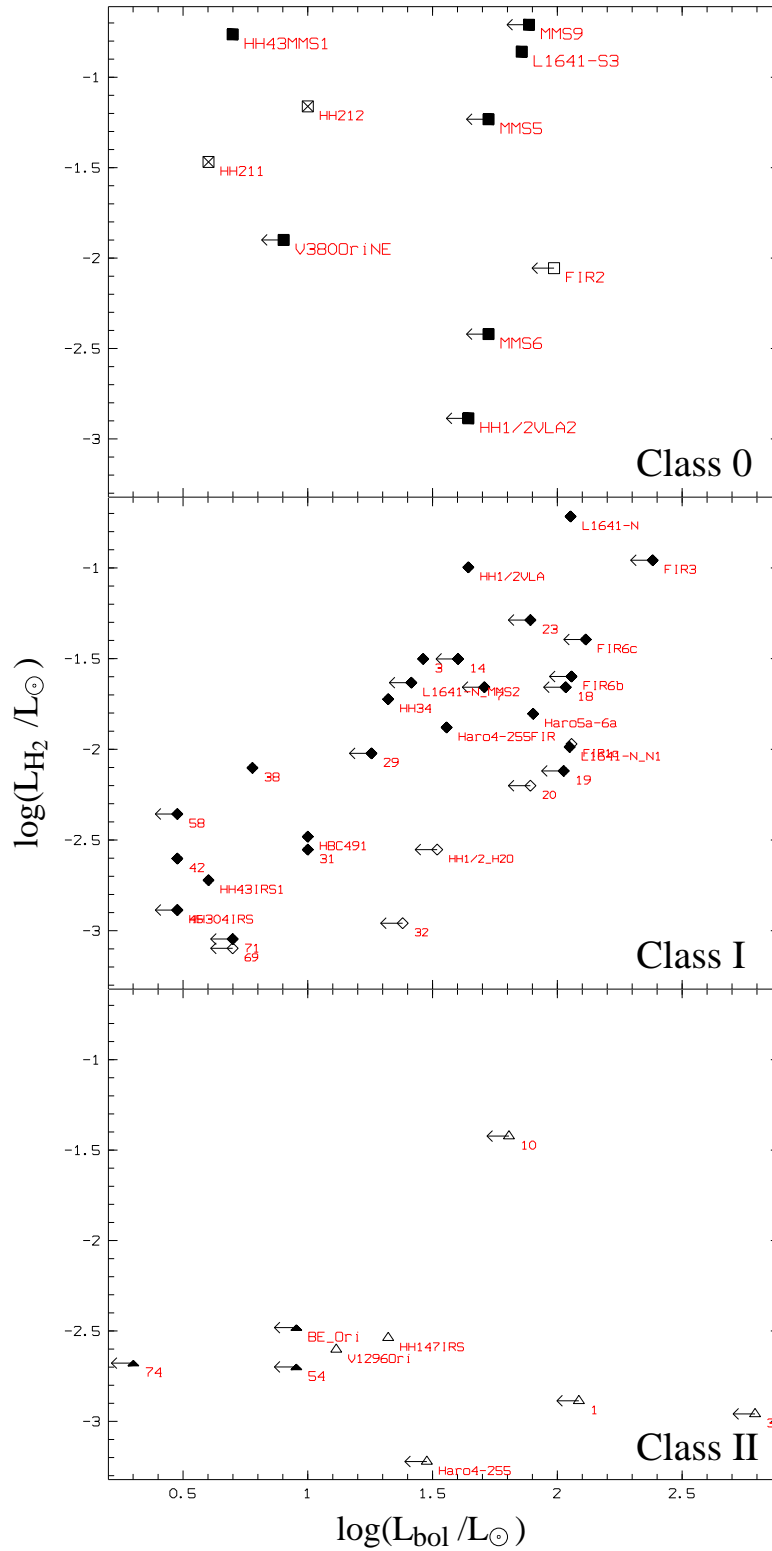


Figure 26: Flow H<sub>2</sub> luminosities as a function of the bolometric luminosities of their driving sources, sorted by the infrared class of the driving source. Filled symbols mark objects from the “certain” group, and open symbols mark objects from the “uncertain” group. Class 0 sources are plotted as squares, Class I sources as diamonds, and Class II sources as triangles. The locations of the Class 0 driven prototype H<sub>2</sub> flows HH 211 and HH 212 are also shown in the upper panel.

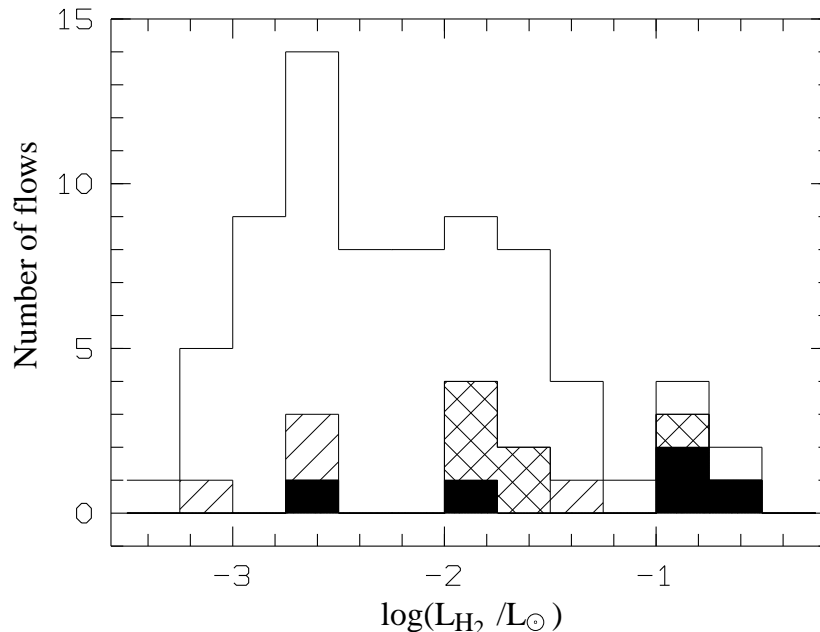


Figure 27: The plot shows the frequency distribution of  $L_{\text{H}_2}$  for H<sub>2</sub> jets associated with high velocity CO for various data sets. The filled histogram represents the distribution of  $L_{\text{H}_2}$  for the CO outflows found in the unbiased survey by Fukui and coworkers (Fukui et al. 1986, 1989; Fukui 1988). The criss-crossed histogram represents H<sub>2</sub> flows likely associated with CO flows found otherwise, and the hashed histogram shows the distribution of  $L_{\text{H}_2}$  for H<sub>2</sub> flows whose association with CO outflows is somewhat uncertain. For comparison, the open histogram shows the frequency distribution of  $L_{\text{H}_2}$  for all H<sub>2</sub> flows found during the present H<sub>2</sub> survey.

The following H<sub>2</sub> jets appear to be associated with high velocity CO: **#3, #6, #17, #49, #53, #55, #59, #61, #64, #72, and #76**. More uncertain CO associations are found for the H<sub>2</sub> flows **#2, #25** (and a number of other suggested flows in the OMC-2/3 area), **#27, #28, #54, and #73**. Only the CO counterparts to the H<sub>2</sub> flows **#17, #49**, possibly **#61, #72, and #76** were detected (i.e., not necessarily discovered) in the unbiased survey by Fukui and coworkers (Fukui et al. 1986, 1989; Fukui 1988). Loosely speaking, the Fukui et al. unbiased survey found only 5 out of more than 70 active H<sub>2</sub> outflows in the survey area, i.e., the detection rate is less than 10% for the unbiased CO survey. All other CO outflows in the area were found either in surveys for CO outflows around known young stars in the area, IRAS sources in the area, or in dedicated searches for CO counterparts to optical flows, i.e., in more or less biased CO outflow searches. In contrast to the “low detection rate” of the unbiased CO search, the unbiased H<sub>2</sub> search presented here detected most and missed only very few of the known CO flows in the area. These are the blueshifted lobe of the CO outflow apparently driven by MMS 8 in OMC-2/3 (Chini et al. 1997b, but see Yu 2000), the OMC-1S outflow found by Schmid-Burgk et al. (1990), possibly the large scale CO lobes in the L1641-N area found by Reipurth et al. (1998), and the blueshifted lobe south of Re 50 N.

In Figure 27 the frequency distributions of  $L_{\text{H}_2}$  are plotted for the H<sub>2</sub> flows associated with flows found by Fukui and coworkers (filled histogram), for flows associated with other CO outflows (criss-crossed and hashed histogram), and for all H<sub>2</sub> flows found during the present H<sub>2</sub> survey. There is a clear trend for the flows associated with CO outflows to be the more H<sub>2</sub> luminous ones. This is particularly the case for the flows found by Fukui and coworkers during their unbiased survey for CO outflows. The H<sub>2</sub> survey is thus able to reveal a population of outflows which is fainter in H<sub>2</sub> emission than the outflows found in searches for high velocity CO.

The findings presented in this section can be summarized as follows: a comparison of the results

of the H<sub>2</sub> survey with published results of searches for high velocity CO flows in the same area demonstrates that H<sub>2</sub> searches are a more powerful tool to locate outflows from young stars. The number of flows discovered through H<sub>2</sub> imaging is considerably larger than the number of flows revealed in CO searches. This is particularly the case, if the (unbiased) H<sub>2</sub> survey is compared to the unbiased CO outflow search done by Fukui and coworkers: the unbiased H<sub>2</sub> search revealed more than 10 times as many outflows as the unbiased CO search. It has furthermore been shown that the H<sub>2</sub> search recovered the large majority of known CO outflows. The H<sub>2</sub> flows found to have a CO counterpart tend to be the brighter H<sub>2</sub> flows. In addition, a large number of fainter flows is found. It is a plausible assumption that fainter H<sub>2</sub> flows are also associated with molecular outflows, which are too weak to be detected in the commonly performed CO searches. The H<sub>2</sub> search thus not only reveals more outflows, but also a population of less energetic and less massive molecular outflows. Follow up CO observations of the H<sub>2</sub> flow sample found in the present work will help to extend the knowledge about molecular outflows to less energetic flows, possibly driven by very low mass objects (brown dwarfs?).

### 5.7 Orientation of the jets with respect to the large scale magnetic field

It is a widely advocated suggestion that the collapse of a cloud may proceed more easily along magnetic field lines (e.g., Mouschovias 1976; Shu et al. 1987), since the partly ionized gas can slide easily along the field lines, but not perpendicular to it, leading to flattened structures oriented perpendicular to the field lines. In some cases, evidence has been found that this may happen on the size scale of molecular clouds. The Mon R2 core is seen to be elongated perpendicular to the large scale magnetic field in that area (Hodapp 1987; Zaritsky et al. 1987), and similar results are found for some clouds in the Taurus complex (Moneti et al. 1984; Tamura et al. 1987; Heyer et al. 1987b), the  $\rho$  Ophiuchi cloud core (Sato et al. 1988), and the NGC 1333 region (Tamura et al. 1988). On the other hand, Vrba et al. (1988) find that the magnetic field in L1641 at a mean position angle of 110° is inclined by only 35° with respect to the cloud position angle (145°), and shows a large scatter around the mean position angle. They conclude that the large scale magnetic field was not important in the collapse of the L1641 cloud. On the other hand, the densest part of the Orion A giant molecular cloud, the integral shaped filament containing OMC-1/2/3, is oriented in a north-south direction, roughly perpendicular to the apparently roughly east-west oriented magnetic field lines in that part of the cloud (Appenzeller 1974; Breger 1976), so maybe only the collapse of this northern part of the cloud has been governed by magnetic fields. In fact, recent 850  $\mu$ m dust polarimetric observations showed that the field is oriented perpendicular to the filament in the OMC-3 region (Matthews & Wilson 2000).

On the smaller scale of a molecular cloud core, there may be two mechanisms leading to disks perpendicular to the field lines. Magnetic braking of the rotating cloud core is more efficient for rotational motions not parallel to the direction of the magnetic field (Mouschovias & Paleologou 1980), thus cloud cores will favourably keep rotational motions with the spin axis parallel to the magnetic field, and lose the spin component perpendicular to the field. When the core then collapses to form a star, a collapse predominantly along the magnetic field lines would result in the formation of a disk perpendicular to the field lines, which in turn would produce an outflow oriented parallel to the field lines. However, observations addressing this point so far did not provide a consistent picture.

On the one hand, a number of young stellar objects are known which appear to have disklike structures perpendicular to the ambient field and/or outflows parallel to the ambient magnetic field. These include the outflow from the Mon R2 core (Loren 1977; Bally & Lada 1983), Cep A (Cohen et al. 1984), and the prototype L1551-IRS5 outflow (Snell et al. 1980; Nagata et al. 1983; Moneti et al. 1984). Hodapp (1984) measured the polarization of a number of the infrared sources driving the Bally & Lada (1983) flows and found evidence for flattened structures perpendicular to the flows; these disks

in turn appeared to be preferentially oriented perpendicular to the ambient magnetic field (implying that the flows are oriented parallel to the field). Sato et al. (1985) found disks perpendicular/flows parallel to the ambient field in more than half of their sample, but not for all of the sources under study. Strom et al. (1986) also claimed that most Herbig-Haro outflows are aligned with the ambient field (70% of all flows include angles less than  $30^\circ$  with the field lines). Heyer et al. (1987a) found the HH 7-11 flow in the NGC 1333 region to be roughly parallel to the ambient field, but the HH 12 flow in the same cloud was found to be misaligned with the field by  $60^\circ$ . Note also that recently many more flows were found in NGC 1333 (Hodapp & Ladd 1995; Bally et al. 1996b) with no recognizable preferred orientation with respect to the field lines. In the case of L1641, Vrba et al. (1988) find that 5 out of the 6 Herbig-Haro flows, that were known in L1641 at that time, were parallel (to within  $\pm 40^\circ$ ) to the mean orientation of the large scale magnetic field. In contrast, Morgan et al. (1991) do not find a preferred orientation of molecular CO flows with the magnetic field orientation nor any other preferred orientation in L1641.

On the other hand, Aitken et al. (1993) find evidence for toroidal magnetic fields in most of the objects in their sample, which are difficult to explain in an object in which the cloud collapsed along the field lines of large scale ambient fields (which would result in poloidal field lines). Heyer et al. (1986) observed a number of cloud cores and did not find evidence for a systematic orientation of the cloud cores perpendicular to the ambient field. Finally, recent  $850\ \mu\text{m}$  polarimetry of pre-stellar cores showed that there is a significant deviation of the field orientation and the orientation of the minor axes of these cores (Ward-Thompson et al. 2000).

To summarize, there is evidence for collapse and subsequent outflow activity along magnetic field lines in many clouds and young stellar objects, but not in all. In some cases, very large differences between flow orientation and ambient field orientation are found.

Besides collapse along magnetic field lines, one might also speculate about other mechanisms working on the size scale of a cloud, which could determine the spin axis of a young star (and consequently its outflow axis). For example the galactic (differential) rotation might supply angular momentum, leading to a spin axis perpendicular to the galactic plane, thus circumstellar disks might be preferentially coplanar with the galactic plane and outflows perpendicular to it.

The large number of flows found in this work in a single molecular cloud with known field orientation naturally suggests to re-investigate the possible relationship between the flow orientations and the field orientation or any other particular orientation. Polarization surveys in order to determine the orientation of the magnetic field in and around the Orion A giant molecular cloud have been carried out by Appenzeller (1974), Breger (1976), and Vrba et al. (1988). The measurements by Appenzeller suggest field lines at a position angle of about  $100^\circ$  in the Orion A region, Bregers measurements in the area around the Orion Nebula also suggest a similar field orientation, and Vrba et al. determined a field position angle of  $110^\circ$  for the L1641 dark cloud south of the Orion Nebula, however with a fairly large scatter in the field direction. I will in the following adopt a position angle of the field lines of  $110^\circ$  according to Vrba et al.

To search for possible overall trends in alignment, Fig. 28 shows a histogram of the frequency of position angles for all flows. There is apparently no preferred flow orientation, and ironically the only bin with no flows in it (from the “certain” group) is just the  $110^\circ$  bin at the position angle of the ambient field. Vrba et al. state that 5 out of 6 Herbig-Haro flows (i.e., 83%) in L1641 are aligned to within  $\pm 40^\circ$  with the ambient field. For comparison, only 36% of the flows in the “certain” group (34% if both “certain” and “uncertain” flows are included) are aligned to within  $\pm 40^\circ$  with the field. For a randomly oriented sample a total of 45% flows would be expected to be aligned to within  $\pm 40^\circ$  with the field, thus a systematic alignment of the flows can be ruled out on the scale of the entire survey field. This result does also not change when other field position angles are assumed; to illustrate this, Fig. 29 shows

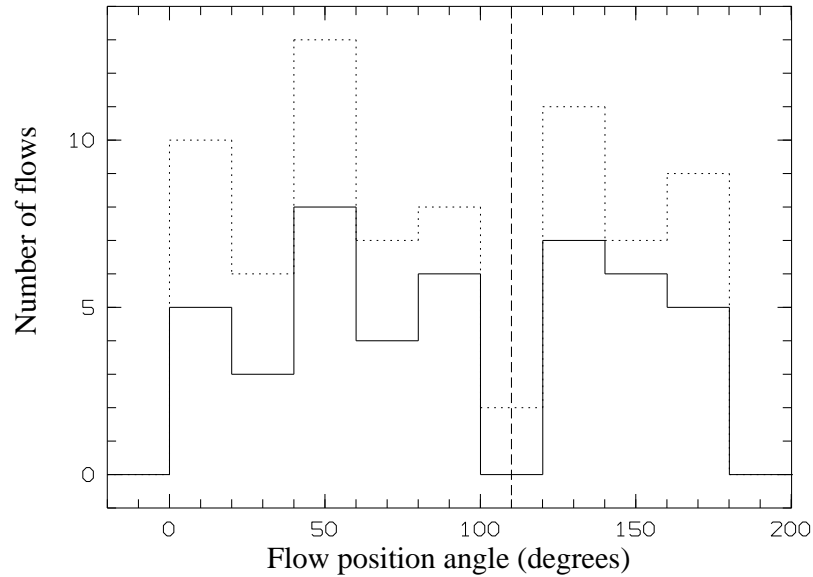


Figure 28: The distribution of flow position angles, including flows from the entire survey field, except for the flows in the Orion Nebula area (flows # 26, # 27, and # 28). The solid histogram shows the distribution of flows from the “certain” group only, the dotted histogram represents all flows (“certain” and “uncertain” group). The dashed vertical line indicates the orientation of the ambient magnetic field ( $110^\circ$ , see Vrba et al. 1988).

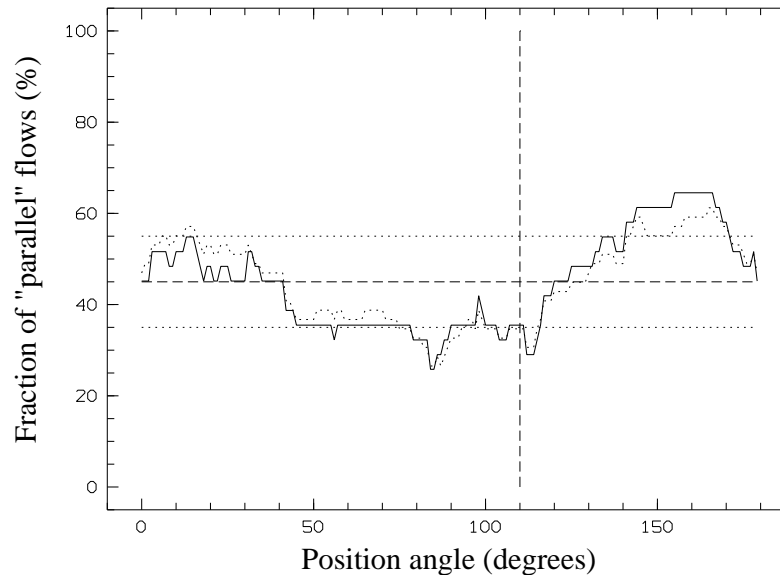


Figure 29: The fraction of flows “parallel” to a given position angle, including flows from the entire survey field, except for the flows in the Orion Nebula area (flows # 26, # 27, and # 28). “Parallel” in this case means “aligned to within  $\pm 40^\circ$ ”, to allow a comparison with the Vrba et al. (1988) statement that 5 out of 6 (83%) of the flows in L1641 are parallel (to within  $\pm 40^\circ$ ) with the ambient large scale field. The solid line represents flows from the “certain” group only, the dotted line all flows (“certain” and “uncertain” group). The dashed horizontal line indicates the fraction of “parallel” flows in a randomly oriented flow sample (45%). The dotted horizontal lines represent the typical statistical variations ( $1\sigma$ ). The dashed vertical line indicates the orientation of the ambient magnetic field as measured by Vrba et al. (1988) of  $110^\circ$ .

the fraction of the flows aligned (to within  $\pm 40^\circ$ ) with an arbitrary position angle. There is only little scatter around the value expected for a randomly oriented flow sample (45%), which can be attributed

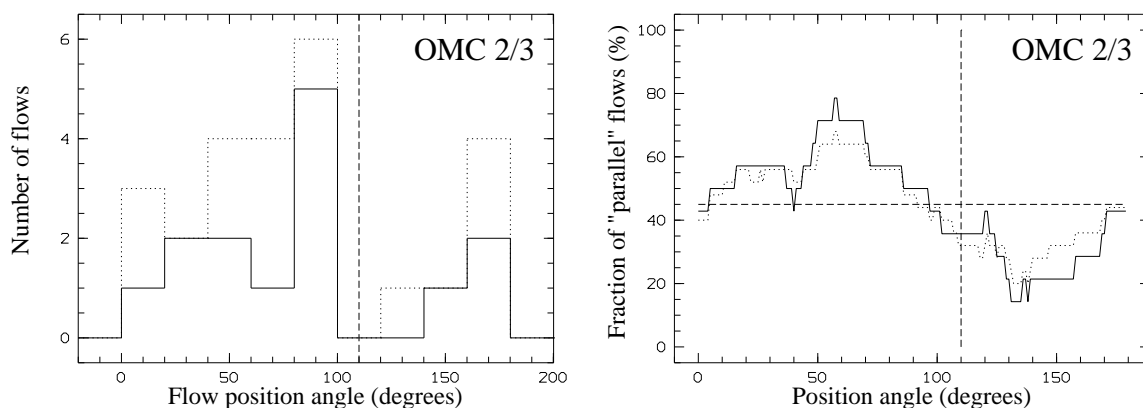


Figure 30: Same as Fig. 28 and Fig. 29, for the flows in OMC-2/3 only (flows # 1 to #25).

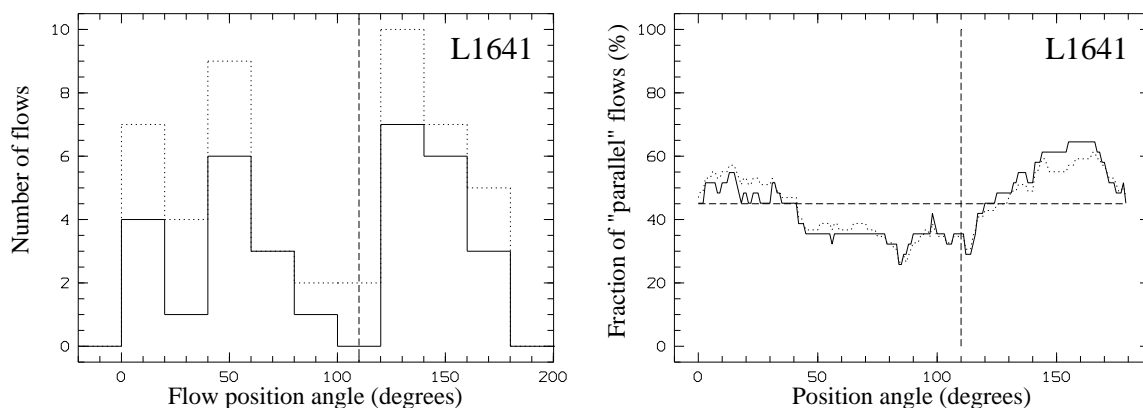


Figure 31: Same as Fig. 28 and Fig. 29, for the flows in L1641 only (flows # 29 to #76).

to statistical fluctuations (with typically 20 flows regarded as “parallel”, the statistical counting error is about 4.5 flows, or 10% of the total of 44 flows in the “certain” group; this statistical error is indicated by the horizontal dotted lines above and below the horizontal dashed line indicating the random sample fraction of 45%). Thus there appears to be no preferred flow orientation at all, neither parallel to the large scale magnetic field nor parallel or perpendicular to the cloud position angle ( $145^\circ$ ; this is also roughly the position angle of the galactic plane close to Orion).

To check whether this result depends on the environment or position of the flows within the cloud, the same analysis was repeated for the dense, highly active northern part of the survey area (i.e., the OMC-2/3 region) and the less active L1641 area south of the Orion Nebula. Again, no preferred flow orientations are recognizable. In the OMC-2/3 part, there may be some excess of flows at a position angle of  $\sim 90^\circ$ , i.e., perpendicular to the north-south running filament containing OMC-2/3. This may be real, but could possibly reflect the fact that flows, which are oriented perpendicular to the filament and break out of it quickly, are simply easier to detect because of the lower extinction further away from the densest part of the clouds. Note also that the smaller sample size of course also produces larger statistical fluctuations. In Fig. 32, the flow position angles (left panel) and the absolute deviations of the flow orientations from the orientation of the ambient field are plotted as a function of the position (declination) of the flows in order to see whether there is a north-south trend or whether there are some regions in the cloud where local alignments of the flows with the large scale field are present. Since the survey area is a rather narrow stripe extending more or less north-south, the declination of the flows is used as a standalone position indicator; for obvious reasons, the declination is plotted as the Y-axis.



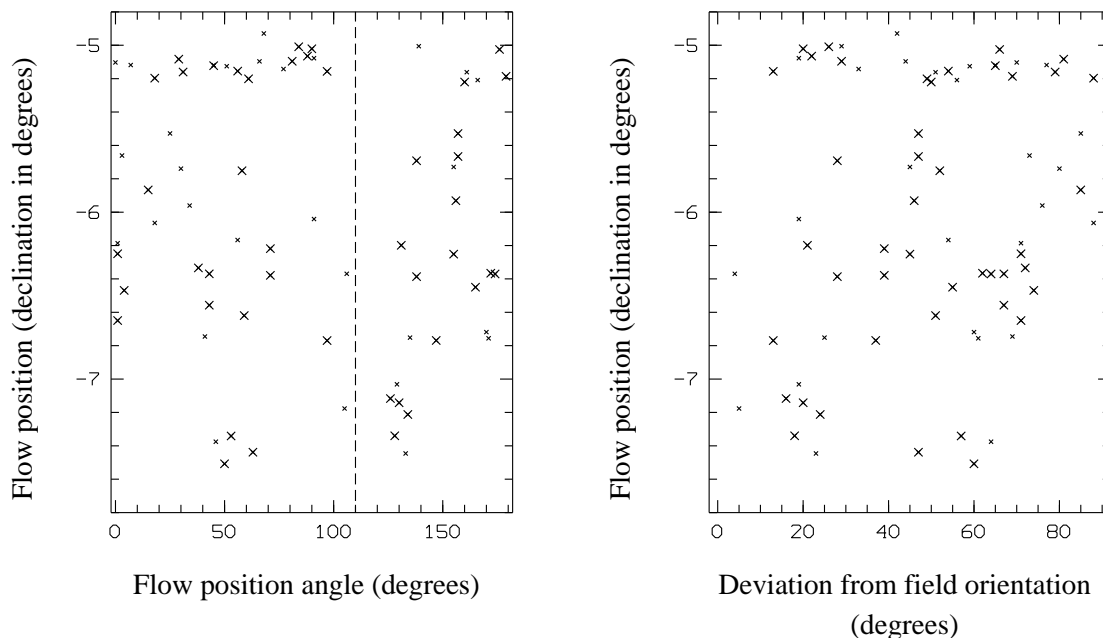


Figure 32: Flow position angles (left panel) and absolute deviation of flow orientations from the ambient field orientation (right panel) as a function of the position (declination) of the flows. To allow an easier comparison, the declination is plotted as the Y-axis. Big crosses mark the flows from the “certain” group, small crosses mark the “uncertain” flows.

No obvious systematic pattern is seen, perhaps with the exception of a slight deficiency of flows with the largest misalignments in the southernmost part of the survey area. Furthermore, there may be some small “clusters”, e.g., at  $\alpha \sim -5.1$ , position angle  $\sim 90^\circ$  (causing the excess of flows perpendicular to the north-south filament in OMC-2/3 noted above), at  $\alpha \sim -7.2$ , position angle  $\sim 130^\circ$ , and at  $\alpha \sim -7.4$ , position angle  $\sim 50^\circ$  (note also that the latter two groups, although closely spaced, are perpendicular to each other). Again, there are not very many flows in that part of the cloud, thus these “clusters” may also be only statistical fluctuations.

Finally, in Fig. 33 the jet lengths,  $H_2$  luminosities  $L_{H_2}$ , and the bolometric luminosities  $L_{bol}$  of the jet driving sources are plotted as a function of the jet position angle (left panels) and as a function of the absolute deviation of the jet position angle from the position angle of the ambient field (right panels). Again, there are no dependencies of these jet properties on the orientation of the jets with respect to the magnetic field or with respect to any other orientation.

To summarize, it appears that the jets in Orion A are randomly oriented, without any preferred orientation. In particular, the jets are neither parallel nor perpendicular to the ambient magnetic field (similar to the result of Matthews & Wilson 2000 for OMC-3 alone), nor are they parallel or perpendicular to the orientation of the molecular cloud (i.e., the galactic plane, to which Orion A is roughly parallel). It thus appears that the orientation of the spin axis of a young stellar object is not determined by the ambient large scale magnetic field orientation or by the galactic rotation. This does not necessarily exclude collapse along magnetic field lines. Observations as well as numerical simulations have shown that the magnetic field orientation on small scales may deviate from the large scale field orientation (Crutcher et al. (in prep.) for NGC 2024; Ostriker et al. 1999 for a low magnetization, turbulent cloud). Thus, although the jet orientations are not related to the orientation of the *large scale field*, they might still originate in disks which collapsed along the *local* field lines. However, recent  $850 \mu\text{m}$  polarization measurements in OMC-3 *do* trace the local magnetic field orientation in the dense cores on fairly small scales, and still Matthews & Wilson (2000) do not find an alignment of the jets in OMC-3

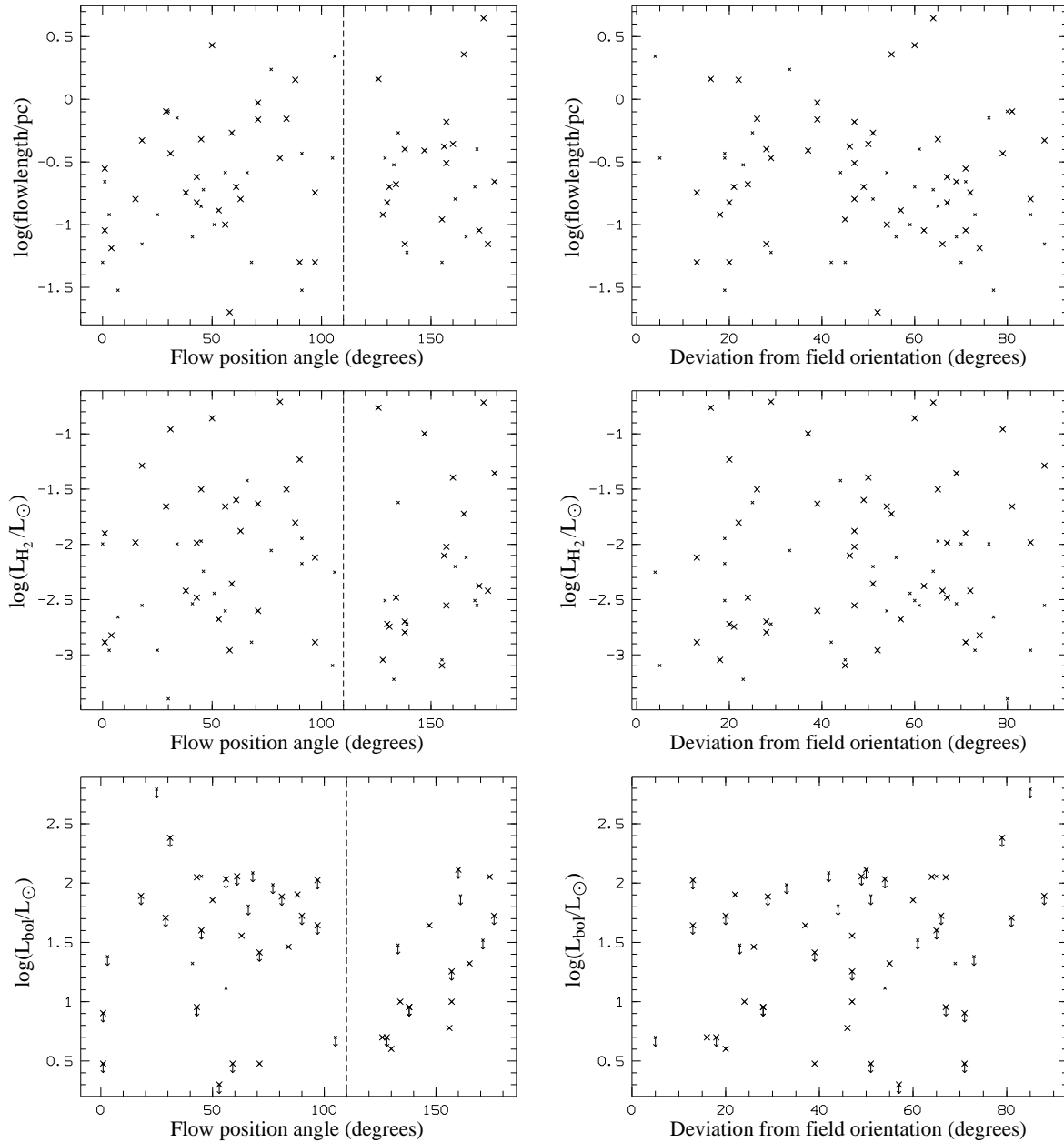


Figure 33: Flow lengths (upper row), H<sub>2</sub> luminosities  $L_{\text{H}_2}$  (middle row), and bolometric luminosities  $L_{\text{bol}}$  of the flow driving sources (lower row) plotted as a function of the flow position angle (left column) and as a function of the deviation of the flow orientation from the ambient magnetic field orientation. Big crosses mark the flows from the “certain” group, small crosses mark the “uncertain” flows.

with the magnetic field. The random orientation of the flows may thus suggest turbulence as the main ingredient in the determination of the spin axis of a star forming core (e.g., Burkert & Bodenheimer 2000), the young stellar object, its accretion disk, and consequently its outflow orientation.

Shu et al. (1987) argue that the collapse in giant molecular clouds and regions of clustered star formation may be “supercritical”, i.e., magnetic fields might not have a strong influence on the collapse. This could also explain the nonalignment of jets and large scale magnetic fields. Notably, in NGC 1333, another cluster forming area and harbouring many outflows, there also seems to be no systematic flow orientation (Hodapp & Ladd 1995; Bally et al. 1996b; Knee & Sandell 2000). Ironically,

the regions which are most likely to harbour a substantial number of outflows which would allow a statistical statement, seem to be the regions in which an alignment with the large scale field would be less likely: the turbulent and supercritical regions being located in giant molecular clouds and/or forming clusters. Thus, although the random orientation of the H<sub>2</sub> jets from the present survey seems to rule out an effect of large scale magnetic fields on the jet orientation, this might be a consequence of the location of the jets in a supercritical giant molecular cloud. The orientation of jets in a subcritical cloud like Taurus, which only allows the formation of a few isolated stars, may still be determined by the large scale fields; unfortunately, only few jets will be there, allowing only a statement based on a very small sample.

Finally, the orientations of the flows seems not to have a significant influence on the flow properties. Particularly, the flow lengths do not depend on the orientation of the flow with respect to the ambient magnetic field, suggesting that the ambient field does not have a large impact on the flow propagation, and does not facilitate or hinder flow propagation parallel or perpendicular to the field. It also seems not to influence strongly the collimation of the flows, which would also presumably lead to differences in flow lengths (a more poorly collimated flow would certainly more easily disperse).

## 6 H<sub>2</sub> Jets and CS cores

Tatematsu et al. (1993; T93 in the following) performed a CS (1–0) survey of a large part of the Orion A molecular cloud in order to detect and to characterize dense molecular cloud cores. The aim of this survey was to compare the cloud core properties in a giant molecular cloud (like Orion A) to those of cores in dark clouds of lower mass (such as, e.g., in Taurus). In total, T93 found 125 cloud cores, with masses ranging from 8 to 1800  $M_{\odot}$ . Since these dense cloud cores are believed to be the sites of ongoing or future star formation, it was reasonable to assume that there should be a significant number of very young stellar objects within this area. Thus the CS survey area offered itself as a target area for the H<sub>2</sub> jet survey: on the one hand, a considerable number of jets could be expected, thus allowing a study of a rich sample, on the other hand, the CS survey covered a small enough area on the sky to allow a sensitive infrared survey to be carried out in a reasonable amount of observing time.

The uniform coverage of the survey area in both, CS and in the infrared, now allows a study of possible relations of core properties with jet activity and properties.

### 6.1 Association of jets with CS cores

Figure 34 shows the locations of the representative positions of the H<sub>2</sub> jets superposed on the T93 CS map (“+” symbols indicate “certain” flows, “×” symbols flows from the “uncertain” group). The cloud cores identified by T93 are marked by circles, with the radii of the circles indicating their extent as given by T93. In the following, when using the term “position of a jet” this will mean “location of its representative position” (as defined in Section 4.1). Ideally and most reasonably, one would like to use the location of the driving source of the jets for the following analysis; however, for many jets no conclusive driving source identification is available so far. As introduced in Section 4.1, the representative position of a flow is the position of the driving source, if there is one identified, or some other characteristic position along the jet path.

The jet survey usually extends beyond the edges of the CS survey area. We thus first have to remove all those flows from the list whose positions are not within the T93 CS map. Local CS maxima on the edge of the CS map were not classified as cores by T93 (without defining the exact meaning of “on the edge”). Therefore I will also reject all flows which lie closer to the edge of the CS map than 0.1 pc, a typical cloud core radius. Thus the following flows are not included in the jet–CS core analysis: #29, #31, #34, #36, #42, #58, #74, and #75. Flow #58, in principle located within the area of core 88, is just on the edge of the CS map and apparently associated with CS emission, nevertheless it will not be included in the analysis of this chapter, because it is too close to the edge of the CS map.

Furthermore, all flows and cores in the immediate vicinity of the Orion Nebula will not be included in the analysis, since the bright nebular emission seriously affects the detectability of flows. We thus exclude all jets and cores between  $\delta = -5^{\circ} 15' 00''$  and  $\delta = -5^{\circ} 30' 00''$  (J2000). This affects the flows #26, #27, and #28, and the CS cores 17 through 41.

This leaves us with a subsample of 65 flows, with 38 belonging to the “certain” group, and 27 to the “uncertain” group, and 100 cloud cores.

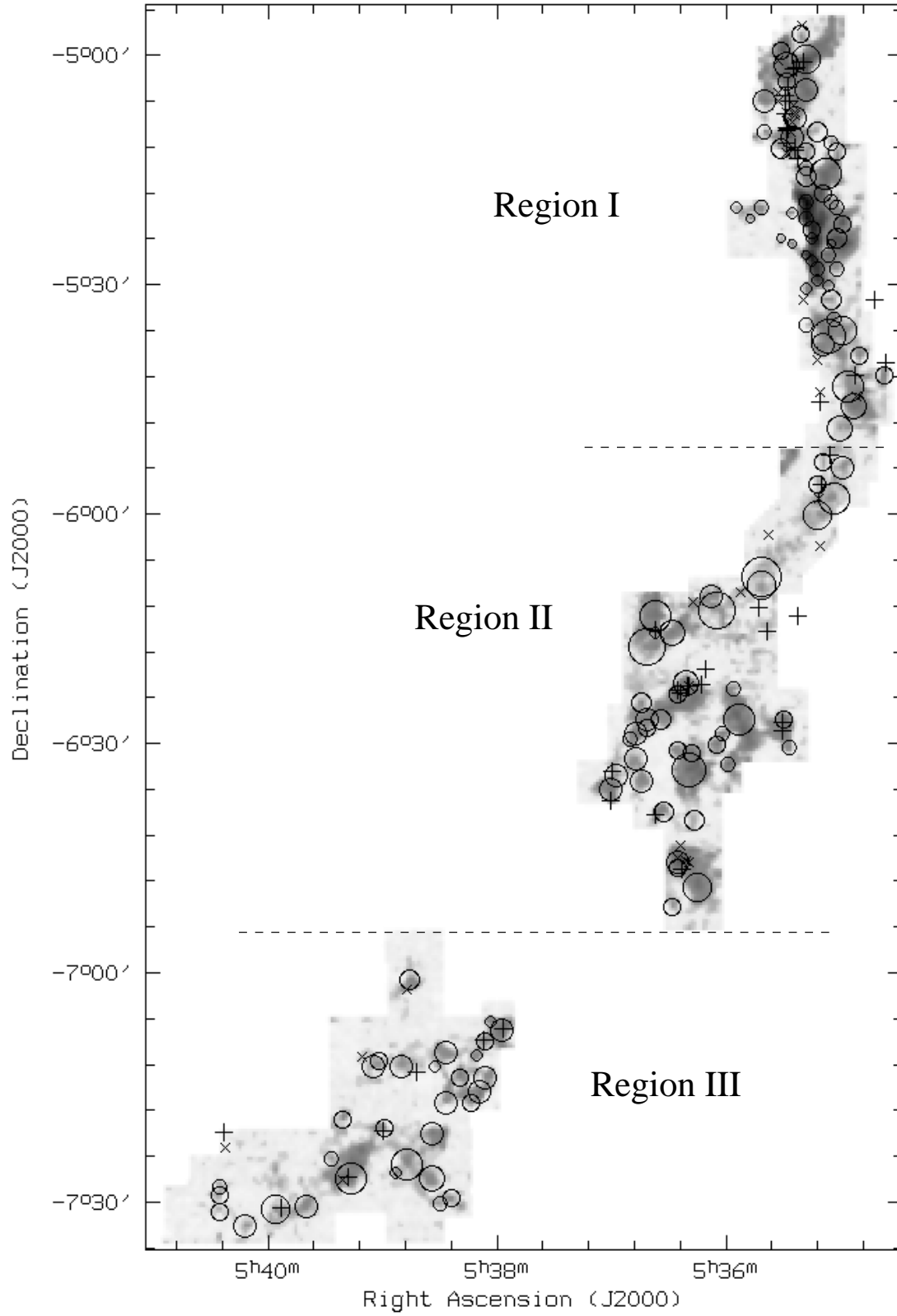


Figure 34: This figure shows the representative positions of the  $H_2$  jets superposed on the CS map of T93. The circles mark the locations of the CS cores identified by T93, with the sizes of the circles indicating their extent. The “+” symbols mark the locations of flows from the “certain” group, the “x” signs mark the positions of flows from the “uncertain” group.

CS-core	Flows “certain”+ “uncertain” No.	Flows “certain”		Flows “uncertain”	
		No.	Id. #	No.	Id. #
3	1	1	<b>3</b>		
4	3	2	<b>4, 5</b>	1	2
8	5	1	<b>14</b>	4	12, 13, 15, 16
11	7	6	<b>17, 18, 19, 21, 23, 24</b>	1	20
13	1			1	22
15	1	1	<b>25</b>		
51	1			1	35
56	1	1	<b>38</b>		
57	1			1	39
65	1	1	<b>46</b>		
67	3	2	<b>49, 53</b>	1	52
69	2	2	<b>51, 54</b>		
71	1	1	<b>55</b>		
86	1	1	<b>57</b>		
89	1	1	<b>59</b>		
91	2			2	62, 63
92	2	2	<b>64, 65</b>		
95	1			1	66
97	1	1	<b>67</b>		
98	1	1	<b>68</b>		
111	1	1	<b>71</b>		
117	2	1	<b>72</b>	1	73
123	1	1	<b>76</b>		

Table 3: List of cores associated with H<sub>2</sub> outflows.

In the following, we will regard a flow as associated with a CS core, when its representative position lies within a circle around the position of the cloud core with the CS core radius as given by T93. In those cases, where two or more cores are seen to overlap at the position of a flow, the flow is regarded to be associated with the core whose central position is closer to the flow position. This concerns the following flows: Flows #4 and #5 are located in the overlap region of cores 3 and 4, but the flow positions are closer to the centre of core 4; flows #51 and #54 are located in the overlap region of cores 67 and 69, but the flow positions are closer to the centre of core 69; also their location on the CS map suggests a relation to core 69 rather than 67.

The individual jet–core associations found by applying the above criteria are listed in Table 3 and also noted in Appendix B. To summarize, 41 jets are associated with cloud cores (27 of the “certain” group, 14 of the “uncertain” group), and 24 are not associated with cloud cores (11 of the “certain”, 13 of the “uncertain” group). Thus, more than 2/3 of the jets are found to be associated with CS cores (27/38 = 71 %, if only the “certain” group is considered, and 41/65 = 69 %, if both “certain” and “uncertain” flows are included).

Of the cloud cores, 23 are found to be associated with outflows, and 77 not, if both “certain” and “uncertain” flows are considered. Dropping the “uncertain” flow candidates leaves 18 CS cores associated with outflows, and 82 not associated. Of the 23 CS cores which are associated with flows, 8 are associated with more than one flow (5 out of 18, if only flows from the “certain” group are counted).

It is reasonable to ask whether the flow–core associations found above are true associations or just chance superpositions of cores and flows. Although a true association cannot be proven based on the available data, there are some indications that most of the claimed associations are presumably real.

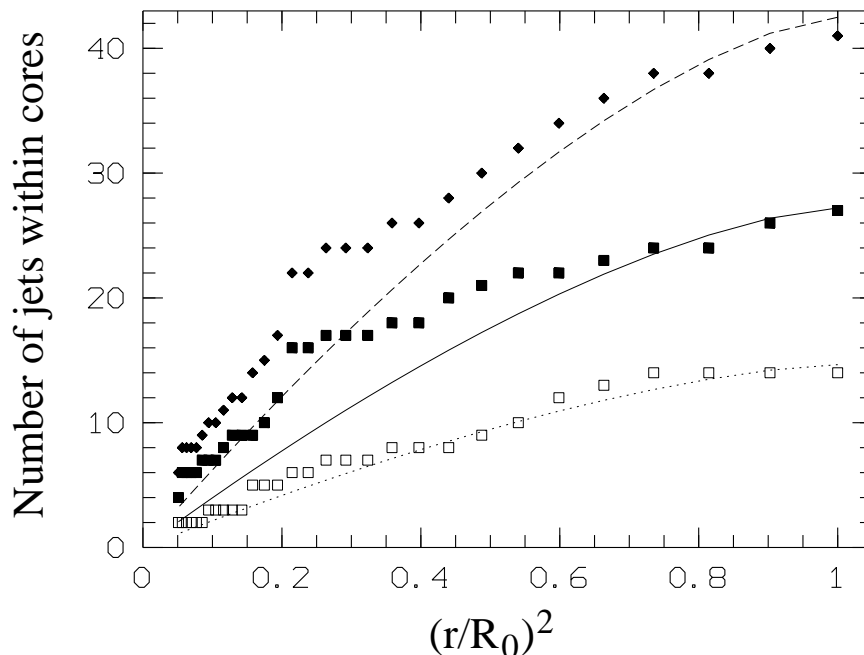


Figure 35: The figure shows the number of jets with their representative positions found in ever smaller areas around the core center positions. The number of jets found within the core area would decrease linearly with decreasing  $(r/R_0)^2$ , if the jets were only seen in projection onto the area covered by the cores. In case the jets were uniformly distributed within the volumes of spherical cores, the number of associated jets would decrease with decreasing  $(r/R_0)^2$  as indicated by the lines (representing  $N_j \propto 1 - (1 - (r/R_0)^2)^{3/2}$  curves). The open squares (and dotted line) represent the number of “uncertain” flows, the filled squares (and the solid line) represent the number of “certain” flows, and the diamonds (and the dashed line) represent the number of both “certain” and “uncertain” jets seen projected on the respective core area. Clearly, there are more jets left over for very small core areas than would be expected for jets uniformly distributed in spherical cores. This indicates a systematic concentration of representative jet positions towards the core centres, supporting the assumption that the bulk of the jets which are claimed to be associated with the cores, are indeed associated with the cores.

First, there is the large fraction of flows which are found to be associated with cores. For a sample of flows scattered randomly over the survey area, the fraction of associated flows should be equal to the fraction of the survey area covered by the cores. The fraction of the survey area covered by the cores is 27 % (where the entire area has been taken to be the original extent of the T93 map, covering 0.72 square degrees, minus a 0.1 pc edge, and cutting out the Orion Nebula area, as has been done in searching for flow–core associations. This leaves 0.57 square degrees, of which 0.15 square degrees are covered by CS cores). The fraction of flows found to be associated with CS cores of  $\sim 70\%$  is much larger than the fraction of the survey area covered by the cores. Thus it is reasonable to assume that in fact most of the flows that have been found to have their representative position within the area covered by the cores, are in fact associated.

Second, the locations of the representative positions of the flows within the core areas are also indicative of an association of the flows. To check this, I assumed ever smaller core radii and again searched for the flows located within the now smaller core areas. The result of this procedure is shown in Fig. 35. The figure shows the number of flows still found to be located within core areas depending on the square of the ratio of the assumed smaller core radii to the actual core radii  $(r/R_0)^2$  (i.e., the ratio of the assumed smaller area to the actual area covered by the cores). The number of “certain” flows is plotted with filled squares, the number of “uncertain flows” with open squares. The diamonds represent the sum of both. For a sample of flows which is only seen projected onto the area of the cores, but otherwise distributed randomly in front and behind the cores, the number of flows seen within the core

areas would decrease linearly with the core areas. This is clearly not the case; instead, more flows are seen closer to the cores central positions than would be expected from a linear decrease of the number of flows with decreasing core areas. This again strongly suggests that the bulk of the flows claimed to be associated is in fact associated with the cores, and not only seen in projection on the area of the cores. Furthermore, for a sample of flows distributed uniformly within the volumes of the (supposedly spherical) cores the number of flows found to be located within the core area should follow a curve given by

$$N_j(r) \propto 1 - (1 - (r/R_0)^2)^{3/2}$$

In Fig. 35 curves of this shape have been plotted scaled such that they approximately match the number of flows found within the areas covered by the cores of full size (the solid line is for the “certain” flows, the dotted line for the “uncertain” flows, the dashed line for the sum of  $N_j$  of both groups). Clearly, for smaller assumed core sizes there is an excess in the number of flows still associated with the cores. This implies that more flows are found close to the central position of the core than would be expected from a uniform distribution of flows within the volumes of the cores: flows are preferentially found close to the centers of the cores, again a strong argument for a true association of the flows with the cloud cores.

Finally, it should be noted that the jets not found to be associated with a cloud core are not necessarily not associated with dense gas. This may in part be due to poor (representative) positions for a number of jets (not for all of them a satisfying driving source location could be obtained). On the other hand, the CS core survey is very likely incomplete for core masses less than about  $50 M_\odot$ . This leaves the possibility that a number of the coreless jets found here are associated with cores with lower mass than has been revealed by T93. This may be particularly the case in dense regions like OMC-2/3.

To summarize this section, it has been shown that a large fraction of the jets found in the H<sub>2</sub> survey is likely to be associated with dense CS cores. Given the generally noted omnipresence of outflows during the earliest phases of star formation, this can be taken as equivalent to the notion that dense cloud cores are in fact the sites of star formation in Orion A, as expected. This is similar to the findings for other star forming regions (e.g., Beichman et al. 1986; Lada et al. 1993).

## 6.2 Properties of cores with and without H<sub>2</sub> jets

T93 derived a number of basic core properties for their sample of cloud cores (line width  $\Delta v$ , radius  $R_{\text{core}}$ , mass  $M_{\text{core}}$ ). In the following section I will compare properties of cores associated with jets with properties of cores apparently not associated with jets. Equating “presence of outflow activity” to “presence of star formation”, this can be regarded as equivalent to a comparison of star forming cores with not star forming cores, and may eventually allow one to draw conclusions on the initial conditions of star formation and on the effect that star formation has on the star forming cores.

There is a systematic gradient in core properties in Orion A from north to south. Thus, not only a comparison of the cores from the entire survey area (excluding the Orion Nebula area) will be done, but also a comparison of the core properties in three different subregions of the survey area, as introduced by T93. The northern area (region I) includes cores 1–52 (except for the “Orion Nebula cores” 17–41), region II includes cores 53–94, and the southernmost area (region III) cores 95–125.

### Core masses

Figure 36 shows the distribution of masses for cores associated with jets (solid line) and for cores without jets (dotted line). It is evident that there is a tendency for jets to be associated preferentially with more massive cores. The histograms show the frequency of cores with/without jets, counting both “certain”



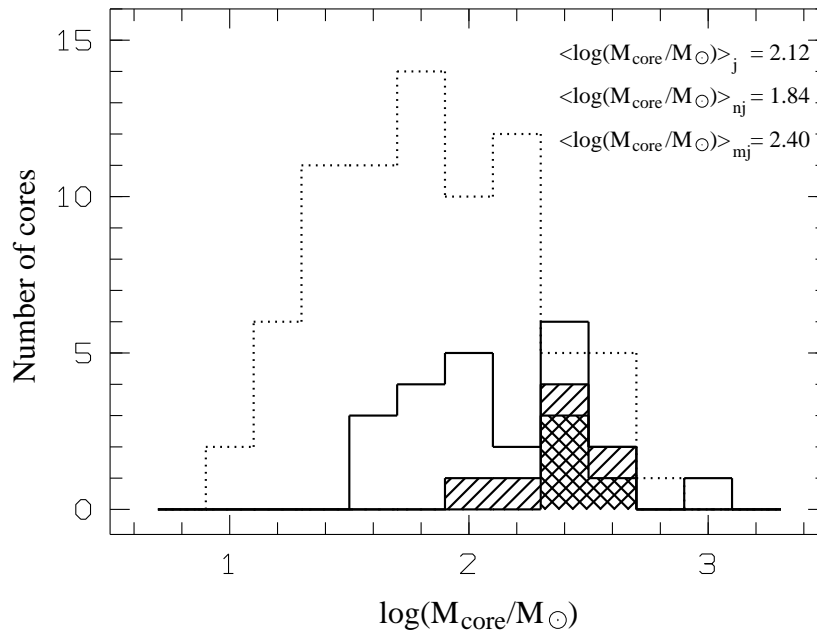


Figure 36: Distribution of core masses (as derived by T93) for cores with jets (solid histogram; both “certain” and “uncertain” jets included) and without jets (dotted histogram). The hashed histogram indicate cores with double jets and the criss-crossed histogram cores with more than two jets. Also noted are the mean values in  $\log(M/M_{\odot})$  for the various groups; the subscript “j” denotes cores with jets, “nj” cores without jets, and “mj” multiple jets (i.e., more than one jet).

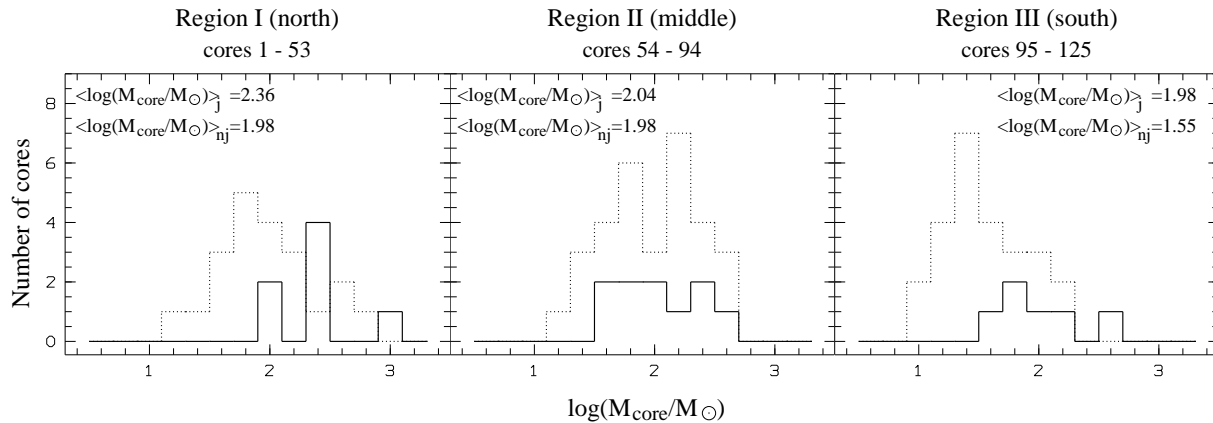


Figure 37: Distribution of core masses (as derived by T93) for cores with jets (solid histograms; both “certain” and “uncertain” jets included) and without jets (dotted histograms). The distributions of core masses are shown for the survey subregions as introduced by T93. The subscripts “j”/“nj” stand for cores with/without jets.

and “uncertain” jets as real. The tendency for jets to be found in more massive cores persists if only the “certain” jets are considered. Then  $\langle \log(M_{\text{core}}/M_{\odot}) \rangle_j = 2.10$ , and  $\langle \log(M_{\text{core}}/M_{\odot}) \rangle_{nj} = 1.87$ . If the masses for cores with jets and without jets are compared for the subregions I, II, and III (Fig. 37), the jets still reside preferentially in more massive cores in each subregion (although this tendency is not very pronounced in subregion II). Finally, as can be seen from Fig. 36, there is a tendency for cores associated with more than one jet to be more massive than cores with only one jet.

### Virial parameters

In order to search for a possible reason for these findings, it may be a reasonable idea to look at the relative importance of the kinetic and gravitational energy of the cores. This can be done using the (dimensionless) virial parameter (see, e.g., Bertoldi & McKee 1992)

$$\alpha_{\text{vir}} = \frac{5\sigma^2 R}{GM} \simeq \frac{2T}{|W|}$$

where  $\sigma$  is the velocity dispersion of the core ( $\sigma = \Delta v / \sqrt{8 \ln 2}$  for a Gaussian line profile with  $\Delta v$  the measured FWHM of the line),  $R$  and  $M$  are the radius and mass of a core,  $G$  the gravitational constant,  $T$  is the total kinetic energy of the core, and  $W$  its gravitational energy ( $W = -3/5 a GM^2/R$ ;  $a$  is a dimensionless parameter of order unity which measures the effects of a nonuniform or nonspherical mass distribution on the gravitational energy). A value of  $\alpha_{\text{vir}} \leq 1$  means that the gravitational binding energy is more important than the kinetic energy, the core is gravitationally bound (but possibly still supported by magnetic fields).  $\alpha_{\text{vir}} > 1$  means that the kinetic energy is more important than gravity; such a core has to be confined by external pressure (otherwise it would disperse) and is unlikely to form stars.

In Figure 38 the distributions of the virial parameter  $\alpha_{\text{vir}}$  are shown for cores associated with jets (solid line) and for cores not associated with jets (dotted line). Cores with multiple jets are shown as the hashed histograms. It is evident that jets are found preferentially in cores with lower values of  $\alpha_{\text{vir}}$ , i.e., in cores with a relatively large importance of gravitational energy compared to kinetic energy. Furthermore, among the cores associated with jets, the cores associated with multiple jets again tend to have systematically lower values of  $\alpha_{\text{vir}}$ . The trend for jets to be found in cores with low  $\alpha_{\text{vir}}$  is also evident if the three survey subregions are considered separately (Fig. 39); note also the general trend for  $\alpha_{\text{vir}}$  to increase when going from region I southwards to region III<sup>3</sup>.

Figure 40 shows a plot of the virial parameter  $\alpha_{\text{vir}}$  against the core masses. Cores associated with jets are indicated with filled symbols (the bigger symbols mark cores with multiple jets), and cores without jets are marked by open symbols. Obviously there is a tendency for  $\alpha_{\text{vir}}$  to increase with decreasing core mass. From this plot it becomes clear, why jets are found preferentially in more massive cores: these are the cores with smaller values of  $\alpha_{\text{vir}}$ , i.e., they are stronger gravitationally bound and thus more prone to star formation.

T93 guessed that (given the uncertainties of the mass estimates) all cores are likely in virial equilibrium, although they found evidence for a power law relation between core mass  $M_{\text{core}}$  and the ratio of the virial mass of a core to its actual mass,  $M_{\text{vir}}/M_{\text{core}}$ , which is equivalent to  $\alpha_{\text{vir}}$ . However, the tendency for star formation to occur more likely in cores with lower  $\alpha_{\text{vir}}$  as observed here shows that the cores with lower  $\alpha_{\text{vir}}$  indeed seem to be gravitationally bound (or at least more likely to be gravitationally bound). The rarity of star formation in the cores with high  $\alpha_{\text{vir}}$  then might indicate that these are predominantly not gravitationally bound. Further support for this idea comes from the finding that  $\alpha_{\text{vir}}$  and the core mass may be related by a power law of the form  $\alpha_{\text{vir}} = \alpha_0 \cdot (M/M_{\odot})^{\epsilon}$ , as is indicated in Fig. 40. A fit to the CS data gives a power law exponent  $\epsilon$  of about  $-0.4$ . Similar power

<sup>3</sup> The absolute values of  $\alpha_{\text{vir}}$  should be taken with care; T93 pointed out that the mass estimates may be very uncertain due to poor knowledge of the relative abundances of CS in the cores, and Wilson et al. (1999) suggest that the core masses are systematically overestimated by a factor of 7; taking such a correction into account,  $\log(\alpha_{\text{vir}})$  would be larger by about 0.8, thus the lowest values of  $\log(\alpha_{\text{vir}})$  would be around 0 (corresponding to  $\alpha_{\text{vir}} \sim 1$ ), all other values would be bigger than that. This would imply that the majority of the cores, particularly the low mass cores (see Fig. 40), would not be gravitationally bound. Either they are transient features, or they are pressure bound: on the larger scales of molecular clumps it is also found that most, (particularly the less massive) clumps are not gravitationally bound; Bertoldi & McKee (1992) argue that these are likely to be pressure bound.

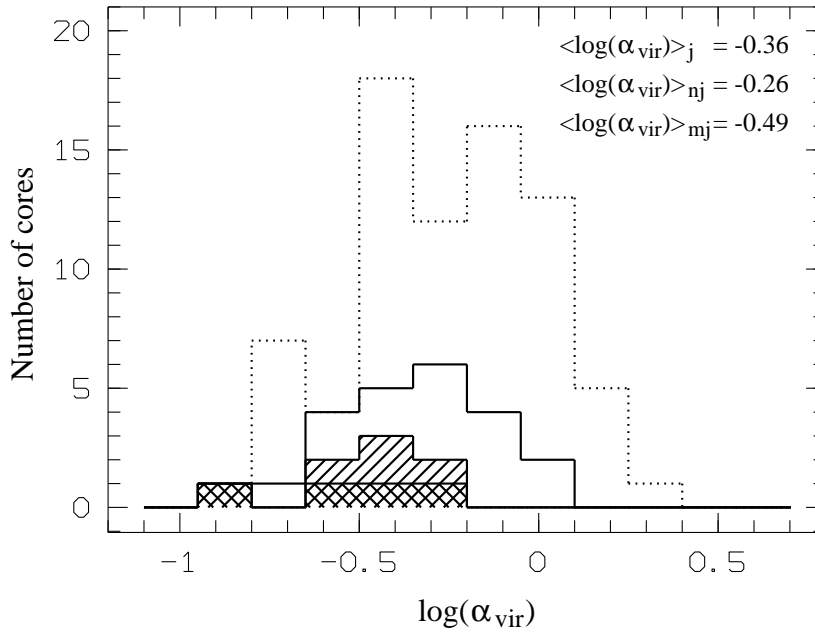


Figure 38: Distribution of the virial parameter  $\alpha_{\text{vir}} = 5\sigma^2 R/(GM)$  for cores with jets (solid histogram; both “certain” and “uncertain” jets included) and without jets (dotted histograms). The hashed histograms indicate cores with double jets and cores with more than two jets are shown by the criss-crossed histogram. Also noted are the mean values in  $\log(\alpha_{\text{vir}})$  for the various groups; the subscript “j” denotes cores with jets, “nj” cores without jets, and “mj” multiple jets (i.e., more than one jet).

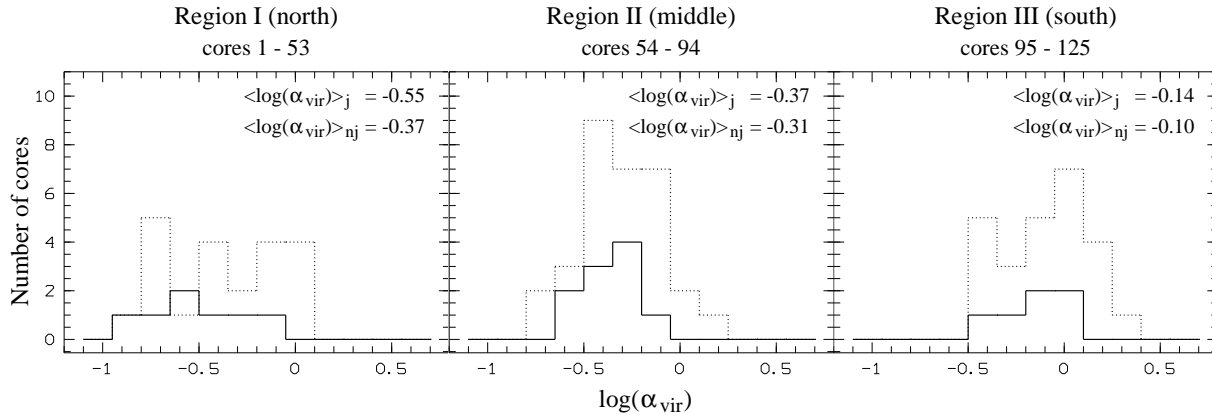


Figure 39: Distribution of the virial parameter  $\alpha_{\text{vir}} = 5\sigma^2 R/(GM)$  for cores with jets (solid histograms; both “certain” and “uncertain” jets included) and without jets (dotted histograms). The distributions of  $\alpha_{\text{vir}}$  are shown for the survey subregions as introduced by T93.

laws, albeit with generally smaller exponent  $\epsilon$ , are also known from other clouds on larger scales for molecular clumps (see, e.g., Loren 1989; Bertoldi & McKee 1992; Williams et al. 1994). Bertoldi & McKee argue that such a power law relation (for  $\alpha_{\text{vir}}$  reasonably greater than 1; see footnote 3) is expected for pressure-confined clumps, with a power law exponent  $\epsilon \sim -2/3$ . The findings that star formation in Orion A occurs more likely in the cores with low  $\alpha_{\text{vir}}$  and high mass, and that  $\alpha_{\text{vir}}$  seems to be related to the core mass by a power law with an exponent  $\epsilon \sim -0.4$  may thus imply that pressure-confinement governs the low-mass cloud cores in Orion A.

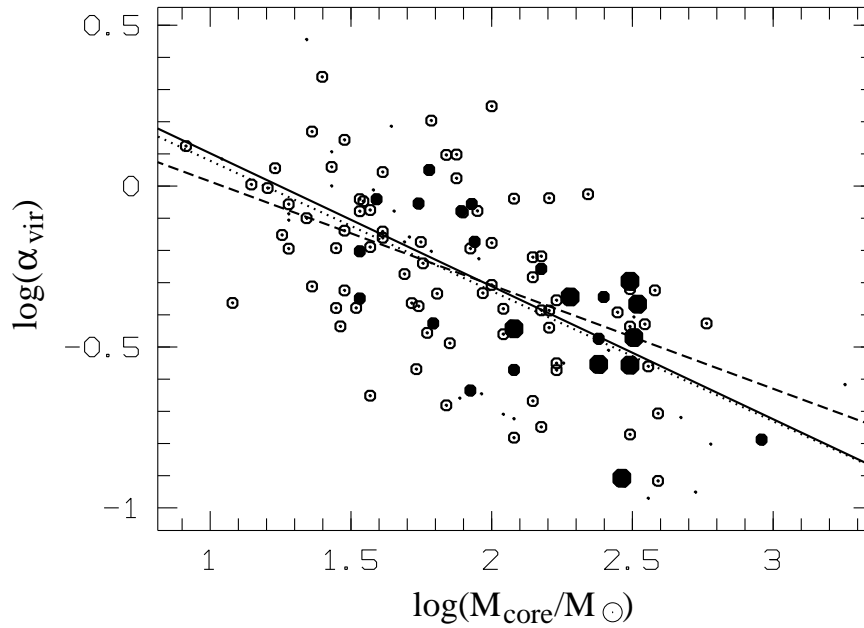


Figure 40: log–log plot of the virial parameter  $\alpha_{\text{vir}}$  versus core masses. The open symbols mark cores without associated jets, the filled symbols mark cores with associated jets, cores associated with multiple jets are marked by bigger symbols. For completeness, the cores in the Orion Nebula area have also been plotted (small dots). The lines mark power law fits of the form  $\alpha_{\text{vir}} = \alpha_0 \cdot (M/M_{\odot})^{\epsilon}$ . The dotted line is for the entire CS core sample (including the Orion Nebula cores; the fit yields  $\alpha_0 = 3.0 \pm 0.7$ ;  $\epsilon = -0.41 \pm 0.04$ ), the solid line represents the cores associated with jets ( $\alpha_0 = 3.3 \pm 2.4$ ;  $\epsilon = -0.41 \pm 0.11$ ), and the dashed line the fit to the cores without associated jets ( $\alpha_0 = 2.2 \pm 0.7$ ;  $\epsilon = -0.32 \pm 0.06$ ).

## Linewidths

Next I will compare the linewidths of the cores with jets with those of the cores without jets. It has already been noted by T93 that cores which are associated with molecular outflows and/or cold IRAS sources tend to have larger linewidths. Similarly, Beichman et al. (1986) and Myers et al. (1988) found larger linewidths in cores associated with cold IRAS sources and/or CO outflows in other star forming regions. This behaviour is usually attributed to the action of outflows stirring up and disrupting the star forming cloud cores, thus terminating accretion and determining the final stellar mass. In addition to the CS linewidth given by T93, I will also include the linewidths measured by Wilson et al. (1999) towards the CS cores (NH<sub>3</sub>, C<sup>18</sup>O (2–1), C<sup>18</sup>O (3–2), and <sup>13</sup>CO (3–2)). NH<sub>3</sub> traces similar densities as CS ( $n > 10^4 \text{cm}^{-3}$ ), whereas the CO lines are excited at lower densities ( $n > 10^3 \text{cm}^{-3}$ ).

Figure 41 shows the distributions of the linewidths of the cores for the various lines for the entire survey area (except for the Orion Nebula area). The left column shows the true number of cores in each  $\Delta v$  bin, whereas in the right column the frequencies of the cores with jets have been scaled up in order to allow a better comparison between the shapes of the distributions for cores with and without jets, and to allow an easier recognition of shifts of both distributions relative to each other. As in Fig. 36, the dotted lined histograms represent the cores without jets, and the solid lined histograms the distributions of cores associated with jets. The hashed histograms again represent cores associated with two jets and cores with more than two jets. There is strong evidence that cores with jets show on average larger linewidths than cores without jets. This is true for the CS line as well as the CO lines. The only exception is the NH<sub>3</sub> linewidth, where possibly cores with jets show smaller linewidths than cores without jets. Fig. 42 shows the distributions of linewidth for the three subregions. The trends seen in the histograms for the total survey area are still present in the individual subregions. It is thus unlikely

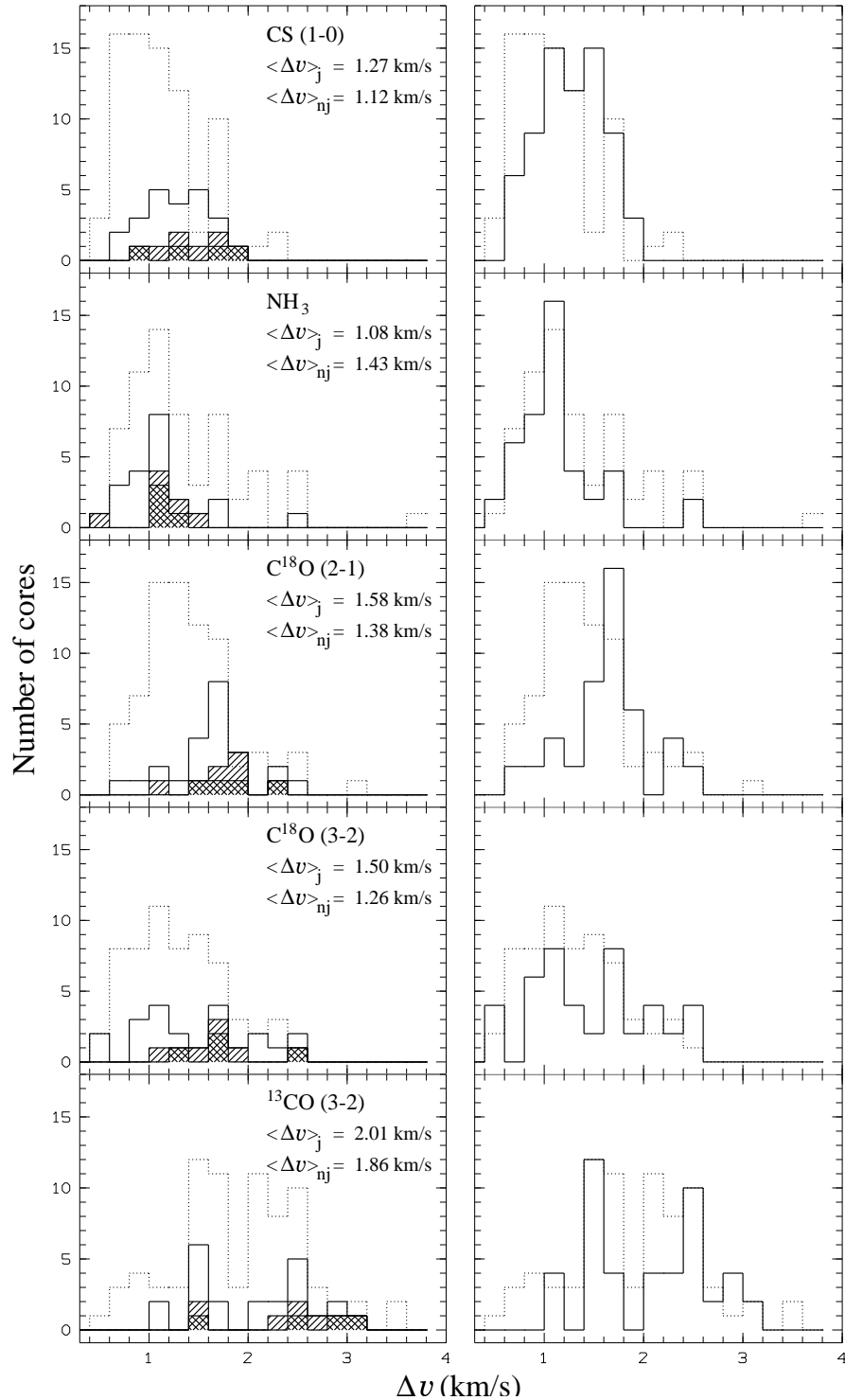


Figure 41: Distribution of line widths of various molecular transitions for cores (entire survey area except for the Orion Nebula area) with jets (solid histograms) and without jets (dotted histogram). The hashed histograms indicate cores with double jets, and multiple (i.e., more than two) jets are marked by the criss-crossed histograms. The left panels show the actual number of cores as histograms, whereas in the right panel the histograms for the cores with jets are shown in a scaled-up version to allow a better comparison of the shapes of the distributions of cores with jets and without jets. The CS (1–0) data are taken from T93, the other data from Wilson et al. (1999). The subscripts “j”/“nj” stand for cores with/without jets.

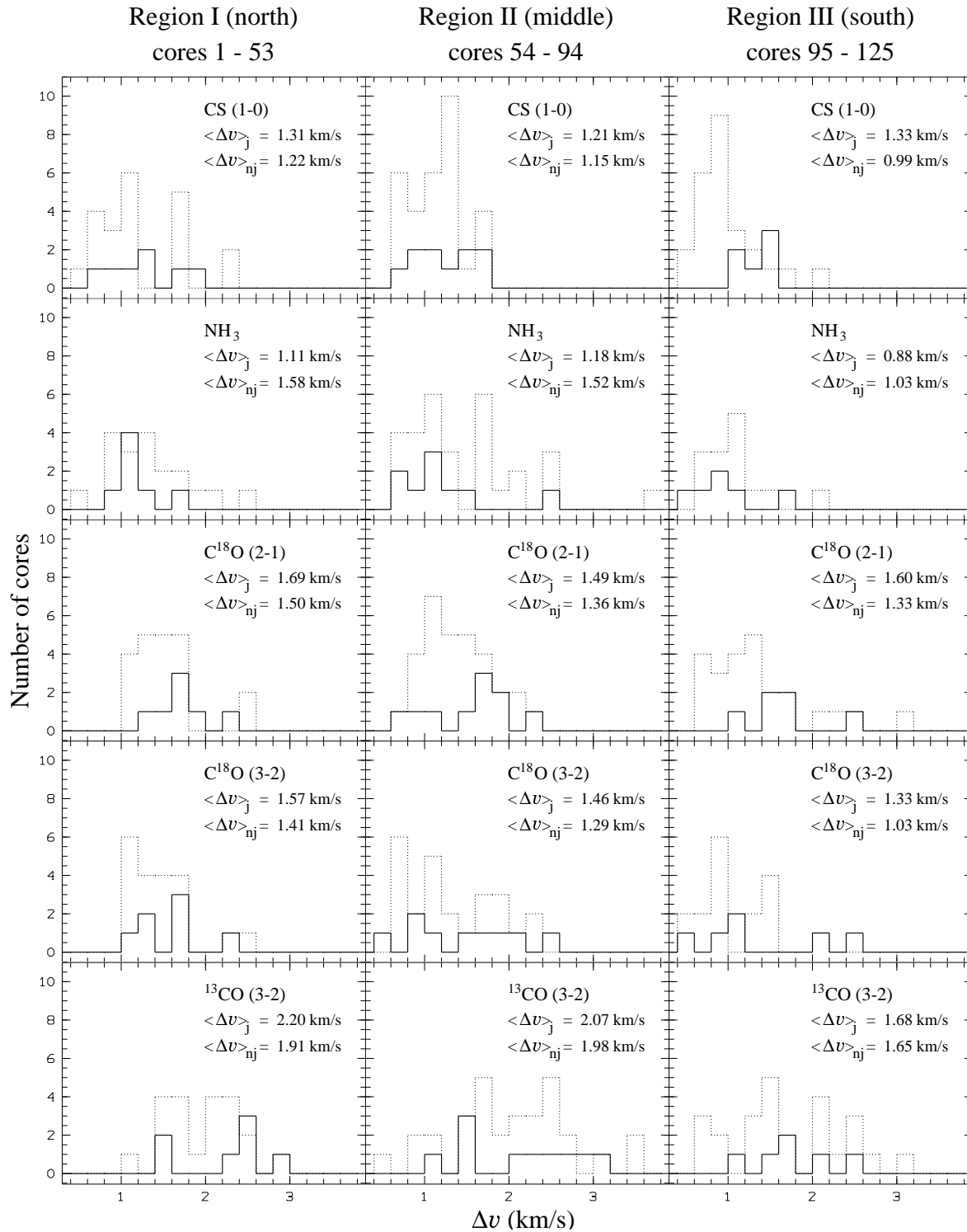


Figure 42: Distribution of line widths of various molecular transitions measured for the cores, shown separately for the northern part of the survey area (except for the Orion Nebula area; left column), the middle part of the survey (middle column), and the southern part of the survey area (right column). The distribution of velocity dispersions for cores associated with jets is indicated by the solid lined histograms, the distributions for cores without jets are shown as dotted lined histograms. The CS (1–0) data are taken from T93, the other data from Wilson et al. (1999). The subscripts “j”/“nj” stand for cores with/without jets.

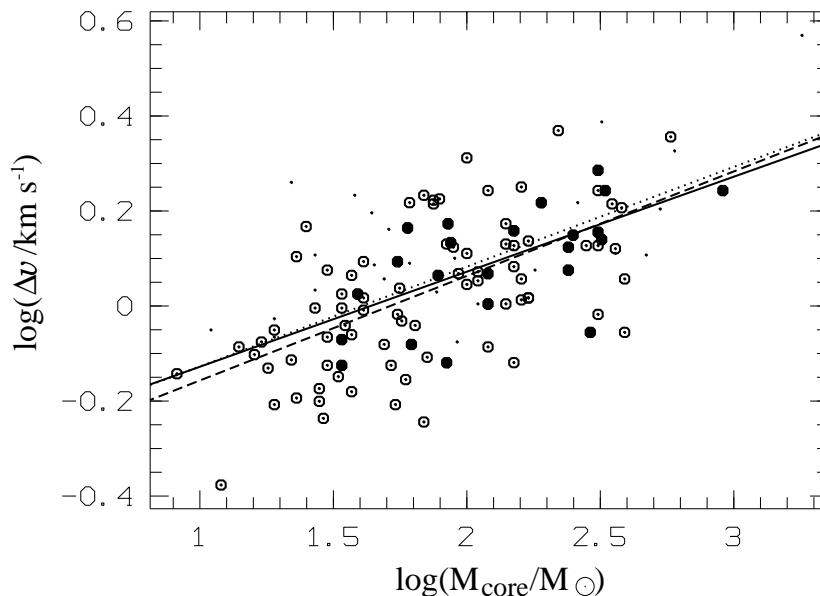


Figure 43: log–log plot of the core linewidths versus core masses. The open symbols mark cores without associated jets, the filled symbols mark cores with associated jets. For completeness, the cores in the Orion Nebula area have also been plotted (small dots). The lines mark power law fits of the form  $\Delta v(\text{km s}^{-1}) = v_0 \cdot (M/M_\odot)^\gamma$ . The dotted line is for the entire CS core sample (including the Orion Nebula cores; the fit yields  $v_0 = 0.46 \pm 0.05$ ;  $\gamma = 0.21 \pm 0.02$ ), the solid line represents the cores associated with jets ( $v_0 = 0.47 \pm 0.14$ ;  $\gamma = 0.20 \pm 0.05$ ), and the dashed line the fit to the cores without associated jets ( $v_0 = 0.42 \pm 0.07$ ;  $\gamma = 0.22 \pm 0.03$ ).

that the trends seen are localized phenomena caused by particular circumstances, e.g., the proximity of the northernmost cores to the Orion Nebula H II region.

Given the general trend for cores with jets to have larger linewidths in the CS and the various CO lines, it is somewhat “strange” that this is not the case for the NH<sub>3</sub> lines. This is even more the case when recalling that CS and NH<sub>3</sub> should trace not too different densities, and that larger NH<sub>3</sub> linewidths have been found in NH<sub>3</sub> cores with CO outflows by Myers et al. (1988). The unexpected behaviour of the NH<sub>3</sub> linewidths as measured by Wilson et al. (1999) may have its explanation in *what* has been observed: Wilson et al. measured the NH<sub>3</sub> linewidths towards the peak positions of the CS cores, not the NH<sub>3</sub> linewidths of NH<sub>3</sub> cores, as did Myers et al. (1988). It is, on the other hand, known that CS cores and NH<sub>3</sub> cores are not the same. This is apparent in the comparison of the NH<sub>3</sub> and CS maps of OMC-2/3 shown by T93. Although CS and NH<sub>3</sub> maxima occur largely at similar positions, the ratio of CS to NH<sub>3</sub> emission varies considerably. Zhou et al. (1989) showed that in a sample of cores mapped both in CS and in NH<sub>3</sub>, the CS emission is generally more extended, the shapes of the CS emission regions can differ substantially, and there can be large offsets between CS and NH<sub>3</sub> peak positions. Thus it may be that the NH<sub>3</sub> linewidths as measured by Wilson et al. are misleading in our context; instead of observing NH<sub>3</sub> towards the CS cores, it would be more meaningful to search all NH<sub>3</sub> cores in the entire survey area, associate flows with the NH<sub>3</sub> cores and then compare the linewidths of NH<sub>3</sub> cores with and without jets, similar to what is done here for the CS cores.

Jets and outflows are often invoked to be an important agent in clearing the environment of a newly born star from remnant cloud material or even to halt accumulation of cloud core material on the star and its disk, thus possibly determining the mass of the star. Larger linewidths in cloud cores associated with embedded IRAS sources (Beichman et al. 1986) and/or CO outflows (Myers et al. 1988) have been taken as evidence that protostars transfer kinetic energy and momentum to their surrounding cloud core through their outflow, thus inducing turbulence in the cloud core, which causes the larger

linewidths. T93 also stated that those Orion CS cores with cold IRAS sources and/or CO outflows also tend to have larger linewidths. He argued that this is in support of Beichman's and Myers' idea. Indeed, the above comparison of the linewidths of cores with and without H<sub>2</sub> jets also reveals this trend: jets are found preferentially in cores with larger linewidths.

However, instead of immediately joining Beichman's and Myers' line of argumentation, it seems worth looking at this phenomenon in a bit more detail. The first thing I noticed in this section is that jets are preferentially found in cores with higher mass. T93 pointed out that there is a power-law relationship between the masses of the CS cores and their linewidth:  $\Delta v(\text{km/s}) \approx 0.43 \cdot M(M_{\odot})^{0.23}$ . Such a relation is not only known for the CS cores in Orion A: Bally et al. (1987) found  $\Delta v(\text{km/s}) \approx 0.54 \cdot M(M_{\odot})^{0.25}$  for the <sup>13</sup>CO clumps in Orion A, and Larson (1981) found this relation to hold over a range of 5 orders of magnitude in cloud masses ( $\sigma(\text{km/s}) \approx 0.42 \cdot M(M_{\odot})^{0.20}$ , fitted by eye;  $\sigma$  is the velocity dispersion, which for a Gaussian line is  $\sigma = 0.18 \cdot \Delta v$ ) for various clouds in various star forming regions. This power law relationship of linewidth and cloud mass thus seems to be fundamental, and is generally explained in the context of a turbulent and/or fractal nature of the clouds (note that there are also other power law relationships between various cloud parameters, most notably the linewidth-size relation  $\Delta v \propto R^p$ , with  $p \sim 0.38$  remarkably close to the value expected for Kolmogoroff turbulence of  $p = 1/3$ ; see Larson 1981; Williams et al. 1994).

Given this  $\Delta v$ - $M$  relationship and the finding that jets tend to be found in cores with larger linewidths and larger masses, it now has to be asked whether the larger linewidths in cores with jets are simply due to the higher masses of the cores. To give an answer to this question, power laws of the form  $\Delta v(\text{km/s}) = v_0 \cdot (M/M_{\odot})^{\gamma}$  have been fitted to the measured linewidths and core masses, first for the entire sample of all 125 cores, then to all cores with associated jets, and for all cores not associated with jets (excluding the Orion Nebula cores). The results are shown in Fig. 43. There, the dotted line marks the relation found for all 125 cloud cores ( $\Delta v(\text{km/s}) = 0.46 \cdot (M/M_{\odot})^{0.21}$ :  $v_0$  and  $\gamma$  are only marginally different from the values given by T93; the differences are presumably due to the different fitting procedures used), the solid line is for the cores with jets ( $\Delta v(\text{km/s}) = 0.47 \cdot (M/M_{\odot})^{0.20}$ ), and the dashed line represents the fit for the cores not associated with jets ( $\Delta v(\text{km/s}) = 0.42 \cdot (M/M_{\odot})^{0.22}$ ; the uncertainties of the fit parameters are given in the figure caption; the power law exponent  $\gamma$  is intriguingly similar to that found by Larson (1981) of  $\gamma = 0.20$ ; Larson used the velocity dispersion  $\sigma$  for his relation, whereas here the FWHM  $\Delta v$  of the CS lines is plotted). It is evident from the plot as well as from the results of the fits that within the uncertainties there is no difference in the  $\Delta v$ - $M$  relationships between cores with jets and cores without jets, neither in the power law exponent  $\gamma$  nor in the normalisation factor  $v_0$ . Thus it seems that cores with jets and cores without jets have undistinguishable linewidths, as long as cores with similar masses are compared. Jets and protostars are just more likely to be found in more massive cores, which generally have larger linewidths, thus simulating intrinsically larger linewidths. Notably, in the study by Beichman et al. (1986), the cores with the protostars and larger linewidths (proposed to be due to the impact of the protostellar outflow on the core) also have the larger masses.

**Summary.** In this section the properties of star forming and not star forming cores have been compared. I have shown that star formation takes places predominantly in cores in which the virial parameter  $\alpha_{\text{vir}}$  is comparably low, i.e., in cores in which the gravitational binding energy is more dominant in comparison to the kinetic energy of internal motions. Furthermore, it appears that the more massive cores have a lower  $\alpha_{\text{vir}}$ , which might imply that the lower mass cores are pressure confined rather than gravitationally bound. Consistently, star formation takes place mainly in the more massive cores.

Other authors have found a tendency for cores with associated outflows and/or forming stars to have larger linewidths. This has been taken as evidence that the forming stars stir up or disrupt their



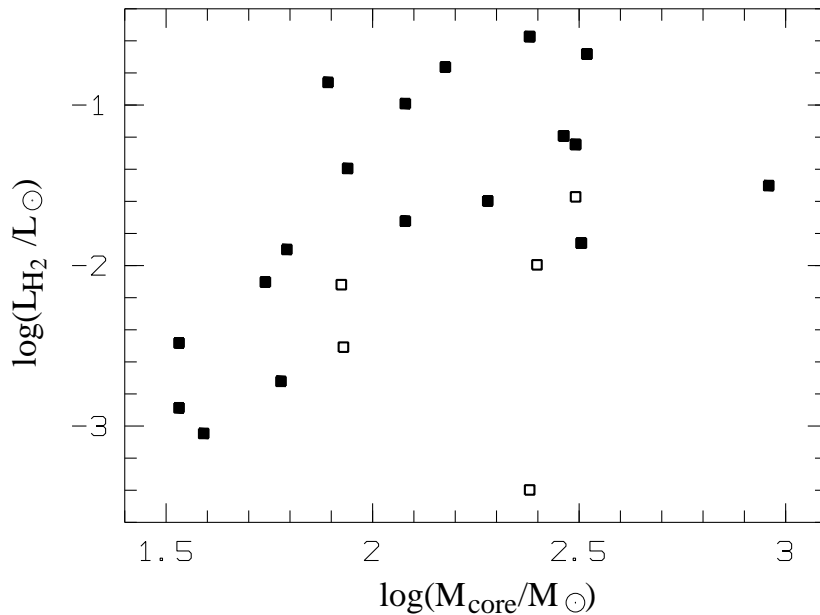


Figure 44:  $H_2$  luminosities of the jets plotted as a function of the masses of the associated CS cores. In case of multiple jets from a CS core, the  $H_2$  luminosities of the individual jets have been added. The open squares mark cores associated only with “uncertain” jets, the filled symbols mark cores associated with at least one “certain” jet.

parent cores via the action of their outflows. A tendency for larger linewidths in cores associated with jets is also found in Orion A. However, I interpret this to be a consequence of the typically higher masses of the star forming cores (and the known tendency for higher mass cores to have larger linewidths), rather than to be an intrinsic property of star forming cores: cores of similar masses have similar linewidths, regardless of their being star forming or not star forming cores. Apparently, protostellar outflows have a less violent impact on the parent cloud cores than has been suggested by others.

### 6.3 Jet- vs. core properties

In the previous section it has been shown that jets are preferentially found in the higher mass, lower  $\alpha_{\text{vir}}$  cores. Furthermore, the subgroup of cores associated with multiple jets have been found again in the more massive, lower  $\alpha_{\text{vir}}$  cores out of the jet harbouring cores. It thus appears reasonable to check whether the properties of the cores are related to other jet properties (i.e., in addition to multiplicity), and whether the core properties have an influence on the outcome of the star formation process.

#### Core mass & jet $H_2$ luminosity

One obvious question is to what extent the core mass influences the properties of the protostar(s) and the associated outflow(s). Figure 44 shows the total  $H_2$  luminosity of the flows plotted as a function of the mass of the core (in cores with multiple jets, the  $H_2$  luminosities of the individual jets have been coadded). There is a clear trend for more luminous flows to be located in more massive cores. Thus it appears that outflow activity (which is tightly connected to accretion activity) is more energetic in more massive cores. This is a reasonable finding, since the more massive cores (having also lower values of  $\alpha_{\text{vir}}$ ) have obviously the potential to form the more massive stars, which will be associated with the more energetic outflows.

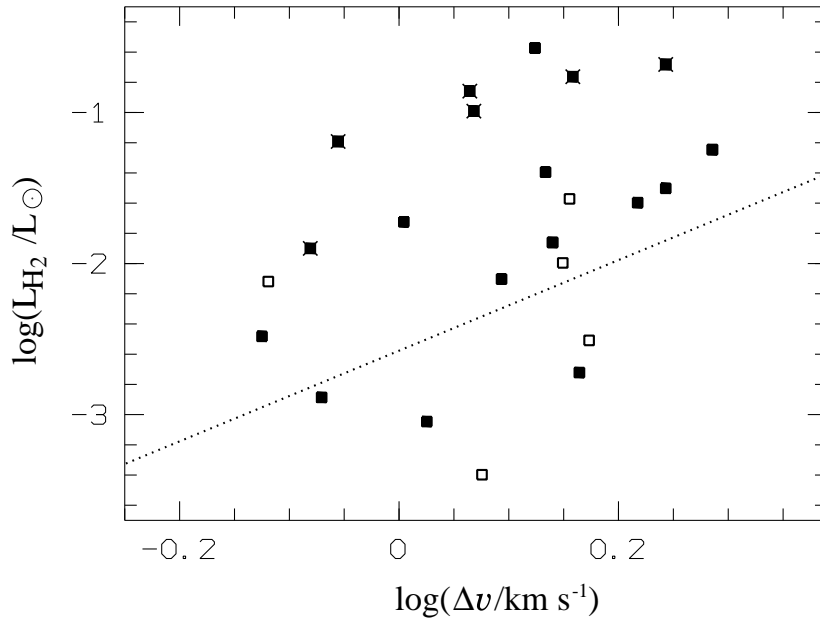


Figure 45: H<sub>2</sub> luminosities of the jets plotted as a function of the linewidth of the associated CS cores. In case of multiple jets from a CS core, the H<sub>2</sub> luminosities of the individual jets have been added. The open squares mark cores associated only with “uncertain” jets, the filled symbols mark cores associated with at least one “certain” jet. Cores associated with a Class 0 driven flow are marked with an additional cross. The dotted line represents a  $L_{\text{H}_2}/L_{\odot} = 2.65 \cdot 10^{-3} \cdot [\Delta v / (\text{km/s})]^3$  relationship as predicted by the Shu et al. model of a collapsing singular isothermal sphere.

### Core linewidth & jet H<sub>2</sub> luminosity

The Shu et al. star formation paradigm (see Section 2.1), based on the collapse of an initially static singular isothermal sphere, suggests a mass accretion rate which is essentially constant over the entire collapse process. It is determined by the effective sound speed  $c_{\text{eff}}$  in the cloud:  $\dot{M}_{\text{acc}} \simeq c_{\text{eff}}^3/G$ . The effective sound speed  $c_{\text{eff}}$  is in turn reflected in the line widths  $\Delta v$  measured towards the cores. Assuming furthermore that a certain fraction of the mass accretion rate is converted into mass outflow rate (e.g.,  $\dot{M}_{\text{out}} \sim 0.3 \times \dot{M}_{\text{acc}}$  in the X-wind model; see Section 2.5) one could expect a correlation between the line widths of the core and the kinetic energy input rate  $L_{\text{now}} = 1/2 \cdot \dot{M}_{\text{out}} \cdot v_{\text{jet}}^2$  of the associated jets. The kinetic energy input rate is eventually indicated by the H<sub>2</sub> luminosity  $L_{\text{H}_2} \propto L_{\text{now}}$  of a jet. Assuming a typical, constant jet velocity (e.g.,  $v_{\text{jet}} = 200$  km/s), this may thus result in a power law dependency of  $L_{\text{H}_2}$  on the core linewidths:  $L_{\text{H}_2} \propto (\Delta v)^3$ .

Figure 45 shows a plot of the total H<sub>2</sub> luminosity of the flows as a function of the linewidth of the jet harbouring core (in cores with multiple jets, the H<sub>2</sub> luminosities of the individual jets have been added). With a lot of good will one might recognize a trend for more luminous jets to be located in cores with larger linewidths, but the correlation is certainly more than doubtful. The dotted line is not a fit to the data, but marks a power law correlation between linewidth and H<sub>2</sub> luminosity as has been suggested above:  $L_{\text{H}_2}/L_{\odot} = 2.65 \cdot 10^{-3} \cdot [\Delta v / (\text{km/s})]^3$ . The normalisation factor  $2.65 \cdot 10^{-3}$  in this relation comes from a number of assumptions:  $L_{\text{H}_2} = 0.1 \times L_{\text{shock}}$ ;  $L_{\text{shock}} = 0.1 \times L_{\text{now}} = 0.1 \times 1/2 \cdot \dot{M}_{\text{out}} \cdot v_{\text{jet}}^2$  (see Section 7.1 for details);  $v_{\text{jet}} = 200$  km/s;  $\dot{M}_{\text{out}} = 0.3 \times \dot{M}_{\text{acc}} = 0.3 \times c_{\text{eff}}^3/G$ ;  $c_{\text{eff}} = \sigma = 0.18 \times \Delta v$ ; the assumed K-band extinction is 1 mag. Although the power law index of 3 appears to represent the expected trend for more luminous jets to be located in larger linewidth cores correctly, the scatter of the data around such a relation is huge. Given the list of assumptions that went into the derivation of the above relation, it would have been a surprise to see such a correlation in the data anyway (but note

that the existence of an equivalent relation between  $\Delta v$  and  $\dot{M}_{\text{flow}}$  has recently been claimed to exist for molecular outflows by Aso et al. 2000).

Interestingly, most flows seem to have a larger  $\text{H}_2$  luminosity than predicted by the combined Shu et al. accretion plus X-wind outflow model. This might point to a systematically higher mass accretion rate than in the Shu et al. star formation picture throughout most of the time during which the protostar is accreting. Furthermore, the cores associated with Class 0 driven flows (marked by crosses in Fig. 45) are all found in the upper part of the plot and might indeed follow a  $L_{\text{H}_2} \propto \Delta v^3$  relationship, albeit with a larger normalization factor than predicted by the Shu et al. model. The remaining jets also follow a  $L_{\text{H}_2} \propto \Delta v^3$  relation a bit more closely, if the Class 0 sources are taken away, with  $L_{\text{H}_2}$  more consistent with the Shu et al. model predictions.

In principle, higher  $\text{H}_2$  luminosities could be obtained by assuming a higher value of  $\epsilon = \dot{M}_{\text{out}}/\dot{M}_{\text{acc}}$ ; however, the value of  $\epsilon = 0.3$  assumed above is already in the upper range of what is usually taken. Instead, the systematically higher  $\text{H}_2$  luminosity in the (less numerous) Class 0 flows might imply the presence of a short, but highly active accretion phase early in the protostellar evolution, with the peak mass accretion rate more than an order of magnitude higher than the Shu et al. value of  $c_{\text{eff}}^3/G$ . Higher, time dependent accretion rates are in fact the result of a number of collapse calculations (e.g., Foster & Chevalier 1993; Tomisaka 1996; Safier et al. 1997; Li 1998). In these calculations, the accretion rate scales as  $\dot{M}_{\text{acc}} = c_{\text{eff}}^3/G \cdot f(t)$ , where  $f(t)$  typically has a strong peak early on and then declines, first rather quickly, then more gradually. This kind of models seems to be better suited than the Shu et al. star formation picture of a constant mass accretion rate to explain the data presented here. Note also that the trend for steadily declining accretion rates found for the Class I sources here might have a smooth continuation in steadily declining accretion rates in the more evolved T Tauri stars disks (Hartmann et al. 1998; Calvet et al. 2000).

**Summary.** To summarize this section, despite the trends for more  $\text{H}_2$ -luminous jets to be located in more massive, larger linewidth cores, no obvious correlations between jet properties and core properties could be established, although they may exist. Presumably the actual evolutionary stage of the flow/protostar is more influential on the current jet properties (particularly its energetics) than the properties of the core from which the protostar is forming. The trend for more luminous flows to be found in more massive cores is reasonable: these cores have the potential to form more massive stars, which will produce more energetic outflows.

The comparison of core linewidths and jet  $\text{H}_2$  luminosities suggest a picture more consistent with star formation scenarios implying a short main accretion phase plus a subsequent slow, declining late accretion phase, rather than the Shu et al. standard star formation picture, which implies a constant mass accretion rate. This conclusion is similar to that of Bontemps et al. (1996a), who also found evidence for stronger outflow (hence accretion) during the (apparently shorter) Class 0 stage, based on a study of a sample of molecular (CO) outflows from Class 0 and Class I protostars.

## 7 Discussion

### 7.1 Jet & protostar statistics in Orion A

**Jets and their driving sources.** The (admittedly incomplete) identification of the jet driving sources allows an investigation of the jet evolution parallel to the driving source evolution. The first interesting thing to notice here is the number of flow/driving source systems found in each infrared class. Comparing the number of Class 0 systems with Class I systems, it is seen that about 4 times as many Class I systems are found. The current consensus about the Class 0 lifetime compared to the Class I lifetime is that the Class I stage lasts for about ten times longer than the Class 0 stage (e.g., André et al. 2000). This estimate is largely based on the detection of two Class 0 and 15-30 Class I objects in the  $\rho$ -Ophiuchus cloud core. Given these lifetime estimates, there should be  $\sim 10$  times more Class I sources than Class 0 sources in Orion as well. Since I found only  $\sim 4$  times more Class I driven flows than Class 0 driven flows, there might be some deficiency of Class I driven flows (for comparison, Gomez et al. 1997 found jets from 60 molecular outflows from virtually all of the Class I sources in their sample). If true, then this might either imply that the Class 0 stage last for some time longer (if compared to the Class I stage) than previously assumed, or that some part of the Class I objects do not drive an outflow (which is detectable in the  $H_2$  jet survey). However, it should be noted that some of the sources classified as Class 0 here may be misidentifications. E.g., the evolutionary stage of HH 1/2 VLA2 is at most a guess, since the only reliable information on that source is its VLA detection, making it likely a very young star. Furthermore, it is often noted that some Class I sources may in fact resemble Class 0 sources in their spectral appearance if they were seen with their disks edge-on (e.g., Sonnhalter et al. 1995; but see André et al. 2000). Thus it may be the case that the Class 0 sample is contaminated by Class I sources. Another point is that flows from Class I sources appear to be systematically fainter than those from Class 0 sources, thus it is more likely that in certain parts of the survey area (e.g., OMC-2/3) some of them were overlooked between the brighter flows from the younger sources and the general extended background emission (although they would have been visible in less confused regions). Taking these arguments into account, it may well be that there are ten times as many flows from Class I sources as from Class 0 sources, in accordance with the relative lifetimes of these stages (which itself is only a soft guess based on only very few examples, rather than a hard fractual number). Thus it seems that the possible deficiency of Class I driven flows is at most a poorly established result. On the other hand, the rather large number of Class 0 driven flows (if compared to the number of Class I driven flows) makes it unlikely that there are Class 0 sources without an  $H_2$  jet: then even more Class I outflow sources would be “missing”.

The situation looks different when the sample of Class I driven flows is compared with the Class II driven flows. The lifetime of the Class II stage is also estimated to be a factor of  $\sim 10$  longer than that of the Class I stage, but *much fewer Class II driven flows are found than Class I driven flows*. This clearly indicates that outflow activity is not a big deal any more at the Class II stage (see also Gomez et al. 1997; Kenyon et al. 1998).

*The distribution of flow driving sources among the infrared classes strongly suggests an evolution of the frequency of outflows with time.* Many (presumably all) Class 0 sources are associated with

outflows. Apparently also a large fraction of the Class I sources is driving an outflow; the (poorly established) deficiency of Class I driven outflows might imply a decline in outflow activity during the late Class I stage. Finally, during the early Class II stage, the outflow activity quickly dies out or fades from view.

A more in depth investigation of this issue will be possible using the ongoing wide field millimetre survey in Orion A, which will (together with additional observations) reveal the full population of young stellar objects in the survey area (in progress, but not part of this thesis).

**Flow lengths.** The analysis of the flow lengths in section 5.4 showed that Class 0 sources are associated with very short, medium sized, and very long outflows, without any preferred or typical flow length. The fraction of very long flows was found to be comparatively high. On the other hand, the Class I driven flows were found to be typically some tenths of a parsec long, with some very short and very long outflows also present. However, the fraction of very long flows for Class I sources is lower than for the Class 0 sources. The flows from Class II sources finally were found to be only rather short.

*These findings suggest an evolution in flow length with time.* Parsec-scale flows seem to be present during a considerable part of the Class 0 stage and a somewhat smaller fraction of the Class I stage. Assuming a continuous evolution, this implies that parsec-scale flows are present during the later part of the Class 0 stage, and during the early Class I stage. Later in the Class I stage, the jets get shorter, until finally in the very early Class II stage only a few, short jets are left over.

The underlying evolution of the driving sources from the Class 0 stage (earliest protostellar stage known, just after onset of accretion, main accretion phase with very strong accretion activity) via the Class I stage (late accretion phase, moderate to low accretion activity) to the Class II stage (only residual accretion activity left) offers a *straightforward explanation* for these findings. Throughout the Class 0 stage, the mass (and therefore energy and momentum supply) by the very actively accreting protostar is strongest. It drives a very powerful jet and is able to push material over large distances through the cloud. The flow evolves from zero length at the beginning to its full parsec-scale extent. Assuming a flow propagation speed of 200 km/s, a flow lobe needs about 2500 years to evolve to a size of 0.5 pc (i.e., a flow of a length of 1 pc, if both lobes are counted). Given the current estimates of the lifetime of the Class 0 stage of 10000-20000 years, 2500 years is a considerable fraction of the Class 0 stage. A fairly high fraction of parsec-scale jets is found among the Class 0 driven flows (1/3, which may indeed be a lower limit, as stated in Sect. 5.4). Furthermore, a certain fraction of Class 0 sources necessarily must have shorter outflows simply because they are so young that they did not yet have the time to build up a parsec-scale flow. Together, this strongly suggests that a very large fraction of protostars (if not all) are driving parsec-scale flows for some of their lifetime, apparently during much of their Class 0 stage and also during the early Class I phase. During the Class I and eventually the Class II stage, the power supply fades, and the protostar cannot provide enough energy/momentum any more to push the jet gas over parsec-scale distances. Since the gas at the head of the parsec-scale flow, which has been ejected from the protostar during its earlier, highly active phase, is finally decelerated, too, the flow will soon stop propagating, and its outermost parts will fade from view.

Is this “fading momentum supply leads to shortening” scenario realistic? It might be argued that a jet continues to propagate until the mass supply terminates entirely. In an ideal, straight jet, the material ejected from the source at any time (even the last gas parcel!) flows down the beam (which is of course also moving at the jet velocity) without any deceleration or energy loss, until it enters and pushes forward the terminating working surface. Jets in reality are not ideal. There is plenty of evidence that much of the jet gas will not just follow older jet gas, which is moving ahead of it at the same velocity. First, there are generally many knots and internal bow shocks along the jet beam. Apparently,

some of the kinetic energy is wasted on the way. Second, jet beams are generally not really straight, but show wiggles and bends. Presumably the jet gas does not flow along the curving path outlined by the wiggling beam. More likely is that the bends and wiggles reflect variations of the ejection direction at the driving source, with the jet gas moving ballistically along the direction it has been ejected (e.g., Heathcote et al. 1996). Thus, much of the jet gas will soon run into some ambient medium, which will generally be moving more slowly. It will be (more or less) continuously decelerated. Besides by the conditions in the ambient material, into which the jet is running, the length of a jet is then essentially determined by the momentum supply rate of the driving source (the more momentum there is, the longer the drag from the ambient medium has to act in order to decelerate the jet gas to rest, and the jet beam propagates further). Assuming a roughly constant jet velocity over time, the momentum supply rate is determined by the mass outflow rate, and thus eventually by the protostellar mass accretion rate. As the mass accretion/ejection rate decreases, the jet length decreases. Note also, that instabilities will more easily affect and disrupt a lighter jet (e.g., Stone 1997), which also helps to keep lighter jets short.

The continuous deceleration of a jet beam has presumably already been observed. Devine et al. (1997) report proper motion and radial velocity measurements on the prototypical HH 34 giant outflow ( $H_2$  jet #55). They show that there is a systematic decrease in the velocity of the Herbig-Haro objects (radial as well as tangential) with increasing distance from the driving source. As suggested by Devine et al. and as shown in more detail by Cabrit & Raga (2000), this is in fact more likely to be due to continuous deceleration of the jet along its path, rather than a gradual increase in ejection velocity. Taken together, this strongly suggests that the jet gas will be decelerated already before it reaches the terminating working surface of the jet. If it is brought to rest before it reaches the terminating working surface, the jet will shorten, as the old terminating working surface loses momentum supply and is subsequently brought to rest.

The evolutionary scenario suggested above implies that the class of giant outflows, which have been discovered during the last years, indeed represents the maximum extent of jets from young stellar objects. The prediction is that no flows should be found which are much longer than a few parsec, with a few exceptions (presumably driven by more luminous sources) reaching a size of order 10 pc. There will be no “hyperjets”, i.e., jets of which the currently found parsec-scale/giant/superjets are just the inner part. The maximum observable extent of young stellar object flows is limited by the evolution of the protostar itself, namely by the limited time span during which it provides sufficient momentum to push the jet gas over large distances in spite of the action of continuous deceleration. In contrast, it is often stated that the maximum observable extent of protostellar outflows is given simply by the maximum length of its path through the molecular cloud, until it breaks out of the cloud and fades from view, but actually extending much further (e.g., Eislöffel 2000). It also seems to be the case that jets can be traced even if they rush through a very tenuous environment: some of the Herbig-Haro objects found to trace the outermost parts of giant outflows are seen on exposures, on which background galaxies can easily be seen: the extinction through this medium must be low, thus the density of the material through which the flow runs, cannot be very high. New sensitive wide field surveys for giant Herbig-Haro flows covering large areas around molecular clouds are necessary to prove or disprove the above suggested scenario.

**$H_2$  luminosities.** The amount of  $H_2$   $2.12\mu\text{m}$  emission that is radiated by a jet ( $L_{2.12}$ ) is obviously a very interesting observable, since it is tightly connected to the energetics and kinematics of the jet. Since the cooling times of shock-excited  $H_2$  are only of order a few years, the  $H_2$  shocks highlight where the jet is right now interacting with the ambient medium (or itself), and how strong this interaction is right at the moment: *in  $H_2$ , we see the sparks that fly as the jet interacts*. It should thus, at least in principle, allow us to estimate the rate at which energy is transferred from the jets to the cloud. This quantity, in turn, will be closely related to the rate at which energy is fed into the jet by the driving source (termed

$L_{\text{now}}$  in the following;  $L_{\text{now}} = 1/2 \cdot \dot{M}_{\text{out}} v_{\text{jet}}^2$ ). Assuming furthermore that the injection velocity of the jet gas is not too different from some typical value ( $v_{\text{jet}} \sim \overline{v_{\text{jet}}}$ ), one can thus estimate the mass outflow rate  $\dot{M}_{\text{out}}$ .  $\dot{M}_{\text{out}}$  finally is tightly related to the protostellar mass accretion rate  $\dot{M}_{\text{acc}}$  (e.g.,  $\dot{M}_{\text{out}} = \epsilon \cdot \dot{M}_{\text{acc}}$ ,  $\epsilon \sim 0.1 \dots 0.3$  in disk wind models, see Section 2.5), which is certainly the key parameter governing the protostellar evolution. Thus the observations of the brightness of the  $\text{H}_2$  jets can be used to obtain valuable informations on the protostellar evolution and may allow one to constrain protostellar evolutionary schemes (particularly those models which predict the protostellar evolution in conjunction with the evolution of the outflow, like the “unification scheme” proposed by Smith 2000).

Momentum and energy supply rates are routinely estimated in the literature for molecular CO outflows. However, in the case of CO outflows, only the *average* supply rates can be measured, as the molecular outflow consists of material which has been accelerated during the entire outflow life time, i.e., the entire evolution of the protostar up to the time it is observed.  $\text{H}_2$  observations provide a truly complementary measure: as only the energy is measured which is right now radiated, one measures also only the energy which is right now injected.  $\text{H}_2$  observations are much more like a snapshot. Not the *average* energy/momentum supply rate is measured, but the *instantaneous* energy/momentum supply rate.  $\text{H}_2$  observations provide a much better time resolution in the study of protostellar outflow evolution and thus the underlying protostar.

**Converting  $L_{\text{H}_2}$  to  $\dot{M}_{\text{acc}}$ !** The problem is, that the relation between the measured  $L_{2.12}$  and the desired final observable  $\dot{M}_{\text{acc}}$  is not trivial. There is a number of factors which have to be taken into account, if  $L_{2.12}$  is to be converted to an estimate of  $\dot{M}_{\text{acc}}$ . A number of those factors are highly uncertain. Still, I will try to give some reasonable  $L_{2.12} \longrightarrow L_{\text{now}} \longrightarrow \dot{M}_{\text{acc}}$  conversion.

Besides the problem of unknown extinction (which will be assumed to be  $A_K = 1$  mag), one first has to understand, which fraction of the kinetic energy supply rate  $L_{\text{now}}$  of the jet that goes into shock fronts is eventually radiated in the observed  $v = 1-0\text{S}(1)$  line. This fraction is determined by a number of factors:

1. Only a certain fraction of the initially available kinetic energy of the jet will be available for consumption in the shock front ( $L_{\text{shock}}$ ). The rest will be kept as kinetic energy by the jet gas (the jet is not brought to rest in a shock, as is indicated by the high proper motions of Herbig-Haro objects and  $\text{H}_2$  shocks) and will be used to accelerate ambient material.
2. Besides radiation, a certain fraction of the energy available for consumption in the shock front will go into other processes, like ionisation of atoms and dissociation of molecules.
3. Only a certain fraction of the totally radiated energy will be radiated by  $\text{H}_2$  molecules ( $L_{\text{H}_2}$ ).
4. Only a certain fraction of  $L_{\text{H}_2}$  will be radiated in the  $v = 1-0\text{S}(1)$  line, which is observed here ( $L_{2.12}$ ).

It is plausible that all these factors depend on the actual properties of the part of the jet causing the shock as well as the properties of the ambient medium. In particular the jet velocity will be a major ingredient as well as the density of the jet and the ambient medium. Also the molecular content of the jet as well as the ambient medium will play a great role (if there are no  $\text{H}_2$  molecules, there will be no  $\text{H}_2$  emission), and also the strength and orientation of the ambient magnetic field will be important (dissociating J-shocks vs. nondissociating C-shocks).

The first of the above items, the fraction of the kinetic energy which is available for consumption by the shock, seems to be the hardest to quantify. Wilkin et al. (1997) discuss the energetics and

momentum distribution of bow shocks produced by two colliding winds, which can be adopted to the problem of a bow shock caused by a jet. They show a plot displaying the fraction of energy which is thermalized, dependent on the efficiency of momentum transfer and the ratio of the wind speeds. For most of their parameter values, this fraction is smaller than 30%. Davis & Eisloffel (1995) present a formula describing the fraction of radiated energy, depending on the ratio of the jet speed to the bow shock speed. According to this formula, the radiated energy is at most 15% of the jet mechanical luminosity; this maximum occurs for  $v_{\text{bow}}/v_{\text{jet}} = 1/3$ , i.e., a very slowly moving bow shock as expected for underdense jets. Taking a higher bow speed, as would be expected for an overdense young stellar object jet, would strongly reduce the fraction of the radiated energy: taking  $v_{\text{bow}}/v_{\text{jet}} = 3/4$  yields a fraction of only 5% of the kinetic energy which is radiated away. Together it seems that a fraction of the order of  $\sim 10\%$  of the kinetic energy being dissipated in the shock is a good guess:  $L_{\text{shock}} \sim 0.1 \cdot L_{\text{now}}$ .

Items (2),(3) and (4) may be obtained from sophisticated numerical molecular bow shock models, yielding about 1% of the total thermalized energy in the  $\text{H}_2 v = 1-0\text{S}(1)$  line ( $L_{2.12} \sim 0.01 \cdot L_{\text{shock}} \sim 0.001 \cdot L_{\text{now}}$ ; Smith, pers. comm.; Smith 1995); in the following I will generally assume that 10% of the thermalized energy is radiated by  $\text{H}_2$  molecules ( $L_{\text{H}_2} \sim 0.1 \cdot L_{\text{shock}}$ ), and 10% of the energy radiated by  $\text{H}_2$  molecules is in the  $v = 1-0\text{S}(1)$  line ( $L_{2.12} \sim 0.1 \cdot L_{\text{H}_2}$ ; the latter value is typical for molecular shocks (e.g., Smith 1995)). Thus, a total fraction of about 0.1% of the kinetic energy of the jet will eventually be emitted at  $2.12 \mu\text{m}$ :  $L_{2.12} \sim 0.001 \cdot L_{\text{now}}$ . This is certainly not more than a very crude order of magnitude estimate and will depend on the case to case circumstances, but may serve as a rough guideline throughout the following discussion. From the estimated kinetic energy input rate  $L_{\text{now}} = 1/2 \cdot \dot{M}_{\text{out}} v_{\text{jet}}^2$ , a momentum supply rate  $F_{\text{now}} = \dot{M}_{\text{out}} v_{\text{jet}}$  and a mass outflow rate  $\dot{M}_{\text{out}}$  may be derived, assuming a typical jet velocity of 200 km/s. Assuming furthermore a mass ejection fraction of  $\epsilon = 0.3$ ,  $L_{2.12}$  may directly be converted to a protostellar disk accretion rate as  $\dot{M}_{\text{acc}} \sim 10^{-7} \cdot (L_{2.12}/10^{-4} L_{\odot}) \cdot M_{\odot} \text{yr}^{-1}$ . Assuming a mass ejection fraction of  $\epsilon = 0.1$ , this has to be multiplied by 3, and correcting for an extinction of  $A_K$  of 1 mag, this has to be multiplied by a factor of 2.5.

The fixed conversion of  $L_{2.12}$  into  $L_{\text{now}}$  implies some more simplifying assumptions. First, it is assumed that the energy pumped into the flow immediately produces the  $\text{H}_2$  emission. In reality, a given parcel of gas injected into the jet may need quite some time before it is shocked, e.g., up to  $10^4$  years before it reaches the terminating working surface of a giant flow. Thus the conversion of  $L_{\text{now}}$  into  $L_{2.12}$  can be expected to be delayed. Second, the generally observed occurrence of internal working surfaces implies that  $L_{2.12}$  is not only delayed, but also smeared out over a certain time interval. A given parcel of jet gas may go through several shocks, losing kinetic energy piece by piece. The delay and smearing out of  $L_{2.12}$  will affect the conclusions drawn from examining the behaviour of  $L_{2.12}$  only, if the timescale over which it is smeared and delayed is comparable to the timescale over which significant changes in the behaviour of the driving engine occur, i.e., presumably only at the earliest evolutionary stages. On the other hand, the smearing out will help to avoid problems when comparing models of continuously working driving engines with the observed jets which generally show evidence for episodic mass ejection events. Third, the assumption that a fixed fraction of  $L_{\text{now}}$  is converted into  $L_{2.12}$  ignores probable variations of the properties of the individual jets and the ambient medium. For example, Völker et al. (1999) find in their jet simulations that more  $\text{H}_2$  emission is seen from pulsed, wiggling jets than from non-pulsed jets. Also the extreme case of an atomic jet running into an atomic medium will obviously produce no  $\text{H}_2$  emission at all.

Giving believe to all the above assumption ( $L_{\text{now}}$  is a fixed multiple of  $L_{\text{H}_2}$ ;  $v_{\text{jet}}$  is equal to a fixed (in time and for all jets) typical velocity,  $\dot{M}_{\text{out}}$  is a fixed (in time and for all protostars) fraction of  $\dot{M}_{\text{acc}}$ ), it is stated: the protostellar mass accretion rate  $\dot{M}_{\text{acc}}$ , the mass outflow rate  $\dot{M}_{\text{out}}$ , the instantaneous momentum supply rate  $F_{\text{now}}$ , and the instantaneous kinetic energy supply rate  $L_{\text{now}}$  are all



proportional to the luminosity  $L_{2.12}$  of a jet in the  $2.12\ \mu\text{m}$  line of molecular hydrogen.

**Back to the observations.** The analysis of the flow  $\text{H}_2$  luminosities in Section 5.5 showed that Class 0 driven jets tend to be more luminous, Class I jets tend to be of intermediate luminosity (with a very broad distribution, some very luminous as well as a number of rather faint Class I jets are also found), and the few Class II driven jets tend to be of very low luminosity. Taking the above arguments serious, this reads: Class 0 sources tend to have high accretion rates, Class I sources have a large range of accretion rates, some rather high, most intermediate, and a number of them fairly low accretion rates; Class II sources are only weakly accreting. This trend becomes even clearer, if the predicted effect of the cloud core sound speed on the accretion rate is taken into account ( $\dot{M}_{\text{acc}} = c_{\text{eff}}^3/G \cdot f(t)$ , with  $f(t) \equiv 1$  in the Shu (1977) star formation paradigm; see Section 6.3). As can be seen in Fig. 45, *the Class 0 driven flows all have  $\text{H}_2$  luminosities (i.e., accretion rates) about 20 to 40 times higher than predicted by the Shu (1977)  $\dot{M}_{\text{acc}} = c_{\text{eff}}^3/G$  relation*, whereas the remaining sources (the large majority of them Class I sources) have  $\text{H}_2$  luminosities/accretion rates consistent with or only a few times higher/lower than expected for a  $\dot{M}_{\text{acc}} = c_{\text{eff}}^3/G$  relation.

Having derived the conversion factor for  $L_{2.12} \rightarrow \dot{M}_{\text{acc}}$ , it should be worthwhile to check how large the estimated accretion rates are. Starting with the prototype  $\text{H}_2$  jets HH 211 and HH 212 ( $L_{2.12} = 34 \cdot 10^{-4} L_{\odot}$  and  $L_{2.12} = 69 \cdot 10^{-4} L_{\odot}$ , respectively), this yields accretion rates of order  $\dot{M}_{\text{acc}} \sim 1 \cdot 10^{-5} M_{\odot}/\text{yr}$  and  $\dot{M}_{\text{acc}} \sim 2 \cdot 10^{-5} M_{\odot}/\text{yr}$ , respectively (corrected for  $A_{\text{K}} = 1$  mag). The  $\text{H}_2$  jets with the highest  $L_{2.12}$  found in the survey have  $L_{2.12} \sim 200 \cdot 10^{-4} L_{\odot}$ , therefore the accretion rates in these systems are of order  $5 \cdot 10^{-5} M_{\odot}/\text{yr}$ . Compared to accretion rates typical of T Tauri stars ( $\dot{M}_{\text{acc}}$  of order  $10^{-7} M_{\odot}/\text{yr}$ ), these estimates are very high. Even the FUOr systems are thought to have accretion rates only a few times higher than those estimated here (of order  $10^{-4} M_{\odot}/\text{yr}$ ), which are however only achieved during limited time intervals. As noted above, particularly the long, young and luminous jets have dynamical timescales which are greater than the time span between FUOr outbursts, thus the  $\text{H}_2$  emission integrated over the jet beam should average out these variations. That means, that these very luminous jets, driven mainly by very young protostars, imply *average* accretion rates only a few times lower than in the short time FUOr outbursts in more evolved (T Tauri) stars. On the other hand, if a star (e.g., of  $1 M_{\odot}$ ) has to accrete the bulk of its mass during the first  $\sim 10^5$  yr (the Class 0 plus Class I life time), an average mass accretion rate of order  $10^{-5} M_{\odot}/\text{yr}$  is inevitable, thus the above estimates are in fact not too high. The more typical values of  $L_{2.12}$  are one to two orders of magnitude lower than the above noted extreme values, implying accretion rates which are one to two orders of magnitude lower. Since the typical  $\text{H}_2$  jet source is a Class I source, and classical T Tauri stars mostly Class II sources, this might point to an evolution of the high accretion rates of  $\text{H}_2$  jet driving sources to the lower accretion rates of T Tauri stars.

The assumption of a fixed (in time) value for the mass ejection fraction  $\epsilon$  presumably has no major impact on this conclusion. The assumed value of  $\epsilon = 0.3$  is in the upper range of what is usually assumed. Taking lower values would increase the resulting mass accretion rate. A time variable ejection fraction would more likely have a maximum early in the stellar evolution (as required, e.g., in the unification scheme presented by Smith 2000, see Sect. 7.2 below). This means that the high accretion rates which resulted for the very young, highly active sources noted above, are still about the same, whereas for more evolved sources the ejection fraction may be somewhat lower (by a factor of a few), and the accretion rates somewhat higher than estimated here. This would however not explain the order of magnitude differences in  $\text{H}_2$  luminosity as observed here. Also the fixed jet velocity will differ in reality by not much more than a factor of two.

**Summary.** As a summary of this Section, it appears that there is a clear evolution, namely a decline, in outflow activity with time, which can be attributed to a decline in mass outflow rate, and consequently to a decline in mass accretion rate in the protostellar system. Jets are found presumably from all Class 0 sources, apparently from a large fraction of the Class I sources, and only from a minor fraction of the Class II sources. The longest, parsec-scale jets are found during the late Class 0 and the early Class I phase. Earlier, the jet (although very powerful) did not yet have the time to expand to its final extent, later on it shortens because of a declining momentum supply. The evolution in H<sub>2</sub> luminosity can also be interpreted as a decline in momentum supply, i.e., accretion activity. The jet may go through the following stages:

Early Class 0	Short (<1 pc) bright (possibly strongly extincted)	V 380 Ori NE (H <sub>2</sub> jet # <b>59</b> ) HH 211, HH 212
Late Class 0 very early Class I	Giant flow (a few parsec) bright	HH 43 giant flow (H <sub>2</sub> jet # <b>67</b> ) L1641-S3 giant flow (H <sub>2</sub> jet # <b>76</b> ) L1641-N giant flow (H <sub>2</sub> jet # <b>49</b> )
Early Class I	Giant flow (a few parsec) getting fainter	HH 34 giant flow (H <sub>2</sub> jet # <b>55</b> ) H <sub>2</sub> jet # <b>51</b>
Most of Class I	subparsec scale flow moderately bright to faint	Haro 4-255 FIR (H <sub>2</sub> jet # <b>72</b> ) H <sub>2</sub> jet # <b>58</b>
Late Class I very early Class II	Short faint (residual H <sub>2</sub> jet)	Haro 4-255 jet (H <sub>2</sub> jet # 73) HH 147/N <sup>3</sup> SK50 (H <sub>2</sub> jet # 63)
Class II	optical T Tauri star jets microjets	

Table 4: The evolution of a protostellar jet.

## 7.2 $L_{\text{H}_2}$ vs. $L_{\text{bol}}$ : Testing the toy model of protostar/outflow evolution

Smith (2000) presents a toy model, aimed at providing an easy to handle, easy to modify description of the simultaneous evolution of the protostellar envelope, the protostellar disk, the protostar, the jet driven by the protostar, and the molecular outflow accelerated by the protostellar jet. The model prescribes a (time-dependent) mass inflow rate and a (time-dependent) jet speed, all other quantities are calculated from the model based on simple assumption about the physics and dynamics of the protostellar system.

In this Section I will do some first, crude steps in order to explore whether this model is able to reproduce the properties of the jet and protostar sample studied in this thesis. This should be regarded as an initial step rather than a thorough, elaborate test of the model. A lot more can be done in future, both from an observational side and from the theoretical side.

The model is a combined protostar and outflow evolution model, and calls for a comparison of jet and protostar properties. Besides the evolutionary stage of the driving sources, I have estimated (or in many cases put some constraints on) the bolometric luminosity of the driving sources, the discussion

of which has been left aside so far in this chapter. As shown in Section 5.5, there is fairly clear evidence for a correlation between  $L_{\text{bol}}$  and  $L_{\text{H}_2}$  for the Class I driven flows. This correlation is absent for the Class II driven flows. For the Class 0 driven flows, it appears that they might have typically higher  $\text{H}_2$  luminosities than Class I sources of similar bolometric luminosity.

The bolometric luminosity of a very young stellar object will be determined by a number of ingredients. On the one hand, there is the luminosity  $L_*$  of the protostellar core, which evolves to a pre-main-sequence star. Accretion is another source of luminosity, which will dominate the bolometric luminosity in the youngest, strongly accreting protostars. The accretion luminosity is determined by the mass of the central object  $M_*$ , its radius  $R_*$  (or better, the radius at which kinetic infall energy is converted to heat), and the mass accretion rate:  $L_{\text{acc}} = G \cdot M_* \dot{M}_{\text{acc}} / R_*$ , and  $L_{\text{bol}} = L_{\text{acc}} + L_*$ . This relation makes a simple interpretation of the  $L_{\text{H}_2}$  vs.  $L_{\text{bol}}$  plots presented in Figs. 25 and 26 difficult.

The absence of any correlation between  $L_{\text{bol}}$  and  $L_{\text{H}_2}$  for the Class II objects is easily explained. Here  $L_{\text{H}_2}$  is essentially determined by the accretion activity of the protostar, which is comparably low at this late stage. Consequently,  $L_{\text{bol}}$  will be determined by the stellar luminosity  $L_*$  rather than by  $L_{\text{acc}}$  and thus be independent of the accretion activity. Then no correlation between  $L_{\text{bol}}$  and  $L_{\text{H}_2}$  can be expected.

The correlation of  $L_{\text{bol}}$  and  $L_{\text{H}_2}$  for the Class I sources is more difficult to explain. It might point to a dominance of  $L_{\text{acc}}$  over  $L_*$ , such that  $L_{\text{bol}}$  is strongly dependent on  $\dot{M}_{\text{acc}}$  (as is  $L_{\text{H}_2}$ ). This however cannot be the full explanation, since  $L_{\text{acc}}$  also depends on the mass of the protostar (which may be close to its final value and not change too much any more; similarly, the radius might be rather fixed), and very likely protostars of different final mass are present in the sample. It is also not clear, if and when the stellar luminosity becomes comparable to the accretion luminosity.

The situation becomes even more difficult to assess for the Class 0 objects, although there it is presumably well justified to take the accretion luminosity as dominating source of luminosity. On the other hand, the masses of the central objects (which are the precursors of stars with varying final masses) are some small, poorly determined fractions of the final stellar masses, and the radii of the protostellar cores presumably are also not fixed at this early stage.

The evolutionary scheme proposed by Smith (2000) offers itself to explore the  $L_{\text{bol}}$  vs.  $L_{\text{H}_2}$  dependencies, and to explain its features, since it yields all of the above quantities. In order to compare the  $L_{\text{H}_2}$  and  $L_{\text{bol}}$  data of the  $\text{H}_2$  jet sample with the unification scheme, I have calculated the evolution of  $L_{\text{now}} = 100 \cdot L_{\text{H}_2}$  and  $L_{\text{bol}}$  from the model for a range of final masses, and plotted the resulting curves into the  $L_{\text{H}_2}$  vs.  $L_{\text{bol}}$  plots for the jet sample (Fig. 47). In doing so, the final mass of the protostar was changed by simply assuming different normalization factors for the mass accretion rate. This might not be a physically meaningful approach, because also the evolutionary time scale might depend on the final mass. However, as long as the evolution of the accretion rate with time is of the same *type* (a peak at the beginning followed by a decline), the shape of the evolutionary track should be the same; changing the time scale would only result in changing the normalization factor of the accretion rate. Since both,  $L_{\text{bol}}$  as well as  $L_{\text{H}_2}$  depend on the accretion rate, this would only result in a shift of the track in both,  $L_{\text{bol}}$  and  $L_{\text{H}_2}$ . That means, one should simply not trust the age and the mass assigned to a given point on a given track. In addition to the tracks, I also plotted the location of the transition from Class 0 to Class I (the point at which the mass of the protostellar core equals the mass of the circumstellar material) as derived from the model for the different final masses as a thick line.

The following assumptions go into the model. First, as noted above, the accretion rate is taken to be time-dependent, with a sharp exponential rise and a subsequent power-law falloff:

$$\dot{M}_{\text{acc}}(t) = \dot{M}_0 (e/\alpha)^\alpha (t/t_0)^{-\alpha} \exp(-t/t_0)$$

Second, the jet velocity is prescribed to have an exponential rise and to approach a final velocity  $v_f$  of

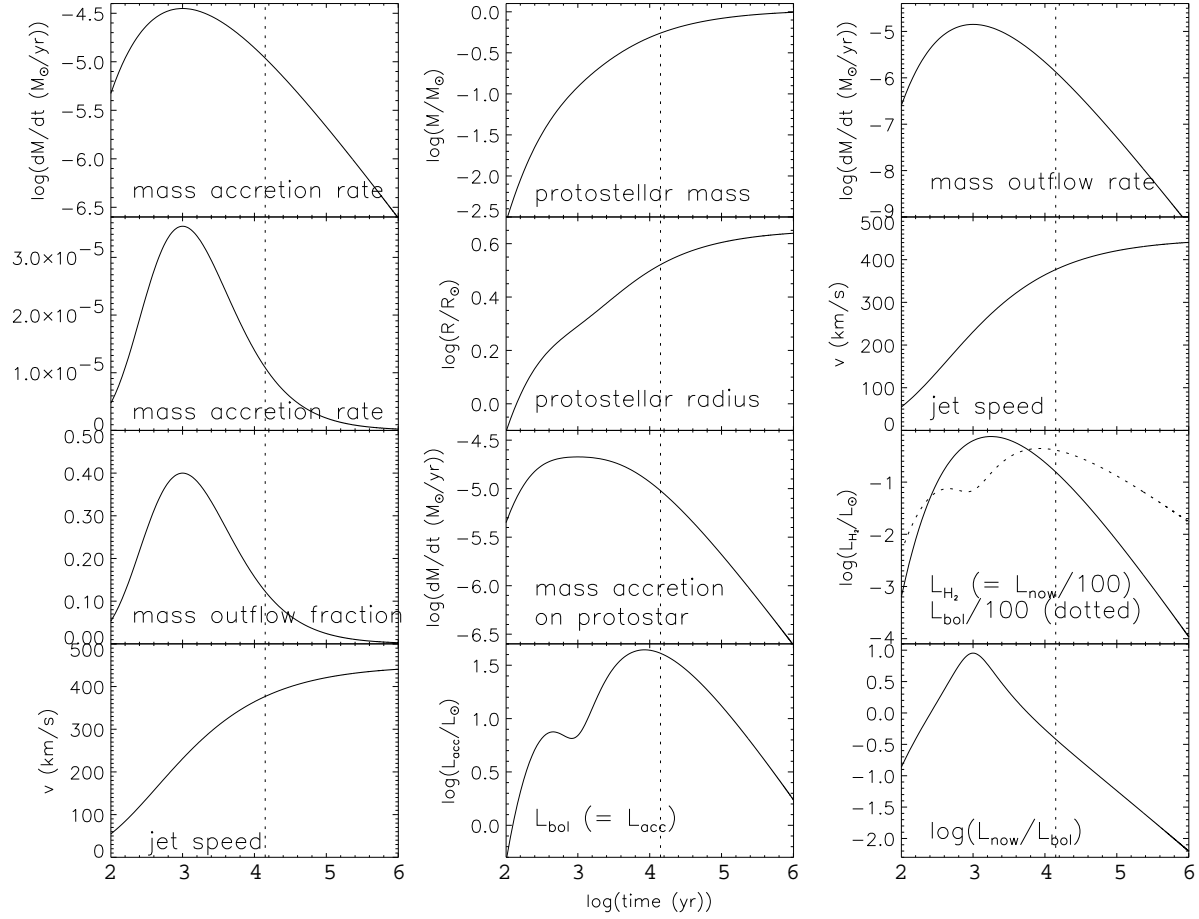


Figure 46: The time evolution of various quantities as predicted by the Smith (2000) unification scheme. The dotted, vertical lines mark the time of the transition from the Class 0 to the Class I stage (i.e., the time at which the circumstellar mass of the model protostar equals the mass of the protostellar core).

450 km/s:

$$v_{\text{jet}} = v_f \exp(-t_1/t)$$

Furthermore, a time dependent ejection fraction  $\epsilon(t) = \eta(\dot{M}_{\text{acc}}(t)/\dot{M}_0)$  is assumed. The mass of the protostellar core is calculated from the accretion rate (minus the ejected mass). The jet speed is fixed to be some multiple of the protostellar escape speed,  $v_{\text{jet}} = \chi \cdot \sqrt{GM_*/R_*}$ , which in turn determines the radius  $R_*$  of the protostellar core. The models makes a number of additional assumptions in order to explain the evolution of the protostellar environment (envelope and disk) as well as the propagation and properties of the jet and the evolution of molecular outflows, which are however not of interest here. The tracks have been calculated using the same parameters as given by Smith (2000): the mass flow time scale  $t_0 = 20000$  yr; the jet speed time scale  $t_1 = 60000$  yr; the mass rate power index  $\alpha = 2.0$ ; the maximum jet ejection fraction  $\eta = 0.4$ ; the jet speed factor  $\chi = 2.12$ ; the final jet speed  $v_f = 450$  km/s. From these inputs,  $L_{\text{H}_2}(t)$  has been calculated as

$$L_{\text{H}_2}(t) = 0.4 \times 0.01 \times 1/2 \cdot \epsilon(t) \dot{M}_{\text{acc}}(t) \cdot v_{\text{jet}}^2(t)$$

(the factor 0.4 is to correct for 1 mag of K-band extinction), and  $L_{\text{bol}}$  as

$$L_{\text{bol}}(t) = L_{\text{acc}}(t) = G \cdot M_*(t) \cdot (\dot{M}_{\text{acc}}(t) - \dot{M}_{\text{out}}(t))/R_*(t)$$

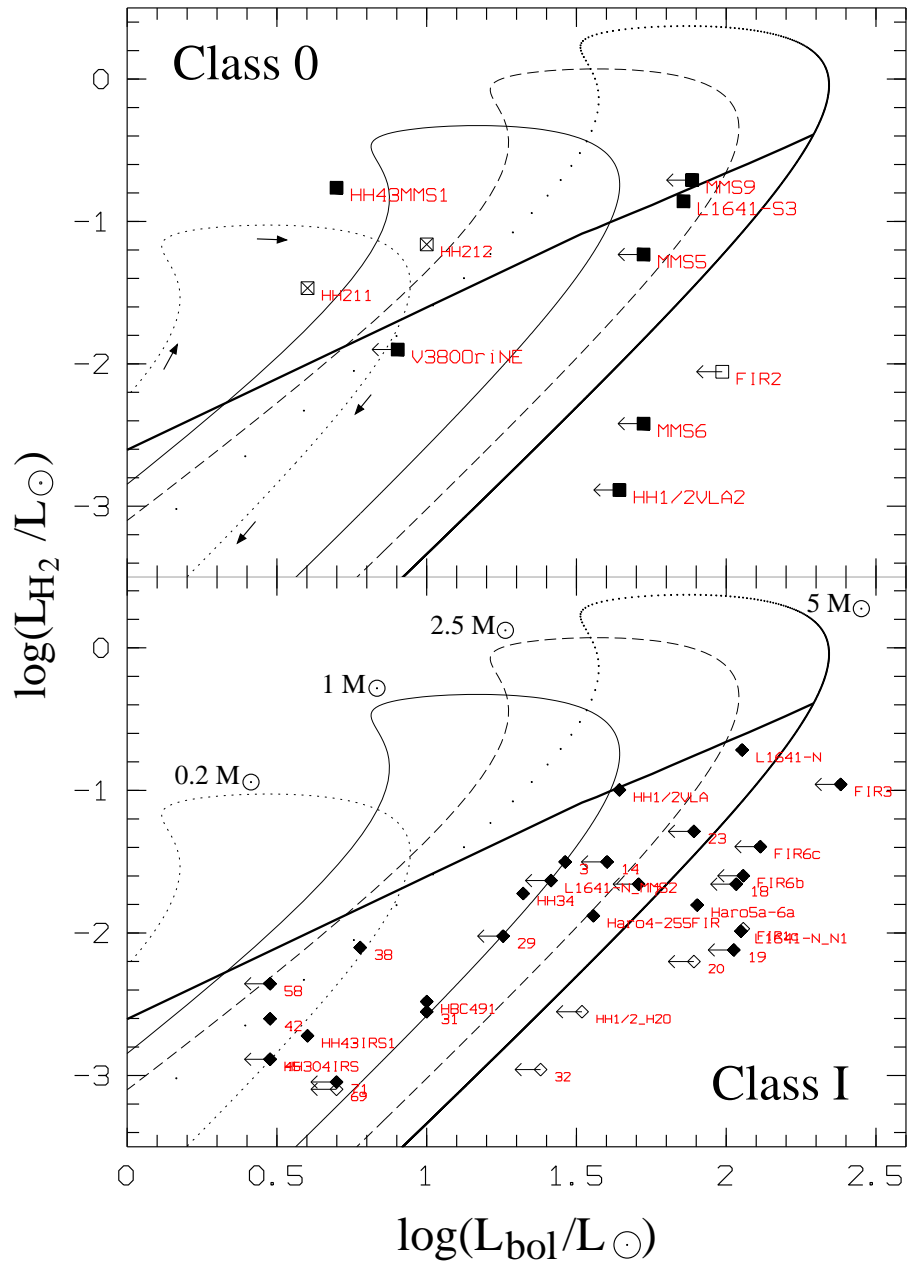


Figure 47: Flow  $L_{\text{H}_2}$  as a function of  $L_{\text{bol}}$  of the jet driving source (see Fig. 26). The curves are evolutionary tracks calculated according to Smith (2000). The dotted line (equally spaced dots) represents the evolution of a  $0.2 M_{\odot}$  protostar, the solid line a  $1 M_{\odot}$ , and the dashed line a  $2.5 M_{\odot}$  protostar. The dotted curve (unequally spaced dots) represents the evolution of a  $5 M_{\odot}$  protostar; here a data point is plotted every 200 years, to show the fast evolution at the beginning (large spaces between dots) versus the slow evolution at the end (small spaces between dots). The thick, almost straight line marks the transition between the Class 0 and Class I stage for protostars of different masses (defined as the time at which the mass in the stellar core equals the circumstellar mass). Class 0 sources should be found above, Class I sources below this line.

The time evolution of the quantities of interest for the present discussion for a  $1 M_{\odot}$  protostar as calculated from the unification scheme (with the same input parameters and assumptions as chosen by Smith 2000) is plotted in Fig. 46, and the  $L_{\text{H}_2}$  vs.  $L_{\text{bol}}$  evolution for protostars with a range of final masses is shown in Fig. 47. As it can be seen from Fig. 47, the  $L_{\text{H}_2}$  vs.  $L_{\text{bol}}$  evolutionary tracks calculated from the unification scheme can indeed approximately reproduce the locations of the Orion A

jets and driving sources in the  $L_{\text{H}_2}$  vs.  $L_{\text{bol}}$  plot. The tracks describe a looplike curve.  $L_{\text{H}_2}$  and  $L_{\text{bol}}$  first both increase very quickly, then  $L_{\text{H}_2}$  reaches a maximum while  $L_{\text{bol}}$  further increases, then  $L_{\text{bol}}$  goes through its maximum while  $L_{\text{H}_2}$  starts to decrease, and finally both quantities decrease (with the ratio of  $L_{\text{H}_2}/L_{\text{bol}}$  smaller than at the beginning). The youngest sources (corresponding to the Class 0 stage) are in fact located at higher  $L_{\text{H}_2}$  and lower  $L_{\text{bol}}$  than the older (Class I) sources.

The *presence* of this loop-like structure is due to the assumed time-dependent mass ejection fraction  $\epsilon(t)$  (introduced in order to explain the molecular outflow data presented by Bontemps et al. 1996a). With the assumed dependency of the protostellar radius on the jet velocity, the ratio of  $L_{\text{now}}/L_{\text{bol}}$  is given by  $\epsilon(t)/[2/\chi^2 - \epsilon(t)]$ . If the ejection fraction  $\epsilon$  was constant, then also the ratio of  $L_{\text{now}}/L_{\text{bol}}$  would be constant, and the loop would reduce to a straight line in Fig. 47. The *shape* of the loop is determined by the times when  $L_{\text{H}_2}$  ( $L_{\text{now}}$ ) reaches its maximum, and when  $L_{\text{bol}}$  reaches its maximum, i.e., by the timescale of the jet velocity evolution in comparison to the mass accretion time scale.

A possible weakness in the calculation of the  $L_{\text{H}_2}$  vs.  $L_{\text{bol}}$  evolutionary tracks may be the dependency of  $L_{\text{bol}}$  on the prescribed jet velocity via the protostellar radius. Although it is argued by Smith (2000) that the radii obtained by this assumption are consistent with stellar evolution models, it might be more reasonable to prescribe the protostellar radius (e.g., as a function of protostellar mass and maybe accretion rate), and to calculate the jet velocity from that using some meaningful assumptions on the relation between jet velocity and the Keplerian velocity at the jet injection point (which may not be at the stellar radius). Furthermore, for a reasonable comparison of  $L_{\text{bol}}$  with any other parameter it would certainly be desirable to get some estimate of the luminosity of the central protostellar core, particularly at later times.

To conclude this section, it has been shown that the Smith (2000) toy model of the simultaneous evolution of a protostar, its environment, and its outflow can reproduce the characteristic locations of the  $\text{H}_2$  jets and their driving sources in the  $L_{\text{H}_2}$  vs.  $L_{\text{bol}}$  plane. Class 0 sources were found to have a tendency towards higher  $L_{\text{H}_2}$  at comparable  $L_{\text{bol}}$  than Class I sources. This is reproduced by  $L_{\text{H}_2}$  vs.  $L_{\text{bol}}$  evolutionary tracks calculated from the model with the “standard” assumptions used by Smith (2000). These tracks describe a loop, with high  $L_{\text{H}_2}$ , but low  $L_{\text{bol}}$  at the beginning. The presence of the loop is due to the assumption of a time-variable mass-ejection fraction  $\epsilon(t)$ , which has a maximum early in the protostellar evolution; this assumption proved to be necessary in order to reproduce the Bontemps et al. (1996a) molecular outflow data. Thus it seems that the  $\text{H}_2$  jet data are in support of this assumption.

Besides the reproduction of the locations of the Class 0 sources from the model, at this point it is probably not wise to investigate more details of the model or to try to get exact fits to the data and estimate masses or ages from the tracks: the observational uncertainties are rather large, and there are much too many parameters and assumptions in the model which could be changed. However, the Orion  $\text{H}_2$  jet sample presented in this thesis may be a valuable base for further explorations and tests for the unification scheme. In particular, this will mean a better determination of the driving source parameters hopefully in the near future (i.e., better SEDs through follow up photometry, and a determination of the circumstellar masses from an already existing 1.3 mm continuum survey). Furthermore, the  $\text{H}_2$  jet sample calls for an investigation of the molecular CO outflows which are presumably associated with the  $\text{H}_2$  jets. Finally, it should always be kept in mind that accretion (and outflow) presumably are episodic, which implies that particularly  $L_{\text{bol}}$  may be strongly variable on short time scales rather than follow a smooth evolution as assumed here.

The compilation of additional data will allow us to test and evolve the “unification scheme” much further than has been shown here. Obvious improvements are the modeling of the shortening of the jet with time (inclusion of a continuous drag), and a more realistic treatment of the protostar itself

(removal of the dependency of the stellar radius (hence the accretion luminosity) on the prescribed jet velocity, inclusion of the stellar luminosity in addition to the accretion luminosity).

### 7.3 Estimated impact of the jets on the Orion A molecular cloud

The estimated lifetimes of giant molecular clouds (a few times  $10^7$  yr, see e.g., Blitz 1993) and the observed low star formation rate pose some problems. The timescale for such a cloud to collapse under its own gravity is less than  $10^7$  years (see below). If all molecular clouds in the galaxy were in free fall collapse, the star formation rate would have to be much larger than is observed (Zuckerman & Palmer 1974). Given the apparently longer lifetimes of giant molecular clouds and the low star formation efficiency, it is clear that the clouds cannot be in free-fall collapse. Instead, there must be some mechanism which counteracts the clouds' self-gravity and stabilizes them against collapse. There seem to be several ways of how to do this, most importantly probably magnetic fields frozen into the cloud material (e.g., Shu et al. 1987). The generally observed supersonic linewidths in molecular clouds suggest turbulent pressure as another supporting agent (Zuckerman & Evans 1974; Larson 1981). However, the problem with this suggestion is that supersonic turbulence is a strongly dissipative phenomenon (both, pure hydrodynamic as well as magnetohydrodynamic turbulence), with decay time scales presumably shorter than the free-fall time scale of a cloud (MacLow 1999; see also Goldreich & Kwan 1974; MacLow et al. 1998, 1999; Stone et al. 1998; Ostriker et al. 1999). Thus, in order to make turbulence a viable support mechanism, one has to search a way to replenish turbulent motions in the cloud.

Ever since the discovery of high velocity molecular flows from forming stars, there has been a debate on whether these flows could inject significant quantities of energy and momentum into the clouds, thus helping to stabilize them against collapse and provide a self-regulation mechanism for star formation. To illustrate this point, the very first paper dealing with the outflow nature of the high velocity molecular gas in OMC-1 by Kwan & Scoville (1976) noted that the outflow would not have a significant impact on the cloud in terms of momentum input. In contrast, Solomon et al. (1981) concluded that an outflow such as OMC-1 might well be the exciting source for the turbulent motions in a giant molecular cloud considering the energy input. These two papers serve to draw attention to a major difficulty in estimating the impact of outflows on the cloud. The outflows are made up of high velocity gas, whereas the turbulent motions supposedly excited by the outflows have much lower velocities. The high velocity gas in the outflows has to transfer its kinetic energy to the cloud gas: the question is, whether this happens in an energy conserving manner (almost all the kinetic energy of the flow is transformed to turbulent kinetic energy, little is radiated away) or in a momentum conserving manner (only a small fraction of the flow kinetic energy can be transferred to the cloud gas, most has to be dissipated). No consensus on the debate has been reached so far. Further discussion of this and related issues can be found in a number of papers (e.g., Norman & Silk 1980; Draine 1983; Bally & Lada 1983; Lada 1985; Fukui 1989; some papers which conclude "Yes, outflows can stabilize clouds or have some significant impact on the cloud" are: Fukui 1989; Morgan et al. 1991; Norman & Silk 1980; Draine 1983; Bally et al. 1999 (to cite only a few); some papers which conclude "No, outflows do not stabilize/significantly influence clouds" are: Bally & Lada 1983; Levreault 1988b)

Virtually all estimates of the feedback of outflows from young stars on the molecular clouds relied on CO outflow observations. A number of probable sources of error are known to affect the derived flow properties, the most serious probably being the estimate of the dynamical life times of the flows (e.g., Padman et al. 1997). This in turn greatly affects the estimated energy and momentum input rates estimated from the CO data. The H<sub>2</sub> survey presented in this thesis allows an alternative approach to this issue. For the first time the H<sub>2</sub> outflow activity has been revealed over a significant portion of a giant molecular cloud, thus making any assumptions about star formation rates, outflow lifetimes, etc.

obsolete: the outflows just have to be counted, or better, their cumulative energy and momentum input as deduced from the H<sub>2</sub> shock emission just has to be added up. Although there are admittedly considerable sources of error with the new approach, it may still be better than the old procedure, or at least provide an independent check.

**The energy and momentum supply rate.** The *maximum* rate at which energy may be transferred from the outflows to the ambient cloud medium is the rate at which energy is provided by the flow driving sources

$$L_{\text{turb}} = \frac{1}{2} \sum_i \dot{M}_{\text{jet},i} \cdot v_{\text{jet},i}^2 =: \frac{1}{2} \dot{M}_{\text{all jets}} \cdot \overline{v_{\text{jet}}^2}$$

Similarly, the (forward) momentum supply rate can be estimated as

$$\begin{aligned} F_{\text{turb}} &= \sum_i \dot{M}_{\text{jet},i} \cdot v_{\text{jet},i} \simeq \dot{M}_{\text{all jets}} \cdot \overline{v_{\text{jet}}} \\ &\simeq 2 \cdot \frac{L_{\text{turb}}}{\overline{v_{\text{jet}}}} \end{aligned}$$

where  $\dot{M}_{\text{all jets}}$  corresponds to the coadded mass loss rates of all protostars, and  $\overline{v_{\text{jet}}}$  stands for the typical outflow velocity, which I will assume to be 200 km/s.  $L_{\text{turb}}$  is an upper limit for the kinetic energy transferred to the cloud, since part of this energy is radiated away. The *minimum* rate at which energy is transferred to the ambient cloud medium is directly indicated by the emitted radiation from the shocks: according to Fischer et al. (1985; see also Beckwith 1980) the amount of energy transferred to the ambient medium per unit time is about the same as is radiated (or better, consumed in the shock  $L_{\text{shock}}$ ; initially at least two times  $L_{\text{shock}}$  had to be present as kinetic energy) given the fact that the material is generally not at rest after passing through the shocks, this is a lower limit only. Since the shocks are known to move rather fast, a considerable amount of energy may still be present after the material went through the shock, implying that the available kinetic energy may still be rather large. Thus the rate at which energy is transferred to the cloud will be somewhere between these extreme values, probably much more than the minimum.

$L_{\text{turb}}$  can be estimated from the H<sub>2</sub> survey by adding up the H<sub>2</sub> luminosities  $L_{\text{H}_2} \simeq 10 \times L_{2.12}$  of all detected knots and multiplying this by a factor of 10 to account for energy radiated by other species than H<sub>2</sub> or consumed through other mechanisms (e.g., ionisation, dissociation; see above). This yields the total rate at which energy is consumed in shocks. Including all knots (i.e., the knots with and without flow associations as well as the features in the Orion Nebula area, but not the OMC-1 outflow) a total H<sub>2</sub> luminosity  $L_{\text{H}_2, \text{tot}}$  of  $0.46 L_{\odot}$  is found (using 1 mag of extinction). This means that in total  $L_{\text{shock}} \sim 5 L_{\odot}$  is radiated (or otherwise consumed) in shocks, and thus a lower limit for the energy input rate  $L_{\text{turb}, \text{min}} = L_{\text{shock}}$  of  $\sim 5 L_{\odot}$  is obtained. According to the above estimate, about 10 times more energy per unit time is actually supplied to the flows than is radiated away (or otherwise consumed) by the shocks. Thus the upper limit for the energy supply rate  $L_{\text{turb}, \text{max}} \sim 10 \times L_{\text{shock}}$  to the cloud may be about  $50 L_{\odot}$ . These two estimates correspond to a minimum momentum supply rate  $F_{\text{turb}, \text{min}}$  of  $60 \times 10^{-5} M_{\odot} \text{ km s}^{-1} \text{ yr}^{-1}$  (at least  $2 \times L_{\text{shock}}$  had to be available as kinetic energy initially) and  $F_{\text{turb}, \text{max}}$  of  $300 \times 10^{-5} M_{\odot} \text{ km s}^{-1} \text{ yr}^{-1}$ , respectively<sup>4</sup>. Together, it appears plausible that the energy supply rate  $L_{\text{turb}}$  of the protostellar driving sources may be a few times  $10 L_{\odot}$ , and the momentum supply rate  $F_{\text{turb}}$  of the order of  $2 \cdot 10^{-3} M_{\odot} \text{ km s}^{-1} \text{ yr}^{-1}$ , assuming strict forward momentum conservation; if motions or MHD waves are induced transverse to the jet propagation direction,  $F_{\text{turb}}$  might well be larger.

<sup>4</sup>This compares pretty well with the coadded momentum input rates obtained by Bontemps et al. (1996a) of  $F_{\text{CO}, \text{all flows}} \simeq 160 \times 10^{-5} M_{\odot} \text{ km s}^{-1} \text{ yr}^{-1}$  for a similarly large sample of young stellar objects of comparable (maybe somewhat lower) masses. This can be taken as an additional justification of the above assumptions regarding the link between kinetic flow energies and shock luminosities.



**The “energy loss factor”.** Before considering the possible impact of this kinetic energy and momentum source on the cloud, there is another point that has to be noted. The discovery that many protostellar jets extend over several parsecs has two implications. On the one hand, it helps to solve the problem that the jets might only influence a very small part of a cloud immediately at the protostars’ location: this is clearly not the case, protostars can apparently influence parts of the cloud which are parsecs away. On the other hand, one must be careful not to overestimate the impact that the jets could have. The great length of the flows also implies that a significant part of the kinetic energy and momentum provided by the driving protostar might get lost to the diffuse interstellar medium, as the jet might propagate beyond the edge of the cloud. The fraction of energy which is lost certainly depends on the relative size of the cloud with respect to the length of the jets. The smaller the cloud, the larger is the chance that flows peak out of the cloud. Thus no generally applicable “energy loss factor” can be given; instead, this issue has to be discussed on a case by case basis. Finally, the above value for the energy supply rate of the protostars has been estimated using the amount of H<sub>2</sub> shock emission in the molecular cloud. It is likely that much of the H<sub>2</sub> emission is from ambient molecular material that is hit by the flow. Thus the above estimates of  $L_{\text{turb}}$  and  $F_{\text{turb}}$  automatically account for the energy loss to the interstellar medium by counting only those parts of the flows which indeed interact with the molecular cloud.

**Which energy/momentum input rate can be regarded to be significant?** Now it has to be assessed whether an energy and momentum input rate as has been estimated above could be significant for a cloud. For this I will consider the gravitational energy  $W$  of a cloud

$$W = \frac{3}{5} a \frac{GM^2}{R}$$

and its momentum  $P$  of internal (presumably turbulent) motions

$$P = Mv_{\text{turb}}$$

which will be estimated assuming that the cloud is in virial equilibrium

$$\begin{aligned} W &= 2 \cdot \mathcal{T} \simeq 2 \cdot \frac{1}{2} Mv_{\text{turb}}^2 \\ \implies P &\simeq \sqrt{M \cdot W} \end{aligned}$$

and the free-fall time scale  $t_{\text{ff}}$  of a cloud

$$t_{\text{ff}} = \sqrt{\frac{3\pi}{32G\rho}} = 2.1 \cdot 10^6 \text{yr} \cdot \left( \frac{\rho}{10^{-21} \frac{\text{g}}{\text{cm}^3}} \right)^{-1/2}$$

where  $G$  is the gravitational constant,  $M$  the mass,  $\rho$  the density, and  $R$  the radius of a cloud.  $\mathcal{T}$  is the kinetic energy from internal motions, and  $a$  is a constant of order unity which measures the effects of a nonuniform or nonspherical mass distribution on the gravitational energy (Bertoldi & McKee 1992).

The kinetic energy and momentum supply rates of the protostars within a cloud will be regarded as potentially significant, if the time  $t_E$  needed to supply a kinetic energy equivalent to  $W$  and the time  $t_P$  to supply a momentum equivalent to  $P$  is comparable to or shorter than the free fall time scale of the cloud.

**The case of a giant molecular cloud.** First, I will discuss the case of a typical giant molecular cloud, having a mass of  $10^5 M_{\odot}$  and a diameter of 35 pc (e.g., Blitz 1993; this also roughly corresponds to the properties of Orion A). Such a cloud would have a mean density  $\rho \sim 1.2 \cdot 10^{-22} \text{g cm}^{-3}$ , corresponding

to a proton density  $n_p \sim 75 \text{ cm}^{-3}$ . This cloud would have a free fall time scale  $t_{ff}$  of order  $6 \cdot 10^6$  years and a gravitational energy  $W$  of  $2.9 \cdot 10^{42} \text{ J}$ . The timescale  $t_{E,GMC}$  needed by the protostellar population to provide an equal amount of kinetic energy is given by  $W/L_{\text{turb}}$ . At this point it is probably well justified to use the above noted upper limit for  $L_{\text{turb}}$  (and to regard it as an actual lower limit), since only a fraction of the entire Orion A cloud has been surveyed in  $\text{H}_2$ . The energy/momentum loss factor induced by the presence of very long giant flows would presumably be rather low in the case of a giant molecular cloud, since even the longest flows are short compared to the diameter of a giant molecular cloud, and most flows will not stick out of the cloud. Even for a clearly elongated cloud such as Orion A, the energy loss to the interstellar medium outside the cloud is probably minor, since even the extent of the cloud perpendicular to the major axis is of order 10-20 pc. Adopting  $L_{\text{turb}} \sim 50 L_\odot$ , the protostellar population in Orion A could provide a kinetic energy equivalent to  $W$  in  $t_{E,GMC} \sim 4.4 \cdot 10^6 \text{ yr}$ , i.e., in about the same time as the free fall time scale of the cloud  $t_{ff} \sim 6 \cdot 10^6 \text{ yr}$ . The momentum  $P_{\text{turb}}$  contained in turbulent motions in the cloud as estimated by assuming that the cloud is in virial equilibrium is  $\sim 3.7 \cdot 10^5 M_\odot \text{ km/s}$  (which is reasonable, since the linewidths of giant molecular clouds imply internal velocities of a few km/s). The assumption of virial equilibrium is probably well justified here, since giant molecular clouds are generally observed to be in virial equilibrium (e.g., Blitz 1993). At a momentum supply rate  $F_{\text{turb}}$  of  $300 \times 10^{-5} M_\odot \text{ km s}^{-1} \text{ yr}^{-1}$ , the protostar population in Orion A would need a time  $t_{P,GMC} \sim 1.25 \cdot 10^8 \text{ yr}$  to provide this amount of momentum. This is much longer than the free fall time of the cloud and also much longer than the estimated life times of giant molecular clouds of a few times  $10^7 \text{ yr}$ . It thus seems plausible that the jets from only the low- to intermediate-mass protostars could have a significant influence on the *energy* budget of an entire giant molecular cloud, but *fail to produce the required momentum*.

**The case of a molecular clump.** Now let's consider the next smaller building blocks of giant molecular clouds, the molecular clumps as revealed, e.g., by the  $^{13}\text{CO}$  observations by Bally et al. (1987) and Nagahama et al. (1998; see also Bertoldi & McKee 1992, Williams et al. 1994 for other giant molecular clouds). The molecular clumps have typical sizes of a few parsec, and masses of a few hundred  $M_\odot$ . I will here consider a clump with a diameter of 3 pc and a mass of  $400 M_\odot$ . This clump would have a mean density of  $1.94 \cdot 10^{-21} \text{ g cm}^{-3}$  (proton density  $n_p \sim 1.2 \cdot 10^3 \text{ cm}^{-3}$ ) and a free fall time scale  $t_{ff} \sim 1.5 \cdot 10^6 \text{ yr}$ . Its gravitational energy would be  $W = 5.54 \cdot 10^{38} \text{ J}$ , and, assuming the clump to be in virial equilibrium, its momentum of internal motions would be  $P_{\text{turb}} \sim 340 M_\odot \text{ km/s}$ . The latter would correspond to a velocity dispersion of the order of 1 km/s; this is somewhat less than is typically observed for molecular clumps. Bertoldi & McKee argue that the internal motions are larger than would be expected for clumps in virial equilibrium, but that the clumps are pressure confined instead of gravitationally bound. The area covered by the  $\text{H}_2$  survey includes  $\sim 10$  of the clumps found by Bally et al. (1987). I will thus assume that 1/10 of the total observed kinetic energy and momentum supply rate is produced in a single typical clump, i.e.,  $L_{\text{turb,clump}} \sim 5 L_\odot$ , and  $F_{\text{turb,clump}} \sim 30 \cdot 10^{-5} M_\odot \text{ km s}^{-1} \text{ yr}^{-1}$ . Given these supply rates, a kinetic energy equivalent to  $W_{\text{clump}}$  could be generated within  $t_{E,\text{clump}} \sim 4.6 \cdot 10^4 \text{ yr}$ , and the clump momentum within  $t_{P,\text{clump}} \sim 1.1 \cdot 10^6 \text{ yr}$ .

The energy/momentum loss factor due to giant flows sticking out of the clump may be significant in this case. The sizes of the giant flows are typically a few parsec, i.e., of the same order as the clump sizes. A flow with its driving source located close to the center of a clump will first have to push its way through the clump, before expanding into the interclump medium. Thus, during a sizable fraction of the flow expansion time (i.e., a sizable fraction of the very energetic Class 0 outflow phase), most energy will be deposited in the clump medium. As is suggested by the relative numbers of parsec-scale and sub-parsec-scale flows, the giant flow phase may last for about 1/5 of the entire outflow time, but is also

more energetic than during the subsequent fading phase. In total, it may be a good guess to assume that about half of the energy and momentum supplied by the protostars gets lost to the interclump medium during the giant flow phase. For a flow with a driving source located close to the surface of the clump, one lobe will stick out of the clump, and one lobe will be within the clump for most of the possible orientations (and reasonable flow lengths and clump sizes). Thus the energy loss factor will also be about 1/2 in this case. On the other hand, there may also be the possibility that the energy/momentum loss factor is effectively reduced again, when a giant flow hits the clump under consideration from the outside (e.g., flow #49, the L1641-N giant flow, originating in clump 4 of Bally et al., may be seen to rush through clump 3 (NGC1999/HH 1/2) at the locations indicated by H<sub>2</sub> features SMZ 6-2 and SMZ 6-4; similarly, Bally et al. note two clumps (5a and 5b) at the positions of HH 33/40, which are actually the terminating working surfaces of the HH 34 giant outflow originating in clump 6). Thus part of the kinetic energy/momentum which gets lost from one clump, might be deposited in a different clump, and part of the energy/momentum getting lost from the clump under consideration might be replenished by flows from other clumps.

Assuming an energy/momentum loss factor of order 1/2, the timescales  $t_{E,\text{clump}}$  and  $t_{P,\text{clump}}$  estimated above have to be scaled up by a factor of 2, yielding  $t_{E,\text{clump}} \sim 10^5$  yr, and  $t_{P,\text{clump}} \sim 2.2 \cdot 10^6$  yr. As in the case of the entire giant molecular cloud, the time needed to generate a kinetic energy equivalent to the gravitational energy of the clump is significantly shorter than the free fall time scale  $t_{ff} \sim 1.5 \cdot 10^6$  yr. And, different to the case of the giant molecular cloud, the protostars may also be able to produce the momentum of the internal motions in a clump in a time comparable to the free fall time scale. Thus the *jets from protostars in the clump may indeed be an important agent of creating turbulence and supporting the clump against collapse*, possibly self-regulating the star formation process in a molecular clump.

**The case of a cloud core.** Finally, the case of a typical CS core, as revealed by Tatematsu et al. (1993) shall be discussed. The average radius of such a core is 0.16 pc, the average mass is  $80 M_{\odot}$ , implying a mean density of  $\rho \sim 3.83 \cdot 10^{-19} \text{ g cm}^{-3}$  ( $n_p = 2.3 \cdot 10^5 \text{ cm}^{-3}$ ) and a free fall time scale  $t_{ff} \sim 1.1 \cdot 10^5$  yr. The gravitational potential energy would be  $W \sim 1.9 \cdot 10^{38}$  J, and the momentum of internal motions (assuming virial equilibrium) would be  $86 M_{\odot} \text{ km s}^{-1}$ . In order to supply a kinetic energy equivalent to  $W$  in a free fall time, an energy supply rate of  $L_{\text{turb}} \sim 0.15 L_{\odot}$  is required, and to provide the momentum, a momentum supply rate of  $\sim 80 \cdot 10^{-5} M_{\odot} \text{ km s}^{-1} \text{ yr}^{-1}$  would be required. The latter value is similar to the lower limit of  $F_{\text{turb,min}} \sim 60 \cdot 10^{-5} M_{\odot} \text{ km s}^{-1} \text{ yr}^{-1}$  derived for the total momentum input rate of all flows in all cores in the cloud. This makes a significant impact of one or a few flows in a core appear unlikely in terms of momentum input. The required energy input rate could in principle be provided by one or a few flows (70 flows produce a few ten  $L_{\odot}$ , i.e., one flow produces on average some tenths of a  $L_{\odot}$ ). However, the small sizes of the cores imply that the large majority of the flows stick out of the cores, and that most of the kinetic energy and momentum is not deposited in the core. Together, *it seems unlikely that the protostars located in a typical core have a significant impact on the harbouring cloud core via their jets*. This is also in accordance with the finding in Sect. 6.2: no difference in linewidths (pointing to stronger internal motions) can be seen in cores with jets, if these are compared to cores without jets with similar masses.

**Summary.** It seems that protostellar jets may have a significant impact on the cloud dynamics particularly at intermediate scales, on molecular clumps with sizes of a few parsec and masses of the order of a few hundred  $M_{\odot}$ . They fail to produce enough momentum in short enough times on larger scales of a giant molecular cloud. They are unlikely to have a major impact on the small scales of dense molecular cloud cores. Given the potential impact of the protostellar jet population on a cloud, it has to be

investigated *how* a jet may transfer its momentum and energy to a molecular cloud. Simulations of the propagation of a jet into an ambient medium are so far restricted to rather short time intervals and do largely focus on the evolution of the jet. Besides a few exceptions, jets are assumed to run into a non-magnetized, uniform density, and quiet environment. In reality, a jet will run into a magnetized medium, first with a steep density gradient as it runs out of the parent core, then through a clumpy medium, which is in nonordered, turbulent motion. *It is not at all clear how the jet interacts with this medium, how it loses energy (and how much), how it transfers momentum, and how its swept up molecular outflow evolves over long time scales.* For example, the excitation of sideways motions or of MHD waves propagating transverse to the jet direction in the ambient medium (for which observational evidence has recently been claimed by Yu et al. 1999) might be important: much more motions in the cloud could be excited than would be allowed under the assumption of strict forward momentum conservation as assumed here.

## 8 Conclusions and future prospects

### 8.1 Conclusions

In this thesis I have presented the results of an unbiased, sensitive, wide field survey for protostellar H<sub>2</sub> jets covering a substantial part of the Orion A giant molecular cloud. Additional data covering a wide wavelength range have been used to search for and characterize the protostellar outflow sources. From these data, the following conclusions have been drawn:

- **There are more than 70 active protostellar jets in the survey area.** The large number of detected H<sub>2</sub> jets is in line with the generally-found ubiquity of energetic outflow activity in star-forming regions. This confirms the paradigm that outflow activity is an integral part of the star-formation process.
- **No single jet has been found with a morphology as clear and simple as seen in the prototypical H<sub>2</sub> jets HH 211 and HH 212.** Although many of the jets are seen to be bipolar, only very few of them show clear signs of symmetric features. A handful of jets shows well-collimated, narrow jet beams, and a few well defined bow shocks are seen. The great majority of the jets has a fairly ill-defined morphology. This is attributed to the turbulent, clumpy medium into which the Orion A jets are propagating.
- **The jets are randomly oriented.** In particular, there is no trend for an alignment of outflow direction with the large-scale ambient magnetic field. Apparently, large-scale magnetic fields do not have a dominant impact on the determination of the spin and symmetry axis in a young stellar object. Instead, the random orientation of the jets suggests random, turbulent motions as the creator of spin motions in the cores.
- **The length of a jet evolves over time, starting short, going through a giant flow phase, and ending as a shrinking jet at later times.** During the Class 0 phase, short, medium-sized, and very long jets are observed, and very long jets are comparatively common: the jets expand from zero length to their full giant flow extent. The large fraction of giant jets among Class 0 driven jets suggests that *every* protostar goes through a giant outflow phase. During the Class I phase, medium-sized jets prevail, with a number of very long and very short jets also present. The jets shorten from their maximum length, and by the Class II stage, only short jets remain. This points to a gradual decrease in momentum supply which can be naturally explained by a decrease in the mass outflow rate and the underlying mass accretion rate. In addition, the shortening of the jets with time requires a continuously acting, decelerating drag on the jets.
- **The H<sub>2</sub> luminosity of a jet decreases with time.** This effect points to a decreasing mass outflow rate with time, under the assumption of a close relation between the H<sub>2</sub> luminosity of a jet and the kinetic energy input rate of the protostellar driving source and a constant jet speed (in time and for all jets). Furthermore, assuming a constant ratio of mass ejection to mass accretion, a decreasing mass accretion rate is implied.

- **The distribution of the jets and their associated driving sources in the  $L_{\text{H}_2}$  vs.  $L_{\text{bol}}$  diagram suggests the presence of a high accretion phase combined with a highly efficient ejection phase.** The “unification scheme” proposed by Smith (2000), a model of the simultaneous evolution of a protostar, its envelope, and its outflow, is able to reproduce the location of the Class 0 and Class I driven jets in the  $L_{\text{H}_2}$  vs.  $L_{\text{bol}}$  diagram. It assumes a mass accretion rate which peaks early in the stellar evolution and declines thereafter. In tandem with the mass accretion rate, the mass ejection fraction goes through a maximum early on and decreases later.
- **Protostars and jets tend to form in quiet cores, i.e., in cores with a low value of the virial parameter  $\alpha_{\text{vir}} = E_{\text{kin}}/E_{\text{grav}}$ .** These are typically cores with higher masses.
- **There is no evidence for jet-induced turbulence in the star forming cores.** Broader molecular lines in cores associated with outflows and with young stellar objects have been taken as evidence for additional, outflow-induced turbulence. In fact, a trend for broader lines in jet-producing cores is also seen for the Orion A cores. However, this is due to the preferred location of jet driving sources in more massive cores, which generally have larger linewidths. When cores with similar masses are compared, there is apparently *no* difference in linewidths for star-forming and non-star-forming cores, and consequently *no* indication for any additional internal motion in the cores induced by the jets.
- **A comparison of jet  $\text{H}_2$  luminosity and core linewidth, as well as the evolution of jet length and  $\text{H}_2$  luminosity with time all favour star formation theories predicting a non-steady accretion rate peaking strongly early in the protostellar evolution.** Collapse calculations predict a mass accretion rate  $\dot{M}_{\text{acc}}$  which is related to the effective sound speed  $c_{\text{eff}}$  in the core as  $\dot{M}_{\text{acc}} = c_{\text{eff}}^3/G \cdot f(t)$ . Assuming  $f(t) \equiv 1$  as in the Shu (1977) standard model should result in a  $c_{\text{eff}}^3$  power law relation between sound speed (as measured by the linewidth  $\Delta v$  of the cloud cores) and flow energetics (as measured by  $L_{\text{H}_2}$ ). In a plot of  $L_{\text{H}_2}$  vs.  $\Delta v^3$ , most sources lie above such a relation. There is a trend for higher  $L_{\text{H}_2}$  in larger linewidth cores, which may follow a  $c_{\text{eff}}^3$  law. If Class 0 and Class I driven jets are treated separately, each group (particularly the Class 0 jets) follows such a relation more closely, with a larger normalization factor for the Class 0 jets (Class 0 jets are brighter). Thus it seems that indeed there is a dependency of the accretion rate on the sound speed, but in a time-variable fashion, with  $f(t)$  peaking early on and then declining.
- **The protostellar jet population provides sufficient momentum to potentially replenish decaying turbulence within intermediate-scale molecular clumps, a few parsec in size and with masses of the order of a few hundred  $M_{\odot}$ .** They fail to provide enough momentum in a short enough time on the large scales of entire giant molecular clouds and on the small scales of dense molecular cloud cores. This result is based on the assumption of strict forward momentum conservation, which allows for the conversion of only a small fraction (of the order of 1 %) of the kinetic energy in a jet to kinetic energy of turbulent cloud motion. In the case of a more efficient deposition of kinetic energy in the cloud, the impact of the jets will be even stronger. In either case, the energy and momentum feedback of protostellar jets on the cloud cannot be neglected.

## 8.2 What next?

One of the prime goals of the present work was to provide a sample of jets which is largely free from selection effects. This sample can be used in the future to address many more of the questions described in Section 1. A number of desirable extensions to the present work have been mentioned at various places in this thesis. These and some further ideas are discussed here at the end of this thesis.

As can be seen best from the list compiled in Appendix C, information on the jet-driving sources is very incomplete. This calls for additional surveys, if possible covering the entire survey area, particularly at longer wavelengths. The wish-list includes:

- An unbiased 1.3 mm continuum survey at the 30 m IRAM millimetre telescope. This survey in fact is already complete. It will allow us to identify additional, deeply-embedded jet-driving sources, and to derive circumstellar dust masses. Moreover, it will provide a census of *all* protostellar objects, particularly Class 0 sources. It will thus be possible to check whether *all* protostars drive jets.
- Follow-up observations of the sources discovered in the 1.3 mm survey at 450/850  $\mu\text{m}$  with SCUBA at the JCMT. These have already been carried out for the southern part of the survey area, and further applications have been submitted. Such observations will allow us to further constrain circumstellar dust masses and the long-wavelength luminosity of the sources.
- High-resolution ground-based mid-infrared imaging will provide photometry of embedded sources particularly in crowded regions like OMC-2/3, and give additional hints on the locations of driving sources. The field-of-view of current mid-infrared cameras are comparatively small, thus only targeted observations will be possible. First observations have already been made using the LWS at the Keck I telescope, and further telescope applications for LWS/Keck and TIMMI2/ESO have been submitted.
- Supplementary near-infrared observations will comprise J- and H-band surveys with Omega Prime at Calar Alto (the J-band survey has been done last winter). An L-band survey with ISAAC/VLT could be used to get a complete census of Class II sources using the L-band excess as an indicator for the presence or absence of a disk in a near-infrared source, but may be prohibitive in terms of observing time.
- A search for infall signatures within the cores should be made. In recent years, millimetre molecular line spectroscopy has revealed the signatures of infalling envelopes in young stars (see Myers et al. 2000 for a review). However, no clear evolutionary tendencies are seen so far. The jet and protostar sample presented in this thesis offers an opportunity to search for evolutionary trends and the relation between infall and outflow.
- Somewhat further in the future, air-borne and space-based mid- to far-infrared observatories (SOFIA, SIRTf) will provide higher spatial resolution and higher sensitivity measurements in the mid- to far-infrared wavelength range. Hopefully these instruments will allow us to fill in the gaps in this work which have been left by the low spatial resolution IRAS data. The mid- to far-infrared wavelength range is very important, since it is here where very young protostars emit most of their radiation, and thus uncertainties in this range introduce major uncertainties in estimates of their bolometric luminosities.
- High-resolution imaging techniques, in particular mid-infrared and (sub)millimetre interferometry (VLTI, ALMA), will allow us to probe the multiplicity of the embedded jet driving sources, the structure of the protostellar envelopes and disks, and the acceleration and collimation regions of protostellar jets.

With respect to the jets themselves, a number of extensions to the research presented here are possible. This might include observations of the jets at other wavelengths and the compilation of kinematical data.

- A search for optical Herbig-Haro objects in and around the survey area will help to check whether there are yet more giant outflows or even longer “hyperjets”. This will test the hypothesis that jets go through a maximum extent and then get shorter again. E.g., it is possible that the present work underestimated the length of the older jets, because their ends might have broken out of the molecular cloud and thus might be invisible to the present H<sub>2</sub> survey.
- A more sensitive search for molecular CO outflows associated with the H<sub>2</sub> jets will allow us to check the relation between H<sub>2</sub> jets and CO outflows (e.g., entraining mechanisms). An evolutionary trend is predicted by the “unification scheme” (Smith 2000): young outflows should be H<sub>2</sub> luminous, but not yet associated with massive CO outflows, whereas more evolved outflows should be faint in H<sub>2</sub>, but should be seen as massive CO outflows, as the mass swept up during the entire outflow life time is still moving.
- Proper motion and radial velocity measurements can help to confirm (or reject) the uncertain candidate jets by showing that they are not only a morphological, but also a kinematical entity. Velocity information is also essential for an interpretation of the H<sub>2</sub> luminosity ( $\propto \dot{M}_{\text{jet}} v_{\text{jet}}^2$ ) and a better estimate of key parameters such as the mass outflow rate, and consequently the mass accretion rate (note, however, that the apparent velocity of H<sub>2</sub> features is not necessarily equal to the jet velocity, e.g., Völker et al. 1999). It is also not known how the jet velocity evolves with time: the velocity evolution is simply prescribed in the “unification scheme” (Smith 2000); a “kinematics survey” is needed to test the validity of this assumption. Finally, measuring the terminal jet velocity in the asymptotic regime (i.e., in the jet beam at reasonable distances from the driving source) is one of the few possibilities to constrain the processes at work in the jet collimation and driving region without having to observe or resolve this region directly.
- Masers, particularly water masers, form in high density, warm molecular post-shock gas in protostellar outflows very close to the driving source (e.g., Hollenbach 1997; Claussen et al. 1997; 1998). At a frequency of 22 GHz (i.e., at radio wavelengths), H<sub>2</sub>O maser emission is not affected by extinction, and can thus be used to probe the optically-obscured jet acceleration and collimation region. The Effelsberg 100 m radio telescope could be used to survey the new jet sample for the presence of H<sub>2</sub>O masers (see, e.g., Wouterloot & Walmsley 1986). Subsequently, radio interferometry can be used to probe the kinematics in the immediate vicinity of the driving source with high angular and spectral resolution, providing proper motion and radial velocity information respectively.

Finally, it may well be worth surveying other clouds in a similar fashion as has been done here, to check to what extent the jets are typical for all star-forming regions or reflect particular conditions of the Orion A cloud. For example, the sound speed in the cores appears to have an impact on the mass accretion rate, hence the mass outflow rate and the jet energetics (this work; Aso et al. 2000). Other clouds, harbouring less turbulent cores, may have generally less energetic, H<sub>2</sub> fainter, but possibly longer lived jets. Less turbulent cloud environments might also favour the production of jets with a clearer morphology, similar to that seen in HH 211 and HH 212, than is seen for the jets in Orion A. Surveys such as the one presented in this thesis will become more efficient in the near future: the successor of Omega Prime at the Calar Alto observatory, Omega 2000, will have more than 4 times the field of view of Omega Prime (Bailer-Jones et al. 2000).



## References

- Adams F.C., Lada C.J., Shu F.H.: 1987, ApJ 312, 788
- Adams F.C., Lada C.J., Shu F.H.: 1988, ApJ 326, 865
- Aitken D.K., Wright C.M., Smith C.H., Roche P.F.: 1993, MNRAS 262, 456
- Ali B., DePoy D.L.: 1995, AJ 109, 709
- Allen D.A., Burton M.G.: 1993, Nature 363, 54
- Allen L.E.: 1996, PhD thesis (University of Massachusetts, Amherst)
- Ambartsumian V.A.: 1954, Comm. Burakan Obs. 13
- André P., Montmerle T.: 1994, ApJ 420, 837
- André P., Ward-Thompson D., Barsony M.: 1993, ApJ 406, 122
- André P., Ward-Thompson D., Barsony M.: 2000, in *Protostars and Planets IV*, eds. V. Mannings, A. Boss, S. Russel (Tucson: University of Arizona Press), 59
- Anglada G.: 1995, Revista Mexicana de Astronomia y Astrofisica, Serie de Conferencias 1, 67
- Appenzeller I.: 1974, A&A 36, 99
- Appenzeller I., Jankovics I., Östreicher R.: 1984, A&A 141, 108
- Appenzeller I., Mundt R.: 1989, A&A Rv. 1, 291
- Aso Y., Tatematsu K., Sekimoto Y., Nakano T., Umemoto T., Koyama K., Yamamoto S.: 2000, ApJS 131, 465
- Aspin C., Reipurth B.: 2000, MNRAS 311, 522
- Axon D.J., Taylor K.: 1984, MNRAS 207, 241
- Bacciotti F.: 1997, in *Herbig-Haro flows and the birth of low mass stars*, IAU 182, eds. B. Reipurth & C. Bertout, 73
- Bacciotti F., Eisloffel J.: 1999, A&A 342, 717
- Bacciotti F., Mundt R., Ray T.P., Eisloffel J., Solf J., Camenzind M.: 2000, ApJ 537, L49
- Bachiller R.: 1996, ARA&A 34, 111
- Bachiller R., Gómez-González J.: 1992, A&ARv 3, 257
- Bachiller R., Guilloteau S., Dutrey A., Planesas P., Martín-Pintado J.: 1995, A&A 299, 857
- Bailer-Jones C.A.L., Bizenberger P., Storz C.: 2000, in *Optical and IR Telescope Instrumentation and Detectors*, SPIE Proceedings Vol. 4008, eds. M. Iye & A.F. Moorwood, 1305
- Bally J.: 1982, in *Symposium on the Orion Nebula to Honor Henry Draper*, New York Academy of Sciences, Annals, vol. 395, 191
- Bally J., Devine D.: 1994, ApJ 428, L65
- Bally J., Devine D.: 1997, in *Herbig-Haro flows and the birth of low mass stars*, IAU 182, eds. B. Reipurth & C. Bertout, 29
- Bally J., Lada C.J.: 1983, ApJ 265, 824
- Bally J., Lane A.P.: 1982, ApJ 257, 612
- Bally J., Devine D., Alten V.: 1996a, ApJ 473, 921
- Bally J., Devine D., Fesen R.A., Lane A.P.: 1995, ApJ 454, 345

- Bally J., Devine D., Reipurth B.: 1996b, ApJ 473, L49
- Bally J., Langer W.D., Stark A.A., Wilson R.W.: 1987, ApJ 312, L45
- Bally J., O'Dell C.R., McCaughrean M.J.: 2000, AJ 119, 2919
- Bally J., Reipurth B., Lada C.J., Billawala Y.: 1999, AJ 117, 410
- Bate M.R.: 1998, ApJ 508, L95
- Bate M.R., Bonnell I.A., Clarke C.J., Lubow S.H., Ogilvie G.I., Pringle J.E., Tout C.A.: 2000, MNRAS 317, 773
- Batrla W., Wilson T.L., Bastien P., Ruf K.: 1983, A&A 128, 279
- Beckwith S.V.W.: 1980, in *Infrared Astronomy*, IAU 96, eds. C.G. Wynn-Williams & D.P. Cruikshank, 167
- Beckwith S.V.W., Sargent A.I.: 1993, in *Protostars and Planets III*, eds. E.H. Levy & J.I. Lunine (Tucson: University of Arizona Press), 521
- Beckwith S., Zuckerman B.: 1982, ApJ 255, 536
- Beckwith S., Gatley I., Matthews K., Neugebauer G.: 1978b, ApJ 223, L41
- Beckwith S., Persson S.E., Neugebauer G., Becklin E.E.: 1978a, ApJ 223, 464
- Beckwith S., Persson S.E., Neugebauer G.: 1979, ApJ 227, 436
- Beckwith S.V.W., Sargent A.I., Chini R.S., Güsten R.: 1990, AJ 99, 924
- Beichman C.A., Myers P.C., Emerson J.P., Harris S., Mathieu R., Benson P.J., Jennings R.E.: 1986, ApJ 307, 337
- Bell K.R., Lin D.N.C.: 1994, ApJ 427, 987
- Bence S.J., Richer J.S., Padman R.: 1996, MNRAS 279, 866
- Bertoldi F., McKee C.F.: 1992, ApJ 395, 140
- Bertout C.: 1989, ARAA 27, 351
- Bertout C., Basri G., Bouvier J.: 1988, ApJ 330, 350
- Bizenberger P., McCaughrean M.J., Birk C., Thompson D., Storz C.: 1998, Proc. SPIE 3354, 825
- Black J.H., Dalgarno A.: 1976, ApJ 203, 132
- Black J.H., van Dishoeck E.F.: 1987, ApJ 322, 412
- Blandford R.D., Payne D.G.: 1982, MNRAS 199, 883
- Blandford R.D., Rees M.J.: 1974, MNRAS 169, 395
- Blitz L.: 1993, in *Protostars and Planets III*, eds. E.H. Levy & J.I. Lunine (Tucson: University of Arizona Press), 125
- Blondin J.M., Fryxell B.A., Königl A.: 1990, ApJ 360, 370
- Blondin J.M., Königl A., Fryxell B.A.: 1989, ApJ 337, L37
- Böhm K.-H.: 1978, A&A 64, 115
- Bohigas J., Torrelles J.M., Echevarría J., Cantó J., Enríquez R., Firmani C., Gutiérrez L., Ruiz E., Salas L.: 1985, RevMexAA 11, 149
- Bonnell I., Bastien P.: 1992, ApJ 401, L31
- Bontemps S., André P., Terebey S., Cabrit S.: 1996a, A&A 311, 858
- Bontemps S., Ward-Thompson D., André P.: 1996b, A&A 314, 477
- Brandner W., Köhler R.: 1998, ApJ 499, L79
- Brandner W., Zinnecker H., Alcalá J.M., Allard F., Covino E., Frink S., Köhler R., Kunkel M., Moneti A., Schweitzer A.: 2000, AJ 120, 950
- Brand P.W.J.L., Moorhouse A., Burton M.G., Geballe T.R., Bird M., Wade R.: 1988, ApJ 334, L103
- Breger M.: 1976, ApJ 204, 789
- Brown A.G.A., de Geus E.J., de Zeeuw P.T.: 1994, A&A 289, 101

- 
- Bührke T., Mundt R., Ray T.P.: 1988, A&A 200, 99
  - Burgarella D., Livio M., O'Dea C.P. (eds.): 1993, *Astrophysical Jets*, Proceedings of the Astrophysical Jet Meeting Baltimore 1992, Cambridge University Press
  - Burkert A., Bodenheimer P.: 2000, ApJ 543, 822
  - Burnham S.W.: 1890, MNRAS 51, 94
  - Burnham S.W.: 1894, Pub. Lick Obs. 2, 175
  - Burrows C.J., Stapelfeldt K.R., Watson A.M., Krist J.E., Ballester G.E., Clarke J.T., Crisp D., Gallagher J.S. III, Griffiths R.E., Hester J., Hoessel J.G., Holtzman J.A., Mould J.R., Scowen P.A., Trauger J.T., Westphal J.A.: 1996, ApJ 473, 437
  - Burton M.G., Brand P.W.J.L., Geballe T.R., Webster A.S.: 1989a, MNRAS 236, 409
  - Burton M.G., Geballe T.R., Brand P.W.J.L.: 1989b, MNRAS 238, 1513
  - Burton M.G., Haas M.R.: 1997, A&A 327, 309
  - Cabrit S., André P.: 1991, ApJ 379, L25
  - Cabrit S., Raga A.: 2000, A&A 354, 667
  - Cabrit S., Edwards S., Strom S.E., Strom K.M.: 1990, ApJ 354, 687
  - Cabrit S., Raga A., Gueth F.: 1997, in *Herbig-Haro flows and the birth of low mass stars*, IAU 182, eds. B. Reipurth & C. Bertout, 163
  - Calvet N., Hartmann L., Strom S.E.: 2000, in *Protostars and Planets IV*, eds. V. Mannings, A. Boss, S. Russel (Tucson: University of Arizona Press), 377
  - Camenzind M.: 1990, Rv. in Mod. Astr. 3, 234
  - Camenzind M.: 1997, in *Herbig-Haro flows and the birth of low mass stars*, IAU 182, eds. B. Reipurth & C. Bertout, 241
  - Cantó J.: 1980, A&A 86, 327
  - Cantó J., Rodríguez L.F.: 1980, ApJ 239, 982
  - Cantó J., Raga A.C., Binette L.: 1989, Rev. Mexicana Astron. Astrof. 17, 65
  - Cantó J., Raga A.C., D'Alessio P.: 2000, MNRAS 313, 656
  - Cantó J., Tenorio-Tagle G., Różyczka M.: 1988, A&A 192, 287
  - Carr J.S.: 1993, ApJ 406, 553
  - Carruthers G.R.: 1970, ApJ 161, L81
  - Casali M.M.: 1992, *JCMT UKIRT Newsletter* 4, 33
  - Cassen P., Shu F.H., Terebey S.: 1986, in *Protostars and Planets II* (Tucson: University of Arizona Press), 448
  - Castets A., Langer W.D.: 1995, A&A 294, 835
  - Cernicharo J., Reipurth B.: 1996, ApJ 460, L57
  - Cernicharo J., Neri R., Reipurth B.: 1997, in *Herbig-Haro flows and the birth of low mass stars*, IAU 182, eds. B. Reipurth & C. Bertout, 141
  - Cerqueira A.H., de Gouveia dal Pino E.M., Herant M.: 1997, ApJ 489, L185
  - Cesaroni R., Wilson T.L.: 1994, A&A 281, 209
  - Chan K.L., Henriksen R.N.: 1980, ApJ 241, 534
  - Chen H., Tokunaga A.T.: 1994, ApJSS 90, 149
  - Chen H., Ohashi N., Umemoto T.: 1996, AJ 112, 717
  - Chen H., Tokunaga A.T., Fukui Y.: 1993a, ApJ 416, 235
  - Chen H., Tokunaga A.T., Strom K.M., Hodapp K.-W.: 1993b, ApJ 407, 639
  - Chen H., Zhao J.-H., Ohashi N.: 1995, ApJ 450, L71
  - Chernin L.M., Masson C.R.: 1995, ApJ 443, 181

- Chernin L.M., Masson C.R., de Gouveia dal Pino E.M., Benz W.: 1994, ApJ 426, 204
- Chernoff D.F., Hollenbach D.J., McKee C.F.: 1982, ApJ 259, L97
- Chini R., Krügel E., Haslam C.G.T., Kreysa E., Lemke R., Reipurth B., Sievers A., Ward-Thompson D.: 1993, A&A 272, L5
- Chini R., Reipurth B., Sievers A., Ward-Thompson D., Haslam C.G.T., Kreysa E., Lemke R.: 1997a, A&A 325, 542
- Chini R., Reipurth B., Ward-Thompson D., Bally J., Nyman L.-A., Sievers A., Billawala Y.: 1997b, ApJ 474, L135 (CRW)
- Chrysostomou A., Hobson J., Davis C.J., Smith M.D., Berndsen A.: 2000, MNRAS 314, 229
- Clarke D.A., Norman M.L., Burns J.O.: 1986, ApJ 311, L63
- Claussen M.J., Marvel K.B., Wootten H.A., Wilking B.A.: 1997, in *Herbig-Haro flows and the birth of low mass stars*, IAU 182, eds. B. Reipurth & C. Bertout, 515
- Claussen M.J., Marvel K.B., Wootten H.A., Wilking B.A.: 1998, ApJ 507, L79
- Cohen M.: 1990, ApJ 354, 701
- Cohen M., Kuhl L.V.: 1979, ApJS 41, 743
- Cohen M., Schwartz R.D.: 1979, ApJ 233, L77
- Cohen M., Bieging J.H., Schwartz P.R.: 1982, ApJ 253, 707
- Cohen M., Emerson J.P., Beichman C.A.: 1989, ApJ 339, 455
- Cohen R.J., Rowland P.R., Blair M.M.: 1984, MNRAS 210, 425
- Coppin K.E.K., Davis C.J., Micono M.: 1998, MNRAS 301, L10
- Corcoran D., Ray T.P.: 1995, A&A 301, 729
- Corcoran M., Ray T.P.: 1998, A&A 331, 147
- Correia J.C., Griffin M., Saraceno P.: 1997, A&A 322, L25
- Cudworth K.M., Herbig G.: 1979, AJ 84, 548
- Davis C.J., Eislöffel J.: 1995, A&A 300, 851
- Davis C.J., Smith M.D.: 1996, A&A 309, 929
- Davis C.J., Berndsen A., Smith M.D., Chrysostomou A., Hobson J.: 2000a, MNRAS 314, 241
- Davis C.J., Dent W.R.F., Matthews H.E., Coulson I.M., McCaughrean M.J.: 2000b, MNRAS 318, 952
- Davis C.J., Eislöffel J., Ray T.P.: 1994, ApJ 426, L93
- Davis C.J., Eislöffel J., Ray T.P., Jennes T.: 1997a, A&A 324, 1013
- Davis C.J., Eislöffel J., Smith M.D.: 1996, ApJ 463, 246
- Davis C.J., Moriarty-Schieven G., Eislöffel J., Hoare M.G., Ray T.P.: 1998a, AJ 115, 1118
- Davis C.J., Ray T.P., Eislöffel J., Corcoran D.: 1997b, A&A 324, 263
- Davis C.J., Smith M.D., Eislöffel J.: 2000c, MNRAS 318, 747
- Davis C.J., Smith M.D., Eislöffel J., Davies J.K.: 1999, MNRAS 308, 539
- Davis C.J., Smith M.D., Moriarty-Schieven G.H.: 1998b, MNRAS 299, 825
- de Gouveia dal Pino E.M., Benz W.: 1993, ApJ 410, 686
- de Gouveia dal Pino E.M., Benz W.: 1994, ApJ 435, 261
- Dent W.R.F., Matthews H.E., Walther D.M.: 1995, MNRAS 277, 193
- Dent W.R.F., Matthews H.E., Ward-Thompson D.: 1998, MNRAS 301, 1049
- Devine D., Bally J., Reipurth B., Heathcote S.: 1997, AJ 114, 2095
- Devine D., Reipurth B., Bally J.: 1999b, AJ 118, 972
- Devine D., Reipurth B., Bally J., Balonek T.J.: 1999a, AJ 117, 2931
- Dopita A.: 1978, A&A 63, 237

- Dopita M.A., Schwartz R.D., Evans I.: 1982, ApJ 263, L73
- Dougados C., Cabrit S., Lavalley C., Ménard F.: 2000, A&A 357, L61
- Downes T.P., Ray T.P.: 1999, A&A 345, 977
- Draine B.T.: 1980, ApJ 241, 1021
- Draine B.T.: 1983, ApJ 270, 519
- Draine B.T., McKee C.F.: 1993, ARA&A 31, 373
- Draine B.T., Roberge W.G.: 1982, ApJ 259, L91
- Draine B.T., Roberge W.G., Dalgarno A.: 1983, ApJ 264, 485
- Dutrey A., Guilloteau S., Duvert G., Prato L., Simon M., Schuster K., Menard F.: 1996, A&A 309, 493
- Dyson J.E.: 1987, in *Circumstellar matter*, IAU 122, eds. I. Appenzeller & C. Jordan, 93
- Eddington A.S.: 1937, Observatory 60, 99
- Edwards S., Snell R.L.: 1984, ApJ 281, 237
- Edwards S., Ray T., Mundt R.: 1993, in *Protostars and Planets III*, eds. E.H. Levy & J.I. Lunine (Tucson: University of Arizona Press), 567
- Eislöffel J.: 1997, in *Herbig-Haro Flows and the Birth of Low Mass Stars*, IAU 182, eds. B. Reipurth & C. Bertout, 93
- Eislöffel J.: 2000, A&A 354, 236
- Eislöffel J., Mundt R.: 1992, A&A 263, 292
- Eislöffel J., Mundt R.: 1997, AJ 114, 280
- Eislöffel J., Davis C.J., Ray T.P., Mundt R.: 1994a, ApJ 422, L91
- Eislöffel J., Mundt R., Böhm K.-H.: 1994b, AJ 108, 1042
- Eislöffel J., Mundt R., Ray T.P., Rodríguez L.F.: 2000a, in *Protostars and Planets IV*, eds. V. Mannings, A. Boss, S. Russel (Tucson: University of Arizona Press), 815
- Eislöffel J., Smith M.D., Davis C.J.: 2000b, A&A 359, 1147
- Elias J.H.: 1980, ApJ 241, 728
- Elsässer H., Staude H.J.: 1978, A&A 70, L3
- Erickson N.R., Goldsmith P.F., Snell R.L., Berson R.L., Huguenin G.R., Ulich B.L., Lada C.J.: 1982, ApJ 261, L103
- Evans N.J. II, Levreault R.M., Harvey P.M.: 1986, ApJ 301, 894
- Falle S.A.E.G., Innes D.E., Wilson M.J.: 1987, MNRAS 225, 741
- Fendt C., Elstner D.: 1999, A&A 349, L61
- Fendt C., Zinnecker H.: 1998, A&A 334, 750
- Field G.B., Somerville W.B., Dressler K.: 1966, ARA&A 4, 207
- Fischer J., Joyce R.R., Simon M., Simon T.: 1982, ApJ 258, 165
- Fischer J., Righini-Cohen G., Simon M.: 1980a, ApJ 238, L155
- Fischer J., Righini-Cohen G., Simon M., Joyce R.R., Simon T.: 1980b, ApJ 240, L95
- Fischer J., Sanders D.B., Simon M., Solomon P.M.: 1985, ApJ 293, 508
- Foster P.N., Chevalier R.A.: 1993, ApJ 416, 303
- Frank, A.: 1998, in *Accretion Processes in Astrophysical Systems: Some Like it Hot!*, eds. Stephen S. Holt and Timothy R. Kallman, AIP Conference Proceedings 431, 513
- Frank A., Mellema G.: 1997, in *Herbig-Haro Flows and the Birth of Low Mass Stars*, IAU 182, eds. B. Reipurth & C. Bertout, 291
- Frank A., Ryu D., Jones T.W., Noriega-Crespo A.: 1998, ApJ 494, L79
- Fridlund C.V.M., Liseau R.: 1998, ApJ 499, L75
- Fukui Y.: 1988, Vista Atr. 31, 217

- Fukui Y.: 1989, in *Low Mass Star Formation and Pre-main Sequence Objects*, ESO Conf. Proc. 33, ed. B. Reipurth, p. 95
- Fukui Y., Iwata T., Mizuno A., Bally J., Lane A.P.: 1993, in *Protostars and Planets III*, eds. E.H. Levy & J.I. Lunine (Tucson: University of Arizona Press), 603
- Fukui Y., Iwata T., Takaba H., Mizuno A., Ogawa H., Kawabata K., Sugitani K.: 1989, *Nature* 342, 162
- Fukui Y., Sugitani K., Takaba H., Iwata T., Mizuno A., Ogawa H., Kawabata K.: 1986, *ApJ* 311, L85
- Fukui Y., Takaba H., Iwata T., Mizuno A.: 1988, *ApJ* 325, L13
- Garden R., Geballe T.R., Gatley I., Nadeau D.: 1986, *MNRAS* 220, 203
- Garden R.P., Russell A.P.G., Burton M.G.: 1990, *ApJ* 354, 232
- Gatley I., Becklin E.E., Matthews K., Neugebauer G., Penston M.V., Scoville N.: 1974, *ApJ* 191, L121
- Gautier T.N. III, Fink U., Larson H.P., Treffers R.R.: 1976, *ApJ* 207, L129
- Genzel R., Stutzki J.: 1989, *ARA&A* 27, 41
- Goldreich P., Kwan J.: 1974, *ApJ* 189, 441
- Gomez M., Whitney B.A., Kenyon S.: 1997, *AJ* 114, 1138
- Goodson A.P., Winglee R.M., Böhm K.-H.: 1997, *ApJ* 489, 199
- Gould R.J., Harwit M.: 1963, *ApJ* 137, 694
- Gould R.J., Salpeter E.E.: 1963, *ApJ* 138, 393
- Gould R.J., Gold T., Salpeter E.E.: 1963, *ApJ* 138, 408
- Grasdalen G.L., Joyce R.R.: 1976, *BAAS* 8, 349
- Gredel R.: 1994, *A&A* 292, 580
- Gredel R.: 1996, *A&A* 305, 582
- Gredel R., Reipurth B.: 1993, *ApJ* 407, L29
- Gredel R., Reipurth B., Heathcote S.: 1992, *A&A* 266, 439
- Guenther E.W., Lehmann H., Emerson J.P., Staude J.: 1999, *A&A* 341, 768
- Gueth F., Guilloteau S.: 1999, *A&A* 343, 571
- Gueth F., Guilloteau S., Bachiller R.: 1996, *A&A* 307, 891
- Guilloteau S., Dutrey A., Gueth F.: 1997, in *Herbig-Haro Flows and the Birth of Low Mass Stars*, IAU 182, eds. B. Reipurth & C. Bertout, 365
- Gull T.R., Harwit M.O.: 1971, *ApJ* 168, 15
- Haro G.: 1952, *ApJ* 115, 572
- Haro G.: 1953, *ApJ* 117, 73
- Hartigan P., Raymond J.: 1993, *ApJ* 409, 705
- Hartigan P., Carpenter J.M., Dougados C., Skrutskie M.F.: 1996, *AJ* 111, 2470
- Hartigan P., Curiel S., Raymond J.: 1989, *ApJ* 347, L31
- Hartigan P., Edwards S., Ghandour L.: 1995, *ApJ* 452, 736
- Hartigan P., Morse J.A., Raymond J.: 1994, *ApJ* 436, 125
- Hartigan P., Raymond J., Hartmann L.: 1987, *ApJ* 316, 323
- Hartmann L., Kenyon S.J.: 1996, *ARA&A* 34, 207
- Hartmann L., MacGregor K.B.: 1982, *ApJ* 259, 180
- Hartmann L., Calvet N., Gullbring E., D'Alessio P.: 1998, *ApJ* 495, 385
- Hartmann L., Kenyon S., Hartigan P.: 1993, in *Protostars and Planets III*, eds. E.H. Levy & J.I. Lunine (Tucson: University of Arizona Press), 497
- Hayashi C.: 1961, *PASJ* 13, 450
- Heathcote S., Reipurth B.: 1992, *AJ* 104, 2193

- 
- Heathcote S., Morse J.A., Hartigan P., Reipurth B., Schwartz R.D., Bally J., Stone J.M.: 1996, AJ 112, 1141
  - Herbig G.H.: 1950, ApJ 111, 11
  - Herbig G.H.: 1951, ApJ 113, 697
  - Herbig G.H.: 1952, J. Roy. Astr. Soc. Canada 46, 222
  - Herbig G.H.: 1974, Lick Obs. Bull. No. 658
  - Herbig G.H., Jones B.F.: 1981, AJ 86, 1232
  - Hester J.J., Stapelfeldt K.R., Scowen P.A.: 1998, AJ 116, 372
  - Heyer M.H., Snell R.L., Goldsmith P.F., Strom S.E., Strom K.M.: 1986, ApJ 308, 134
  - Heyer M.H., Strom S.E., Strom K.M.: 1987a, AJ 94, 1653
  - Heyer M.H., Vrba F.J., Snell R.L., Schloerb F.P., Strom S.E., Goldsmith P.F., Strom K.M.: 1987b, ApJ 321, 855
  - Heyvaerts J., Norman C.: 1989, ApJ 347, 1055
  - Heyvaerts J., Norman C.: 1997, in *Herbig-Haro Flows and the Birth of Low Mass Stars*, IAU 182, eds. B. Reipurth & C. Bertout, 275
  - Hillenbrand L.: 1997, AJ 113, 1733
  - Hirth G.A., Mundt R., Solf J.: 1997, A&AS 126, 437
  - Hodapp K.-W.: 1984, A&A 141, 255
  - Hodapp K.-W.: 1987, A&A 172, 304
  - Hodapp K.-W.: 1999, AJ 118, 1338
  - Hodapp K.-W., Deane J.: 1993, ApJS 88, 119
  - Hodapp K.-W., Ladd E.F.: 1995, ApJ 453, 715
  - Hollenbach D.J.: 1997, in *Herbig-Haro Flows and the Birth of Low Mass Stars*, IAU 182, eds. B. Reipurth & C. Bertout, 181
  - Hollenbach D.J., Shull J.M.: 1977, ApJ 216, 419
  - Hollenbach D.J., Werner M.W., Salpeter E.E.: 1971, ApJ 163, 165
  - Jensen E.L.N., Donar A.X., Mathieu R.D.: 2000, in *Birth and Evolution of Binary Stars*, Poster Proceedings of IAU Symposium 200, eds. B. Reipurth & H. Zinnecker, 85
  - Johnson J.J., Gehrz R.D., Jones T.J., Hackwell J.A., Grasdalen G.L.: 1990, AJ 100, 518
  - Johnstone D., Bally J.: 1999, ApJ 510, L49 (JB)
  - Jones T.J., Mergén J., Odewahn S., Gehrz R.D., Gatley I., Merril K.M., Probst R., Woodward C.E.: 1994, AJ 107, 2120
  - Joy A.H.: 1942, PASP 54, 15
  - Joy A.H.: 1945, ApJ 102, 168
  - Kant I.: 1755, *Allgemeine Naturgeschichte und Theorie des Himmels*
  - Kenyon S.J., Hartmann L.: 1987, ApJ 323, 714
  - Kenyon S.J., Brown D.I., Tout C.A., Berling P.: 1998, AJ 115, 2491
  - Knee L.B.G., Sandell G.: 2000, A&A 361, 671
  - Königl A.: 1982, ApJ 261, 115
  - Königl A.: 1989, ApJ 342, 208
  - Königl A.: 1991, ApJ 370, L39
  - Königl A., Pudritz R.E.: 2000, in *Protostars and Planets IV*, eds. V. Mannings, A. Boss, S. Russel (Tucson: University of Arizona Press), 759
  - Königl A., Ruden S.P.: 1993, in *Protostars and Planets III*, eds. E.H. Levy & J.I. Lunine (Tucson: University of Arizona Press), 641

- Kreysa E., Gemünd H.-P., Gromke J., Haslam C.G.T., Reichertz L., Haller E.E., Beeman J.W., Hansen V., Sievers A., Zylka R.: 1998, *SPIE Proc.* 3357, 319
- Kudoh T., Shibata K.: 1997, *ApJ* 474, 362
- Kudoh T., Matsumoto R., Shibata K.: 1998, *ApJ* 508, 186
- Kutner M.L., Evans N.J. II, Tucker K.D.: 1976, *ApJ* 209, 452
- Kutner M.L., Tucker K.D., Chin G., Thaddeus P.: 1977, *ApJ* 215, 521
- Kwan J.: 1977, *ApJ* 216, 713
- Kwan J., Scoville N.: 1976, *ApJ* 210, L39
- Kwan J., Tadamaru E.: 1988, *ApJ* 332, L41
- Lada C.J.: 1985, *ARA&A* 23, 267
- Lada C.J.: 1987, in: Peimbert M., Jugaku J. (eds.), *Star forming regions*. IAU 115, 1
- Lada C.J., Wilking, B.A.: 1984, *ApJ* 287, 610
- Lada E.A., Strom K.M., Myers P.C.: 1993, in *Protostars and Planets III*, eds. E.H. Levy & J.I. Lunine (Tucson: University of Arizona Press), 245
- Lada E.A., Bally J., Stark A.A.: 1991, *ApJ* 368, 432
- Lane A.P.: 1989, in *Low Mass Star Formation and Pre-Main Sequence Objects*, ESO Conf. Proc. 33, ed. B. Reipurth, 331
- Lane A.P., Bally J.: 1986, *ApJ* 310, 820
- Laplace P.S.: 1796, *Exposition du système du monde*
- Larson R.B.: 1969, *MNRAS* 145, 271
- Larson R.B.: 1981, *MNRAS* 194, 809
- Levreault R.M.: 1988a, *ApJS* 67, 283
- Levreault R.M.: 1988b, *ApJ* 330, 897
- Lee J.-K., Burton M.G.: 2000, *MNRAS* 315, 11
- Lis D.C., Serabyn E., Keene J., Dowell C.D., Benford D.J., Phillips T.G., Hunter T.R., Wang N.: 1998, *ApJ* 509, 299 (LSK)
- Li W., Evans N.J. II, Lada E.A.: 1996, *ApJ* 488, 277
- Li Z.-Y.: 1998, *ApJ* 493, 230
- London R., McCray R., Chu S.-I.: 1977, *ApJ* 217, 442
- Loren R.B.: 1977, *ApJ* 215, 129
- Loren R.B.: 1989, *ApJ* 338, 925
- Lynden-Bell D., Pringle J.E.: 1974, *MNRAS* 168, 603
- Lynds B.T.: 1962, *ApJS* 7, 1
- MacLow M.-M., Klessen R.S., Burkert A., Smith M.D.: 1998, *Phys. Rev. Lett.* 80, 2754
- MacLow M.-M.: 1999, *ApJ* 524, 169
- MacLow M.-M., Klessen R., Heitsch F.: 1999, in *Optical and Infrared Spectroscopy of Circumstellar Matter*, eds. S. Klose, E. Guenther, & B. Stecklum, (ASP: San Francisco), 177
- Maddalena R.J., Morris M., Moscowitz J., Thaddeus P.: 1986, *ApJ* 303, 375
- Mader S.L., Zealey W.J., Parker Q.A., Mashedier M.R.W.: 1999, *MNRAS* 310, 331
- Masson C.R., Chernin L.M.: 1992, *ApJ* 387, L47
- Masson C.R., Chernin L.M.: 1993, *ApJ* 414, 230
- Mathieu R.D.: 1994, *ARA&A* 32, 465
- Matthews B.C., Wilson C.D.: 2000, *ApJ* 531, 868
- McCaughrean M.J.: 1988, PhD thesis (Edinburgh University)
- McCaughrean M.J. (editor): 2000, *The Orion Complex revisited*, in prep.



- McCaughrean M.J., MacLow M.-M.: 1997, AJ 113, 391
- McCaughrean M.J., O'Dell C.R.: 1996, AJ 111, 1977
- McCaughrean M.J., Stauffer J.R.: 1994, AJ 108, 1382
- McCaughrean M.J., Rayner J.T., Zinnecker H.: 1994, ApJ 436, L189
- McCaughrean M.J., Stapelfeldt K.R., Close L.M.: 2000, in *Protostars and Planets IV*, eds. V. Mannings, A. Boss, S. Russel (Tucson: University of Arizona Press), 485
- McKee C.F., Draine B.T.: 1991, Science 252, 397
- McKee C.F., Hollenbach D.J.: 1980, ARA&A 18, 219
- McMullin J.P., Mundy L.G., Blake G.A.: 1994, ApJ 437, 305
- Mendoza E.E. V: 1966, ApJ 143, 1010
- Mendoza E.E. V: 1968, ApJ 151, 977
- Menten K.M., Reid M.J.: 1995, ApJ 445, L157
- Mezger P.G., Sievers A.W., Haslam C.G.T., Kreysa E., Lemke R., Mauersberger R., Wilson T.L.: 1992a, A&A 256, 631
- Mezger P.G., Sievers A.W., Zylka R., Haslam C.G.T., Kreysa E., Lemke R.: 1992b, A&A 265, 743
- Mezger P.G., Zylka R., Wink J.E.: 1990, A&A 228, 95
- Micono M., Davis C.J., Ray T.P., Eislöffel J., Shetrone M.D.: 1998a, ApJ 494, L227
- Micono M., Massaglia S., Bodo G., Rossi P., Ferrari A.: 1998b, A&A 333, 1001
- Moneti A., Reipurth B.: 1995, A&A 301, 721
- Moneti A., Helfer H.L., McMillan R.S., Perry M.L., Pipher J.L.: 1984, ApJ 282, 508
- Morgan J.A., Bally J.: 1991, ApJ 372, 505
- Morgan J.A., Schloerb P.F., Snell R.L., Bally J.: 1991, ApJ 376, 618
- Moro-Martín A., Cernicharo J., Noriega-Crespo A., Martín-Pintado J.: 1999, ApJ 520, L111
- Morse J.A., Hartigan P., Cecil G., Raymond J.C., Heathcote S.: 1992, ApJ 399, 231
- Morse J.A., Hartigan P., Heathcote S., Raymond J.C., Cecil, G.: 1994, ApJ 435, 738
- Morse J.A., Heathcote S., Cecil G., Hartigan P., Raymond J.C.: 1993a, ApJ 410, 764
- Morse J.A., Heathcote S., Hartigan P., Cecil G.: 1993b, AJ 106, 1139
- Motte F., André P., Neri R.: 1998, A&A 336, 150
- Mouschovias T.C.: 1976, ApJ 207, 141
- Mouschovias T.C., Paleologou E.V.: 1980, ApJ 237, 877
- Mundt R.: 1985, in *Protostars and Planets II* (Tucson: University of Arizona Press), 414
- Mundt R.: 1988, in *Formation and Evolution of Low Mass Stars*, NATO ASI 241, eds. A.K. Dupree & M.T.V.T. Lago, 257
- Mundt R., Eislöffel J.: 1998, AJ 116, 860
- Mundt R., Fried J.W.: 1983, ApJ 274, L83
- Mundt R., Brugel E.W., Bührke T.: 1987, ApJ 319, 275
- Mundt R., Ray T.P., Bührke T., Raga A., Solf J.: 1990, A&A 232, 37
- Mundt R., Ray T.P., Raga A.: 1991, A&A 252, 740
- Mundy L.G., Looney L.W., Welch W.J.: 2000, in *Protostars and Planets IV*, eds. V. Mannings, A. Boss, S. Russel (Tucson: University of Arizona Press), 355
- Myers P.C., Evans N.J. II, Ohashi N.: 2000, in *Protostars and Planets IV*, eds. V. Mannings, A. Boss, S. Russel (Tucson: University of Arizona Press), 217
- Myers P.C., Fuller G.A., Mathieu R.D., Beichman C.A., Benson P.J., Schild R.E., Emerson J.P.: 1987, ApJ 319, 340
- Myers P.C., Heyer M., Snell R.L., Goldsmith P.F.: 1988, ApJ 324, 907

- Nadeau D., Geballe T.R.: 1979, ApJ 230, L169
- Nagahama T., Mizuno A., Ogawa H., Fukui Y.: 1998, AJ 116, 336
- Nagata T., Sato S., Kobayashi Y.: 1983, A&A 119, L1
- Najita J., Edwards S., Basri G., Carr J.: 2000, in *Protostars and Planets IV*, eds. V. Mannings, A. Boss, S. Russel (Tucson: University of Arizona Press), 457
- Nakano T., Hasegawa T., Norman C.: 1995, ApJ 450, 183
- Neuhäuser R.: 1997, Science 276, 1363
- Noriega-Crespo A.: 1997, in *Herbig-Haro Flows and the Birth of Low Mass Stars*, IAU 182, eds. B. Reipurth & C. Bertout, 103
- Noriega-Crespo A., Garnavich P.M.: 1994, AJ 108, 1432
- Noriega-Crespo A., Garnavich P.M., Curiel S., Raga A.C., Ayala S.: 1997, ApJ 486, L55
- Norman C., Silk J.: 1979, ApJ 228, 197
- Norman C., Silk J.: 1980, ApJ 238, 158
- Norman M.L., Smarr L., Winkler K.-H.A., Smith M.D.: 1982, A&A 113, 285
- O'Dell C.R., Hartigan P., Lane W.M., Wong S.K., Burton M.G., Raymond J., Axon D.J.: 1997, AJ 114, 730
- Ogura K.: 1995, ApJ 450, L23
- Ogura K., Walsh J.R.: 1991, AJ 101, 185
- Olberg M., Reipurth B., Booth R.S.: 1991, A&A 259, 252
- Osterbrock D.E.: 1962, ApJ 136, 359
- Ostriker E.C., Gammie C.F., Stone J.M.: 1999, ApJ 513, 259
- O'Sullivan S., Ray T.P.: 2000, A&A 363, 355
- Ouyed R., Pudritz R.E.: 1997a, ApJ 482, 712
- Ouyed R., Pudritz R.E.: 1997b, ApJ 484, 794
- Ouyed R., Pudritz R.E.: 1999, MNRAS 309, 233
- Padgett D.L., Brandner W., Stapelfeldt K.R., Strom S.E., Terebey S., Koerner D.: 1999, AJ 117, 1490
- Padman R., Bence S.J., Richer J.S.: 1997, in *Herbig-Haro flows and the birth of low mass stars*, IAU 182, eds. B. Reipurth & C. Bertout, 123
- Parker N.D., Padman R., Scott P.F.: 1991, MNRAS 252, 442
- Pendleton Y., Werner M.W., Capps R., Lester D.: 1986, ApJ 311, 360
- Pravdo S.H., Rodriguez L.F., Curiel S., Cantó J., Torrelles J.M., Becker R.H., Sellgren K.: 1985, ApJ 293, L35
- Pringle J.E.: 1989, in *Low Mass Star Formation and Pre-Main Sequence Objects*, ESO Conf. Proc. 33, ed. B. Reipurth, 89
- Prosser C.F., Stauffer J.R., Hartmann L., Soderblom D.R., Jones B.F., Werner M.W., McCaughrean M.J.: 1994, ApJ 421, 517
- Pudritz R.E., Norman C.A.: 1983, ApJ 274, 677
- Pudritz R.E., Norman C.A.: 1986, ApJ 301, 571
- Pudritz R.E., Ouyed R.: 1997, in *Herbig-Haro flows and the birth of low mass stars*, IAU 182, eds. B. Reipurth & C. Bertout, 259
- Raga A.C., Böhm K.-H.: 1985, ApJS 58, 201
- Raga A., Cabrit S.: 1993, A&A 278, 267
- Raga A.C., Cantó J.: 1989, ApJ 344, 404
- Raga A.C., Cantó J., Binette L., Calvet N.: 1990, ApJ 364, 601
- Raga A.C., Cantó J., Cabrit S.: 1998, A&A 332, 714

- Raga A.C., Cantó J., Calvet N., Rodríguez L.F., Torrelles J.M.: 1993, A&A 276, 539
- Raga A.C., Mellema G., Lundqvist P.: 1997, ApJS 109, 517
- Rayner J., McLean I., McCaughrean M.J., Aspin C.: 1989, MNRAS 241, 469
- Ray T.P., Mundt R., Dyson J., Falle S.A.E.G., Raga A.: 1996, ApJ 468, L103
- Ray T.P., Muxlow T.W.B., Axon D.J., Brown A., Corcoran D., Dyson J., Mundt R.: 1997, Nature 385, 415
- Rees M.J.: 1978, MNRAS 184, 61P
- Reipurth B.: 1985a, A&AS 61, 319
- Reipurth B.: 1985b, A&A 143, 435
- Reipurth B.: 1989a, in *Low Mass Star Formation and Pre-Main Sequence Objects*, ESO Conf. Proc. 33, ed. B. Reipurth, 247
- Reipurth B.: 1989b, Nature 340, 42
- Reipurth B.: 1989c, A&A 220, 249
- Reipurth B.: 1999, *A general catalogue of Herbig-Haro objects*, 2. edition, electronically published at <http://casa.colorado.edu/hhcat>
- Reipurth B.: 2000, in *The formation of binary stars*, IAU 200, eds. H. Zinnecker, R. Mathieu, in prep.
- Reipurth B., Bally J.: 1986, Nature 320, 336
- Reipurth B., Graham J.A.: 1988, A&A 202, 219
- Reipurth B., Heathcote S.: 1991, A&A 246, 511
- Reipurth B., Heathcote S.: 1992, A&A 257, 693
- Reipurth B., Heathcote S.: 1997, in *Herbig-Haro flows and the birth of low mass stars*, IAU 182, eds. B. Reipurth & C. Bertout, 3
- Reipurth B., Olberg M.: 1991, A&A 246, 535
- Reipurth B., Zinnecker H.: 1993, A&A 278, 81
- Reipurth B., Bally J., Devine D.: 1997, AJ 114, 2708
- Reipurth B., Bally J., Graham J.A., Lane A.P., Zealey W.J.: 1986, A&A 164, 51
- Reipurth B., Chini R., Krügel E., Kreysa E., Sievers A.: 1993a, A&A 273, 221
- Reipurth B., Devine D., Bally J., 1998, AJ 116, 1396
- Reipurth B., Heathcote S., Roth M., Noriega-Crespo A., Raga A.C.: 1993b, ApJ 408, L49
- Reipurth B., Heathcote S., Yu K.C., Bally J., Rodríguez L.F.: 2000a, ApJ 534, 317
- Reipurth B., Rodríguez L.F., Chini R.: 1999a, AJ 118, 983
- Reipurth B., Yu K.C., Heathcote S., Bally J., Rodríguez L.F.: 2000b, AJ 120, 1449
- Reipurth B., Yu K.C., Rodríguez L.F., Heathcote S., Bally J.: 1999b, A&A 352, L83
- Richer J., Shepherd D., Cabrit S., Bachiller R., Churchwell E.: 2000, in *Protostars and Planets IV*, eds. V. Mannings, A. Boss, S. Russel (Tucson: University of Arizona Press), 867
- Rieke G.H., Lebofsky M.J.: 1985, ApJ 288, 618
- Rodríguez L.F.: 1997, in *Herbig-Haro flows and the birth of low mass stars*, IAU 182, eds. B. Reipurth & C. Bertout, 88
- Rodríguez L.F., Delgado-Arellano V.G., Gómez Y., Reipurth B., Torrelles J.M., Noriega-Crespo A., Raga A.C., Cantó J.: 2000, AJ 119, 882
- Rodríguez L.F., Ho P.T.P., Torrelles J.M., Curiel S., Cantó J.: 1990, ApJ 352, 645
- Safier P.N., McKee C.F., Stahler S.W.: 1997, ApJ 485, 660
- Sandell G., Zealey W.J., Williams P.A., Taylor K.N.R., Storey J.V.: 1987, A&A 182, 237
- Sargent A.I., Beckwith S.: 1987, ApJ 323, 294
- Sato S., Nagata T., Nakajima T., Nishida M., Tanaka M., Yamashita T.: 1985, ApJ 291, 708

- Sato S., Tamura M., Nagata T., Kaifu N., Hough J., McLean I.S., Garden R.P., Gatley I.: 1988, MNRAS 230,321
- Schmid-Burgk J., Güsten R., Mauersberger R., Schulz A., Wilson T.L.: 1990, ApJ 362, L25
- Schultz A.S.B., Colgan S.W.J., Erickson E.F., Kaufman M.J., Hollenbach D.J., O'Dell C.R., Young E.T., Chen H.: 1999, ApJ 511, 282
- Schwartz R.D.: 1975, ApJ 195, 631
- Schwartz R.D.: 1977a, ApJ 212, L25
- Schwartz R.D.: 1977b, ApJS 35, 161
- Schwartz R.D.: 1978, ApJ 223, 884
- Schwartz R.D.: 1983, ARA&A 21, 209
- Schwartz R.D., Cohen M., Williams P.M.: 1987, ApJ 322, 403
- Schwartz R.D., Williams P.M., Cohen M., Jennings D.G.: 1988, ApJ 334, L99
- Shu F.H.: 1977, ApJ 214, 488
- Shu F.H., Shang H.: 1997, in *Herbig-Haro flows and the birth of low mass stars*, IAU 182, eds. B. Reipurth & C. Bertout, 225
- Shu F.H., Adams F.C., Lizano S.: 1987, ARA&A 25, 23
- Shu F.H., Lizano S., Ruden S.P., Najita J.: 1988, ApJ 328, L19
- Shu F., Najita J., Galli D., Ostriker E., Lizano S.: 1993, in *Protostars and Planets III*, eds. E.H. Levy & J.I. Lunine (Tucson: University of Arizona Press), 3
- Shu F.H., Najita J., Ostriker E., Wilkin F., Ruden S., Lizano S.: 1994, ApJ 429, 781
- Shu F.H., Najita J.R., Shang H., Li Z.-Y.: 2000, in *Protostars and Planets IV*, eds. V. Mannings, A. Boss, S. Russel (Tucson: University of Arizona Press), 789
- Shu F.H., Ruden S.P., Lada C.J., Lizano S.: 1991, ApJ 370, L31
- Shull J.M., Draine B.T.: 1987, in *Interstellar Processes*, eds. D.J. Hollenbach & H.A. Thronson, 283
- Shull J.M., Beckwith S.: 1982, ARA&A 20, 163
- Simon T., Joyce R.R.: 1983, ApJ 265, 864
- Smith A.M.: 1973, ApJ 179, L11
- Smith M.D.: 1986, MNRAS 223, 57
- Smith M.D.: 1991, MNRAS 252, 378
- Smith M.D.: 1994a, A&A 289, 256
- Smith M.D.: 1994b, MNRAS 266, 238
- Smith M.D.: 1995, A&A 296, 789
- Smith M.D.: 2000, Irish Astr. J. 27, 25
- Smith M.D., Brand P.W.J.L.: 1990, MNRAS 242, 495
- Smith M.D., MacLow M.-M.: 1997, A&A 326, 801
- Smith M.D., Brand P.W.J.L., Moorhouse A.: 1991a, MNRAS 248, 451
- Smith M.D., Brand P.W.J.L., Moorhouse A.: 1991b, MNRAS 248, 730
- Smith M.D., Eisloffel J., Davis C.J.: 1998, MNRAS 297, 687
- Smith M.D., Smarr L., Norman M.L., Wilson J.R.: 1983, ApJ 264, 432
- Smith M.D., Suttner G., Yorke H.W.: 1997b, A&A 323, 223
- Smith M.D., Suttner G., Zinnecker H.: 1997a, A&A 320, 325
- Snell R.L., Loren R.B., Plambeck R.L.: 1980, ApJ 239, L17
- Solf J.: 1989, in *Low Mass Star Formation and Pre-Main Sequence Objects*, ESO Conf. Proc. 33, ed. B. Reipurth, 399

- Solf J.: 1997, in *Herbig-Haro flows and the birth of low mass stars*, IAU 182, eds. B. Reipurth & C. Bertout, 63
- Solomon P.M., Huguenin G.R., Scoville N.Z.: 1981, ApJ 245, L19
- Sonnhalter C., Preibisch T., Yorke H.W.: 1995, A&A 299, 545
- Spitzer L., Drake J.F., Jenkins E.B., Morton D.C., Rogerson J.B., York D.G.: 1973, ApJ 181, L116
- Stahler S.W.: 1994, ApJ 422, 616
- Stahler S.W., Walter F.M.: 1993, in *Protostars and Planets III*, eds. E.H. Levy & J.I. Lunine (Tucson: University of Arizona Press), 405
- Stanke T., Zinnecker H.: 2000, in *Birth and Evolution of Binary Stars*, Poster Proceedings of IAU Symposium 200, eds. B. Reipurth & H. Zinnecker, 38
- Stanke T., McCaughrean M.J., Zinnecker H.: 1998, A&A 332, 307
- Stanke T., McCaughrean M.J., Zinnecker H.: 1999, A&A 350, L43
- Stanke T., McCaughrean M.J., Zinnecker H.: 2000, A&A, 355, 639
- Stapelfeldt K.R., Burrows C.J., Krist J.E.; WFPC2 Science Team: 1997, in *Herbig-Haro flows and the birth of low mass stars*, IAU 182, eds. B. Reipurth & C. Bertout,
- Stapelfeldt K.R., Krist J.E., Ménard F., Bouvier J., Padgett D.L., Burrows C.J.: 1998, ApJ 502, L65
- Stapelfeldt K.R., Scoville N.Z., Beichman C.A., Hester J.J., Gautier T.N. III: 1991, ApJ 371, 226
- Staude H.J., Elsässer H.: 1993, A&ARv 5, 165
- Stone J.M.: 1997, in *Herbig-Haro flows and the birth of low mass stars*, IAU 182, eds. B. Reipurth & C. Bertout, 323
- Stone J.M., Norman M.L.: 1993, ApJ 413, 210
- Stone J.M., Norman M.L.: 1994a, ApJ 420, 237
- Stone J.M., Norman M.L.: 1994b, ApJ 433, 746
- Stone J.M., Ostriker E.C., Gammie C.F.: 1998, ApJ 508, L99
- Strömgren B.: 1939, ApJ 89, 526
- Strom K.M., Strom S.E.: 1993, ApJ 412, L63
- Strom K.M., Margulis M., Strom S.E.: 1989a, ApJ 346, L33
- Strom K.M., Newton G., Strom S.E., Seaman R.L., Carrasco L., Cruz-Gonzalez I., Serrano A., Grasdalen G.L.: 1989b, ApJSS 71, 183
- Strom K.M., Strom S.E., Kenyon S.J., Hartmann L.: 1988b, AJ 95, 534
- Strom K.M., Strom S.E., Merrill K.M.: 1993, ApJ 412, 233
- Strom K.M., Strom S.E., Wenz M., Wolff S.C., Morgan J.: 1986, ApJS 62, 39
- Strom S.E., Strom K.M., Edwards S.: 1988a, in *Galactic and extragalactic star formation*, eds. R.E. Pudritz, M. Fich, p. 53
- Strom S.E., Strom K.M., Grasdalen G.L., Sellgren K., Wolff S., Morgan J., Stocke J., Mundt R.: 1985, AJ 90, 2281
- Suttner G., Smith M.D., Yorke H.W., Zinnecker H.: 1997, A&A 318, 595
- Tamura M., Nagata T., Sato S., Tanaka M.: 1987, MNRAS 224, 413
- Tamura M., Yamashita T., Sato S., Nagata T., Gatley I.: 1988, MNRAS 231, 445
- Tatematsu K., Umemoto T., Kameya O., Hirano N., Hasegawa T., Hayashi M., Iwata T., Kaifu N., Mikami H., Murata Y., Nakano M., Nakano T., Ohashi N., Suanada K., Takaba H., Yamamoto S.: 1993, ApJ 404, 643 (T93)
- Tatematsu K., Umemoto T., Kameya O., Heyer M.H., Hirano N., Kameya O., Jaffe D.T.: 1998, ApJS 118, 517
- Taylor K.N.R., Storey J.W.V., Sandell G., Williams P.M., Zealey W.J.: 1984, Nature 311, 236
- Tedds J.A., Brand P.W.J.L., Burton M.G.: 1999, MNRAS 307, 337

- Terquem C., Eisloffel J., Papaloizou J.C.B., Nelson R.P.: 1999, ApJ 512, L131
- Tomisaka K.: 1996, PASJ 48, L97
- Treffers R.R., Fink U., Larson H.P., Gautier T.N. III: 1976, ApJ 209, 793
- Uchida Y., Shibata K.: 1985, PASJ 37, 515
- Velusamy T., Langer W.D.: 1998, Nature 392, 685
- Vlahakis N., Tsinganos K., Sauty C., Trussoni E.: 2000, MNRAS 318, 417
- Völker R., Smith M.D., Suttner G., Yorke H.W.: 1999, A&A 343, 953
- Vrba F.J., Strom S.E., Strom K.M.: 1988, AJ 96, 680
- Ward-Thompson D., Kirk J.M., Crutcher R.M., Greaves J.S., Holland W.S., André P.: 2000, ApJ 537, L135
- Werner M.W., Harwit M.: 1968, ApJ 154, 881
- Wilkin F.P., Canto J., Raga A.C.: 1997, in *Herbig-Haro Flows and the Birth of Low Mass Stars*, IAU 182, eds. B. Reipurth & C. Bertout, 343
- Wilking B.A., Blackwell J.H., Mundy L.G.: 1990b, AJ 100, 758
- Wilking B.A., Blackwell J.H., Mundy L.G., Howe J.E.: 1989, ApJ 345, 257
- Wilking B.A., Schwartz R.D., Mundy L.G., Schultz A.S.B.: 1990a, AJ 99, 344
- Williams J.P., de Geus E.J., Blitz L.: 1994, ApJ 428, 693
- Wilner D.J., Lay O.P.: 2000, in *Protostars and Planets IV*, eds. V. Mannings, A. Boss, S. Russel (Tucson: University of Arizona Press), 509
- Wilson T.L., Mauersberger R.: 1991, A&A 244, L33
- Wilson T.L., Mauersberger R., Gensheimer P.D., Muders D., Bieging J.H.: 1999, ApJ 525, 343
- Wiseman J., Wootten A., Zinnecker H., McCaughrean M.J.: 2000, submitted to ApJ Letters
- Wolf-Chase G., Barsony M., O'Linger J.A.: 2000, AJ 120, 1467
- Wolfire M.G., Königl A.: 1991, ApJ 383, 205
- Wolstencroft R.D., Scarrott S.M., Warren-Smith R.F., Walker H.J., Reipurth B., Savage, A.: 1986, MNRAS 218, 1
- Wouterloot J.G.A., Walmsley C.M.: 1986, A&A 168, 237
- Wouterloot J.G.A., Henkel C., Walmsley C.M.: 1989, A&A 215, 131
- Wu Y., Huang M., He J.: 1996, A&AS 115, 283
- Yorke H.W., Bodenheimer P., Laughlin G.: 1993, ApJ 411, 274
- Yu K.C.: 2000, PhD thesis (University of Colorado)
- Yu K.C., Bally J., Devine D.: 1997, ApJ 485, L45
- Yu K.C., Billawala Y., Bally J.: 1999, AJ 118, 2940
- Zaritsky D., Shaya E.J., Scoville N.Z., Sargent A.I., Tytler D.: 1987, AJ 93, 1514
- Zavagno A., Molinari S., Tommasi E., Saraceno P., Griffin M.: 1997, A&A 325, 685
- Zealey W.J., Suters M.G., Randall P.R.: 1993, PASAu 10, 203
- Zealey W.J., Williams P.M., Sandell G.: 1984, A&A 140, L31
- Zealey W.J., Williams P.M., Taylor K.N.R., Storey J.W.V., Sandell G.: 1986, A&A 158, L9
- Zhou S., Wu Y., Evans N.J. II, Fuller G.A., Myers P.: 1989, ApJ 346, 168
- Zinnecker H., Mathieu R.D. (editors): 2000, *The Formation of Binary Stars*, IAU 200, in prep.
- Zinnecker H., Tscharnuter W.M.: 1984, in *Proceedings of the Workshop on Star Formation*, held in Edinburgh, 4-6 October 1983, ed. R.D. Wolstencroft, 83
- Zinnecker H., McCaughrean M.J., Wilking B.A.: 1993, in *Protostars and Planets III*, eds. E.H. Levy & J.I. Lunine (Tucson: University of Arizona Press), 429
- Zinnecker H., Mundt R., Geballe T.R., Zealey W.J.: 1989, ApJ 342, 337
- Zinnecker H., Bastien P., Arcoragi J.-P., Yorke H.W.: 1992, A&A 265, 726

- Zinnecker H., McCaughrean M.J., Rayner J.T.: 1998, *Nature* 394, 862
- Zinnecker H., Krabbe A., McCaughrean M.J., Stanke T., Stecklum B., Brandner W., Padgett D.L., Stapelfeldt K.R., Yorke H.W.: 1999, *A&A* 352, L73
- Ziurys L.M., Friberg P.: 1987, *ApJ* 314, L49
- Ziurys L.M., Wilson T.L., Mauersberger R.: 1990, *ApJ* 356, L25
- Zuckerman B., Evans N.J. II: 1974, *ApJ* 192, L149
- Zuckerman B., Palmer P.: 1974, *ARA&A* 12, 279
- Zuckerman B., Kuiper T.B.H., Rodriguez-Kuiper E.N.: 1976, *ApJ* 209, L137

## A The H<sub>2</sub> features

In this section a compilation of all H<sub>2</sub> emission line features is presented. Figure 13 gives an overview over the entire survey area, with the areas covered by the 9 individual survey fields indicated. In the following for each of the 9 survey fields an overview map is given with the features or groups of features marked by ellipses and labelled. In addition, a table is presented giving closeup views of the H<sub>2</sub> features. For each feature, the image section containing the respective feature as seen through the 2.12 μm narrow band filter (H<sub>2</sub> filter), the broad band K' filter (continuum image), and the continuum subtracted image is given. The size scale is indicated by a scale bar, measuring 20'', in each H<sub>2</sub> close-up image. The position for each feature is given, or the positions of some prominent parts of the respective feature, together with the total brightness of the feature (2.12 μm line flux) and brightnesses of prominent parts of the respective feature, and the tentative flow association. Finally, a comment on morphology is given, the associated optical Herbig-Haro object number (if applicable), and for the OMC-2/3 sources in Field 1 also the YBD number designated to the features by Yu et al. (1997).

In all images shown, north is up and east to the left.



### A.1 Field 1

#### H<sub>2</sub> features: Overview

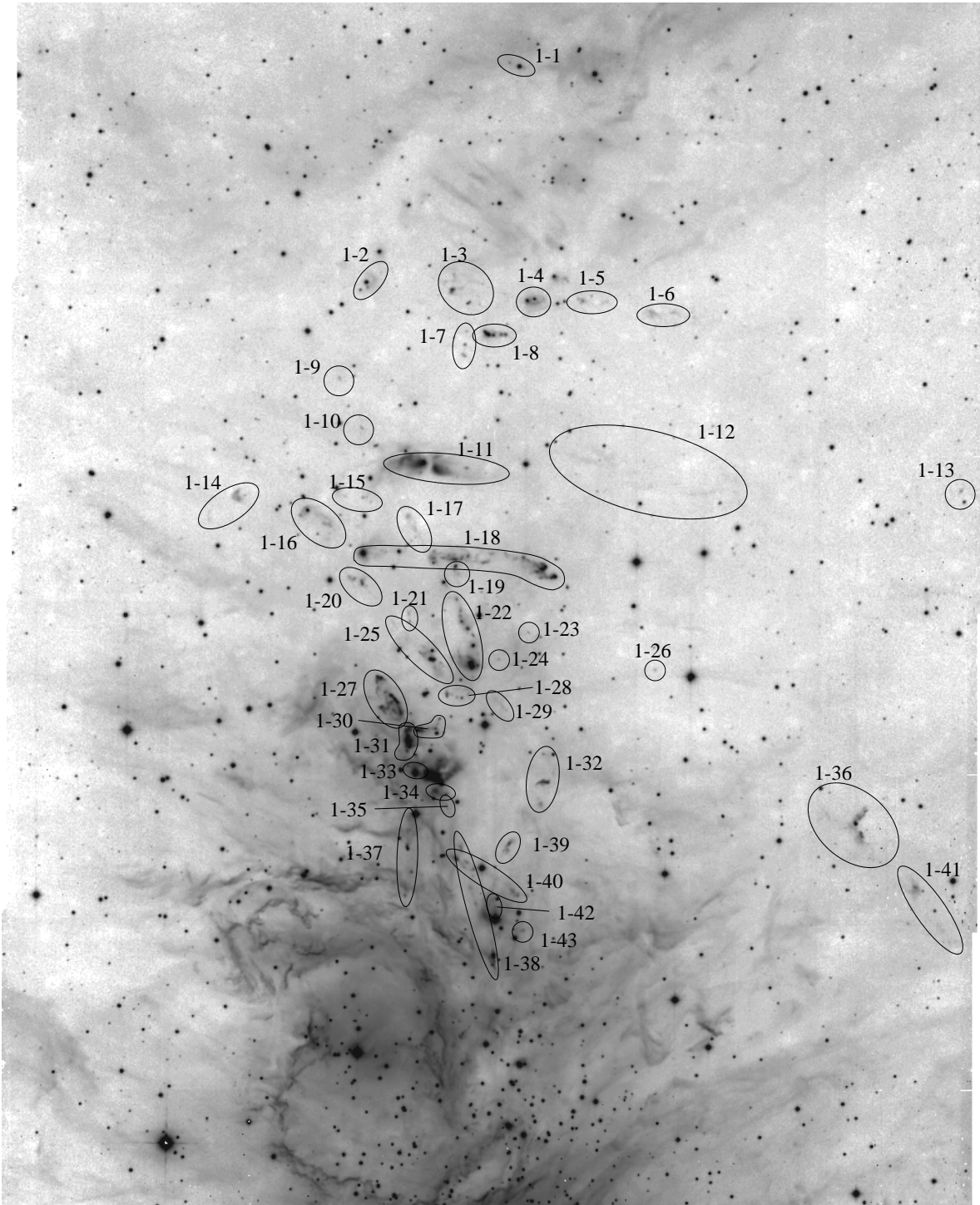
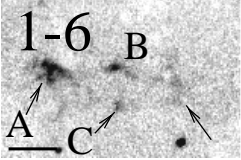
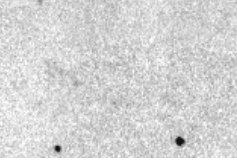
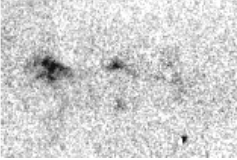
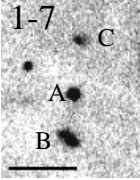
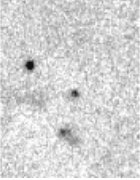
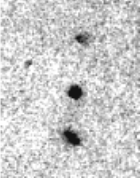
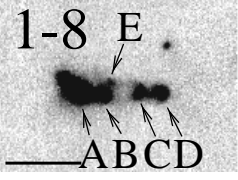

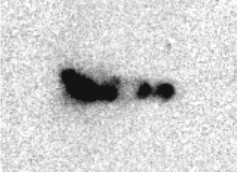
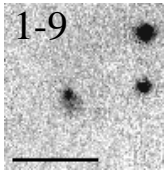
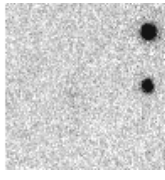
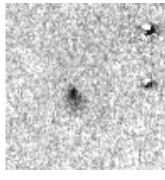
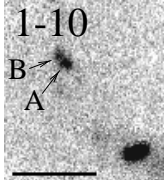
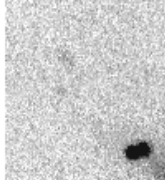
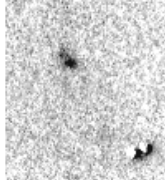


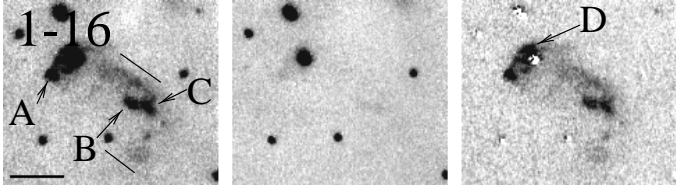
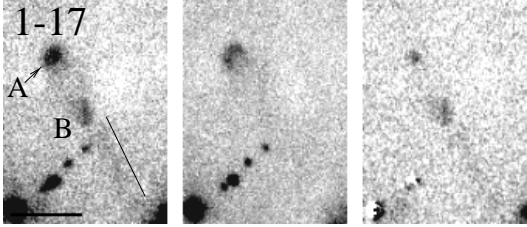
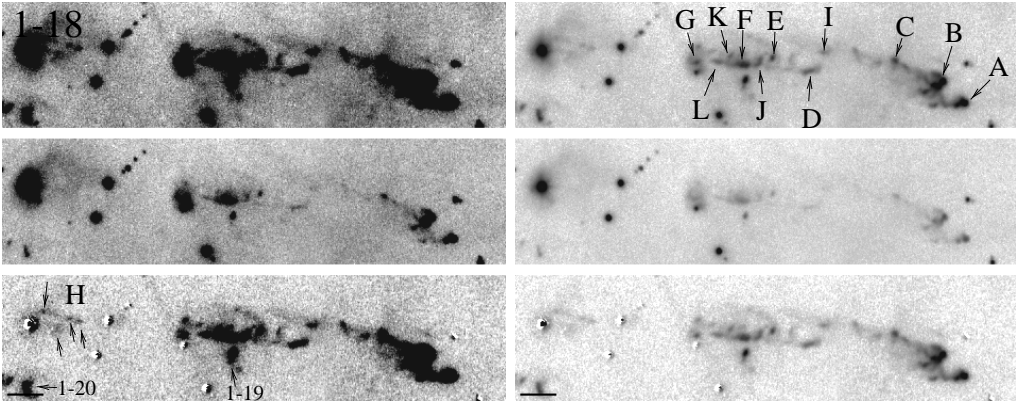
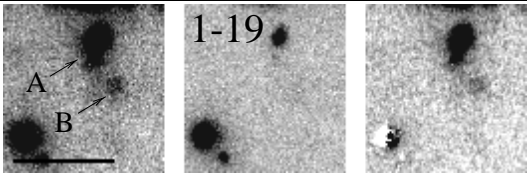
Figure 48: H<sub>2</sub> features in Field 1 (the OMC-2/3 area)

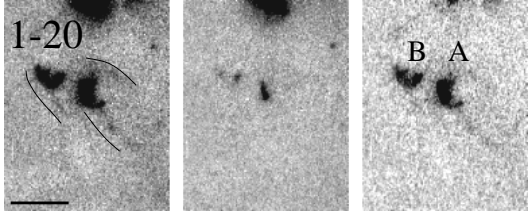

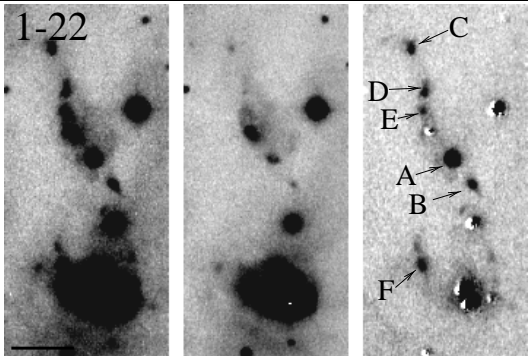
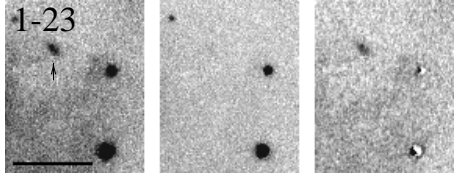
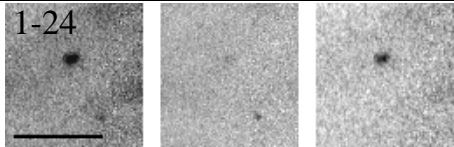
H<sub>2</sub> features: Details

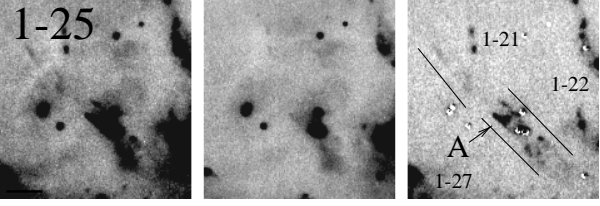
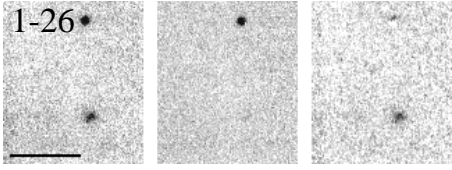
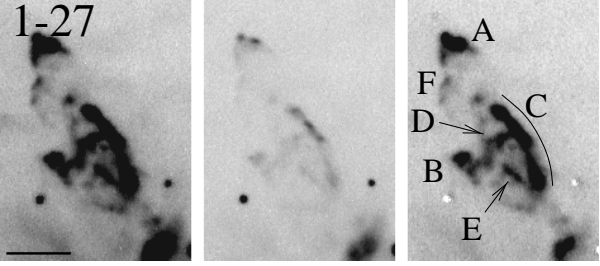
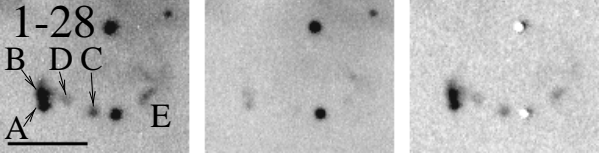
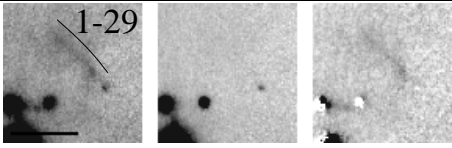
Feature	RA (J2000)	DEC	H <sub>2</sub> Flux (10 <sup>-17</sup> $\frac{W}{m^2}$ )	Flow	Comment
1-1			~ 2.1	1	Two compact knots to the E and W of a star
A	5 35 19.9	-4 55 41	~ 1.5		
B	5 35 18.7	-4 55 47	~ 0.6		
1-2			~ 3	2	Two compact knots associated with some reflection nebulosity, some more diffuse emission Bright knot
A	5 35 31.4	-5 00 20	2.0		
B	5 35 30.3	-5 00 02	~ 0.4		
1-3			~ 20	3 (?)	Group of compact and filamentary features Bright compact knot, bowshock? YBD 42 Filamentary feature; YBD 41 Faint compact feature; YBD 36 Filamentary feature; YBD 50
A	5 35 24.4	-5 00 21	15.4		
B	5 35 24.3	-5 00 02	~ 1.2		
C	5 35 23.6	-5 00 18	~ 0.9		
D	5 35 25.0	-5 00 12	~ 1.1		
1-4			~ 10	3	Knotty filament extending over 25'' east of knot A; associated with reflection nebulosity Compact knot; YBD 7
A	5 35 16.9	-5 00 32	~ 1.4		
1-5			~ 6	3	E-W oriented group of compact and filamentary features Double knot, bowshock? YBD 3 (together with B)  Filamentary feature; YBD 2
A	5 35 13.7	-5 00 33	~ 3.4		
B	5 35 14.0	-5 00 31	~ 0.8		
C	5 35 11.9	-5 00 33	~ 1.4		

Feature	RA (J2000)	DEC	H <sub>2</sub> Flux (10 <sup>-17</sup> $\frac{W}{m^2}$ )	Flow	Comment
  					
1-6			~ 15	<b>3</b>	E-W oriented group of diffuse and filamentary features; very faint diffuse H <sub>2</sub> emission further west; HH 331
A	5 35 07.9	-5 00 46	~ 7.8		Diffuse knots; YBD 1
B	5 35 06.2	-5 00 44	~ 1.9		Faint compact feature
C	5 35 05.9	-5 01 01	~ 0.8		Faint compact feature
  					
1-7			~ 6	<b>4</b>	N-S oriented chain of 3 compact knots
A	5 35 23.2	-5 01 27	~ 2.8		YBD 30
B	5 35 23.2	-5 01 41	~ 2.1		NE-SW extended; YBD 32
C	5 35 23.1	-5 01 12	~ 0.9		YBD 28
  					
1-8			~ 93	<b>5</b>	E-W oriented chain of bright compact knots; HH 293
A	5 35 21.3	-5 01 15	~ 57		Eastern end of chain; brightest knot; 9'' long extension towards NE; YBD 17
D	5 35 19.8	-5 01 15	~ 6.8		Western end of chain; YBD 19 (together with C)
  					
1-9	5 35 33.5	-5 02 11	~ 1.3	<b>7</b>	Small cometary feature heading due NE (small bow shock?); tip at given position
  					
1-10	5 35 31.6	-5 03 14	~ 1.6	<b>7</b>	Double knot; knot A at given position, knot B 2'' N, 2'' E; YBD 76

Feature	RA (J2000)	DEC	H <sub>2</sub> Flux (10 <sup>-17</sup> $\frac{W}{m^2}$ )	Flow	Comment
1-11			~ 8	6	E-W oriented chain of knots extending to the E and W of bipolar reflection nebula Haro 5a/6a; HH 294
A	5 35 24.8	-5 04 00	~ 3.2		Short E-W oriented chain of knots; YBD 46
B	5 35 22.9	-5 04 00	~ 2.6		Bright compact knot; YBD 27
C	5 35 21.3	-5 04 07	~ 0.4		Faint compact knot
D	5 35 27.1	-5 03 54	~ 1.8		Short E-W oriented chain of knots
1-12	5 35 07.0	-5 04 10	~ 15	6	Group of very faint large filaments centered roughly at given position extending about 2'8 to 6' W of Haro 5a/6a; flux measurement highly uncertain
1-13	5 34 42.1	-5 04 18	~ 2.3	6	Elliptical knot; HH 295E
1-14			~ 16	? (8 ?)	
A	5 35 41.9	-5 04 40	~ 15		Bow shaped feature heading due ESE; YBD 80, HH 330
B	5 35 44.2	-5 05 04	~ 0.9		Curving filamentary feature
1-15			~ 2.4	? (8 ?)	E-W oriented group of 3 compact knots
A	5 35 31.5	-5 04 39	~ 1.5		YBD 75
B	5 35 31.2	-5 04 37	~ 0.6		
C	5 35 33.0	-5 04 37	~ 0.3		

Feature	RA (J2000)	DEC	H <sub>2</sub> Flux (10 <sup>-17</sup> $\frac{W}{m^2}$ )	Flow	Comment
					
1-16			~ 40	14? (10??)	Large group of compact and diffuse features
A	5 35 36.6	-5 05 01	~ 4		YBD 79 (together with D)
B	5 35 34.7	-5 05 11	~ 2		YBD 78 (together with C)
C	5 35 34.2	-5 05 13	~ 2.3		
D	5 35 36.2	-5 04 52	~ 4.5		
					
1-17			~ 2	7	Faint knots and diffuse emission features in a row
A	5 35 27.7	-5 05 01	~ 1.1		Compact knot, associated with U shaped reflection nebulosity
B	5 35 27.1	-5 05 17	~ 1.3		Diffuse feature; more diffuse faint emission further SSW; YBD 59
					
1-18			~ 310	9	E-W oriented group of partly very bright features; C = YBD 8, D = YBD 16, E = YBD 25, F = YBD 40, I = YBD 15, J = YBD 29, K = YBD 43, L = YBD 48; HH 357
A	5 35 15.5	-5 06 12	~ 45		Tip of bright bow shock; YBD 4
B	5 35 16.3	-5 06 01	~ 95		Wake of bright bow shock; YBD 5
G	5 35 25.5	-5 05 51	~ 4.9		Diffuse feature associated with continuum nebulosity at center of 1-18; YBD 54
H	5 35 27.1	-5 05 17	~ 3	(10??)	Group of faint knots; YBD 70
					
1-19			~ 16	11	2 knots south of 1-18; YBD 39
A	5 35 23.7	-5 06 00	~ 14		Bright cometary knot; tip of bow shock?
B	5 35 23.5	-5 06 10	~ 1.3		Faint diffuse feature

Feature	RA (J2000)	DEC	H <sub>2</sub> Flux ( $10^{-17} \frac{W}{m^2}$ )	Flow	Comment
					
1-20			~ 25	<b>14</b>	2 compact bright features with trailing filaments; fragmented bow shock heading due NE
A	5 35 31.4	-5 06 23	~ 12		YBD 74
B	5 35 32.2	-5 06 18	~ 6		YBD 77
					
1-21			~ 3.5	12	2 compact knots in N-S oriented group
A	5 35 27.4	-5 07 11	1.9		N-S elongated; YBD 61
B	5 35 27.5	-5 07 01	1.5		N-S elongated; YBD 63
					
1-22			~ 35	<b>7</b>	N-S oriented group of compact knots; HH 385
A	5 35 22.6	-5 07 17	11.3	(13??)	Bright compact knot; YBD 24
B	5 35 22.2	-5 07 25	2.7	(13??)	Compact knot; YBD 21
C	5 35 23.5	-5 06 41	3.0		Compact knot; YBD 38
D	5 35 23.2	-5 06 56	3.0		Compact knot; YBD 33
E	5 35 23.3	-5 07 02	2.3		Compact knot; YBD 31
F	5 35 23.3	-5 07 51	5.7	(15??)	N-S oriented filamentary knot; YBD 34
					
1-23	5 35 17.6	-5 07 21	~ 1	?	Compact knot
					
1-24	5 35 20.0	-5 07 55	~ 1	?(7/13?)	Compact knot

Feature	RA (J2000)	DEC	H <sub>2</sub> Flux ( $10^{-17} \frac{W}{m^2}$ )	Flow	Comment
					
1-25			~ 15	<b>14</b>	System of knots and filaments oriented NE-SW; resembles limb brightened tubelike structure (marked by the lines); YBD 49, YBD 53, YBD 58; HH 383
A	5 35 26.2	-5 07 50	~ 5.4		Triangular feature; YBD 58
					
1-26	5 35 07.0	-5 08 05	~ 0.9	?	Compact knot
					
1-27			~ 280	<b>17/18</b>	Group of bright knots, bow shocks, and filaments; F = YBD 73
A	5 35 30.0	-5 08 20	~50	<b>17</b>	Bright bow shock; YBD 72
B	5 35 29.6	-5 08 57	~30	<b>18</b>	Bow shock (?); YBD 71
C	5 35 28.3	-5 08 51	~80	<b>17</b>	Bright curved filament; YBD 67, YBD 69
D	5 35 28.8	-5 08 51	~11	<b>17</b>	Bow shock (?)
E	5 35 28.5	-5 09 02	~ 5	<b>18</b>	Filament; YBD 68
					
1-28			~ 11	<b>14/16 (?)</b>	Group of compact knots
A	5 35 24.2	-5 08 40	~4.1		YBD 45 (together with B)
B	5 35 24.3	-5 08 37	~4.1		
C	5 35 23.4	-5 08 42	~1.1		YBD 37
D	5 35 23.9	-5 08 39	~0.8		
E	5 35 22.5	-5 08 37	~0.9		Filament; YBD 23
					
1-29	5 35 19.9	-5 08 48	~ 3	<b>14/16 ?</b>	NE-SW oriented filamentary structure

Feature	RA (J2000)	DEC	H <sub>2</sub> Flux (10 <sup>-17</sup> $\frac{W}{m^2}$ )	Flow	Comment
1-30			~ 15	<b>19</b>	E-W oriented feature; some knots NW of knot A; HH 384
A	5 35 25.2	-5 09 21	~ 6	<b>19</b>	Compact knot; western end of E-W feature; YBD 52
B	5 35 26.7	-5 09 23	~ 4	<b>19</b>	Diffuse knot; eastern end of E-W feature
C	5 35 25.0	-5 09 15	~ 1.6	(20?)	Faint compact knot; YBD 51
D	5 35 24.9	-5 09 10	~ 1.5	(20?)	Diffuse faint feature
1-31			~ 55	<b>17</b> (?)	Group of knots around bright continuum source
A	5 35 27.3	-5 09 39	~ 15		Bright knot; flux poorly determined, because close to saturated stars
B	5 35 27.5	-5 09 32	~ 16		Bright knot
C	5 35 27.6	-5 09 25	~ 12		Diffuse knot; YBD 65 (together with D)
D	5 35 27.3	-5 09 22	~ 11		Diffuse feature
E	5 35 28.2	-5 09 49	~ 1	?	Diffuse faint feature
1-32			~ 40	<b>25</b>	Large N-S oriented group of knots and filaments
A	5 35 16.2	-5 10 25	~ 31	<b>25/14</b> ?	Bright, E-W elongated filamentary feature; HH 44
B	5 35 16.5	-5 10 53	~ 4		Diffuse feature
C	5 35 16.2	-5 09 51	~ 1.7		Compact knot; YBD 6
D	5 35 15.4	-5 10 12	~ 1.2		Faint diffuse feature
E	5 35 14.9	-5 10 37	~ 0.5		Faint filament
1-33			~ 4	?(20/17?)	Loose group of faint compact knots
A	5 35 26.4	-5 10 18	~ 1.6		
B	5 35 27.2	-5 10 10	~ 0.7		



Feature	RA (J2000)	DEC	H <sub>2</sub> Flux (10 <sup>-17</sup> $\frac{W}{m^2}$ )	Flow	Comment
1-34			~ 11	<b>17</b>	Bow shaped knotty feature; part of bow shock heading due SW?
A	5 35 24.2	-5 10 42	~ 6.5		Brightest part of bow; tip of bow shock? YBD 44
1-35			~ 1.5	<b>23(?)</b>	Two compact faint knots
A	5 35 24.1	-5 10 58	~ 0.8		
B	5 35 24.2	-5 10 55	~ 0.6		
1-36			~ 70	?	Group of knots, filaments, and diffuse emission features
A	5 34 49.7	-5 11 24	~ 19		Compact double knot, diffuse emission
B	5 34 49.9	-5 11 00	~ 32		SE-NW oriented filamentary structure
1-37			~ 70	<b>21</b>	N-S oriented group of compact features
A	5 35 27.3	-5 11 49	~ 28		Comma shaped compact feature; part of bow shock? YBD 62
B	5 35 26.9	-5 12 19	~ 5.8	(22?)	Compact knot; YBD 60
C	5 35 27.4	-5 12 48	~ 4.9	(22?)	Compact knot, some filamentary emission to the N; YBD 64, YBD 66
D	5 35 27.2	-5 11 28	~ 2.7		Three compact knots
E	5 35 27.2	-5 11 13	~ 4.6		Diffuse structure

Feature	RA (J2000)	DEC	H <sub>2</sub> Flux (10 <sup>-17</sup> $\frac{W}{m^2}$ )	Flow	Comment
1-38			~ 80	<b>23</b>	ENE-SSW oriented chain of features
A	5 35 20.1	-5 14 05	~ 70		Large bright triangular knotty feature; deformed bow shock? YBD 14
B	5 35 21.6	-5 12 55	~ 2.7		Compact faint knot; YBD 18
C	5 35 21.8	-5 12 45	~ 0.7		Compact faint knot
D	5 35 22.0	-5 12 36	~ 2.3		Diffuse faint knot; YBD 20
E	5 35 23.0	-5 11 45	~ 0.6		Compact faint knot associated with continuum nebulosity
1-39			~ 20	<b>25</b>	Filament & three compact knots
A	5 35 18.9	-5 11 40	~ 14		SE-NW oriented filamentary feature; YBD 11
B	5 35 19.0	-5 11 49	~ 3.8		Compact knot; YBD 12 (together with C)
C	5 35 19.3	-5 11 50	~ 1.0		Faint compact knot
1-40			~ 40	<b>24</b>	ENE-WSW oriented, HH 211 like group of knots and filaments; YBD 9, YBD 10, YBD 19, YBD 22, YBD 26, YBD 35
A	5 35 23.3	-5 12 00	~ 10		Diffuse feature; YBD 35
B	5 35 18.4	-5 12 42	~ 13		Group of compact knots; YBD 9, YBD 10
1-41			~ 20	?	Diffuse patch (knot A) and some more diffuse emission further SW
A	5 34 45.2	-5 12 29	~ 18		Diffuse patch

Feature	RA (J2000)	DEC	H <sub>2</sub> Flux (10 <sup>-17</sup> $\frac{W}{m^2}$ )	Flow	Comment
1-42			~ 3.5	<b>25</b>	Short chain of faint compact knots
A	5 35 20.0	-5 12 59	~ 1.4		
B	5 35 20.2	-5 12 53	~ 0.8		
C	5 35 20.3	-5 12 49	~ 0.7		
1-43			~ 3.5	?	Three nearby compact knots
A	5 35 17.8	-5 13 28	~ 1.5		
B	5 35 17.6	-5 13 27	~ 1.7		

## A.2 Field 2

### H<sub>2</sub> features: Overview

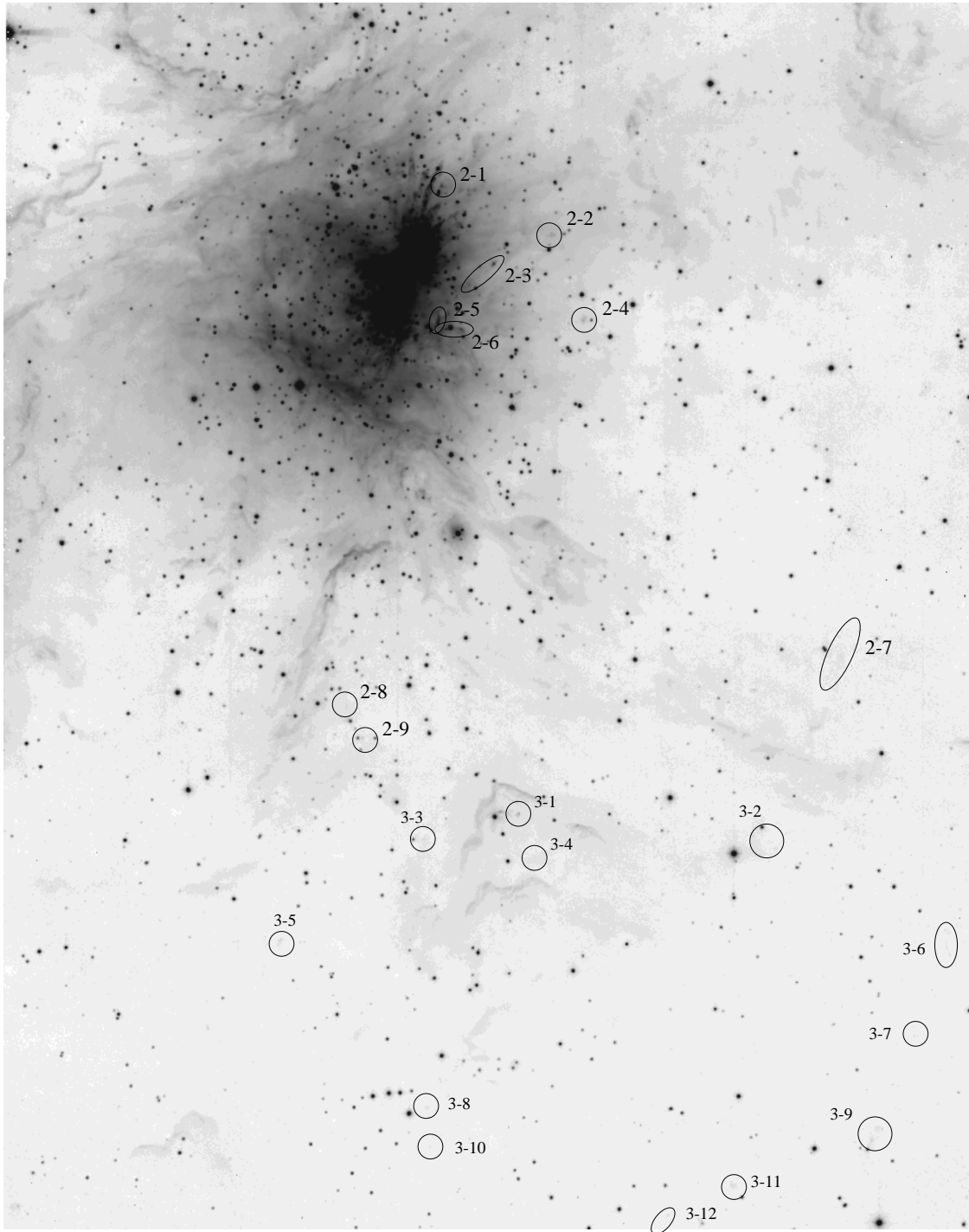
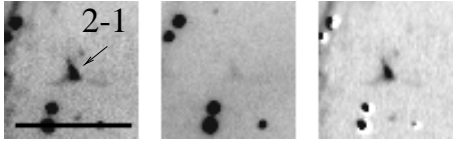
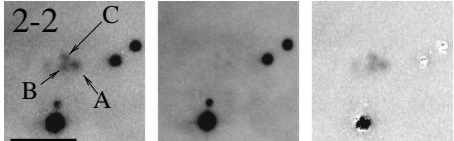
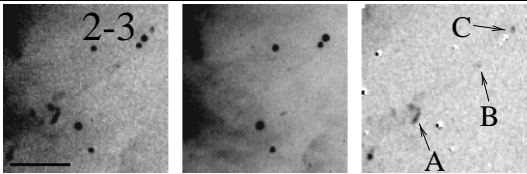
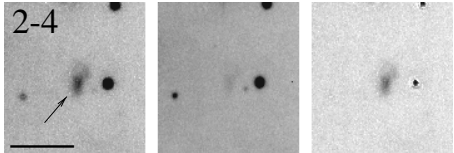
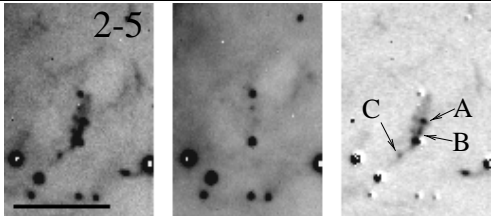
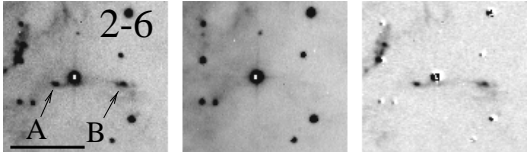
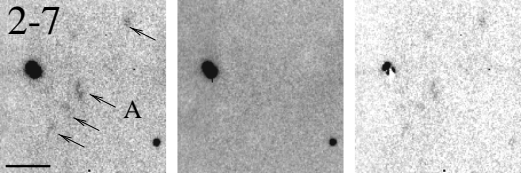
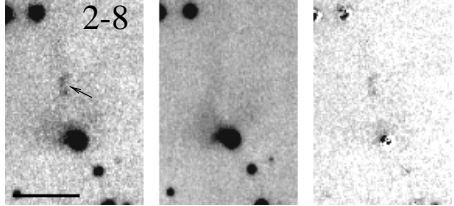
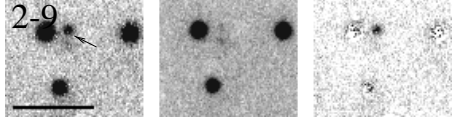


Figure 49: H<sub>2</sub> features in Field 2 (the Orion Nebula area)

H<sub>2</sub> features: Details

Feature	RA (J2000)	DEC	H <sub>2</sub> Flux ( $10^{-17} \frac{W}{m^2}$ )	Flow	Comment
					
2-1	5 35 11.4	-5 20 53	~ 27	?	Bright triangular knot
					
2-2	5 35 02.3	-5 21 50	~ 8	<b>26</b>	Three compact nearby knots centered at given position
					
2-3			~ 50	<b>26</b>	SE-NW running chain of knots
A	5 35 09.0	-5 22 51	~ 21		Bright bowshaped feature
B	5 35 07.6	-5 22 36	~ 1.8		Compact knot
C	5 35 06.9	-5 22 23	~ 6		Compact knot
D	5 35 10.0	-5 23 07	~ 15		Bright extended knot
					
2-4	5 34 59.8	-5 23 32	~ 8	<b>28 (?)</b>	Extended feature
					
2-5			~ 75	<b>27</b>	SE-NW running, short chain of compact knots embedded in fainter ovoidal shaped emission
A	5 35 11.5	-5 23 35			Compact knot
B	5 35 11.6	-5 23 38			Compact knot
C	5 35 11.8	-5 23 43	~ 11		Compact knot
					
2-6			~ 80	<b>28</b>	E-W oriented group of features; probably more H <sub>2</sub> emission further west
A	5 35 10.9	-5 23 46	~ 24		Compact knot
B	5 35 09.6	-5 23 46	~ 54		Compact knot

Feature	RA (J2000)	DEC	H <sub>2</sub> Flux ( $10^{-17} \frac{W}{m^2}$ )	Flow	Comment
					
2-7 A	5 35 10.9	-5 23 46	~ 2.7 ~ 1.7	29	SE-NW oriented group of diffuse features Compact knot
					
2-8	5 35 18.5	-5 31 25	~ 0.6	30	Faint double knot
					
2-9	5 35 17.1	-5 32 02	~ 1.1	30	Single compact knot

### A.3 Field 3

#### H<sub>2</sub> features: Overview

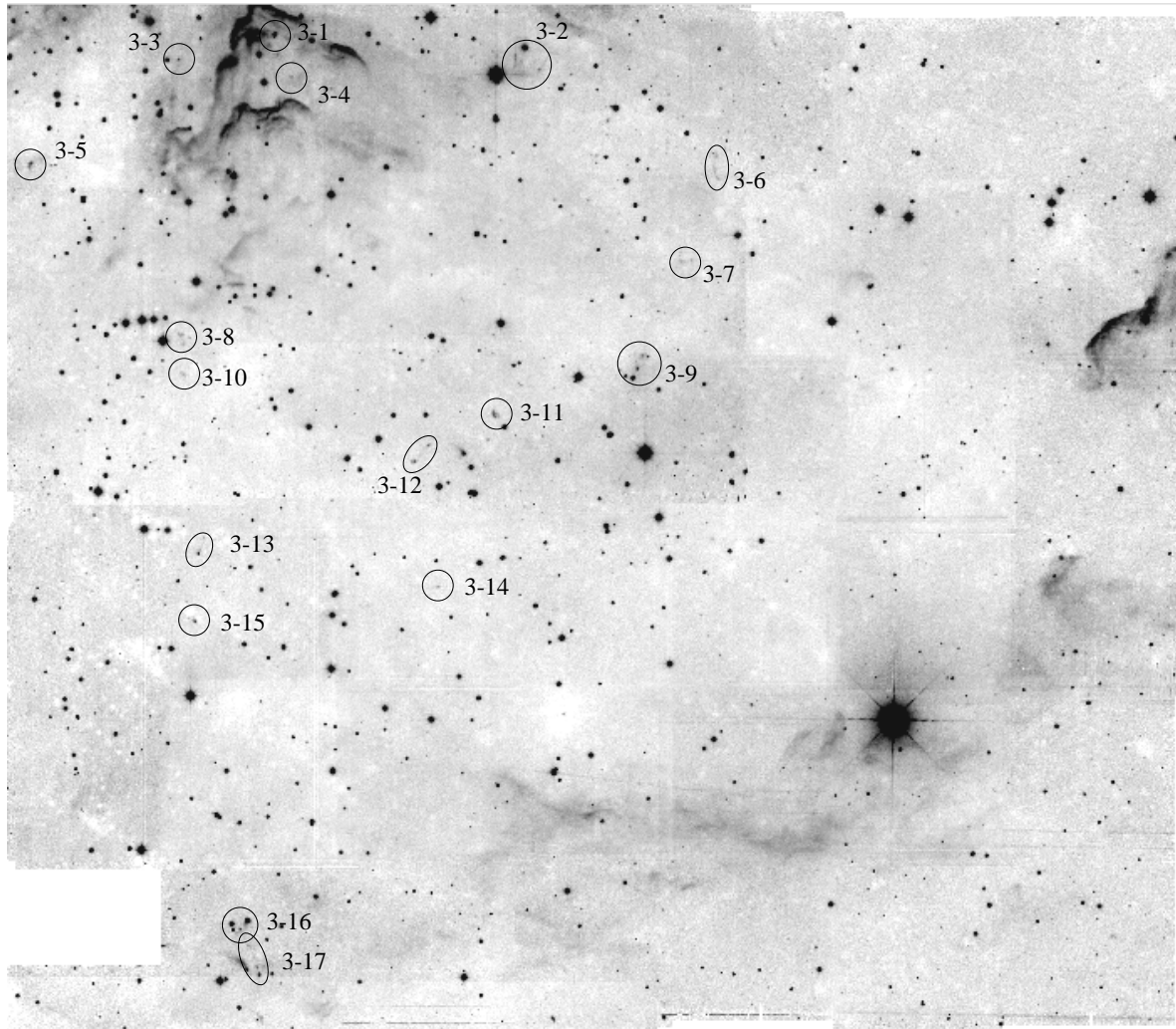
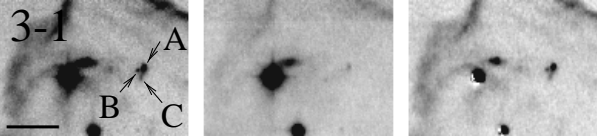
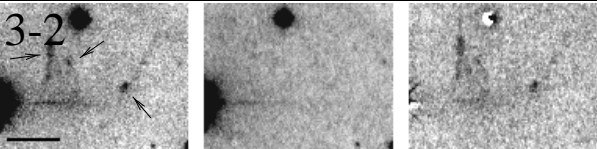

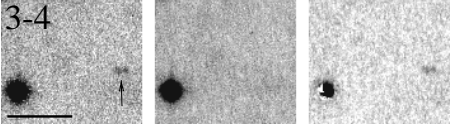



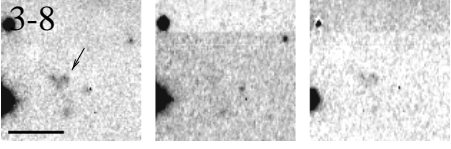
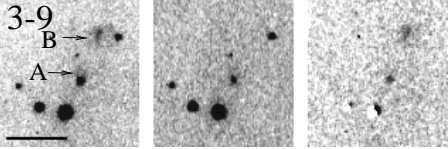
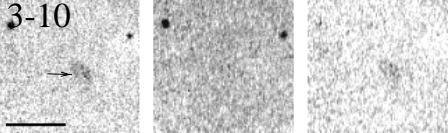
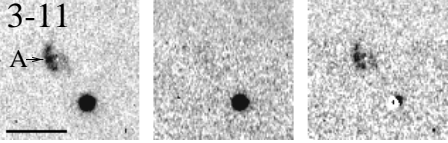
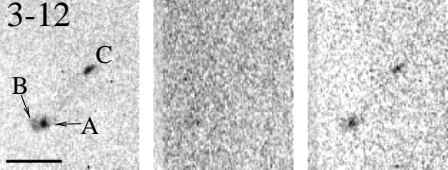
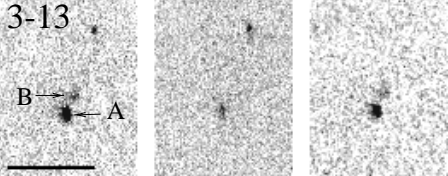
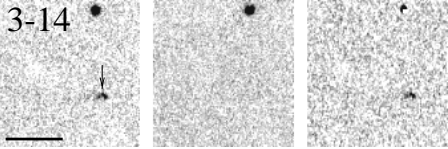



Figure 50: H<sub>2</sub> features in Field 3 (the area south of the Orion Nebula)

H<sub>2</sub> features: Details

Feature	RA (J2000)	DEC	H <sub>2</sub> Flux ( $10^{-17} \frac{W}{m^2}$ )	Flow	Comment
					
3-1	5 35 04.3	-5 33 30	4.2	?	Small V-shaped feature (small bow shock?); position refers to tip of "V" (knot A)
					
3-2	5 34 17.3	-5 36 01	~12	<b>29</b>	Group of knotty filaments centered at given position
					
3-3	5 35 12.0	-5 34 03	0.6	?	Single knot
					
3-4	5 35 03.0	-5 34 21	0.4	?	Two small faint adjacent knots
					
3-5	5 35 23.6	-5 36 09	2.3	?	Diffuse double knot
					
3-6	5 34 29.3	-5 36 00	~ 1.5	<b>31 (?)</b>	Bow shaped filament, extends over ~ 30''N-S
					
3-7	5 34 31.4	-5 37 51	~ 1	<b>31 (?)</b>	2 faint compact knots, some diffuse emission
					
3-8	5 35 11.4	-5 39 27	~ 1	<b>32 (?)</b>	Small group of faint diffuse knots



Feature	RA (J2000)	DEC	H <sub>2</sub> Flux ( $10^{-17} \frac{W}{m^2}$ )	Flow	Comment
					
3-9			~ 2	<b>31</b>	2 faint compact knots, possibly more diffuse H <sub>2</sub> emission further SE
A	5 34 35.3	-5 39 59	0.5		Compact knot, associated with continuum source
B	5 34 34.9	-5 39 44	1.5		Diffuse patch
					
3-10	5 35 11.2	-5 40 14	~ 0.7	32 (?)	Faint diffuse patch
					
3-11	5 34 46.5	-5 40 54	2.7	?	3 knots embedded in diffuse emission
					
3-12			~ 2.5	<b>33</b>	3 knots; knot A and knot C connected by very faint bridge of emission
A	5 34 52.8	-5 41 52	1.2		Compact knot
C	5 34 51.7	-5 41 33	0.7		Elongated knot
					
3-13	5 35 09.7	-5 43 45	1.5	34 (?)	1 bright knot (A), 1 faint knot (B), possibly some more emission NW of knot B; position refers to knot A
					
3-14	5 34 50.6	-5 44 20	0.6	35 (??)	2 small nearby faint knots
					
3-15			~ 1.8	<b>36</b>	3 nearby knots
A	5 35 09.9	-5 45 04	1.2		Extended knot
C	5 35 10.4	-5 45 00	0.3		Faint compact knot

Feature	RA (J2000)	DEC	H <sub>2</sub> Flux ( $10^{-17} \frac{W}{m^2}$ )	Flow	Comment
3-16			~ 12.6	<b>37</b>	Bright bow and faint knot
A	5 35 05.4	-5 50 57	12.4	<b>37</b>	Bright bowshaped feature, apex heading NNW
B	5 35 06.2	-5 51 11	0.2	?	Faint knot
3-17			~ 4	<b>37</b>	3 knots in line
A	5 35 04.4	-5 52 00	2.4		Bright compact knot
B	5 35 04.6	-5 51 51	0.7		Faint ~ N-S elongated feature
C	5 35 05.3	-5 51 26	0.7		Faint compact knot

### A.4 Field 4

#### H<sub>2</sub> features: Overview

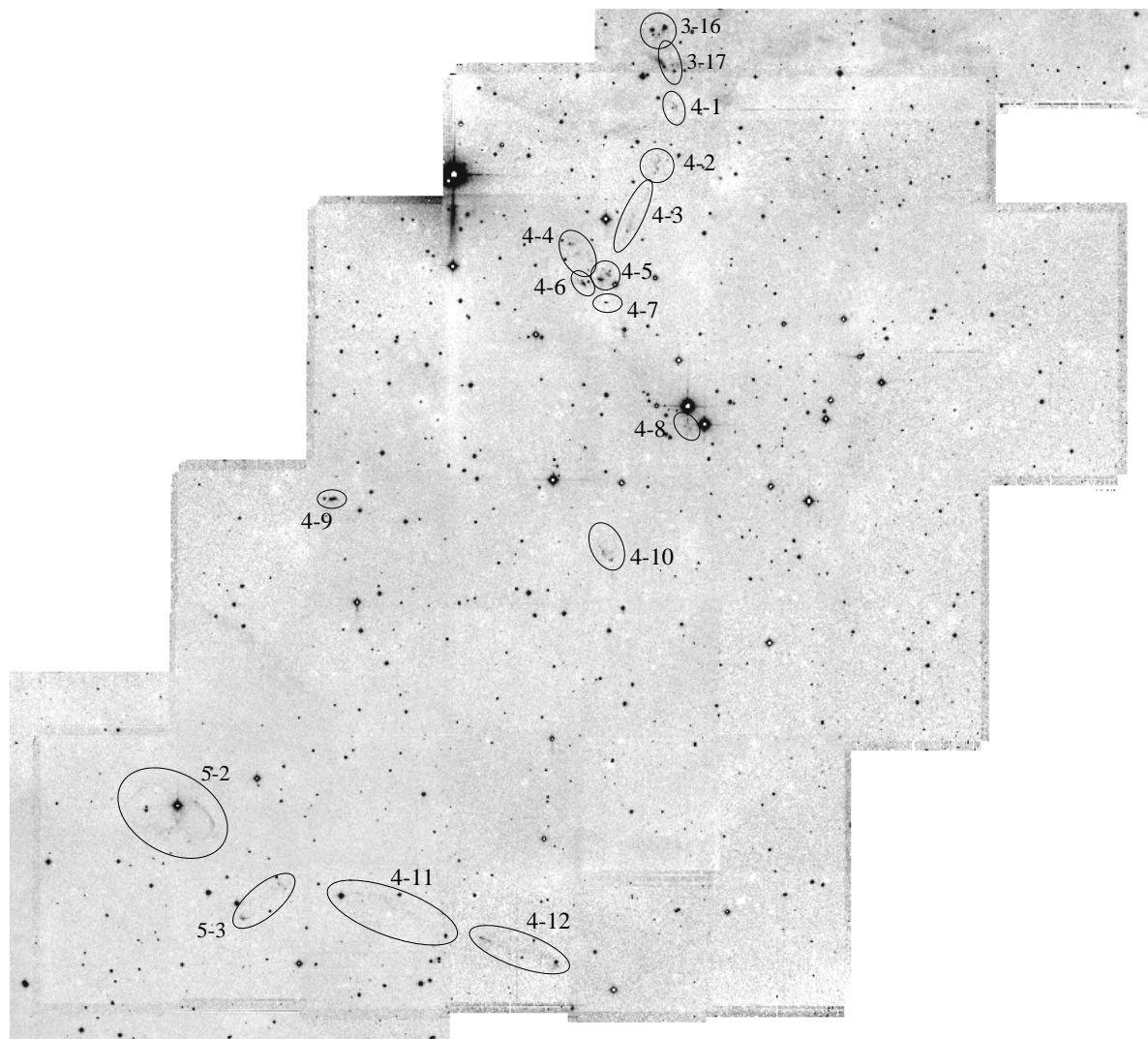
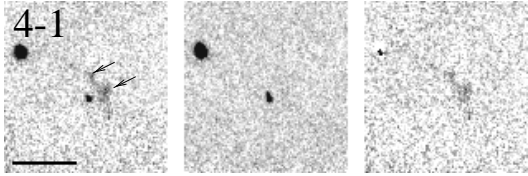
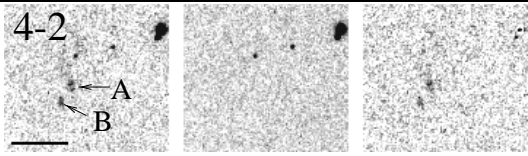
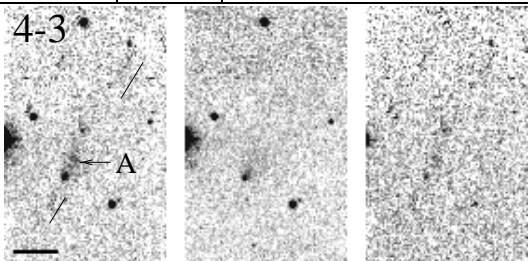
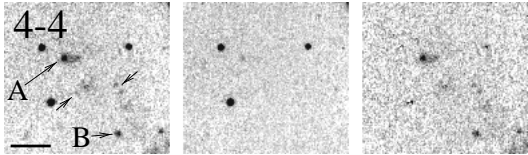
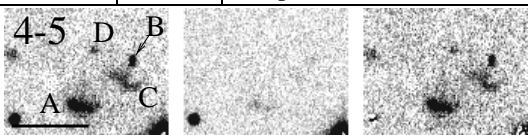
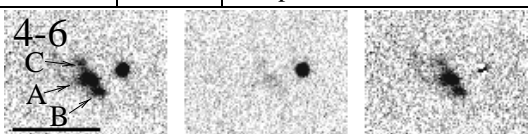

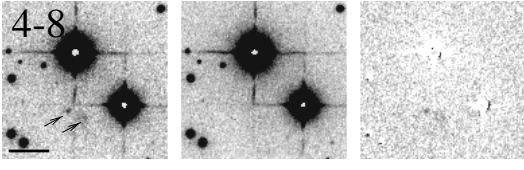
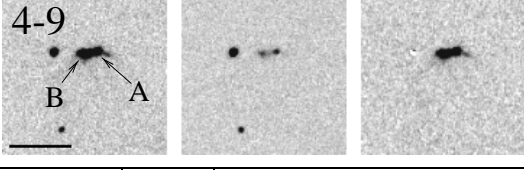
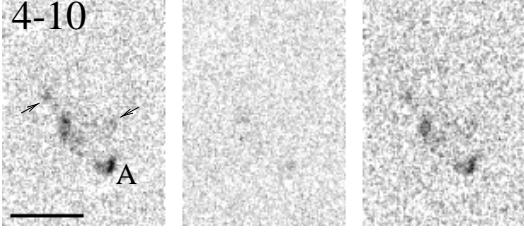
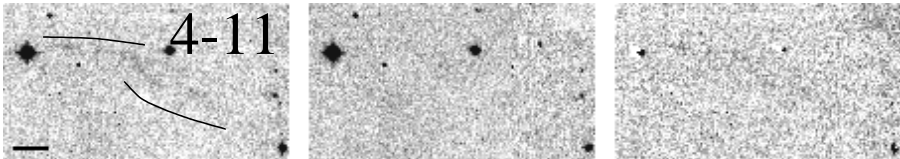
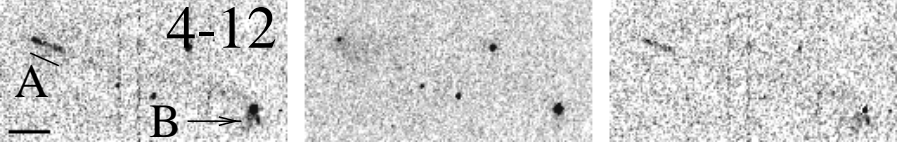


Figure 51: H<sub>2</sub> features in Field 4

H<sub>2</sub> features: Details

Feature	RA (J2000)	DEC	H <sub>2</sub> Flux ( $10^{-17} \frac{W}{m^2}$ )	Flow	Comment
					
4-1	5 35 04.2	-5 52 50	~0.8	38 (?)	faint extended feature
					
4-2			0.9	38	2 faint compact knots
A	5 35 05.9	-5 54 22	0.4		
B	5 35 06.1	-5 54 27	0.5		
					
4-3			~ 2	38	Very faint linear feature, length 100'', PA 155°
A	5 35 08.5	-5 55 45	0.5		
					
4-4			~4.5	? (39 ?)	2 compact knots & some fainter features
A	5 35 14.4	-5 56 13	2.0		Knot with tail pointing W
B	5 35 12.5	-5 56 51	0.8		Compact knot
					
4-5			8.9	38 (39 ?)	Group of knots
A	5 35 11.4	-5 57 04	4.4		~ E-W elongated knot
B	5 35 10.4	-5 56 52	0.6		Compact knot
					
4-6	5 35 13.0	-5 57 11	3.8	? (39 ?)	Three compact nearby knots; position refers to knot A

Feature	RA (J2000)	DEC	H <sub>2</sub> Flux ( $10^{-17} \frac{W}{m^2}$ )	Flow	Comment
					
4-7	5 35 10.7	-5 57 37	1.6	? (39 ?)	Compact E-W elongated knot
					
4-8	5 35 02.4	-6 00 38	0.7	? (39 ?)	2 faint knots; position refers to middle between knots
					
4-9	5 35 37.0	-6 02 29	10.7	? (40 ?)	2 bright nearby knots on E-W oriented filament
					
4-10	5 35 09.7	-6 03 53	~ 4.5	? (41 ?)	Group of extended knots; bow shock like morphology (?); position refers to knot A
					
4-11	5 35 31.0	-6 12 20	~ 1	42	2 very faint filaments centered roughly at given position; flux measurement very uncertain
					
4-12			~ 3	42	Linear feature, some more diffuse emission
A	5 35 21.5	-6 13 10	1.4		Linear feature, length 16'', PA 70°; position gives middle of feature
B	5 35 14.6	-6 13 46	1.4		Diffuse feature

## A.5 Field 5

### H<sub>2</sub> features: Overview

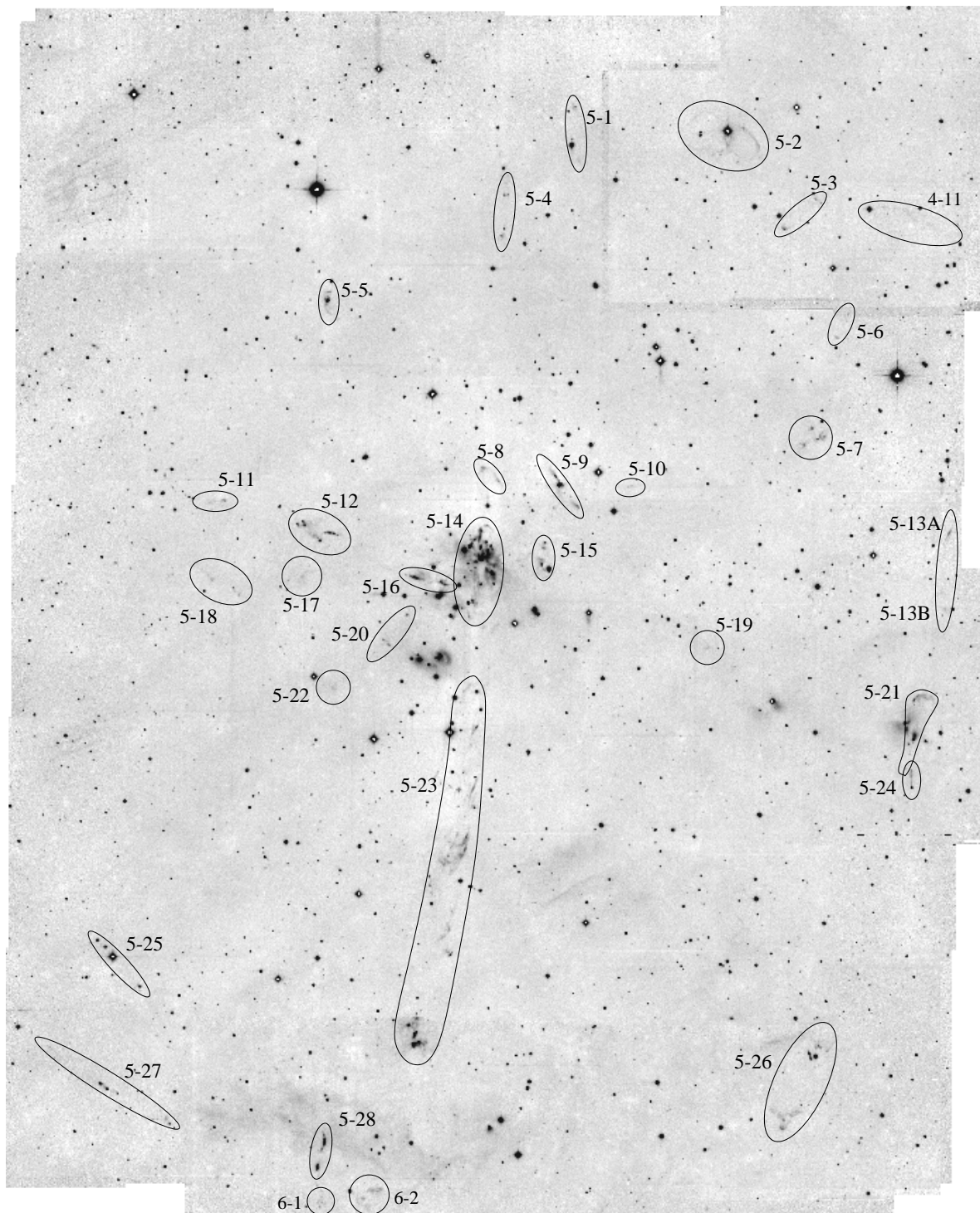


Figure 52: H<sub>2</sub> features in Field 5 (the area around the L1641-N cluster)

H<sub>2</sub> features: Details

Feature	RA (J2000)	DEC (J2000)	H <sub>2</sub> Flux ( $10^{-17} \frac{W}{m^2}$ )	Flow	Comment
5-1			~1.0	(49 ?)	2 faint patches; HH 306
A	5 36 09.2	-6 09 27	~0.5		
B	5 36 08.7	-6 10 56	~0.5		
5-2	5 35 51.8	-6 10 00	~4	43	Bipolar filamentary lobe structures around V 1296 Ori
5-3			~2.9	44	2 compact knots & 1 bowshaped feature
A	5 35 41.9	-6 11 52	0.6		compact elongated knot
B	5 35 41.2	-6 12 00	0.4		compact knot
C	5 35 45.2	-6 12 44	1.9		bowshaped feature
5-4			~2	45/49 (?)	3 compact knots & some extended emission in N-S group
A	5 36 17.0	-6 11 54	0.6		compact knot
B	5 36 16.6	-6 11 53	0.4		compact knot
C	5 36 17.1	-6 13 03	0.9		extended knot & extended emission


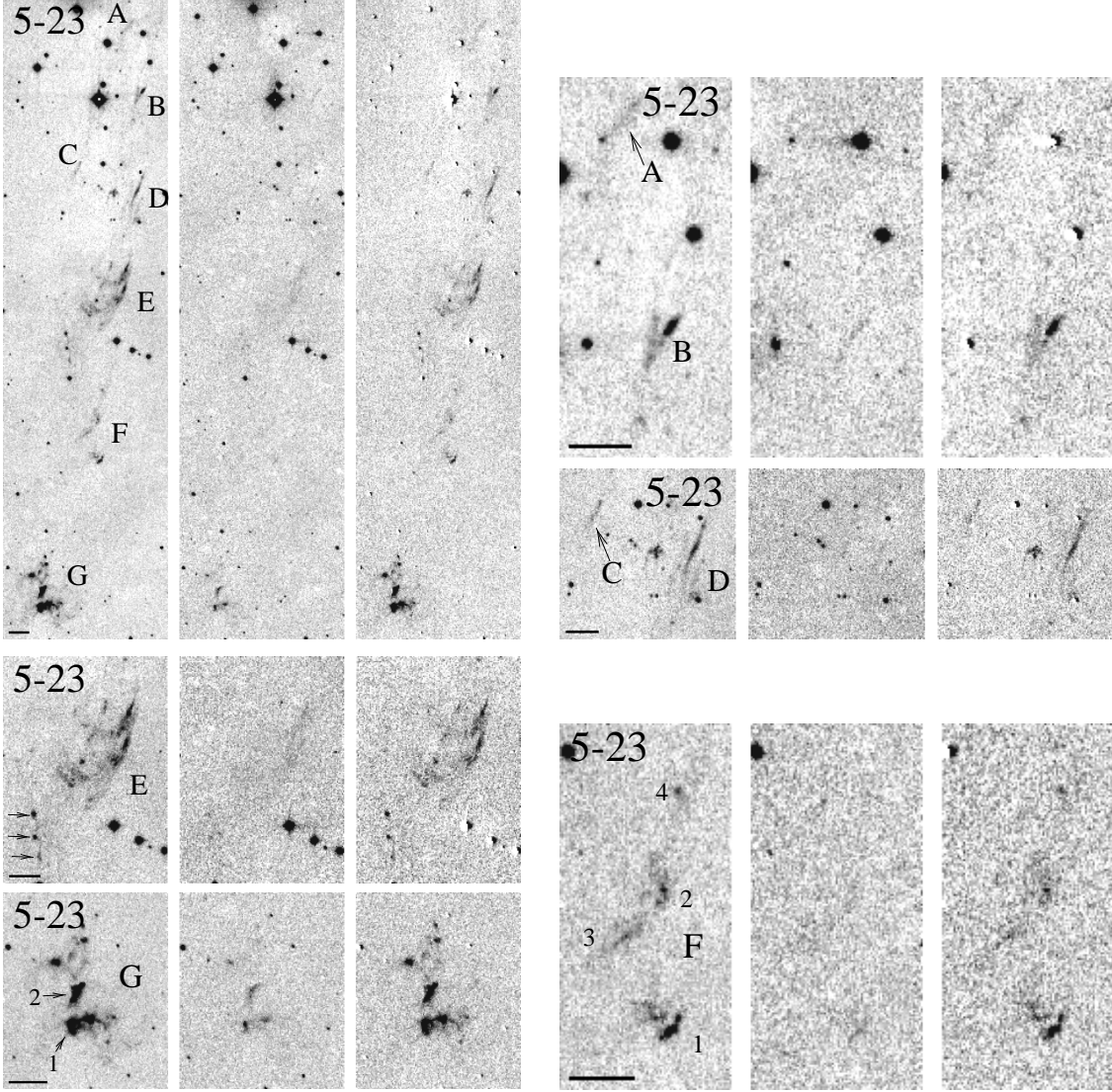
Feature	RA (J2000)	DEC	H <sub>2</sub> Flux (10 <sup>-17</sup> $\frac{W}{m^2}$ )	Flow	Comment
5-5			~2	<b>46</b>	3 E-W elongated knots N and S of bipolar reflection nebula; HH 304
A	5 36 36.7	-6 14 43	1.1		E-W elongated knot
B	5 36 36.7	-6 14 52	0.3		compact knot
C	5 36 36.6	-6 15 19	0.5		diffuse feature
5-6			~1.2	<b>47</b>	2 compact knots & bowshaped feature in NW-SE group
A	5 35 39.2	-6 15 44	0.8		bowshaped feature
B	5 35 37.9	-6 15 05	0.4		2 compact knots, some more fainter emission
5-7			~6.5	52 (?)	3 diffuse extended features
A	5 35 40.4	-6 18 32	3.0		
B	5 35 41.7	-6 18 18	1.8		
C	5 35 42.6	-6 18 47	1.6		
5-8			~2.2	<b>49</b>	Diffuse feature N of L 1641-N cluster; HH 303
A	5 36 18.9	-6 19 36	1.7		Extended triangular feature
B	5 36 17.1	-6 19 55	1.4		NE-SW oriented filament

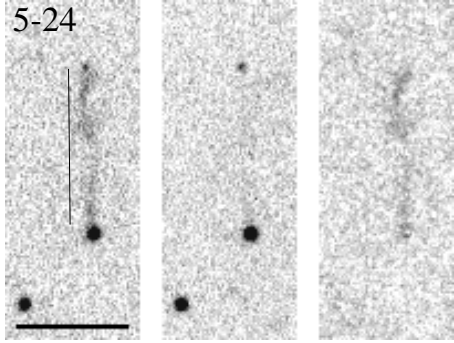
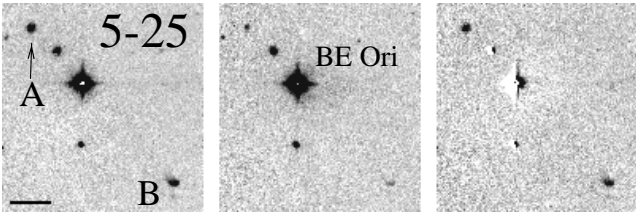
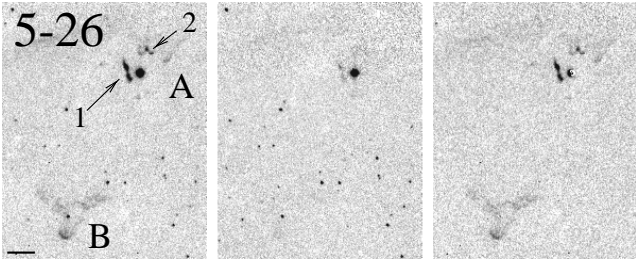
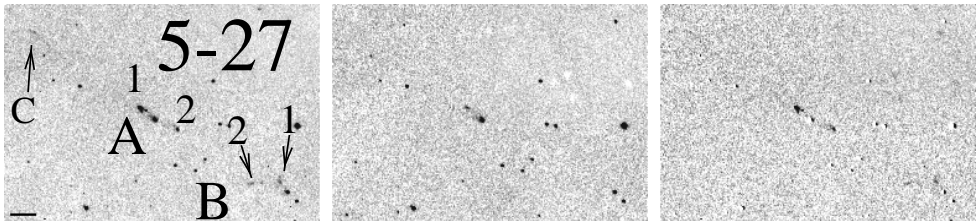


Feature	RA (J2000)	DEC	H <sub>2</sub> Flux ( $10^{-17} \frac{W}{m^2}$ )	Flow	Comment
5-9			~5.3	<b>48</b>	NE-SW oriented filamentary structure at PA 37°, length 84"; HH 299
A	5 36 10.7	-6 19 46	3.3		filamentary knot
B	5 36 08.1	-6 20 36	1.7		cometary knot
5-10	5 36 02.1	-6 20 01	~0.3	52 (?)	Single faint E-W elongated knot
5-11	5 36 48.1	-6 20 36	~2.2	<b>51</b>	Diffuse faint patch; HH 302
5-12			~20	<b>51</b>	Group of bright knots, filaments and diffuse extended emission; HH 301
A	5 36 39.0	-6 21 16	1.6		Slightly extended knot
B	5 36 39.2	-6 21 10	1.3		Compact knot
C	5 36 39.8	-6 21 15	1.3		2 small knots
D	5 36 37.2	-6 21 42	2.2		Bright resolved compact knot
E	5 36 35.9	-6 21 29	4.4		knotty filament at PA 80°, length 27"
5-13			~2.7	<b>55</b>	Group of faint features
A	5 35 26.1	-6 21 10	1.8		Filament at PA -31°, length 21"; not on continuum image, but known Herbig-Haro object HH 85E
B	5 35 26.4	-6 23 20	0.6		Faint diffuse feature; HH 126

Feature	RA (J2000)	DEC	H <sub>2</sub> Flux (10 <sup>-17</sup> $\frac{W}{m^2}$ )	Flow	Comment
5-14	5 36 19.3	-6 22 06	~48	<b>49/53</b>	Rich group of knots and filaments around L 1641-N cluster centered roughly on given position.
A1	5 36 20.3	-6 21 46	7.7	<b>53</b>	Bright bow shaped knot
A2/3	5 36 20.1	-6 21 41	1.7	<b>49</b>	2 small knots
B	5 36 19.1	-6 21 48	3.5	<b>49</b>	N-S elongated knot
C	5 36 19.0	-6 22 08	6.6	<b>53</b>	2 bright knots
D	5 36 18.2	-6 21 56	2.4	<b>49</b>	3 knots in ~ N-S row
E	5 36 17.9	-6 21 46	2.5	<b>49</b>	E1: three nearby small knots, E2: fainter knot
F	5 36 18.5	-6 21 39	1.7	<b>49</b>	Three nearby small knots
G	5 36 19.1	-6 21 25	6.6	<b>49</b>	N-S elongated jetlike feature
5-15			~6.7	<b>50</b>	~5 knots & extended emission in N-S group
A	5 36 11.8	-6 21 38	1.1		compact knot
B	5 36 11.9	-6 21 48	1.1		E-W elongated feature
C	5 36 12.1	-6 22 15	2.2		compact N-S elongated knot
5-16			~15	<b>51</b>	~E-W oriented H <sub>2</sub> features associated with some continuum nebulosity
A	5 36 26.5	-6 22 41	9.6		E-W filament
B	5 36 23.2	-6 22 50	5.0		group of knots & filament

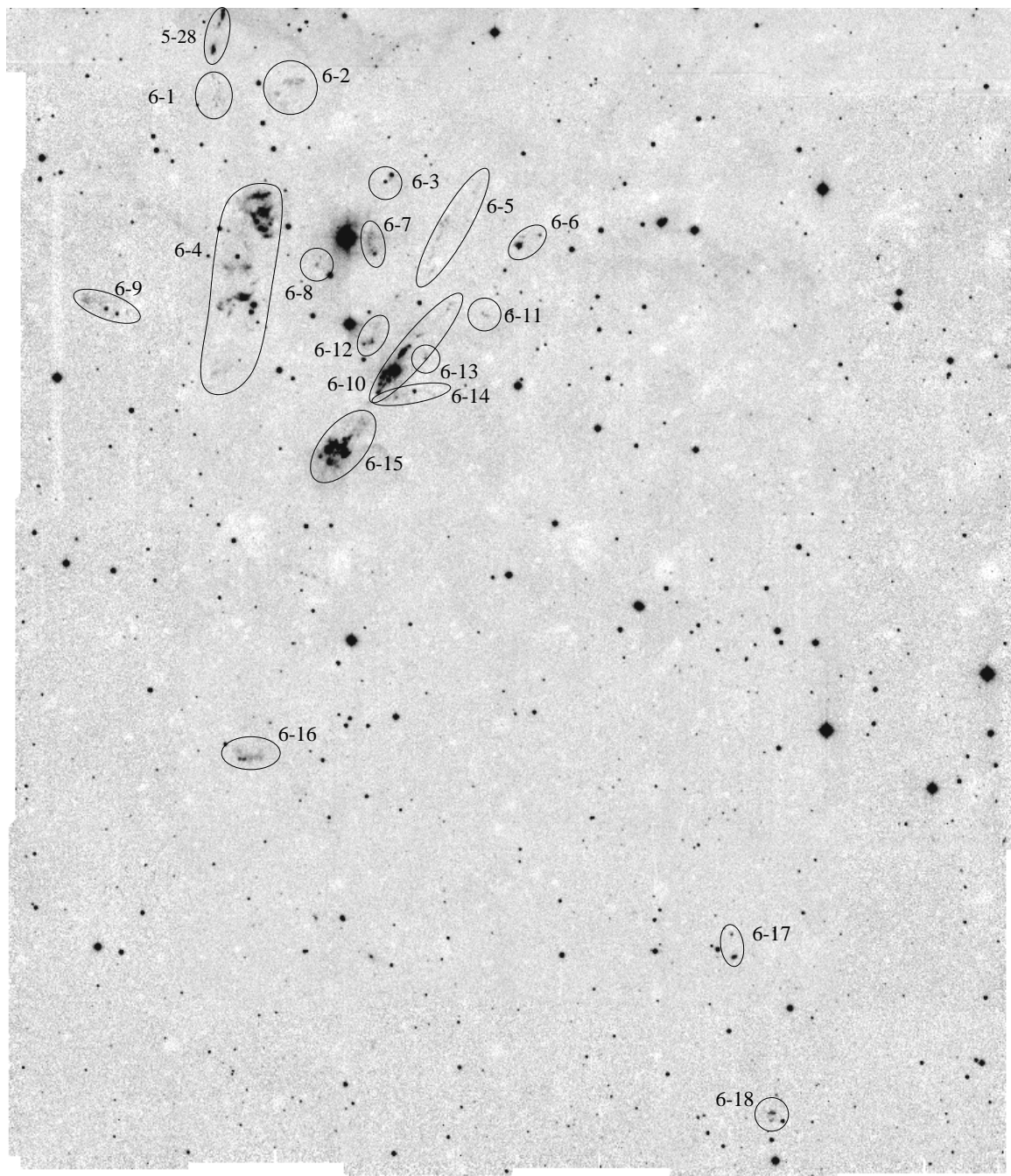
Feature	RA (J2000)	DEC	H <sub>2</sub> Flux (10 <sup>-17</sup> $\frac{W}{m^2}$ )	Flow	Comment
5-17	5 36 39.1	-6 22 44	~1.2	52 (?)	Diffuse faint patch; HH 298E
5-18			~1.5	52 (?)	3 diffuse faint patches
A	5 36 49.4	-6 22 52	0.8		
B	5 36 46.2	-6 23 16	0.5		
C	5 36 46.7	-6 23 08	0.2		
5-19	5 35 53.2	-6 24 31	~0.6	? (51/48?)	Diffuse faint patch
5-20			~2.5	54	3 compact knots & diffuse faint emission form group extending in a NW-SE direction
A	5 36 27.2	-6 23 44	0.9		extended knot
B	5 36 29.8	-6 24 26	0.6		compact knot
C	5 36 29.3	-6 24 35	0.8		double knot
D	5 36 30.9	-6 24 48	0.2		faint knot
5-21			~7	55	Group of features around HH 34 IRS
A	5 35 28.7	-6 25 47	6.5		large bow N of HH 34 IRS
B	5 35 30.0	-6 27 12	~0.4		Faint string of knots (HH 34 jet)
C	5 35 29.4	-6 26 35	~0.1		Very faint short string (HH 34 counterjet)

Feature	RA (J2000)	DEC	H <sub>2</sub> Flux ( $10^{-17} \frac{W}{m^2}$ )	Flow	Comment
			5-22		
5-22	5 36 35.3	-6 25 49	0.7	54	Faint diffuse patch, possibly bowllike morphology
5-23					
5-23			~100	49	Large group of knots/filaments extending N-S over 10/5
A	5 36 20.2	-6 25 45	0.7		Faint diffuse filament
B	5 36 19.4	-6 26 53	4.1		V-shaped filamentary structure
C	5 36 23.6	-6 28 12	1.1		Faint filament
D	5 36 21.0	-6 28 39	8.2		Cross-like group of knots; filament
E	5 36 21.6	-6 30 22	25		Large group of filamentary structures; compact knots further SE
F	5 36 21.7	-6 33 14	6.5		Diffuse group of filamentary knots; position refers to F1
G	5 36 25.1	-6 35 43	53		Group of bright extended knots

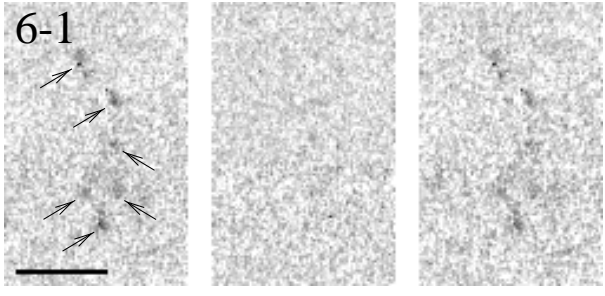
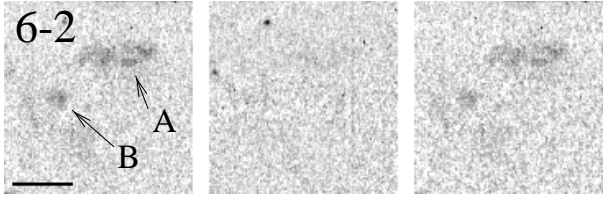
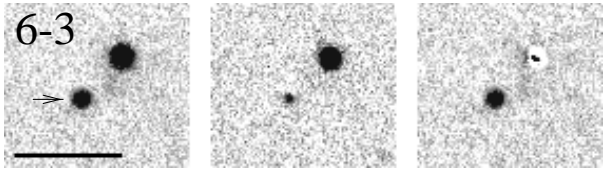
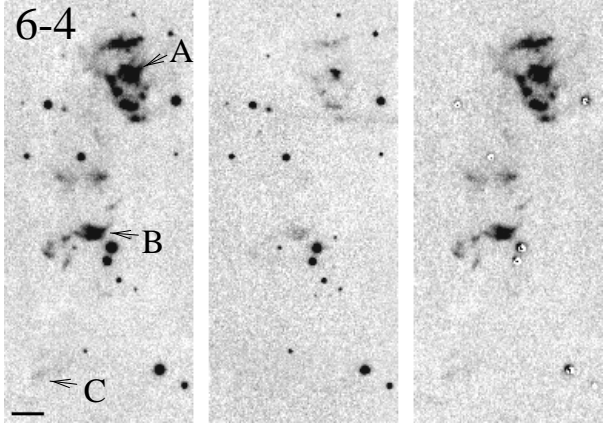
Feature	RA (J2000)	DEC	H <sub>2</sub> Flux ( $10^{-17} \frac{W}{m^2}$ )	Flow	Comment
					
5-24	5 35 29.9	-6 28 04	2.4	56	N-S elongated linear feature at PA 1.5°, length 30''
					
5-25			5.2	57	2 bright compact knots NE and SW of BE Ori, possibly faint H <sub>2</sub> emission further SW; HH 292
A	5 37 01.7	-6 33 00	2.8		Compact knot
B	5 36 56.8	-6 34 17	2.4		Comma-shaped cometary knot
					
5-26			20	55	2 groups of knots and filaments
A	5 35 40.6	-6 35 52	10		Compact knots; HH 87
B	5 35 43.8	-6 37 53	9.5		Faint bow & large diffuse faint wake; HH 88
					
5-27			~7	58	Group of knots bipolar around nebulous star
A1	5 37 01.2	-6 37 00	2.9		Bow NE of star
A2	5 36 59.1	-6 37 17	1.2		Bright knot SW of star
B	5 36 54.3	-6 37 59	1.8		Group of faint knots further SW of star
C	5 37 06.9	-6 36 03	1.0		Faint filament further NE of star

Feature	RA (J2000)	DEC	H <sub>2</sub> Flux ( $10^{-17} \frac{W}{m^2}$ )	Flow	Comment
5-28			~ 19	<b>59</b>	2 groups of knots forming N-S oriented feature
A	5 36 35.6	-6 38 33	11.9		Bright knotty N-S oriented filament, length 35''
B	5 36 36.3	-6 39 17	6.8		Bright $\Lambda$ -shaped group of knots

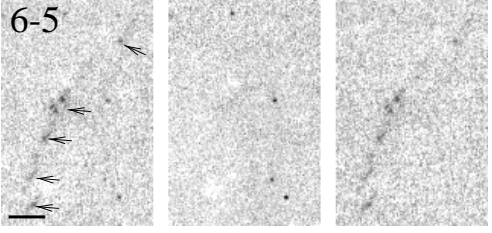
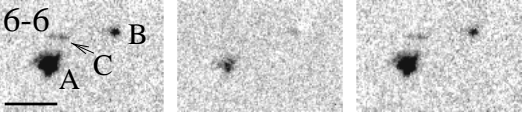
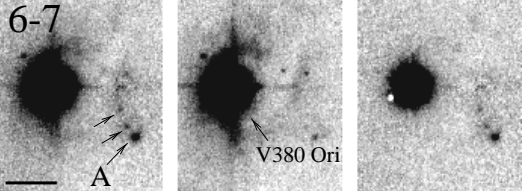
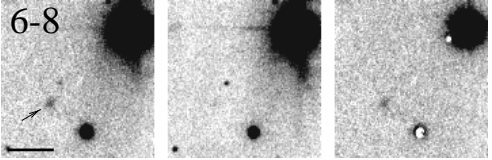
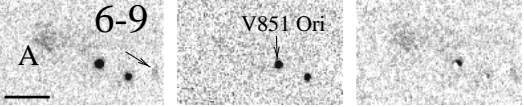
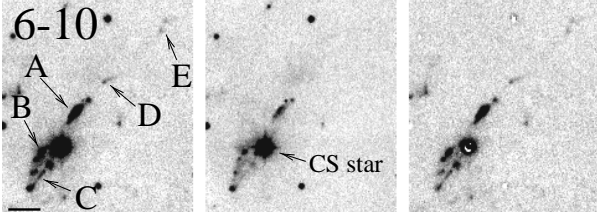
## A.6 Field 6

H<sub>2</sub> features: OverviewFigure 53: H<sub>2</sub> features in Field 6 (the HH 1/2 and V 380 Ori area)

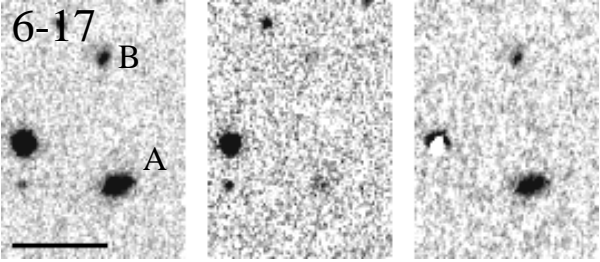
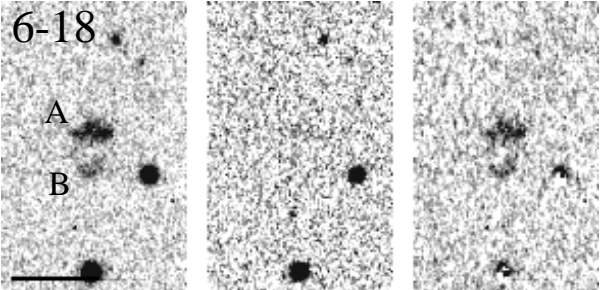
H<sub>2</sub> features: Details

Feature	RA (J2000)	DEC	H <sub>2</sub> Flux ( $10^{-17} \frac{W}{m^2}$ )	Flow	Comment
					
6-1	5 36 36.0	-6 40 07	~ 1.1	59	Group of 6 small faint knots centered at given position
					
6-2			~ 4.5	49	2 large diffuse faint features
A	5 36 29.8	-6 39 51	3.5		
B	5 36 31.1	-6 40 07	1.0		
					
6-3	5 36 22.3	-6 41 50	~ 2.3	60 (?)	Single bright very compact knot; HH 35
					
6-4			~ 150	49	N-S extending group of partly very bright extended knots
A	5 36 32.2	-6 42 30	108		Group of compact bright knots
B	5 36 33.6	-6 44 10	35		Group of filamentary, partly bowshaped knots
C	5 36 35.4	-6 45 40	1.5		faint, diffuse



Feature	RA (J2000)	DEC	H <sub>2</sub> Flux ( $10^{-17} \frac{W}{m^2}$ )	Flow	Comment
					
6-5	5 36 17.2	-6 42 38	~ 3.7	61 (?)	Chain of faint knots centered at given position, PA $-31^\circ$ , length $120''$
					
6-6			~ 10	62 (??)	Group of compact knots; HH 3
A	5 36 11.5	-6 43 04	8.1		Triangular bright feature
B	5 36 09.6	-6 42 51	1.1		Compact knot
C	5 36 11.1	-6 42 53	0.4		E-W elongated filamentary knot
					
6-7	5 36 23.0	-6 43 16	~ 2.6	60 (?)	Chain of faint knots extending NE of knot A, length $17''$ ; position refers to knot A
					
6-8	5 36 27.6	-6 43 31	~ 0.7	?	Single faint small knot
					
6-9	5 36 44.6	-6 44 28	~ 2.8	?	Diffuse faint patch around V 851 Ori; position refers to V 851 Ori; HH 36
					
6-10			~ 35	<b>64</b>	Group of features NW of HH 1/2 VLA1 around the Cohen-Schwartz star (CS star)
A	5 36 20.6	-6 45 14	19	(62 ??)	Bright, NW-SE elongated feature
B	5 36 22.1	-6 45 40	7.7	(62 ??)	NW-SE elongated feature
C	5 36 22.1	-6 45 55	~6		HH 1/2 VLA1 jet
D	5 36 19.3	-6 44 52	1.1	(62 ??)	NW-SE elongated filamentary faint knot
E	5 36 17.0	-6 44 17	0.7	(62 ??)	2 faint knots

Feature	RA (J2000)	DEC	H <sub>2</sub> Flux (10 <sup>-17</sup> $\frac{W}{m^2}$ )	Flow	Comment
6-11					
6-11	5 36 14.1	-6 44 27	~ 1.0	?	2 faint knots
6-12					
6-12			~ 4.6	63	2 extended knots & some diffuse emission; HH 147
A	5 36 23.1	-6 45 01	2.7		Extended feature with compact core
B	5 36 23.8	-6 45 05	1.6		Compact knot
6-13					
6-13	5 36 18.8	-6 45 20	~ 0.8	61	Small faint knot associated with continuum source
6-14					
6-14			~ 2	65	E-W chain of small faint knots, diffuse very faint emission; HH 144
A	5 36 22.0	-6 46 11	0.3		Compact knot
B	5 36 21.1	-6 46 09	0.7		
C	5 36 18.1	-6 46 04	0.2		
6-15					
6-15	5 36 25.2	-6 47 12	125	64	Rich group of bright knots; HH 2; position refers to knot A
6-16					
6-16	5 36 33.1	-6 53 24	13	49	2 bright compact knots at southern rim of an E-W elongated large diffuse feature; position refers to knot A

Feature	RA (J2000)	DEC	H <sub>2</sub> Flux ( $10^{-17} \frac{W}{m^2}$ )	Flow	Comment
<div style="display: flex; justify-content: space-around; align-items: center;"> <div style="text-align: center;"> <p>6-17</p>  </div> </div>					
6-17			4	?	2 compact knots
A	5 35 53.1	-6 57 12	3		
B	5 35 53.3	-6 56 45	1		
<div style="display: flex; justify-content: space-around; align-items: center;"> <div style="text-align: center;"> <p>6-18</p>  </div> </div>					
6-18			3.5	?	2 nearby extended knots; HH 127
A	5 35 49.8	-7 00 17	3		E-W extended feature
B	5 35 49.8	-7 00 26	0.5		

## A.7 Field 7

### H<sub>2</sub> features: Overview

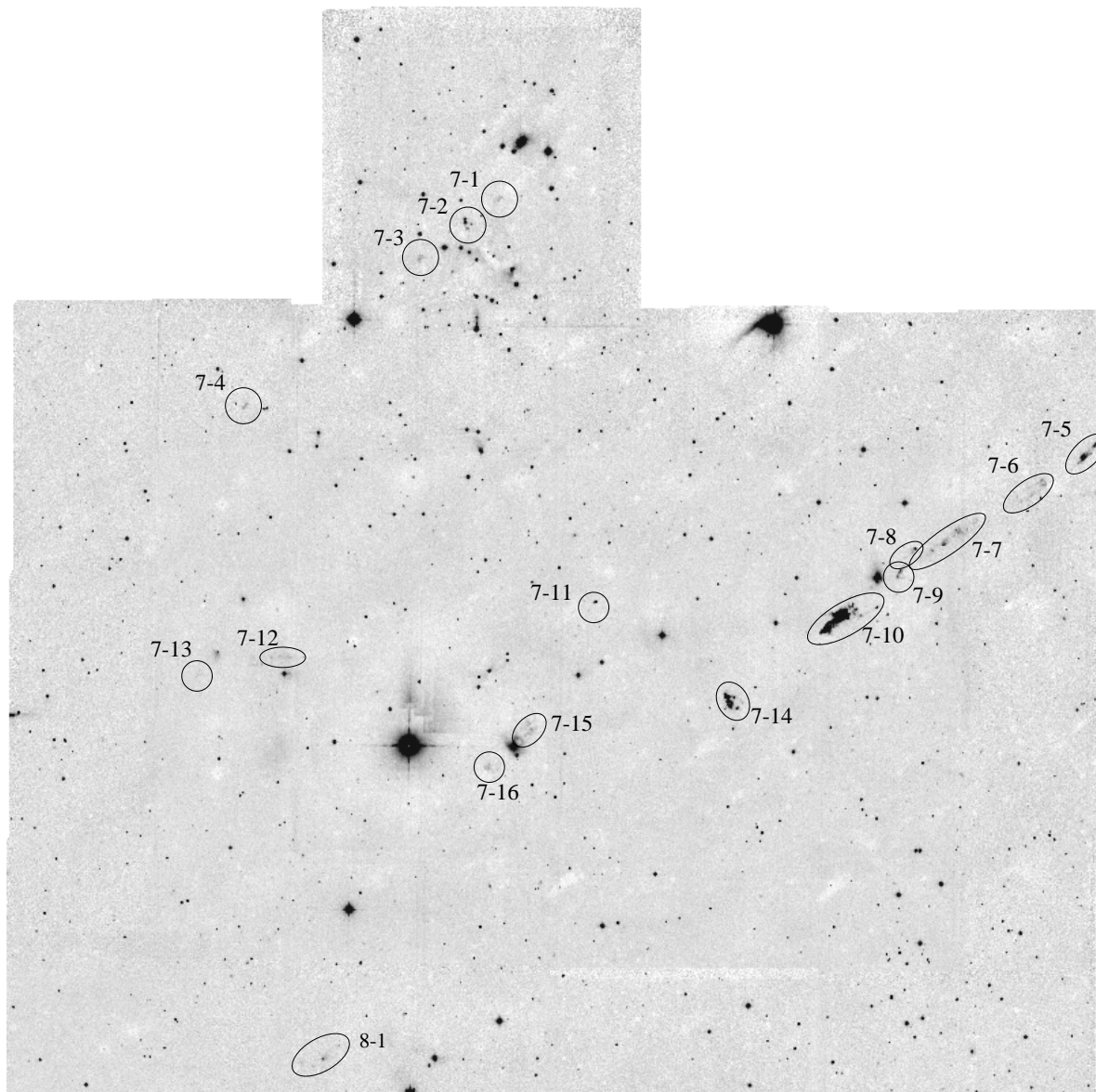


Figure 54: H<sub>2</sub> features in Field 7 (the L1641-C and HH 43 area)

H<sub>2</sub> features: Details

Feature	RA (J2000)	DEC	H <sub>2</sub> Flux ( $10^{-17} \frac{W}{m^2}$ )	Flow	Comment
7-1	5 38 45.1	-6 59 30	~ 0.8	66 (?)	Diffuse patch
7-2					
7-2			~ 1.5	66 (?)	3 compact knots & some diffuse emission
A	5 38 48.2	-7 00 15	0.9		Double knot
B	5 38 47.8	-7 00 07	0.4		Compact knot
7-3					
7-3	5 38 52.7	-7 01 00	~ 1.4	66 (?)	Diffuse patch
7-4					
7-4	5 39 09.6	-7 04 37	~ 1.2	66 (?)	Faint elongated feature
7-5					
7-5			~ 18	<b>67</b>	Large extended feature; HH 64
A	5 37 47.6	-7 05 31	14		
B	5 37 46.4	-7 05 14	3.5		
7-6					
7-6	5 37 51.5	-7 06 10	~ 3.5	<b>67</b>	Extended low surface brightness feature

Feature	RA (J2000)	DEC	H <sub>2</sub> Flux (10 <sup>-17</sup> $\frac{W}{m^2}$ )	Flow	Comment
7-7			~ 8	<b>67</b>	Group of compact knots & some extended emission Bowlike feature
A	5 38 01.1	-7 07 41	3.3		
B	5 37 59.6	-7 07 22	3.3		Group of faint small knots embedded in diffuse emission
C	5 38 02.2	-7 07 50	0.9		2 faint small nearby knots embedded in diffuse emission
7-8	5 38 03.9	-7 07 48	~ 3	<b>68</b>	Small bow pointing to the NW with trailing emission to the SE; position refers to tip of bow (knot A)
7-9	5 38 05.5	-7 08 30	~ 3.8	<b>67</b>	Bow pointing to the SE, northern flank brighter; position refers to tip of bow (knot A); HH 43X
7-10	5 38 10.8	-7 09 25	~ 205	<b>67</b>	Large group of very bright knots; bow shock morphology (pointing to the SE); position refers to brightest knot (knot B2); HH 43
7-11			2.4	?	2 compact knots
A	5 38 34.9	-7 09 12	2.2		E-W elongated knot
B	5 38 35.6	-7 09 25	0.2		Small faint knot

Feature	RA (J2000)	DEC	H <sub>2</sub> Flux ( $10^{-17} \frac{W}{m^2}$ )	Flow	Comment
7-12			1.0	69 (?)	2 faint diffuse features
A	5 39 06.6	-7 10 42	0.4		
B	5 39 04.8	-7 10 41	0.6		
7-13	5 39 13.8	-7 11 10	~0.2	69 (?)	Very faint knot
7-14	5 38 21.6	-7 11 35	36	<b>67</b>	Group of bright knots centered at given position; HH 38
7-15	5 38 41.1	-7 12 20	~4	<b>70</b>	Group of diffuse faint knots NW of HBC 491; position refers to knot A; HH 449
7-16	5 38 45.1	-7 13 16	1.3	<b>70</b>	Faint diffuse extended feature SE of HBC 491

## A.8 Field 8

### H<sub>2</sub> features: Overview

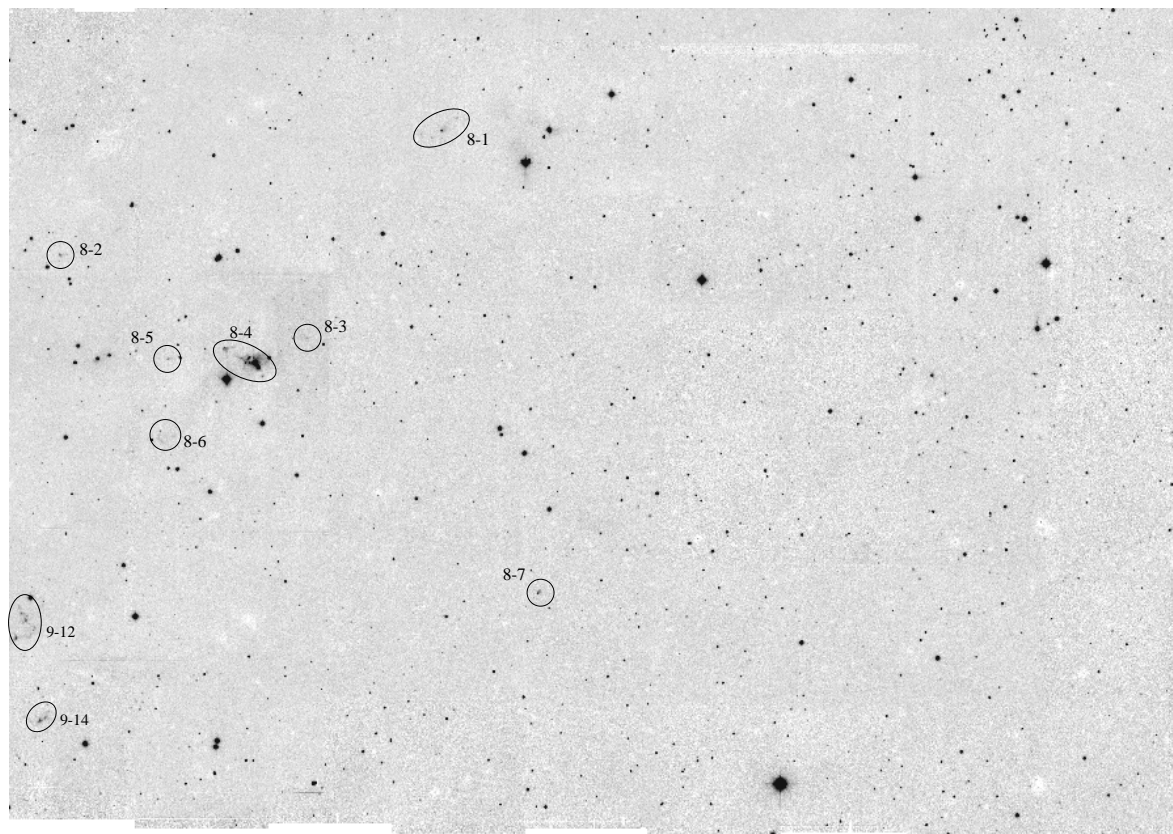
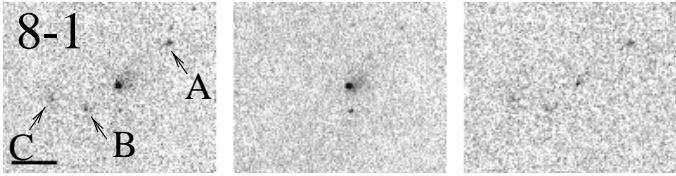
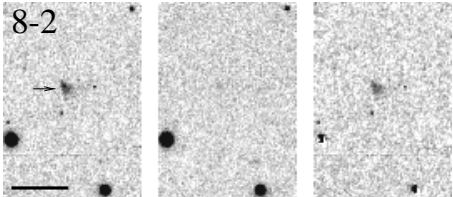
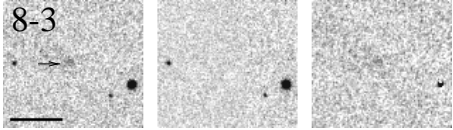
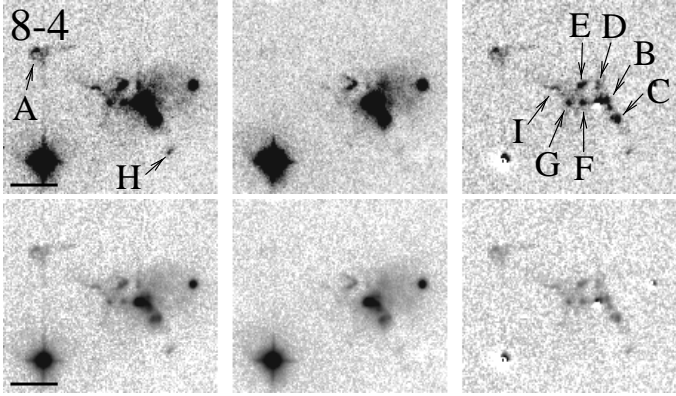
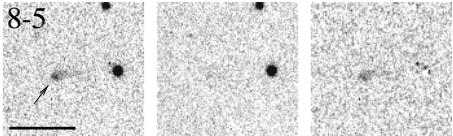
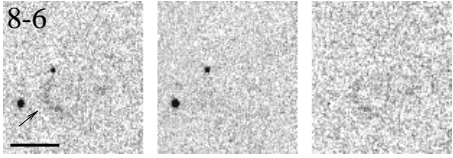
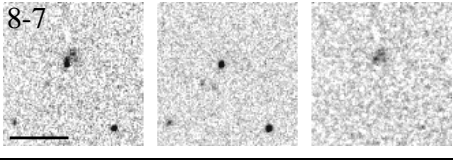


Figure 55: H<sub>2</sub> features in Field 8



H<sub>2</sub> features: Details

Feature	RA (J2000)	DEC	H <sub>2</sub> Flux (10 <sup>-17</sup> $\frac{W}{m^2}$ )	Flow	Comment
					
8-1			~ 1.5	71	3 small faint knots around nebulous continuum source
A	5 38 59.2	-7 20 03	0.4		
B	5 39 01.8	-7 20 33	0.4		
C	5 39 02.8	-7 20 29	0.6		
					
8-2	5 39 39.3	-7 23 40	1.3	? (72 ?)	Single triangular knot
					
8-3	5 39 14.1	-7 25 40	0.5	?	Faint diffuse feature
					
8-4			~ 19	72	Group of knots around Haro 4-255 FIR Bow shock like morphology
A	5 39 22.4	-7 25 59	3		
B	5 39 19.2	-7 26 16	1.6		
G	5 39 20.3	-7 26 19	0.9		Base of jet?
					
8-5	5 39 28.2	-7 26 15	0.4	?	Single knot

Feature	RA (J2000)	DEC	H <sub>2</sub> Flux ( $10^{-17} \frac{W}{m^2}$ )	Flow	Comment
			8-6 		
8-6	5 39 29.1	-7 28 17	~1	73	Diffuse bow, apex at given position; HH 470
			8-7 		
8-7	5 38 50.1	-7 31 57	~0.6	? (72 ?)	Single knot

## A.9 Field 9

### H<sub>2</sub> features: Overview

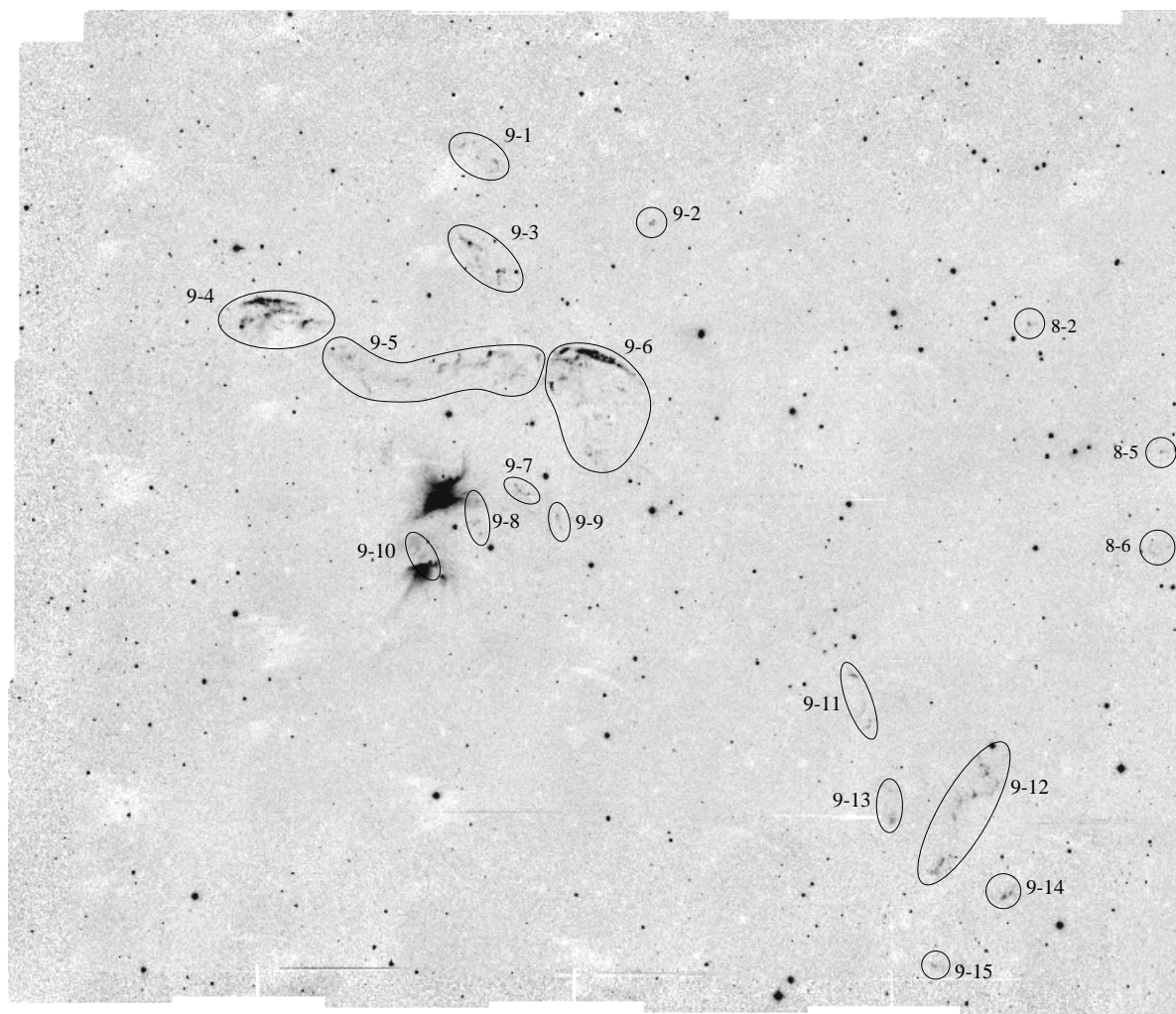
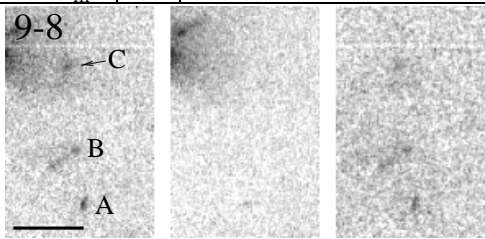
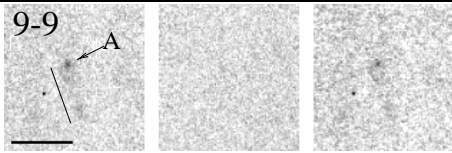
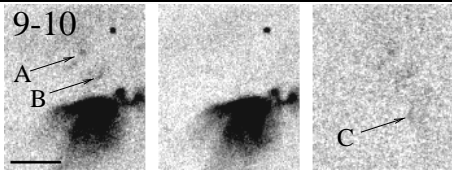
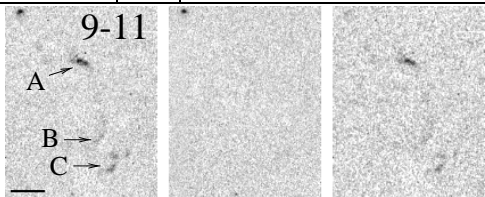
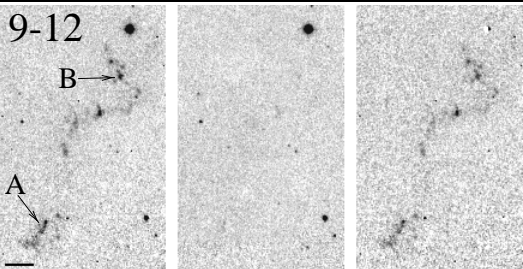


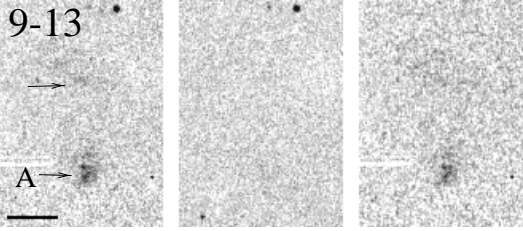
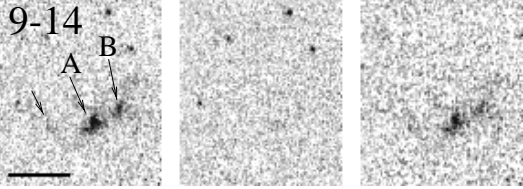

Figure 56: H<sub>2</sub> features in Field 9

H<sub>2</sub> features: Details

Feature	RA (J2000)	DEC	H <sub>2</sub> Flux ( $10^{-17} \frac{W}{m^2}$ )	Flow	Comment
9-1			~ 1.8	<b>74</b>	3 small faint knots around double continuum source
A	5 40 23.7	-7 20 33	1.0		Elongated feature
B	5 40 24.1	-7 20 45	0.2		Very faint
C	5 40 26.4	-7 20 13	0.6		Elongated feature
9-2	5 40 10.7	-7 21 45	1.5	<b>74 ?</b>	Three nearby knots embedded in some faint diffuse emission centered at given position
9-3			~ 9	<b>75/76 ?</b>	Group of knots and filaments
A	5 40 25.8	-7 22 13	3.5		Bright knot
B	5 40 23.4	-7 22 47	1.6		Bright elongated knot
9-4			~ 68	<b>76</b>	Large group of knots and curving filaments
A	5 40 42.9	-7 23 28	29		Bright, E-W oriented, knotty curved filament
B	5 40 41.4	-7 23 41	5.8		Diffuse, E-W oriented, knotty curved filament
C	5 40 39.2	-7 23 53	6.9		Bright elongated knot
D	5 40 44.3	-7 23 54	4.9		Diffuse feature

Feature	RA (J2000)	DEC	H <sub>2</sub> Flux (10 <sup>-17</sup> $\frac{W}{m^2}$ )	Flow	Comment
9-5			~ 20	<b>76</b>	~ E-W oriented chain of diffuse filamentary knots
A	5 40 23.9	-7 24 28	4.3		Bright compact knot
	5 40 37.0	-7 24 24			Eastern end of chain
	5 40 19.9	-7 24 32			Western end of chain
9-6			~ 100	<b>76</b>	Group of bright curved filaments and knots
A	5 40 15.3	-7 24 25	~ 45		Bright curved double filament
B	5 40 17.8	-7 24 24	7.3		Bright elongated feature
C	5 40 18.8	-7 25 07	2.3		Bright elongated feature; HH 65
9-7			3.0	?	3 compact knots connected by faint bowshaped filament
A	5 40 21.3	-7 27 17	0.4		
B	5 40 20.5	-7 27 21	0.5		
C	5 40 21.6	-7 27 10	0.4		

Feature	RA (J2000)	DEC	H <sub>2</sub> Flux ( $10^{-17} \frac{W}{m^2}$ )	Flow	Comment
					
9-8			~ 1.5	?	3 faint knots in N-S oriented group
A	5 40 24.4	-7 28 10	~ 1.1		~ N-S oriented
B	5 40 24.8	-7 27 58	~ 1		NW-SE elongated feature
C	5 40 24.8	-7 27 31	0.4		
					
9-9			~ 0.8	?	Faint filament extending SSW from knot A at PA 19°, length 20''
A	5 40 18.1	-7 27 47	0.5		
					
9-10			~ 1.2	?	3 faint diffuse features close to Re50 reflection nebula
A	5 40 29.5	-7 28 31	~ 0.2		
B	5 40 29.1	-7 28 41	~ 0.6		
C	5 40 28.8	-7 28 55	~ 0.4		
					
9-11			~ 3.1	<b>76</b>	3 filamentary features
A	5 39 53.3	-7 30 57	1.5		
B	5 39 52.5	-7 31 41	~ 0.5		
C	5 39 52.0	-7 31 56	~ 1.1		
					
9-12			~ 20	<b>76</b>	Large system of filamentary knots embedded in diffuse extended emission
A	5 39 45.8	-7 34 44	~ 1.2		
B	5 39 42.3	-7 32 53	~ 1.1		

Feature	RA (J2000)	DEC	H <sub>2</sub> Flux ( $10^{-17} \frac{W}{m^2}$ )	Flow	Comment
			 <p>9-13</p>		
9-13	5 39 49.9	-7 33 54	2.5	76 ?	Diffuse patch
			 <p>9-14</p>		
9-14	A 5 39 40.5 B 5 39 40.0	-7 35 25 -7 35 21	~ 3.6 ~ 2 ~ 1	76	2 diffuse knots
			 <p>9-15</p>		
9-15	5 39 46.3	-7 36 52	1.2	76 ?	Diffuse knot

## B The H<sub>2</sub> flows

In this section a list of outflows identified from the H<sub>2</sub> survey is given.

First, I give for each field an overview, with the candidate outflows regarded as rather certain marked by black solid lines and a number printed in black bold letters, and the candidate flows regarded as uncertain marked with black dashed lines and a number printed in black normal letters. On these maps the H<sub>2</sub> features as listed in Appendix A are also marked as in the overview maps with grey symbols.

The following table is organized as follows: Column 1 assigns a running number to each flow; flows which I regard as rather certain are marked with bold-printed numbers, flows which I regard as uncertain are marked with normal letters. Columns 2 and 3 give a representative flow position (the position of its driving source, if there is one identified, otherwise either a suspected source position, if the morphology of the flow strongly suggests one, or the position of a prominent H<sub>2</sub> feature in the flow, or the approximate geometric centre of the flow). Column 4 contains a list of H<sub>2</sub> features thought to belong to the respective flow, columns 5 and 6 the length of the flow, measuring its angular extend in arcminutes, and its projected length in parsec, assuming a distance of 450 pc to the Orion A cloud. Column 7 gives the position angle of the flow (corrected for the rotation angle of the Omega Prime array on the sky), and column 8 the luminosity  $L_{2.12}$  in the  $v = 1-0\text{S}(1)$  line (no correction for extinction (which is unknown) was applied). The total H<sub>2</sub> luminosity  $L_{\text{H}_2}$ , which accounts for emission in other H<sub>2</sub> lines, may be calculated by multiplying  $L_{2.12}$  by 10, the total energy dissipated in shocks  $L_{\text{shock}}$  by multiplying  $L_{2.12}$  by 100, and the instantaneous energy supply rate of the protostellar driving source  $L_{\text{now}}$  by multiplying  $L_{2.12}$  by 1000. An estimate of the mass accretion rate of the protostar may be obtained as  $\dot{M}_{\text{acc}} \sim 10^{-7} \cdot (L_{2.12}/10^{-4}L_{\odot}) \cdot M_{\odot}\text{yr}^{-1}$  (this assumes a jet velocity of 200 km/s and a mass ejection fraction  $\epsilon$  of 0.3; with  $\epsilon$  of 0.1,  $\dot{M}_{\text{acc}}$  would be 3 times larger). To correct for an extinction of  $A_K = 1$ , this has to be multiplied by 2.5. Column 9 contains the association of the flows with the CS cores found by Tatematsu et al. (1993); this field is left empty, if the flow is outside the area covered by the CS survey or too close to its edge, a dash marks the flows apparently not associated with a CS core, and the flag ON (#26, #27, and #28) marks those flows which are not included in the analysis in Chapter 6, because they are too close to the Orion Nebula. I also give the H<sub>2</sub> luminosity and length of the two prototype H<sub>2</sub> jets HH 212 and HH 211, since they are frequently used for comparison throughout this work.

In addition, a note on flow morphology and other details is given for each flow.

“RN” stands for “reflection nebulosity” in the following.



B.1 Overview maps

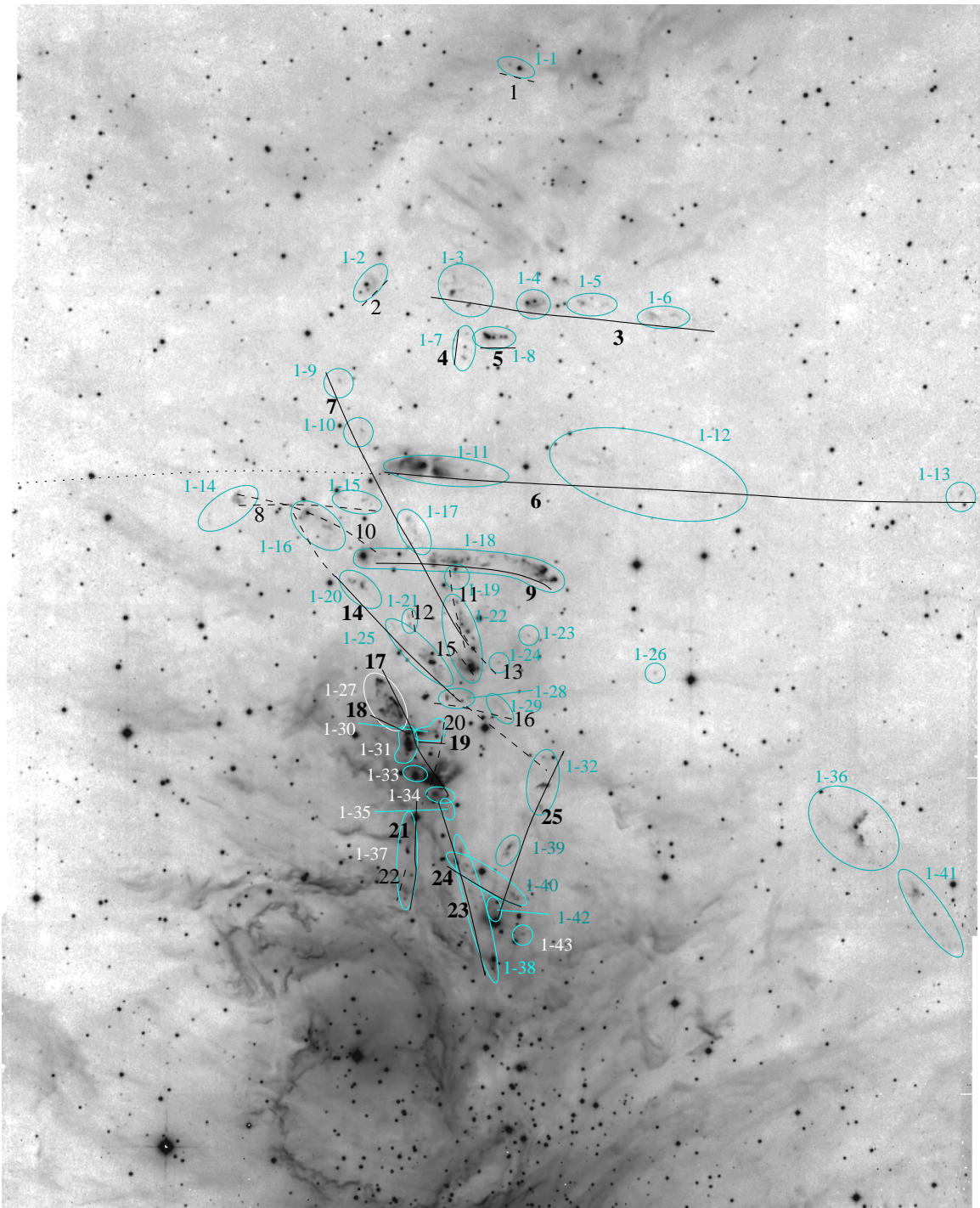
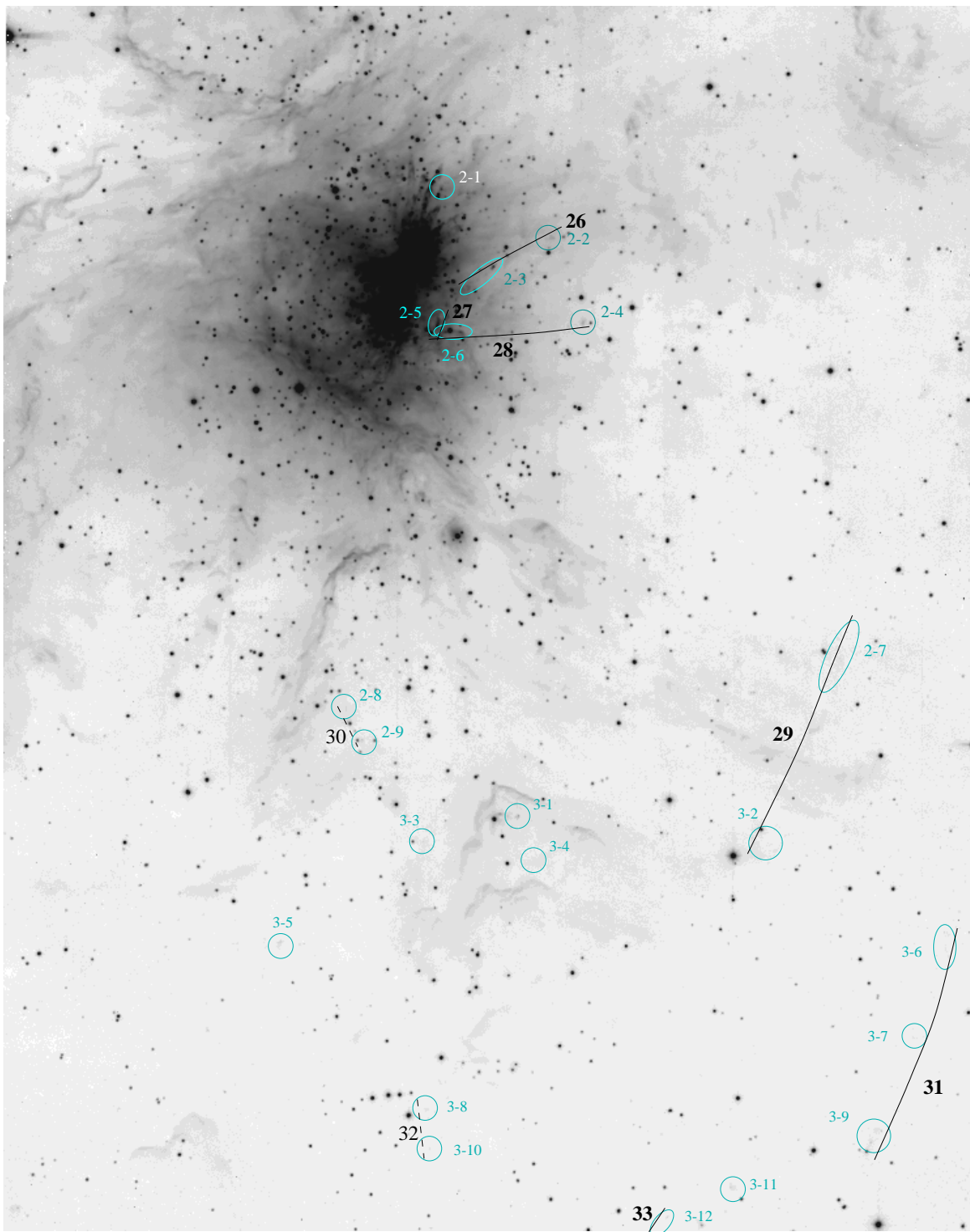


Figure 57: Jets in Field 1 (the OMC-2/3 area)



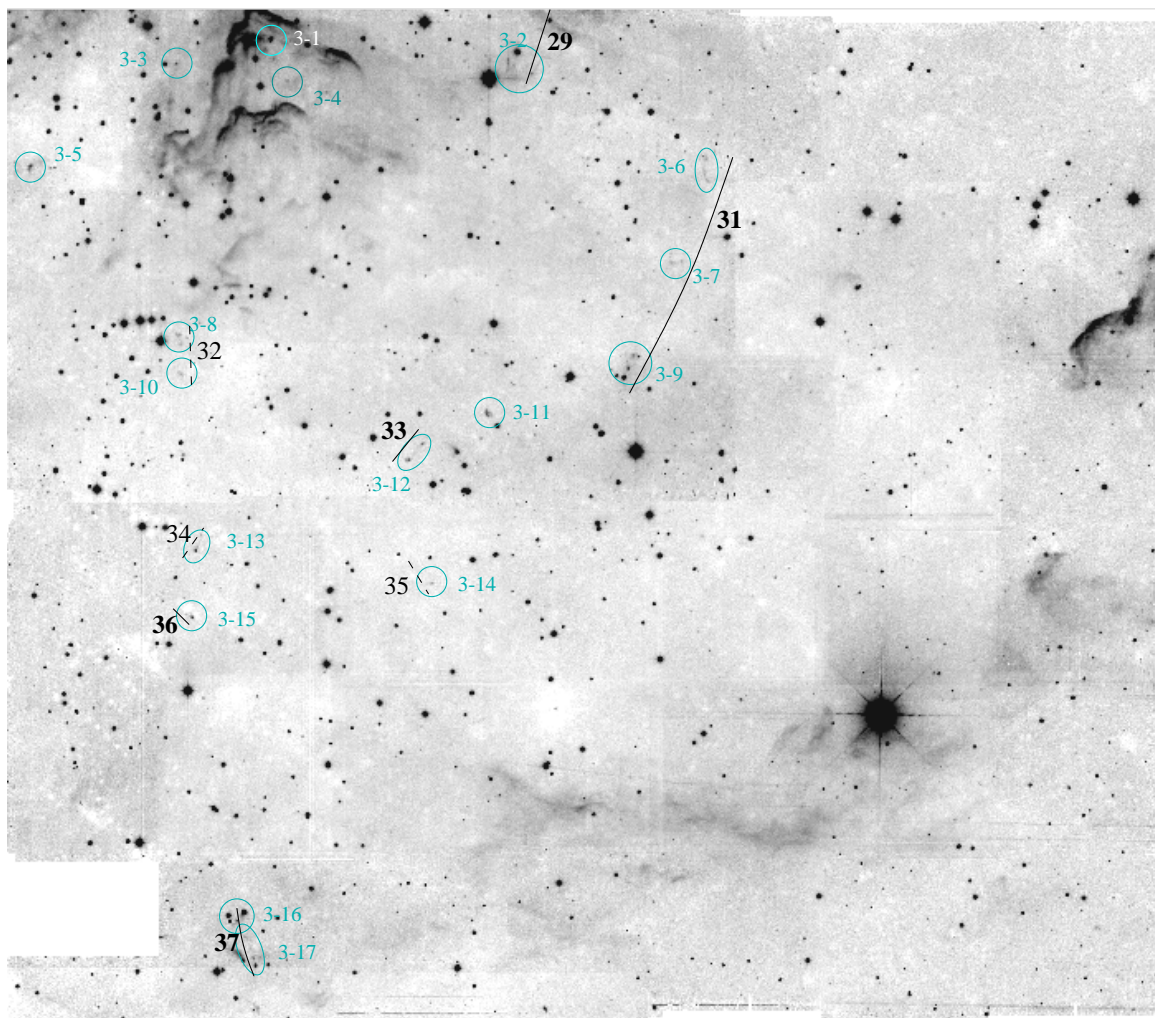


Figure 59: Jets in Field 3 (the area south of the Orion Nebula)

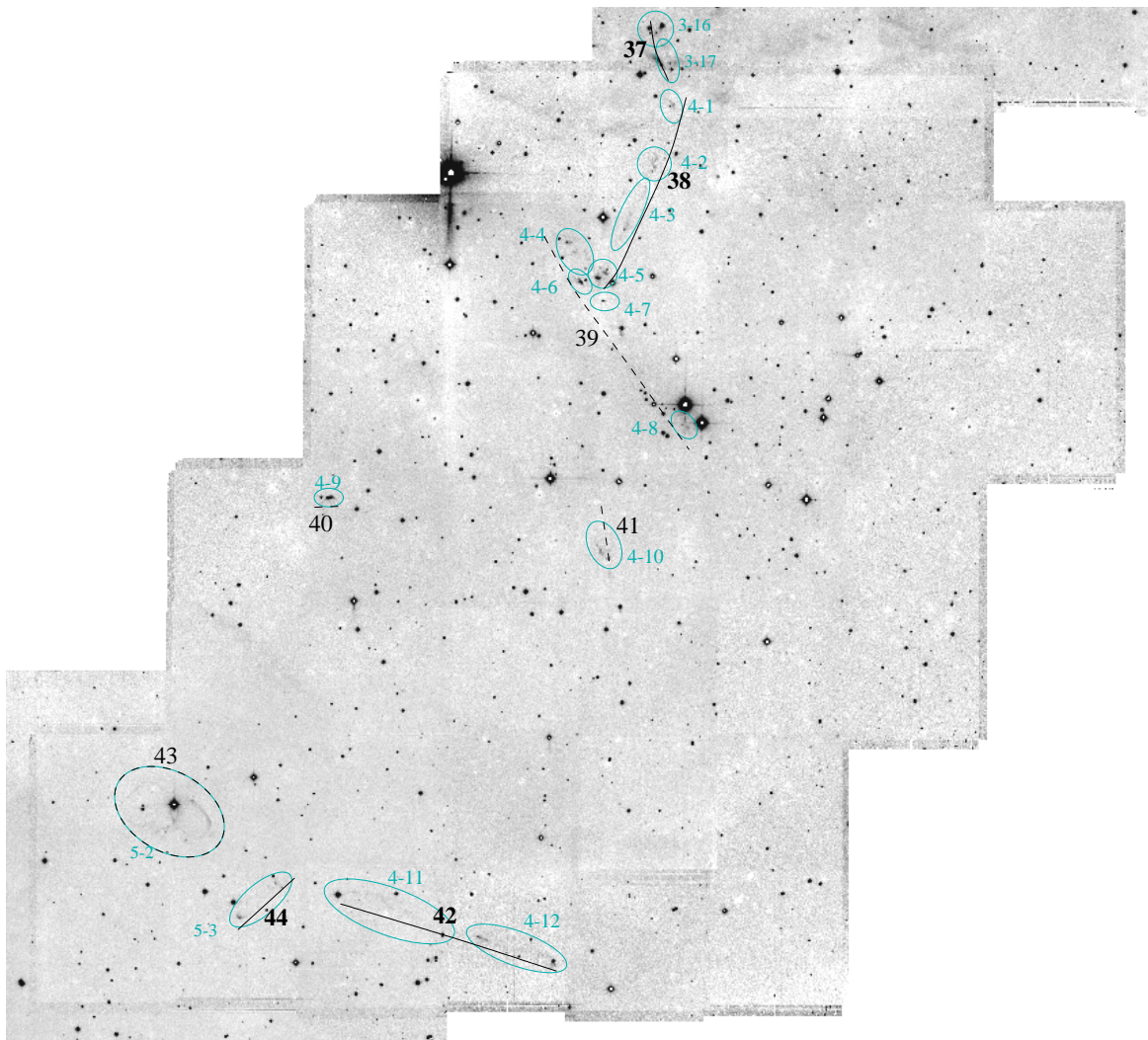


Figure 60: Jets in Field 4

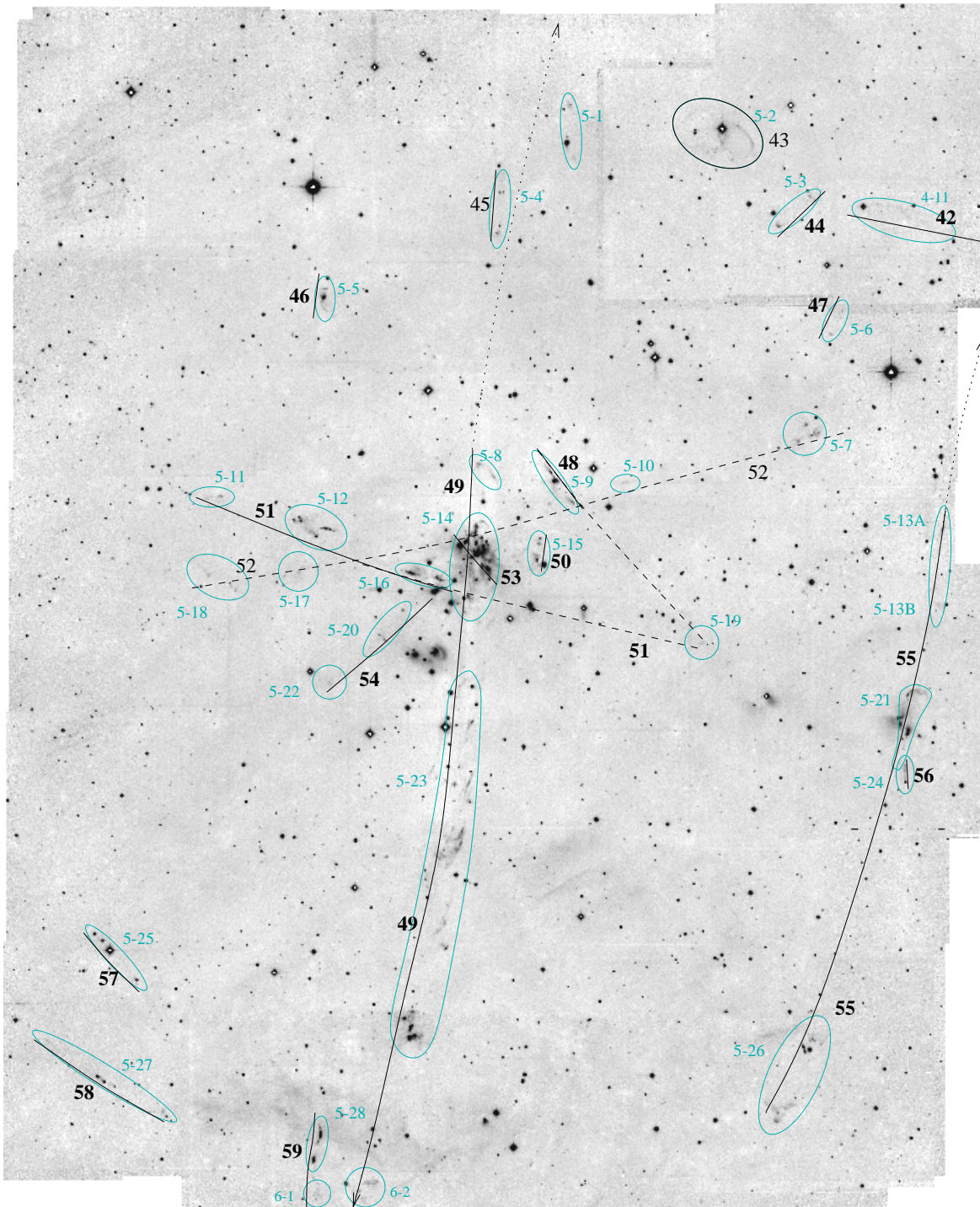


Figure 61: Jets in Field 5 (the area around the L1641-N cluster)

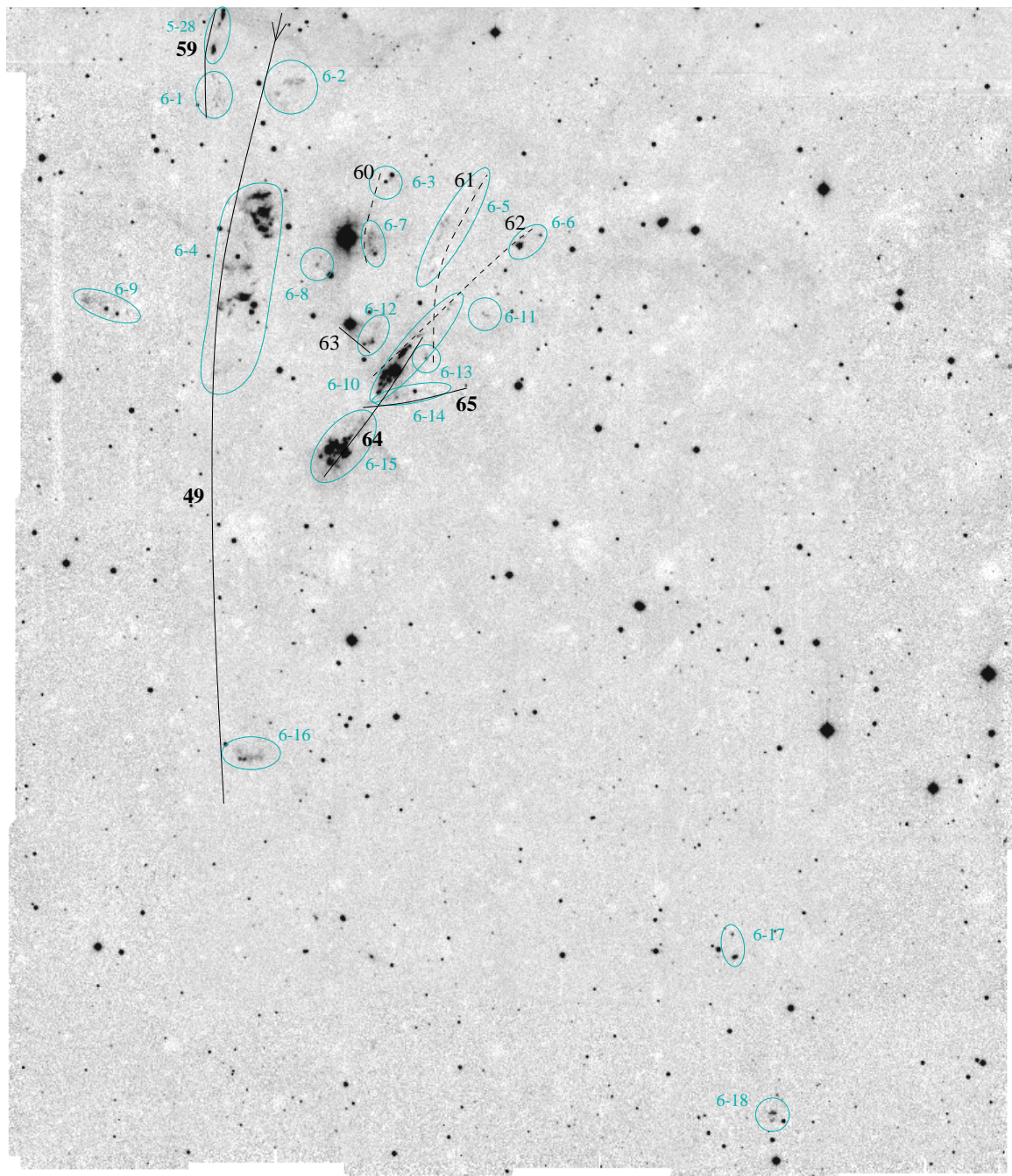


Figure 62: Jets in Field 6 (the HH 1/2 and V 380 Ori area)

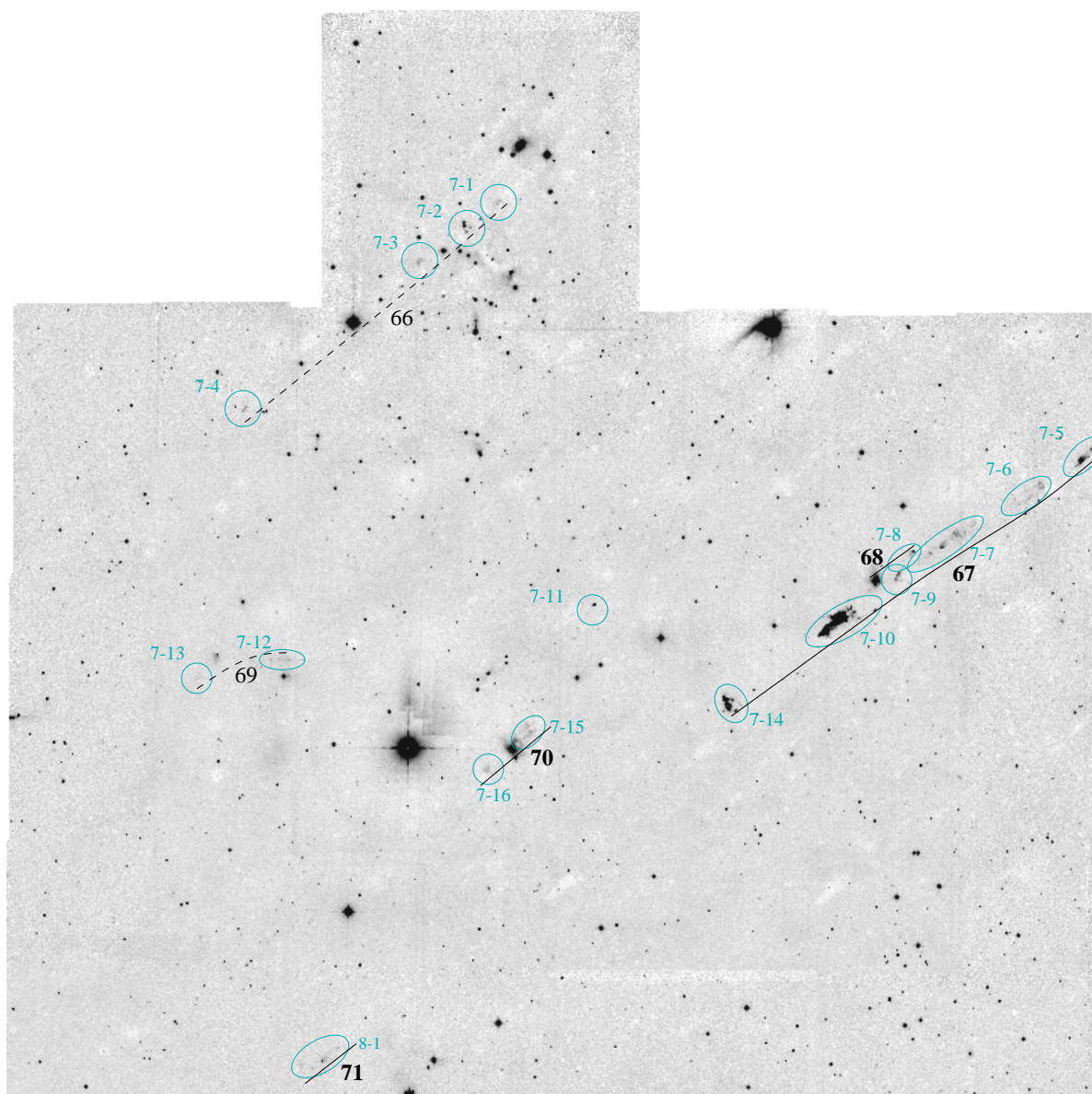


Figure 63: Jets in Field 7 (the L1641-C and HH 43 area)

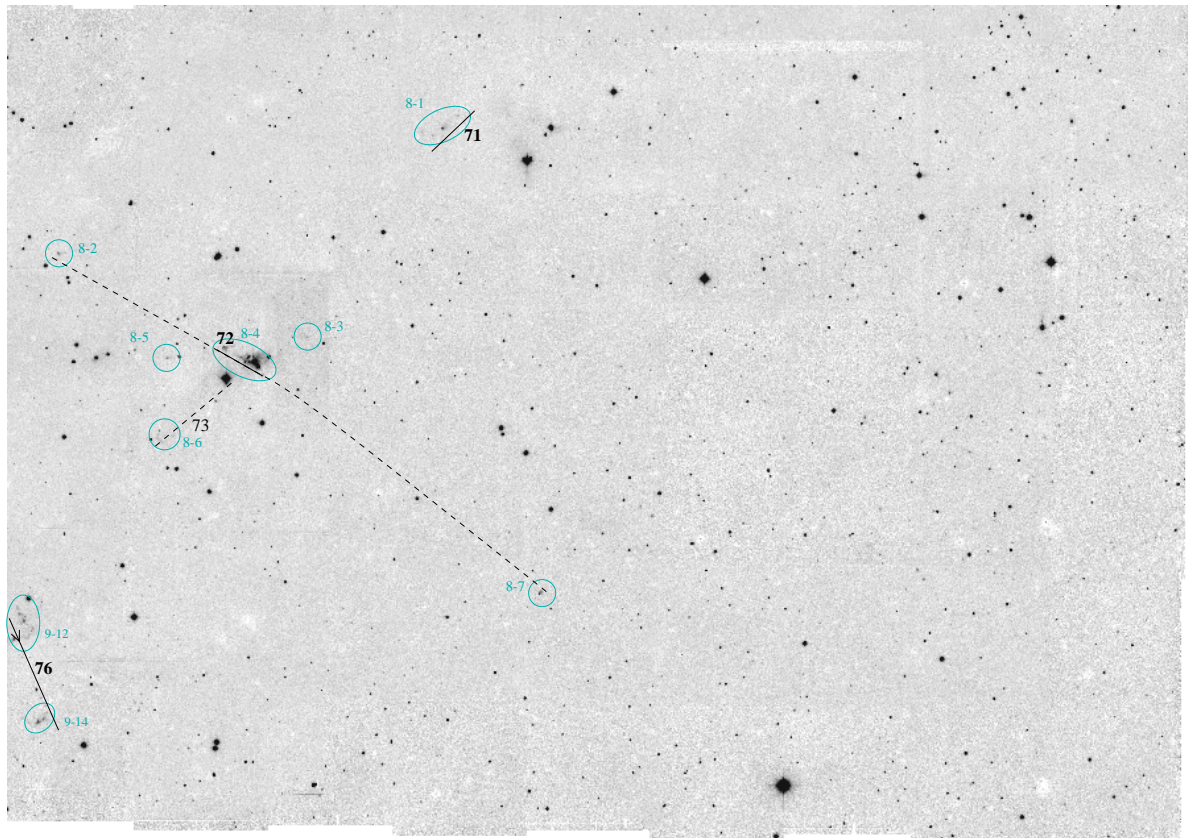


Figure 64: Jets in Field 8



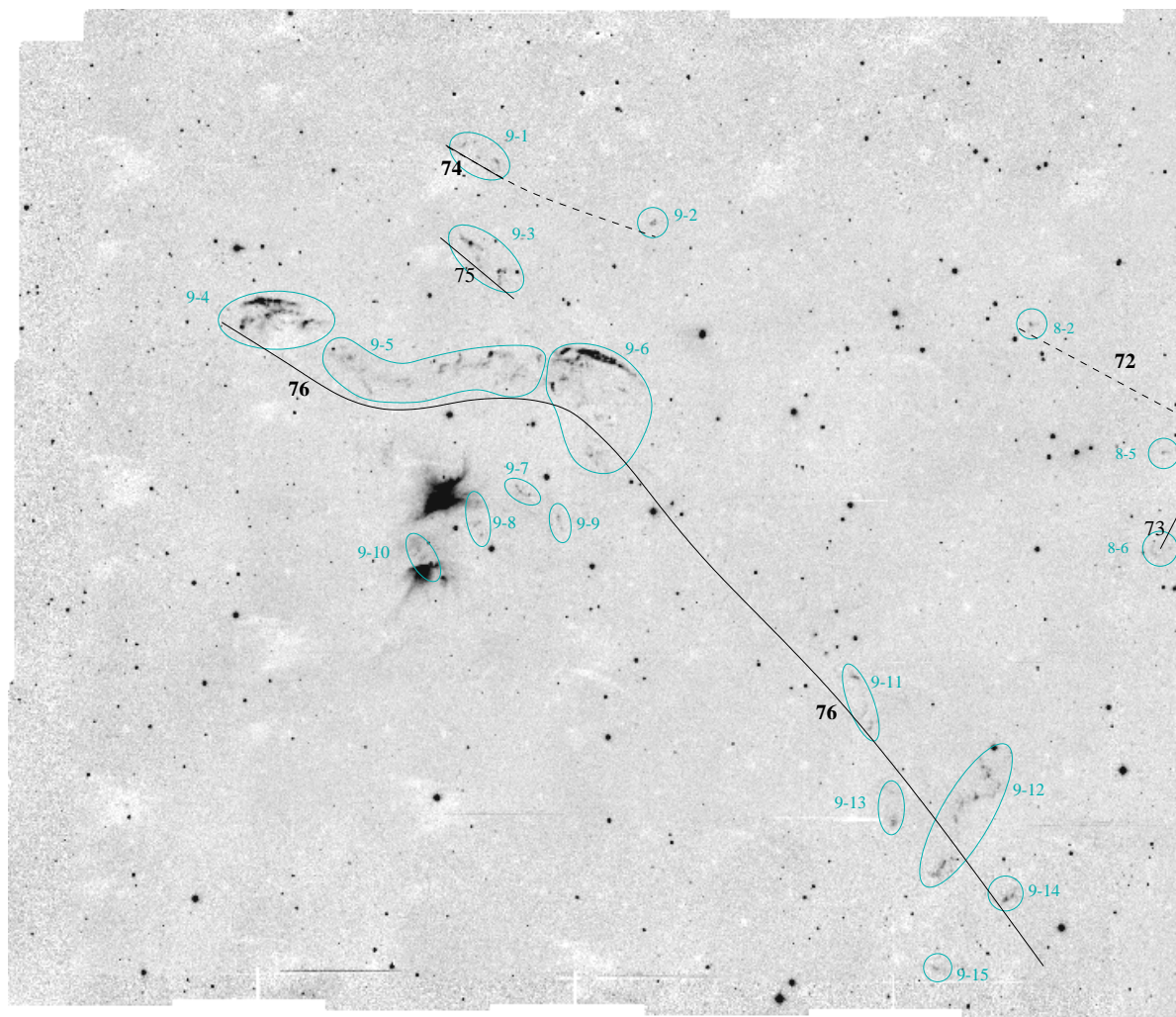


Figure 65: Jets in Field 9 (the Re50/L1641-S/L1641-S3 area)

B.2 List of H<sub>2</sub> flows

Flow #	RA (J2000)	DEC (J2000)	H <sub>2</sub> features SMZ	Length		PA	$L_{2,12}$ $10^{-4}L_{\odot}$	CS core
Field 1								
1	5 35 19.1	-4 55 46	1-1	0'34	0.05	68	1.3	—
2	5 35 31.5	-5 00 21	1-2	0'43	0.06	-41	1.9	4
3	5 35 18.2	-5 00 33	1-4, 1-5, 1-6; 1-3(?)	5'23	0.70	84	31.5	3
4	5 35 23.4	-5 01 31	1-7	0'53	0.07	-4	3.8	4
5	5 35 22.4	-5 01 16	1-8	0'42	0.05	90	58.6	4
6	5 35 26.4	-5 03 54	1-11, 1-12, 1-13	11'	1.43	88	15.7	—
7	5 35 27.8	-5 05 00	1-9, 1-10, 1-17, 1-22; 1-24(?)	6'	0.80	29	22.0	—
8	5 35 31.5	-5 04 39	1-15, 1-14	2'83	0.37	-89	11.3	—
9	5 35 26.2	-5 05 46	1-18 A-G; H(?)	2'62	0.34	81	195.2	—
10	5 35 31.4	-5 05 48	1-18 H, 1-16, 1-14(?)	2'	0.26	66	37.8	—
11	5 35 23.5	-5 06 11	1-19; 1-22(?)	0.30(?)	0.05(?)	~ 0	10.1	—
12	5 35 27.4	-5 07 07	1-21	0'23	0.03	7	2.2	8
13	5 35 23.1	-5 07 09	1-22 A, B; 1-22 E (?); 1-24(?)	1'08	0.14	45	10.7	8
14	5 35 28.1	-5 07 20	1-20, 1-25, 1-28(?), 1-29(?), 1-32 A(?), 1-16(?)	3'43	0.48	45	31.5 (79)	8
15	5 35 23.3	-5 07 32	1-22 F	0'76	0.10	~ 51	3.6	8
16	5 35 24.3	-5 08 33	1-28, 1-29	1'33	0.17	77	8.8	8
17	5 35 27.5	-5 09 37	1-27 A, C, D, 1-34, 1-31 C, D(?)	2'84	0.37	31	110.2	11
18	5 35 27.5	-5 09 17	1-27 B, E	0'75	0.10	56	22.0	11
19	5 35 26.7	-5 09 24	1-30 B-A	0'38	0.05	-83	7.6	11
20	5 35 25.5	-5 09 41	1-30 C, D, (A); 1-33 A, C	1'25	0.16	-19	6.3	11
21	5 35 27.2	-5 11 11	1-37 E...C	1'70	0.22	-1	44.1	11
22	5 35 27.2	-5 12 32	1-37 B-C	0'62	0.08	-14	7.6	13
23	5 35 22.8	-5 11 50	1-38, 1-35 (?)	3'60	0.47	18	51.6	11
24	5 35 23.3	-5 12 03	1-40	1'52	0.20	61	25.2	11
25	5 35 21.4	-5 13 14	1-42, 1-39, 1-32	3'33	0.44	-20	40.3	15
Field 2								
26	5 35 10.9	-5 23 12	2-3, 2-2	2'58	0.34	-55	36.5	—ON
27	5 35 11.6	-5 23 41	2-5 (C ?)	0'22	0.03	-19	40.9	—ON
28	5 35 10.9	-5 23 46	2-6; 2-5 C(?); 2-4(?)	0'38	0.05	89	63.0	—ON
29	5 34 40.7	-5 31 44	2-7, 3-2	5'	0.66	-23	9.5	—
30	5 35 18.2	-5 31 42	2-8, 2-9	0'90	0.12	25	1.1	—
Field 3								
31	5 34 35.3	-5 39 59	3-9, 3-7; 3-6(?)	2'42	0.31	-23	2.8	—
32	5 35 11.3	-5 39 39	3-8, 3-10	0'90	0.12	3	1.1	—
33	5 34 51.6	-5 41 31	3-12	0'57	0.07	-42	1.6	—
34	5 35 09.7	-5 43 45	3-13	0'37	0.05	-25	0.9	—
35	5 34 50.7	-5 44 21	3-14	0'7(?)	0.8(?)	30(?)	0.4	51
36	5 35 09.9	-5 45 06	3-15	0'18	0.02	58	1.1	—
37	5 35 04.4	-5 52 01	3-16 (A), 3-17	1'20	0.16	15	10.4	—
Field 4								
38	5 35 08.8	-5 55 53	4-2, 4-3, 4-5; 4-1(?)	3'25	0.42	-24	7.9	56
39	5 35 10.7	-5 57 37	4-4, 4-6, 4-5(?), 4-7, 4-8	5'51	0.71	34	10.1	57
40	5 35 36.9	-6 02 29	4-9	0'25	0.03	-89	6.7	—
41	5 35 09.7	-6 03 53	4-10	>0'5	>0.07	~18	2.8	—
42	5 35 21.9	-6 13 06	4-11, 4-12	5'33	0.69	71	2.5	—

Table 5: List of H<sub>2</sub> flows

Flow #	RA (J2000)	DEC (J2000)	H <sub>2</sub> features SMZ	Length (pc)		PA	$L_{2,12} 10^{-4} L_{\odot}$	CS core
Field 5								
43	5 35 51.9	-6 10 01	5-2	2'	0.26	56	2.5	—
44	5 35 41.8	-6 11 55	5-3	1':50	0.20	-49	1.8	—
45	5 36 17.1	-6 11 10	5-4	1':67	0.22	1	1.3	—
46	5 36 36.8	-6 14 58	5-5	0':66	0.09	1	1.3	65
47	5 35 37.9	-6 15 06	5-6	0':83	0.11	-25	0.8	—
48	5 36 10.0	-6 20 02	5-9; 5-19(?)	1':40	0.18	38	3.8	—
49	5 36 19.6	-6 22 13	5-14, 5-8, 5-23, 6-2, 6-4, 6-16; 5-1(?), 5-4(?)	34'	4.43	-6	192.1	67
50	5 36 12.1	-6 21 58	5-15	0':68	0.09	-8	4.2	—
51	5 36 24.8	-6 22 42	5-16, 5-12, 5-11; 5-19(?)	7':24	0.94	71	23.3	69
52	5 36 19.1	-6 22 09	5-7, 5-10, 5-17, 5-18	17':4	2.20	-74	5.6	67
53	5 36 18.8	-6 22 10	5-14 A1, C, Q	1':15	0.15	43	10.3	67
54	5 36 23.5	-6 23 11	5-20, 5-22	3':05	0.40	-42	2.0	69
55	5 35 29.7	-6 26 59	5-21, 5-13, 5-26	17':5	2.28	-15	18.9	71
56	5 35 29.8	-6 28 07	5-24	0':50	0.065	4	1.5	—
57	5 36 59.8	-6 33 27	5-25	1':84	0.24	43	3.3	86
58	5 37 00.2	-6 37 10	5-27	4':17	0.54	59	4.4	—
59	5 36 36.4	-6 38 58	5-28, 6-1	2':17	0.28	1	12.6	89
Field 6								
60	5 36 23.6	-6 43 07	6-3, 6-7	1':50	0.20	-10	3.1	—
61	5 36 18.9	-6 45 21	6-5, 6-13	3':10	0.40	-9	2.8	—
62	5 36 20.2	-6 45 06	6-6, 6-10 B, A, D, E	4':17	0.54	-45	23.9	91
63	5 36 25.0	-6 44 42	6-12	0':60	0.08	41	2.9	91
64	5 36 22.8	-6 46 07	6-10, 6-15	3'	0.39	-33	100.8	92
65	5 36 22.9	-6 46 10	6-14	1':38	0.18	-83	1.3	92
Field 7								
66	5 38 48.2	-7 01 53	7-1, 7-2, 7-3; 7-4(?)	2':63	0.34	-51	3.1	95
67	5 37 57.6	-7 07 00	7-5, 7-6, 7-7, 7-9, 7-10, 7-14	11':17	1.45	-54	172.6	97
68	5 38 07.3	-7 08 31	7-8	1':18	0.15	-50	1.9	98
69	5 39 11.8	-7 10 35	7-12, 7-13	2':63	0.34	~ -75	0.8	—
70	5 38 42.7	-7 12 44	7-15, 7-16	1':67	0.21	-46	3.3	—
Field 8								
71	5 39 00.8	-7 20 23	8-1	0':93	0.12	-52	0.9	111
72	5 39 19.6	-7 26 18	8-4, 8-2(?), 8-7(?)	1':25	0.16	63	13.2	117
73	5 39 22.2	-7 26 45	8-6	2':33	0.30	-47	0.6	117
Field 9								
74	5 40 25.3	-7 20 28	9-1, 9-2(?)	1'	0.13	53	2.1	—
75	5 40 24.6	-7 22 31	9-3	1':47	0.19	46	5.7	—
76	5 39 55.1	-7 30 27	9-4, 9-5, 9-6, 9-11, 9-12, 9-13, 9-14, 9-15; 9-3(?)	20':5	2.7	~ 50	138.5	123
HH 212	5 43 51.1	-1 03 01		3':9	0.51		69	
HH 211	3 43 56.6	32 00 53		1':8	0.157		34	

Table 6: List of H<sub>2</sub> flows (continued)

### B.3 Notes on individual flows

1. Two knots east and west of IR star (candidate source); position refers to this star.
2. Two knots & some more diffuse emission; associated with IR–RN and star; flow position refers to H<sub>2</sub> knot 1-2 A.
3. Chain of compact knots and filamentary structures; flow position refers to the candidate driving source IRS 1.
4. North–south extending chain of compact knots; flow position refers to the candidate driving source CRW MMS6.
5. East-west extending chain of bright compact knots; well collimated jet; flow position refers to the candidate driving source CRW MMS5.
6. East–west extending system of compact knots (close to bipolar Haro 5a/6a RN); weak filamentary structures further west; in addition to the H<sub>2</sub> features noted here presumably HH 41, HH 42, HH 128, and HH 129 (11' to the east) are part of this flow (see Reipurth et al. 1997); length measured over the H<sub>2</sub> features only (including the HH objects east of Haro 5a/6a, the flow would extend over a total of about 24'/3.1 pc); the position refers to the candidate driving source CRW MMS7 (Haro 5a/6a).
7. Long, narrow chain of compact features; apparently well collimated flow; H<sub>2</sub> features 1-22 and 1-24 may form independent flow (# 13). Flow position refers to the candidate driving source (U–shaped continuum nebula associated with 1-17 A).
8. 1-15: chain of compact knots; the prolongation of a line through these knots leads through 1-14; very uncertain. Flow position refers to 1-15 A
9. Broad, well defined, collimated, bright flow. Flow position refers to candidate driving source CRW MMS9.
10. Possible flow from CRW MMS10 or bright IR source nearby 1-18 H, very uncertain. Flow position refers to bright IR source nearby 1-18 H.
11. Very uncertain: 1-19 is presumably a bow shock in a flow running south–north; possibly parts of 1-22 belong to this flow. Flow position refers to 1-19 B. The length and H<sub>2</sub> luminosity is measured over 1-19 only.
12. 2 knots, possibly marking north–south oriented flow; knots are elongated along suspected flow direction; well collimated (?). Flow position refers to middle of gap between the two knots.
13. Possibly well collimated flow from CRW FIR1c. Flow position refers to suspected K'-band counterpart to FIR1c.
14. Long chain of H<sub>2</sub> knots and partly optically visible HH–objects; well collimated; the full extend of the flow is not clear; the length is measured over 1-20 to 1-28; adding 1-16 and 1-32, the flow extends over 1 pc. The flow position refers to the suspected driving source.
15. 1-22 F and some additional knots may be flow from bright NIR source south–west of 1-22 F or FIR1b; very uncertain. Flow position refers to FIR1b. The length and position angle are measured from the bright IR source out to the H<sub>2</sub> features.
16. 1-28: chain of compact knots: jet? 1-29: possibly part of a bow shock; very uncertain. Flow position refers to candidate driving source CRW FIR2.
17. 1-27 A, C, D: Spindle shaped outflow lobe running from south–west to north–east; 1-27 A bow shock; 1-34 lies symmetrically to 1-27 A about the candidate outflow source. Flow position refers to candidate driving source (K'-counterpart to CRW FIR3).
18. Flow # 18 superimposed on flow # 17; spindle shaped outflow lobe, similar to # 17, but smaller; counterlobe not seen. Flow position refers to candidate driving source.
19. Short, well collimated H<sub>2</sub> and optical Jet flowing through narrow illuminated cavity. Flow position refers to the candidate driving source at the base of the cavity.
20. All knots are located roughly along a line, but this flow identification is regarded to be very uncertain. The flow position refers to the candidate driving source (also very uncertain).

21. North–south running chain of compact features, presumably originating somewhere in the FIR3/4/5 complex, but no driving source identified. Knots 1-37 B and C may form independent flow (see # 22). Flow position refers to northernmost H<sub>2</sub> feature (1-37 E).
22. 1-37 B and C may form a spindle shaped flow independent from # 21. No driving source identified; the flow position refers to the middle between 1-37 B and C.
23. Chain of compact knots (1-35 A,B; 1-37 E, D, C, B) on a line running through 1-37 A (bow shock?) suggesting a well collimated jet beam. The flow position refers to the candidate driving source.
24. Spindle shaped, partly limb brightened outflow lobe. The driving source is close to 1-40 A, 1-40 B appears to be the leading working surface. There is no counterflow visible.
25. Poorly defined, apparently poorly collimated flow. The flow position refers to the candidate driving source CRW FIR6c; however, the source identification is uncertain.
26. Chain of knots, presumably collimated jet. 2-3 A appears to be a bow shock in the flow. The flow position refers to the candidate driving source.
27. Short, highly collimated jet beam embedded in a spindle shaped cocoon. The flow position refers to the southern end of the jet, which is presumably close to the driving source, which itself is not identified. There is no counterflow detected. The association of knot 2-5 C with this flow is not clear.
28. East–west oriented chain of H<sub>2</sub> features. The length is measured over 2-6 only. The total length, measured over 2-5 C, 2-6, and 2-4, is about 3'/0.4 pc. The flow is apparently well collimated. The flow position refers to 2-6 A (no source identified).
29. System of faint H<sub>2</sub> features distributed bipolar around the driving source. 3-2 appears to be a large bow shock. The flow position refers to the driving source.
30. Two knots, north and south of a red nebulous star, very uncertain. The flow position refers to the red star.
31. Not very well defined chain of features, possibly defining flow from K' continuum source close to 3-9 A; alternatively there may be a flow running from the north–west to the south–east. The length is measured over 3-9 and 3-7 only; adding 3-6, the length is 4'/5/0.6 pc. The flow position refers to the K' continuum source close to 3-9 A.
32. Faint knots to the north and south of a faint, slightly extended continuum source (regarded as the candidate driving source), but very uncertain. The flow position refers to the candidate driving source.
33. Knot 3-12 C together with the faint emission between C and A delineate a short, faint, well collimated jet beam, which ends in a working surface outlined by knots A and B. The source of the flow is presumably located at the north–western end of the jet (close to knot C); the flow position refers to this north–western end. There is no counter flow detected.
34. Knots 3-13 A and B and possibly some more faint emission along their connecting line may delineate a short, well collimated jet (very uncertain). The flow position refers to 3-13 A (no driving source identified).
35. Possibly shock in flow from weak IRAS source 40'' north–east of 3-14; extremely uncertain. The flow position refers to H<sub>2</sub> feature 3-14.
36. 3 knots in a row: short, faint collimated jet. Flow position refers to 3-15 A (no source identified).
37. Features in 3-17 define narrow, well collimated jet. 3-16 A is a bright bow shock on jet axis. The source presumably is close to 3-17 A, the flow position refers to 3-17 A. There is no counter flow detected.
38. 4-2 and 4-3 define a faint, narrow, very well collimated flow; 4-5 (and possibly 4-6 and 4-7) may form a terminating working surface. The flow position refers to the candidate driving source.
39. Very poorly defined flow, very uncertain. Flow position refers to H<sub>2</sub> knot 4-7 (no source identified).
40. Either short, bright, narrow jet or tip of a bow shock in a flow from IRAS 05331–0606 to the south–south–west; very uncertain. Flow position refers to H<sub>2</sub> knot 4-9 A.
41. 4-10 is presumably a bow shock in a flow from the north; very uncertain. The flow position refers to H<sub>2</sub> knot 4-10 A (no driving source identified).
42. 4-12 A apparently is a faint, narrow, very well collimated jet beam, with the driving source at its eastern end. 4-12 B seems to be a bow shock ahead of this jet. 4-11 appears to delineate the counter flow, but is very faint. The flow position refers to the candidate driving source.

43. Filamentary structures forming bipolar bubble-like structures to the east and west of V 1296 Ori, possibly indicating a very poorly collimated flow from that star. The flow position refers to the candidate driving source V 1296 Ori.
44. 5-3 seems to outline a flow from north-west, with knots A and B outlining the (apparently rather broad) flow itself, and feature C being a bow shock like working surface. The flow position refers to knot A (no driving source identified).
45. Group of knots extending south from the candidate driving source (a red, nebulous star north of 5-4 A/B); uncertain. 5-4 may also belong to the northern lobe of a large flow from the L 1641-N cluster. The flow position refers to the candidate driving source.
46. North-south oriented bipolar H<sub>2</sub> and optical HH flow from nebulous star. Knot B is very compact and may indicate a well collimated jet, knot A is elongated in an east-west direction and may be a bow shock like structure. The flow position refers to the candidate driving source.
47. 5-6 B may indicate faint, well collimated jet beam. 5-6 A appears to be a bow shock in a flow from the direction of feature B. The flow position refers to knot 5-6 B.
48. 5-9 is a narrow, jetlike filament, the connection of 5-19 with 5-9 is not clear, but there may be some more very faint emission between 5-19 and 5-9. The position of the driving source is also not clear, but it may be located between 5-9 B and D or to the southwest of 5-9 B, between 5-9 B and 5-19. The length of the flow is measured over 5-9 only. The flow position refers to H<sub>2</sub> feature 5-9 D.
49. L 1641-N giant flow (Stanke et al. 1998; 2000). Only a small fraction of the northern lobe of the flow is detected in H<sub>2</sub> (5-14 B, G, P (?), 5-8), but this lobe is traced by optical HH-objects over a length of more than 6 pc (Reipurth et al. 1998, Mader et al. 1999). The southern lobe detected in the infrared extends over 4 pc (but may continue further south, beyond the edge of the mosaic 6). The length given in the table is measured over the H<sub>2</sub> features only, from 5-8 down to 6-16. Some other H<sub>2</sub> features north of the L 1641-N cluster (5-1 and 5-4) may also belong to this flow. The H<sub>2</sub> features line out a rather broad path, but still the flow appears to be rather well collimated (the underlying flow is presumably also narrower than the path seen in H<sub>2</sub>, since the H<sub>2</sub> features probably are bowshocks which are much wider than the flow). The path also appears to show some bendings, indicating time variable direction of ejection. The flow position refers to the candidate driving source.
50. Short, roughly spindle-shaped flow. There is no driving source identified, but presumably it is located between 5-15 B and D. The flow position refers to the middle between 5-15 B and D.
51. Roughly east-west oriented flow originating in millimetre source between 5-16 A and B. 5-16 A, 5-12, and 5-11 form the eastern lobe of the flow, the counter flow is indicated by 5-16 B (and possibly 5-19). The length is measured over 5-16, 5-12, and 5-11, the total length of the flow may be about 2 pc, assuming that it is symmetric about its driving source. The morphology of 5-16 A and B seem to indicate that the flow here is interacting with the walls of its outflow cavity (possibly traced by some reflection nebulosity). 5-12 and 5-11 may be large bow shocks, and are also detected at optical wavelengths (Reipurth et al. 1998, Mader et al. 1999). The flow position refers to the candidate driving source.
52. This may be another large scale flow from somewhere in the L 1641-N cluster, but very uncertain. The flow position refers to the center of the cluster.
53. Short flow from the center of the L 1641-N cluster. The jet beam itself is not visible, but 5-14 A1 is apparently a bright bow shock pointing away from the cluster center (see also Stanke et al. 1998). The flow position refers to the candidate driving source.
54. Jet from an edge on star+disk system. The flow position refers to the candidate driving source.
55. HH 34 giant flow (Bally & Devine 1994; Devine et al. 1997; Eisloffel & Mundt 1997). The length is measured over the H<sub>2</sub> features seen here only. HH 38/43 further north-west is also an H<sub>2</sub> bright object, but not on the mosaic presented here. In total, the flow extends over more than 3 pc. The HH 34 inner jet (5-21 B) is detected in the H<sub>2</sub> line here for the first time. The counter jet (5-21 C) is detected for the first time at all. The flow position refers to the driving source.
56. Short collimated flow. The flow position refers to the middle of the H<sub>2</sub> feature (there is no driving source identified, but there is a faint continuum source at each end of the feature).

57. Two bright features with a morphology suggestive of small compact bow shocks in a bipolar configuration around BE Ori. The compactness of the bow shocks suggests the presence of a highly collimated jet beam, which itself is not visible neither as H<sub>2</sub> jet nor as optical HH jet (Mader et al. 1999). The flow position refers to the candidate driving source BE Ori.
58. Group of H<sub>2</sub> features in a roughly symmetric bipolar configuration around fan shaped infrared source (candidate driving source). 5-27 A consists of two features, both suggestive of bow shocks heading away from the driving source. 5-27 B and C appear to be a symmetric pair of bow shocks at a greater distance from the driving source. The flow position refers to the candidate driving source.
59. The H<sub>2</sub> features 5-28 and 6-1 form the infrared counterpart to the north-south oriented bipolar molecular outflow V 380 Ori NE (Levreault 1988a; Morgan et al. 1991; Davis et al. 2000b). They indicate the presence of a well collimated, precessing jet. The flow position refers to the candidate driving source.
60. Very poorly defined flow, very uncertain. The flow position refers to the north-eastern knot of 6-7.
61. Flow consisting of faint features from H<sub>2</sub>O maser/VLA source (Pravdo et al. 1985) coincident with 6-13. The morphology of this flow is not well defined, the true shape is unclear, possibly 6-11 or 6-6 are also part of a flow from that source. The flow position refers to the candidate driving source.
62. This flow almost certainly is not real: on the one hand, the H<sub>2</sub> and K' data alone suggest that there may be a well collimated flow from a compact source (partly continuum, partly H<sub>2</sub> line emission) at the given position. However, this source is coincident with the tip of the very bright HH-object HH 1, and the continuum emission seen presumably is emission from other lines in the K' filter, and the H<sub>2</sub> feature 6-10 presumably is some part of the HH 1/2 flow. This conclusion however is based on optical data, not on the infrared data. Based on the infrared data alone, one would have to identify this as a likely jet. Thus I list it as a candidate flow here, but as a very uncertain one.
63. Several H<sub>2</sub> and optical HH knots associated with reflection nebulosity suggesting a flow cavity from star N<sup>3</sup>SK50 and a rather poorly collimated flow through the cavity (e.g., Davis et al. 1994; Corcoran & Ray 1995). There is no counterflow detected. The flow position refers to the candidate driving source N<sup>3</sup>SK50.
64. HH 1/2 outflow system. 6-10 C indicates a very well collimated jet beam, which flows through an illuminated cavity seen as conical reflection nebula. 6-10 B appears to indicate the interaction of a less collimated flow component with the wall of the cavity. 6-10 A is part of the bow shock HH 1. 6-10 D and E seem to indicate a continuation of the flow beyond HH 1, or may belong to a different flow. In the counter lobe, only the bow shock HH 2 (6-15) is seen. The flow position refers to the presumable driving source HH 1/2 VLA1.
65. Faint, well collimated H<sub>2</sub>/HH flow (e.g., Bohigas et al. 1985; Strom et al. 1985; Reipurth et al. 1993b). There is no counterflow detected. The flow position refers to the candidate driving source HH 1/2 VLA2.
66. All features roughly are located along a line, but may as well belong to individual, unknown flows. There is no source identified, the flow position refers to H<sub>2</sub> feature 7-2 A.
67. HH 43/38/64 giant flow (see Stanke et al. 2000). Well collimated, but apparently rather broad jet. The north-western lobe is probably even longer than visible here. The flow position refers to the presumable driving source HH 43 MMS1.
68. Bow shock in jet from HH 43 IRS1, filament (jet beam?) extending back from bow shock towards IRS. The supposed jet direction appears to be perpendicular to the dark lane intersecting the HH 43 reflection nebulosity. There is no counter flow detected. The flow position refers to the presumable driving source HH 43 IRS1.
69. Some very weak H<sub>2</sub> features close to a nebulous continuum source. The morphology of the flow (which is itself very uncertain) is only very poorly constrained. The flow position refers to the candidate driving source.
70. Short, probably well collimated HH–/H<sub>2</sub> flow from HBC 491 (Strom et al. 1986). The reflection nebulosity associated with this star suggests the presence of an outflow cavity. The flow position refers to the apparent driving source HBC 491.
71. Faint H<sub>2</sub> knots distributed in a roughly bipolar configuration around a very weak infrared continuum source. The compactness of knots A and B may suggest a well collimated flow. The flow position refers to the presumable driving source (the nebulous infrared source).

72. Jet from Haro 4-255 FIR source. Well collimated jet beam (8-4 I, G) terminates in bow shock like working surface (8-4 A; see also Davis & Eisloffel 1995). The association of 8-2 and 8-7 with this flow is uncertain, the length of the flow given here is measured over 8-4 only. The flow position refers to the presumable driving source.
73. The T Tauri star Haro 4-255 drives a well collimated HH jet (Aspin & Reipurth 2000), which terminates in a bow shock which is also detected as H<sub>2</sub> feature (8-6). However, based on the H<sub>2</sub> data alone, this flow would not have been recognized, and is thus listed as an uncertain detection only. The flow position refers to the driving source Haro 4-255.
74. H<sub>2</sub> knots distributed in a roughly symmetric bipolar configuration around a very weak K' continuum source. The H<sub>2</sub> features appear to outline a pair of bow shocks from this infrared source. The flow morphology is only very poorly constrained. The flow position refers to the apparent driving source.
75. Group of H<sub>2</sub> features possibly outlining a flow from one of the K' continuum sources associated with 9-3 A and 9-3 B. Alternatively, 9-3 may be part of the giant flow from L 1641-S3 MMS1 (# 76). The flow position refers to the middle between 9-3 A and B.
76. L 1641-S3 giant flow (see Stanke et al. 2000). Either a rather poorly collimated or a strongly bending flow from L 1641-S3 MMS1. The counter flow (features 9-11, 9-12, 9-13, 9-14, 9-15) presumably extends over a larger distance as is seen here. The flow position refers to the apparent driving source.



## C The outflow driving sources

In this section I present a list of candidate driving sources for the outflows listed.

The Table 7/8/9/10 contains for each flow with an identified driving source its position and available photometric data, including photometry/upper limits derived from own observations (imaging at  $0.816\mu\text{m}$  and K'-band, initial 1.3 mm measurements, and in a few cases  $10\mu\text{m}$  photometry from TIMMI), photometry derived from publicly available IRAS data (coadded and HIRES processed maps), photometry derived from the Johnstone & Bally (1999, JB) 450/850  $\mu\text{m}$  maps (kindly provided by Doug Johnstone as FITS files), and millimetre/submillimetre data from the literature (Chini et al. 1997b; Lis et al. 1998; Reipurth et al. 1993a; Zavagno et al. 1997; Dent et al. 1998).

These data are then used to construct spectral energy distributions to estimate or constrain the bolometric luminosities ( $L_{\text{bol}}$ ) of the jet driving sources and to constrain their evolutionary stage according to the infrared classification scheme by Lada (1987) and André et al. (1993). This is done by adapting a set of curves to the measurements, namely “bluebody” spectra adopted from Dent et al. (1998) for the long-wavelength part, and star+disk models taken from Kenyon & Hartmann (1987) and Adams et al. (1988) for the shorter-wavelength part. It should be emphasized that these curves were only used to derive the luminosities and to estimate the spectral slope of the sources, not to constrain any details about the central source (e.g. temperature and luminosity) or the circumstellar environments (e.g. disk properties, dust properties and masses, envelope geometry or masses).

Furthermore, for each jet a short note on the suggested driving source is given, containing informations on the source morphology, detection/nondetection in the various data sets, various additional informations, and possible alternatives.

The indices in the Table 7/8/9/10 have the following meaning:

(n): see note on individual source below

- (1): IRAS Point Source Catalog
- (2): IRAS upper limits derived from ADDSCAN/HIRES maps
- (3): derived from own 1.3 mm map
- (4): derived from JB 450/850  $\mu\text{m}$  maps
- (5): taken from Chini et al. (1997b) (CRW)
- (6): taken from Cohen (1990)
- (7): taken from Dent et al. (1998)
- (8): taken from Lis et al. (1998) (LSK)
- (9): taken from Reipurth et al. (1993a)
- (10): taken from Strom et al. (1989b)
- (11): taken from Zavagno et al. (1997)
- (12): taken from McCaughrean et al. (1994)

## C.1 Candidate driving sources

#	RA (2000)	DEC	0.8 $\mu\text{m}$ I-mag	2.2 $\mu\text{m}$ K'-mag	IRAS fluxes				mm/submm		$L_{\text{bol}}$ ( $L_{\odot}$ )	IR- Class $\alpha_{\text{IR}}$
					12 $\mu\text{m}$ (Jy)	25 $\mu\text{m}$ (Jy)	60 $\mu\text{m}$ (Jy)	100 $\mu\text{m}$ (Jy)	$\lambda$ : ( $\mu\text{m}$ )	Flux (Jy)		
Field 1												
1	5 35 19.1	-4 55 46	20.5	11.1	<15 <sup>2</sup>	<47 <sup>2</sup>	<1800 <sup>2</sup>	<3900 <sup>2</sup>	450: < 2 <sup>4</sup>		< 122	II <sup>n</sup>
2	?	?	?	?			?		850: < 0.3 <sup>4</sup>		?	?
3	5 35 18.2	-5 00 33	>21	12.2	<2 <sup>2</sup>	<2 <sup>2</sup>	<50 <sup>2</sup>	<500 <sup>2</sup>	450: $\leq$ 7 <sup>4</sup>		$\lesssim$ 29	I <sup>n</sup>
4	5 35 23.4	-5 01 31	>21	>17.5	<2 <sup>2</sup>	<3 <sup>2</sup>	<50 <sup>2</sup>	<300 <sup>2</sup>	850: $\leq$ 1 <sup>4</sup>		< 53	0 <sup>5,n</sup>
									350: 72 <sup>5</sup>			
									450: 37 <sup>5</sup>			
									800: 8.6 <sup>5</sup>			
									850: $\sim$ 7.4 <sup>4</sup>			
									1100: 4.4 <sup>5</sup>			
									1300: 2.7 <sup>5</sup>			
									2000: 0.96 <sup>5</sup>			
5	5 35 22.4	-5 01 16	>21	>17.5	<2 <sup>2</sup>	<3 <sup>2</sup>	<50 <sup>2</sup>	<300 <sup>2</sup>	350: 45 <sup>8</sup>		< 53	0 <sup>5,n</sup>
									450: $\sim$ 15 <sup>4</sup>			
									850: $\sim$ 2.5 <sup>4</sup>			
									1300: 0.4 <sup>5</sup>			
6	5 35 26.4	-5 03 54	>21	$\leq$ 11.8	4.48 <sup>1</sup>	32 <sup>1</sup>	$\sim$ 100 <sup>2</sup>	<200 <sup>2</sup>	350: 40 <sup>5</sup>		$\lesssim$ 80	I ( $\sim$ 2.3)
									450: 18 <sup>5</sup>			
									800: 2.5 <sup>5</sup>			
									850: $\sim$ 2.1 <sup>4</sup>			
									1100: 0.9 <sup>5</sup>			
									1300: 0.8 <sup>5</sup>			
									2000: < 0.5 <sup>5</sup>			
7	5 35 27.8	-5 05 00	>21	$\sim$ 14.6	<4 <sup>3</sup>	<15 <sup>3</sup>	<100 <sup>3</sup>	<200 <sup>3</sup>	450: $\sim$ 3 <sup>4</sup>		< 51	I <sup>n</sup>
									850: $\sim$ 0.5 <sup>4</sup>			
8	?	?	?	?			?		?		?	?
9	5 35 26.2	-5 05 46	neb.	neb.	<4 <sup>2</sup>	<10 <sup>2</sup>	<150 <sup>2</sup>	<300 <sup>2</sup>	350: 42 <sup>5</sup>		< 77	0 <sup>5,n</sup>
									450: 21 <sup>5</sup>			
									800: 3.0 <sup>5</sup>			
									850: $\sim$ 1.7 <sup>4</sup>			
									1100: 1.0 <sup>5</sup>			
									1300: 0.8 <sup>5</sup>			
									2000: < 0.32 <sup>5</sup>			
10	5 35 31.4	-5 05 48	16.0	<8	<4 <sup>2</sup>	$\sim$ 5 <sup>2</sup>	<150 <sup>2</sup>	<300 <sup>2</sup>	450: < 2 <sup>4</sup>		< 64	II (-0.8)
									850: < 0.3 <sup>4</sup>			
11	?	?	?	?			?		?		?	?
12	?	?	?	?			?		?		?	?
13	5 35 23.1	-5 07 09	>21	13.7	<2 <sup>2</sup>	24.8 <sup>1</sup>	$\sim$ 297 <sup>1,2</sup>	<300 <sup>2</sup>	350: 23 <sup>5</sup>		$\sim$ 114	I ( $\sim$ 2.8)
									450: 11 <sup>5</sup>			
									800: 1.7 <sup>5</sup>			
									850: $\sim$ 0.8 <sup>4</sup>			
									1100: 0.6 <sup>5</sup>			
									1300: 0.36 <sup>5</sup>			
									2000: < 0.30 <sup>5</sup>			

Table 7: List of candidate driving sources

#	RA (2000)	DEC (2000)	0.8 $\mu\text{m}$ I-mag	2.2 $\mu\text{m}$ K'-mag	IRAS fluxes				mm/submm		$L_{\text{bol}}$ ( $L_{\odot}$ )	IR- Class $\alpha_{\text{IR}}$
					12 $\mu\text{m}$ (Jy)	25 $\mu\text{m}$ (Jy)	60 $\mu\text{m}$ (Jy)	100 $\mu\text{m}$ (Jy)	$\lambda$ : ( $\mu\text{m}$ )	Flux (Jy)		
Field 1												
14	5 35 28.1	-5 07 20	>21	>17.5	<4 <sup>2</sup>	<10 <sup>2</sup>	<250 <sup>2</sup>	<300 <sup>2</sup>	450: $\sim 3^4$	< 40	I <sup>n</sup>	
15	5 35 23.3	-5 07 32	?	?	<3 <sup>2</sup>	<10 <sup>2</sup>	<250 <sup>2</sup>	<300 <sup>2</sup>	850: $\sim 0.6^4$ 350: $18^8$ 450: $\sim 5^4$ 850: $\sim 1^4$ 1300: $\sim 0.2^5$	?	no ID	
16	5 35 24.3	-5 08 33	>21	>17.5	<5 <sup>2</sup>	<15 <sup>2</sup>	<250 <sup>2</sup>	<350 <sup>2</sup>	350: $30^5$ 450: $16^5$ 800: $2.4^5$ 850: $\sim 1.4^4$ 1100: $0.7^5$ 1300: $0.6^5$ 2000: $0.5^5$	< 97	0 <sup>n</sup>	
17	5 35 27.5	-5 09 37	$\sim 19$	<8.2	<10 <sup>2</sup>	$\sim 30^2$	$\sim 1000^2$	$\sim 2000^2$	350: $36^8$ 450: $\sim 12^4$ 850: $\sim 2.4^4$ 1300: $\sim 0.7^5$	< 241	I ( $\sim 0.7$ )	
18	5 35 27.5	-5 09 17	>21	$\sim 15.4$	$\leq 5^2$	<30 <sup>2</sup>	<1000 <sup>2</sup>	<2000 <sup>2</sup>	450: $< 3^4$ 850: $< 0.6^4$	< 108	I <sup>n</sup>	
19	5 35 26.7	-5 09 24	$\sim 19$	$\sim 12.1$	$\leq 5^2$	<30 <sup>2</sup>	<1000 <sup>2</sup>	<2000 <sup>2</sup>	450: $\leq 5^4$ 850: $\leq 1^4$	< 106	I ( $\sim 2.5$ )	
20	5 35 25.5	-5 09 41	>21	$\sim 15.2$	<5 <sup>2</sup>	<20 <sup>2</sup>	<1000 <sup>2</sup>	<2000 <sup>2</sup>	450: $< 3^4$ 850: $\leq 0.6^4$	< 78	I <sup>n</sup>	
21	?	?	?	?		?			?	?	?	
22	?	?	?	?		?			?	?	?	
23	5 35 22.8	-5 11 50	>20	$\sim 13$	<10 <sup>2</sup>	<15 <sup>2</sup>	$\leq 500^2$	<1500 <sup>2</sup>	450: $\sim 3.5^4$ 850: $\sim 0.5^4$	< 78	I <sup>n</sup>	
24	5 35 23.3	-5 12 03	>20	$\sim 13$	<10 <sup>2</sup>	<15 <sup>2</sup>	$\leq 500^2$	<1500 <sup>2</sup>	350: $15^8$ 450: $\sim 7^4$ 850: $\sim 1.1^4$ 1300: $\sim 0.3^5$	< 114	I <sup>n</sup>	
25	5 35 21.4	-5 13 14	>20	>17	<10 <sup>2</sup>	<20 <sup>2</sup>	$\leq 400^2$	<1000 <sup>2</sup>	350: $18^8$ 450: $\sim 8^4$ 850: $\sim 1.5^4$ 1300: $\sim 0.45^5$	< 130	I <sup>n</sup>	
Field 2												
26	5 35 10.9	-5 23 12	>16	$\sim 13.6$	conf.				450: $< 8^4$ 850: $< 1.5^4$	?	II <sup>n</sup>	
27	?	?	?	?	?				?	?	?	
28	?	?	?	?	?				?	?	?	
29	5 34 40.7	-5 31 44	>20.8	$\sim 15.8$	<3 <sup>2</sup>	<4 <sup>2</sup>	<100 <sup>2</sup>	<300 <sup>2</sup>	450: $\lesssim 1.5^4$ 850: $\sim 0.5^4$	< 18	I <sup>n</sup>	
30	5 35 18.2	-5 31 42	$\sim 16.5$	$\sim 10.5$	<7 <sup>2</sup>	<15 <sup>2</sup>	<250 <sup>2</sup>	<500 <sup>2</sup>	450: $< 2^4$ 850: $< 0.1^4$	< 620	II <sup>n</sup>	
Field 3												
31	5 34 35.3	-5 39 59	>21	$\sim 15.8$	<1 <sup>2</sup>	$\sim 3^2$	<15 <sup>2</sup>	<50 <sup>2</sup>	450: $< 2^4$ 850: $\sim 0.12^4$	$\lesssim 10$	I $\sim 2.7$	
32	5 35 11.3	-5 39 39	>21	$\sim 16.9$	<2 <sup>2</sup>	<7 <sup>2</sup>	<50 <sup>2</sup>	<250 <sup>2</sup>	450: $< 1^4$ 850: $< 0.1^4$	< 24	I <sup>n</sup>	

Table 8: List of candidate driving sources (continued)

#	RA (2000)	DEC	0.8 $\mu$ m I-mag	2.2 $\mu$ m K'-mag	IRAS fluxes				mm/submm $\lambda$ : Flux ( $\mu$ m) (Jy)	$L_{\text{bol}}$ ( $L_{\odot}$ )	IR- Class $\alpha_{\text{IR}}$
					12 $\mu$ m (Jy)	25 $\mu$ m (Jy)	60 $\mu$ m (Jy)	100 $\mu$ m (Jy)			
Field 3											
<b>33</b>	5 34 51.6	-5 41 31	>21	>17.5	<1 <sup>2</sup>	<2 <sup>2</sup>	<15 <sup>2</sup>	<80 <sup>2</sup>	450: < 1 <sup>4</sup> 850: $\sim$ 0.1 <sup>4</sup>	< 9	n.a.
34	?	?	?	?			?		?	?	?
35	?	?	?	?			?		?	?	?
<b>36</b>	?	?	?	?			?		?	?	?
<b>37</b>	?	?	?	?			?		?	?	?
Field 4											
<b>38</b>	5 35 08.8	-5 55 53	>20.5	$\sim$ 16.7	<0.3 <sup>2</sup>	$\leq$ 0.5 <sup>2</sup>	$\leq$ 5 <sup>2</sup>	<30 <sup>2</sup>	n.a.	$\lesssim$ 6	I $\sim$ 2.2
39	?	?	?	?			?		n.a.	?	?
40	?	?	?	?			?		n.a.	?	?
41	?	?	?	?			?		n.a.	?	?
<b>42</b>	5 35 21.9	-6 13 06	>21.3	$\sim$ 16.6	$\leq$ 0.3 <sup>2</sup>	$\leq$ 0.5 <sup>2</sup>	5.04 <sup>1</sup>	<15 <sup>2</sup>	n.a.	$\lesssim$ 3	I $\sim$ 3
Field 5											
43	5 35 51.9	-6 10 01	11.5	<10	2.04 <sup>1</sup>	4.99 <sup>1</sup>	7.05 <sup>1</sup>	<15 <sup>2</sup>	n.a.	$\sim$ 13	II $\lesssim$ 0
<b>44</b>	?	?	?	?			?		n.a.	?	?
45	5 36 17.1	-6 11 10	$\sim$ 20.6	$\sim$ 14	<0.2 <sup>2</sup>	$\leq$ 0.2 <sup>2</sup>	$\leq$ 4 <sup>2</sup>	<15 <sup>2</sup>	n.a.	$\sim$ 3	I $\sim$ 1
<b>46</b>	5 36 36.8	-6 14 58	$\sim$ 18.9	$\sim$ 13.1	<0.2 <sup>2</sup>	<0.3 <sup>2</sup>	<4 <sup>2</sup>	<15 <sup>2</sup>	n.a.	< 3	I <sup>m</sup>
<b>47</b>	?	?	?	?			?		n.a.	?	?
<b>48</b>	?	?	?	?			?		n.a.	?	?
<b>49</b>	5 36 19.6	-6 22 13	>21	$\sim$ 14.4	0.48 <sup>1</sup>	16.39 <sup>1</sup>	206.3 <sup>1</sup>	487 <sup>1</sup>	conf. <sup>n</sup>	< 113	I $\sim$ 3
<b>50</b>	?	?	?	?			?		?	?	?
<b>51</b>	5 36 24.8	-6 22 42	>21	>17	$\sim$ 0.3 <sup>2</sup>	$\sim$ 3 <sup>2</sup>	<50 <sup>2</sup>	<150 <sup>2</sup>	1300: $\sim$ 0.25 <sup>3</sup>	< 26	I $\gtrsim$ 3
52	?	?	?	?			?		?	?	?
<b>53</b>	5 36 18.8	-6 22 10	>21	>16.5	0.48 <sup>1</sup>	16.39 <sup>1</sup>	206.3 <sup>1</sup>	487 <sup>1</sup>	350: 53.5 <sup>11n</sup> 450: 30.6 <sup>11n</sup> 800: 5.14 <sup>11n</sup> 1100: 1.99 <sup>11n</sup> 1300: 1.29 <sup>11n</sup>	$\lesssim$ 112	I $\gtrsim$ 3.5
<b>54</b>	5 36 23.5	-6 23 11	$\sim$ 18.1	$\sim$ 10.7	<0.3 <sup>2</sup>	<0.5 <sup>2</sup>	<30 <sup>2</sup>	<150 <sup>2</sup>	1300: < 0.03 <sup>3</sup>	< 9	II <0
<b>55</b>	5 35 29.7	-6 26 59	$\sim$ 18.3	$\sim$ 12.6	$\leq$ 0.5 <sup>2</sup>	8.5 <sup>1</sup>	27.3 <sup>1</sup>	117 <sup>1</sup>	350: 11.9 <sup>7</sup> 450: 6.14 <sup>7</sup> 800: 1.28 <sup>7</sup> 870: 1.25 <sup>9</sup> 1100: 0.6 <sup>7</sup> 1300: 0.42 <sup>9</sup>	$\sim$ 21	I $\sim$ 1.7
<b>56</b>	?	?	?	?			?		?	?	?
<b>57</b>	5 36 59.8	-6 33 27	13.5	8.1	0.81 <sup>1</sup>	0.67 <sup>1</sup>	<3.3 <sup>1,2</sup>	<30 <sup>2</sup>	n.a.	< 9	II -0.55
<b>58</b>	5 37 00.2	-6 37 10	>21	13.5	<0.2 <sup>2</sup>	<0.2 <sup>2</sup>	<2 <sup>2</sup>	<20 <sup>2</sup>	n.a.	< 3	I <sup>m</sup>

Table 9: List of candidate driving sources (continued)

#	RA (2000)	DEC	0.8 $\mu\text{m}$ I-mag	2.2 $\mu\text{m}$ K'-mag	IRAS fluxes				mm/submm		$L_{\text{bol}}$ ( $L_{\odot}$ )	IR- Class $\alpha_{\text{IR}}$
					12 $\mu\text{m}$ (Jy)	25 $\mu\text{m}$ (Jy)	60 $\mu\text{m}$ (Jy)	100 $\mu\text{m}$ (Jy)	$\lambda$ : ( $\mu\text{m}$ )	Flux (Jy)		
Field 5												
<b>59</b>	5 36 36.4	-6 38 58	>21	>17	<0.5 <sup>2</sup>	<0.5 <sup>2</sup>	<5 <sup>2</sup>	$\leq 100^2$	450: 6.36 <sup>11</sup> 800: 1.26 <sup>11</sup> 1100: 0.45 <sup>11</sup> 1300: 0.55 <sup>11</sup>	< 8	0	
Field 6												
60	?	?	?	?					?	?	?	
61	5 36 18.9	-6 45 21	>21	$\sim 16.7$	$\leq 0.4^2$	$\sim 4^2$	$\leq 80^2$	$\leq 200^2$	450: 7.81 <sup>11</sup> 800: 1.29 <sup>11</sup> 1100: 0.45 <sup>11</sup> 1300: 0.32 <sup>11n</sup>	< 33	I $\sim 3$	
62	5 36 20.2	-6 45 06	?	16					?	?	?	
63	5 36 25.0	-6 44 42	14.5	8.1	1.24 <sup>1</sup>	5.4 <sup>1</sup>	<30 <sup>2</sup>	$\leq 200^2$	350: 6.52 <sup>11</sup> 450: 3.69 <sup>11</sup> 800: 0.76 <sup>11</sup> 1100: 0.29 <sup>11</sup> 1300: 0.22 <sup>11n</sup>	$\gtrsim 21$	II -0.1	
<b>64</b>	5 36 22.8	-6 46 07	>21	>17	<0.3 <sup>2</sup>	$\leq 1.5^2$	$\leq 80^2$	$\leq 200^2$	870: 1.67 <sup>9n</sup> 1300: 0.65 <sup>9n</sup>	$\gtrsim 44$	0-I <sup>n</sup>	
<b>65</b>	5 36 22.9	-6 46 10	>21	>17	<0.3 <sup>2</sup>	$\leq 1.5^2$	$\leq 80^2$	$\leq 200^2$	1300: < 0.5 <sup>n</sup>	< 44	0 (?)	
Field 7												
66	?	?	?	?					?	?	?	
<b>67</b>	5 37 57.6	-7 07 00	>21	>17.5	<0.2 <sup>2</sup>	<0.2 <sup>2</sup>	2.41 <sup>6</sup>	19.5 <sup>6</sup>	1300: $\sim 0.5^3$	$\gtrsim 5$	0	
<b>68</b>	5 38 07.3	-7 08 31	>21	$\sim 12.4$	0.38 <sup>10</sup>	1.13 <sup>10</sup>	$\sim 4^2$	$\sim 15^2$	1300: 0.05 <sup>9</sup>	$\gtrsim 4$	I $\sim 0.3$	
69	5 39 11.8	-7 10 35	>21	$\sim 15.3$	<0.2 <sup>2</sup>	<1 <sup>2</sup>	<10 <sup>2</sup>	<20 <sup>2</sup>	1300: < 0.1 <sup>3</sup>	< 5	I <sup>n</sup>	
<b>70</b>	5 38 42.7	-7 12 44	14.1	8.4 <sup>10</sup>	2.24 <sup>10</sup>	3.41 <sup>10</sup>	4.15 <sup>10</sup>	<20 <sup>2</sup>	1300: < 0.1 <sup>3</sup>	$\sim 10$	I $\sim 0.15$	
Field 8												
<b>71</b>	5 39 00.8	-7 20 23	>21	$\sim 15.4$	<0.2 <sup>2</sup>	$\leq 0.3^2$	<3 <sup>2</sup>	<20 <sup>2</sup>	1300: < 0.1 <sup>3</sup>	< 5	I <sup>n</sup>	
<b>72</b>	5 39 19.6	-7 26 18	$\sim 18.3$	$\sim 11.8$	<0.5 <sup>2</sup>	4.2 <sup>1</sup>	67 <sup>1</sup>	139 <sup>1</sup>	1300: $\sim 0.8^3$	$\sim 36$	I $\sim 1$	
73	5 39 22.2	-7 26 45	12.9	8.3 <sup>10</sup>	0.82 <sup>1</sup>	<1 <sup>2</sup>	<67 <sup>2</sup>	<139 <sup>2</sup>	1300: $\leq 0.1^3$	< 30	II -0.6	
Field 9												
<b>74</b>	5 40 25.3	-7 20 28	$\sim 21$	$\sim 17$	<0.2 <sup>2</sup>	<0.2 <sup>2</sup>	<2 <sup>2</sup>	<15 <sup>2</sup>	n.a.	< 2	II <sup>n</sup>	
75	?	?	?	?					?	?	?	
<b>76</b>	5 39 55.1	-7 30 27	>21	$\sim 16.4$	$\sim 0.18^{10}$	8.8 <sup>1</sup>	157 <sup>1</sup>	272 <sup>1</sup>	350: 34.7 <sup>11</sup> 450: 16.3 <sup>11</sup> 800: 3.19 <sup>11</sup> 1100: 1.23 <sup>11</sup> 1300: 0.85 <sup>11</sup> 1300: $\sim 0.6^3$	$\sim 72$	0	
HH 212	5 43 51.1	-1 03 01		> 18	<0.25 <sup>1</sup>	$\sim 0.31^1$	17.33 <sup>1</sup>	59.46 <sup>1</sup>	450: 3.17 <sup>7</sup> 800: 0.61 <sup>7</sup> 1100: 0.23 <sup>7</sup>	10	0	
HH 211	3 43 56.6	32 00 53		> 18	<0.25 <sup>2</sup>	<0.6 <sup>2</sup>	<4 <sup>2</sup>	<20 <sup>2</sup>	350: 18.0 <sup>7</sup> 450: 10.2 <sup>7</sup> 800: 2.0 <sup>7</sup> 1100: 0.93 <sup>7</sup> 2700: 0.025 <sup>12</sup>	< 4	0	

Table 10: List of candidate driving sources (continued)

## C.2 Notes on individual objects

1. Suspected source: opt./IR star between H<sub>2</sub> knots; flow position refers to this star; IRAS: no point source associated, confusion with IRAS 05327–0457 70'' east; no source detected at 450/850 μm; not on CRW 1.3 mm map. Conservatively classified as Class II, but SED only very poorly defined; may also be Class I.
2. Source identification unclear; H<sub>2</sub> knots associated with opt./IR RN, red star; IRAS: no point source associated, confusion with extended emission; there are 5 nearby 450/850 μm-peaks; not on CRW 1.3 mm map. Flow position refers to H<sub>2</sub> knot 1-2.
3. Suspected source: IRS 1; compact K-band source associated with IR RN; IRAS: no point source associated, IRAS 05328–0501 70'' north-west, no source found on HIRES maps, confusion with extended emission; NW–SE filament of submm/mm emission (~ between CRW MMS2 and MMS3); possibly associated with ~7 Jy peak on JB 450 μm map. Detected at 3.6 cm as VLA1 by Reipurth et al. (1999a). Tentatively classified as Class I (no opt. det., K-band det., submm det., but SED poorly defined).
4. Suspected source: CRW MMS6 (on jet axis); no opt./IR counterpart; IRAS: no point source associated, possibly ~50 Jy source in 60 μm HIRES map (confusion with MMS5, see below); MMS6 detected for  $\lambda \geq 350 \mu\text{m}$  (CRW, LSK, JB), position taken from JB 850 μm-map. Detected at 3.6 cm as VLA3 by Reipurth et al. (1999a). Evolutionary stage Class 0 as suggested by CRW; SED:  $L_{\text{bol}}/L_{\text{submm}} < 26$  consistent with this classification.
5. Suspected source: CRW MMS5 (15'' east of eastern end of jet); IRAS: no point source associated, possibly ~50 Jy source in 60 μm HIRES map; MMS5 detected for  $\lambda \geq 350 \mu\text{m}$  (CRW, LSK, JB), position taken from JB 850 μm-map. Evolutionary stage Class 0 as suggested by CRW; SED:  $L_{\text{bol}}/L_{\text{submm}} < 54$  (presumably much less) consistent with this classification.
6. Source: CRW MMS7, associated with bipolar opt./IR RN Haro 5a/6a (Wolstencroft et al. 1986); K-band peak close to mm source position, obscured at optical wavelengths; IRAS: point source IRAS 05329–0505; PSC gives only upper limit at 60 μm, but the HIRES map shows a ~100 Jy source, PSC upper limit at 100 μm (27 Jy) seems to be too low; MMS7 detected for  $\lambda \geq 350 \mu\text{m}$  (CRW, LSK, JB), position taken from JB 850 μm-map. Detected at 3.6 cm as VLA4 by Reipurth et al. (1999a).  $\alpha_{\text{IR}} \sim 2.3 \Rightarrow$  Class I.
7. Suspected source: U-shaped IR nebula associated with 1-17 A opening towards SW in jet direction; IRAS: no point source associated, at 60/100 μm confusion with extended emission and IRAS 05329–0505; weak 450/850 μm peak in JB maps. CRW MMS8, MMS9, and FIR1c lie also on the jet axis and may be the source. Tentatively classified as Class I, SED poorly constrained.
8. No source identified; flow position refers to 1-15 A.
9. Suspected source: CRW MMS9; associated with some opt./IR nebulosity; IRAS: no point source associated, no source visible in HIRES maps, confusion with extended emission and IRAS 05329–0508; MMS9 detected at  $\lambda \geq 350 \mu\text{m}$  (CRW, LSK, JB), position taken from JB 850 μm-map. Detected at 3.6 cm as VLA5 by Reipurth et al. (1999a). Classification as Class 0 (see CRW):  $L_{\text{bol}}/L_{\text{submm}} < 80$  (probably much less; source is only detected at submillimetre wavelengths).
10. Suspected source (very uncertain): IR-bright star associated with opt./IR RN or nearby CRW MMS10; position and photometry refer to IR star; IRAS: no point source associated, IR star possibly as weak 25 μm source on HIRES maps detected; IR star not detected at mm/submm wavelengths.  $\alpha_{\text{IR}} \sim -0.8 \Rightarrow$  Class II (uncertain, because saturated on K'-band image). Alternatively, Reipurth et al. (1999a) VLA6 (located at the westernmost knot of 1-18 H, between CRW MMS9 and CRW MMS10, may be the driving source.
11. No source identified; 1-19 may be the northern tip of a flow from the CRW FIR1c complex to the south. Flow position refers to 1-19 B.
12. No conclusive source identification; there is a nearby 450/850 μm peak; flow position refers to the middle of the gap between the two H<sub>2</sub> knots; IRAS: no nearby pointsource, no source on HIRES maps, at longer wavelengths confusion with IRAS 05329–0508 (70'' east of 1-21).
13. Suspected source: CRW FIR1c (IRAS 05329–0508); jet itself uncertain; position refers to suspected K'-band counterpart to FIR1c; IR source associated with IR RN; not detected at optical wavelengths; IRAS: FIR1c = IRAS 05329–0508, upper limit at 12 μm derived from coadded/HIRES maps, PSC gives upper limit at 60 μm, but maps show distinct peak with a flux of about 300 Jy, upper limit at 100 μm derived from

- coadded/HIRES maps, confusion; FIR1c detected at  $\lambda \geq 350 \mu\text{m}$  (CRW, LSK, JB). Possibly detected at 3.6 cm as VLA7 by Reipurth et al. (1999a).  $\alpha_{\text{IR}} \sim 2.8 \Rightarrow$  Class I.
14. Suspected source: 450/850  $\mu\text{m}$  peak NW of 1-25 (uncertain), CRW FIR1a and FIR2 are also located close to the jet axis; no opt./NIR source detected; IRAS: no pointsource associated, no source on HIRES maps, confusion; submm peak detected at  $\lambda \geq 350 \mu\text{m}$  (CRW, LSK, JB), position taken from JB 850  $\mu\text{m}$  map. Conservatively classified as Class I;  $L_{\text{bol}}$  very poorly constrained by IRAS upper limits, i.e.  $L_{\text{bol}}/L_{\text{submm}}$  may be much less and the source may be a low luminosity Class 0 source. Alternatively, the infrared star superimposed on 1-25 A may be the driving source; this star also seems to be associated with a 3.6 cm VLA source (Reipurth et al. (1999a) VLA9).
  15. Source identification unclear; possibly CRW FIR1b or bright nebulous opt./IR stars SE of 1-22 F; position refers to FIR1b (CRW); IRAS: no point source associated, confusion with extended emission and IRAS 05329–0508 for both candidate sources; FIR1b detected at  $\lambda \geq 350 \mu\text{m}$  (CRW, LSK, JB), no submm/mm emission detected from opt./IR stars. No SED plot/luminosity/evolutionary stage derived because of unclear source identification.
  16. Suspected source: CRW FIR2; no opt./K'–band counterpart detected; IRAS: no point source associated, no source visible on HIRES maps; FIR2 detected at  $\lambda \geq 350 \mu\text{m}$  (CRW, LSK, JB); position taken from CRW. Classified as Class 0, since not detected shortward of 350  $\mu\text{m}$ ;  $L_{\text{bol}}/L_{\text{submm}} < 150$  (probably much less) consistent with this classification.
  17. Suspected source: CRW FIR3; very red nebulous opt./IR star between H<sub>2</sub> knots 1-31 A and B may be counterpart to FIR3; position refers to this star; IRAS: no point source directly associated, but IRAS 05329–0512 is located only 45'' south of FIR3, 25  $\mu\text{m}$  map clearly reveals source at position of FIR3 ( $\sim 30$  Jy); there is a  $\sim 1000$  Jy peak in the 60  $\mu\text{m}$  maps at roughly the position of FIR3, there is also a  $\sim 2000$  Jy peak at 100  $\mu\text{m}$ , the position of that peak is somewhat uncertain, but seems to be closer to FIR3 than to IRAS 05329–0512; for the determination of the SED the 50/100  $\mu\text{m}$  fluxes given by Pendleton et al. (1986; 50  $\mu\text{m}$ : 500 Jy, 100  $\mu\text{m}$ : 1670 Jy) are used. FIR3 is detected at  $\lambda \geq 350 \mu\text{m}$  (CRW, LSK, JB).  $\alpha_{\text{IR}} \sim 0.7 \Rightarrow$  Class I.
  18. Suspected source in small NIR nebula 20'' north of CRW FIR3 (uncertain); not detected in the optical; IRAS: possibly faint (5 Jy) source in 12  $\mu\text{m}$  HIRES map (but possibly confusion with #19), at longer wavelengths confusion with FIR3; no counterpart found at submm/mm wavelengths. Tentatively classified as Class I (no opt. counterpart, nebulous K-band source, possible 12  $\mu\text{m}$  det.  $\Rightarrow \alpha_{\text{IR}} \sim 4$ ).
  19. Source: very red star at the base of a conical opt./IR RN, position refers to this star; IRAS: possibly faint (5 Jy) source in 12  $\mu\text{m}$  HIRES map (but possibly confusion with #18), at longer wavelengths confusion with FIR3; submm/mm: confusion with FIR3.  $\alpha_{\text{IR}} \sim 2.5 \Rightarrow$  Class I.
  20. Suspected source (very uncertain): possibly faint, small IR nebula on jet axis; photometry and position refer to this source; IRAS: no point source associated, confusion with IRAS 05329–0512 and FIR3; submm/mm: confusion with FIR3. Presumably Class I (detected at K' (nebulous), not detected at optical), SED poorly defined.
  21. No source identified; source probably somewhere to the north in CRW FIR3/4/5 complex (Reipurth et al. (1999a) VLA12 lies north of the H<sub>2</sub> chain on a line through the H<sub>2</sub> features); flow position refers to northernmost H<sub>2</sub> knot in jet (1-37 E).
  22. No source identified; flow position refers to middle of gap between knots 1-37 B and C.
  23. Suspected source: fan shaped IR nebula associated with 1-38 E; position refers to this source; IRAS: no point source associated, HIRES maps show nearby 60  $\mu\text{m}$  peak (may as well be associated with #24), confusion with CRW FIR6 and OMC-1; possibly weak 450/850  $\mu\text{m}$  source. Presumably Class I (detected at K', not detected at optical, detected at submm).
  24. Suspected source: nebulous IR source associated with H<sub>2</sub> knot 1-40 A; coincident with CRW FIR6b; IRAS: no point source associated, HIRES maps show nearby 60  $\mu\text{m}$  peak (may as well be associated with #23); FIR6b is detected at  $\lambda \geq 350 \mu\text{m}$  (CRW, LSK, JB); position taken from CRW. Possibly associated with Reipurth et al. (1999a) VLA14.  $L_{\text{bol}}/L_{\text{submm}} \leq 300$ ;  $\alpha_{\text{IR}} \sim 2.4 \Rightarrow$  Class I.
  25. Source identification unclear; candidate source: CRW FIR6c lies on axis defined by 1-32 and 1-39 (alternatively bright star south of 1-42 may be driving source); position and photometry refers to FIR6c; no

- opt./IR counterpart found; IRAS: no point source associated, no source found on HIRES maps (maybe at  $60\ \mu\text{m}$ ), confusion with OMC-1; FIR6c is detected at  $\lambda \geq 350\ \mu\text{m}$  (CRW, LSK, JB); position taken from CRW.  $L_{\text{bol}}/L_{\text{submm}} \leq 300 \Rightarrow$  Class I; IRAS measurements uncertain, possibly also Class 0.
26. Source identification unclear; candidate source: red star at given position; no optical counterpart found (but bright background of Orion nebula); IRAS: confusion with OMC-1; 450/850  $\mu\text{m}$ : source on E-W filament. Tentatively classified as Class II, but SED very poorly defined.
  27. Source presumably at southern end of jet, but not identified; flow position refers to southern end of jet; IRAS: confusion with OMC-1; 450/850  $\mu\text{m}$ : no source found, confusion with OMC-1.
  28. Source presumably east of 2-5 C in Orion-S core, but not identified; flow position refers to 2-6 A; IRAS: confusion with OMC-1; 450/850  $\mu\text{m}$ : no source found, confusion with OMC-1.
  29. Source: faint IR star at base of fan-shaped opt./IR RN; position refers to IR star; star not detected at optical; IRAS: no point source associated, no source found on HIRES maps; detected in JB 450/850  $\mu\text{m}$  maps. Tentatively classified as Class I (obscured at I, visible at K', strong 850  $\mu\text{m}$  emission), but SED poorly defined.
  30. Suspected source: opt./IR star associated with opt./IR RN; position refers to this star; IRAS: no point source associated, no source found on HIRES maps, confusion with emission from Orion nebula; 450/850  $\mu\text{m}$ : no source found. Conservatively classified as Class II, but SED poorly defined (poor IRAS upper limits).
  31. Source identification unclear; suspected source: diffuse IR source at given position; photometry refers to this source (alternatively the flow may be driven by a source somewhere to the north of 3-6); no optical counterpart detected; IRAS: no point source associated, possibly weak 25  $\mu\text{m}$  source on HIRES maps; weak 850  $\mu\text{m}$  source detected in JB maps.  $\alpha_{\text{IR}} \sim 2.7 \Rightarrow$  Class I (measured from 2.1 to 25  $\mu\text{m}$ ).
  32. Suspected source: faint, extended K'-band source  $11''$  to the south of 3-8; no optical counterpart found; IRAS: no point source associated, no HIRES source found; no 450/850  $\mu\text{m}$  source detected in JB maps. Tentatively classified as Class I, very uncertain.
  33. No source identified; suspected source position at NW end of jet; no source detected at opt./NIR; IRAS: no point source associated, no HIRES source found; possibly weak 450/850  $\mu\text{m}$  emission detected in JB maps. IR classification impossible.
  34. No source identified; no nearby IRAS point source or HIRES source; no nearby 450/850  $\mu\text{m}$  source on JB maps.
  35. Source identification unclear; flow position refers to H<sub>2</sub> knot; possibly flow from weak 100  $\mu\text{m}$  IRAS-HIRES source and possibly weak 850  $\mu\text{m}$  source  $40''$  NE; very uncertain.
  36. No source identified; flow position refers to H<sub>2</sub> knot 3-15 A; IRAS: no nearby point source or HIRES source; no nearby 450/850  $\mu\text{m}$  source on JB maps.
  37. No source identified; source presumably south of 3-17 A, flow position refers to H<sub>2</sub> knot 3-17 A; no opt./IR continuum source associated; IRAS: no point source associated, no HIRES source found around and to the south of 3-17 A, confusion with E-W ridge of extended emission.
  38. Source: diffuse K'-band source on jet axis; position refers to this source; no optical counterpart found; IRAS: no point source associated, possibly very weak 25/60  $\mu\text{m}$  source on HIRES maps.  $\alpha_{\text{IR}} \sim 2.2 \Rightarrow$  Class I.
  39. Source identification unclear; flow position refers to H<sub>2</sub> knot 4-7; IRAS: no point source associated, on the HIRES maps there may be a faint 12  $\mu\text{m}$  source at about the position of 4-5 A, and there appears to be 100  $\mu\text{m}$  emission close to the given position.
  40. No source identified; flow position refers to H<sub>2</sub> knot 4-9 A; possibly IRAS 05331-0606 ( $40''$  W,  $130''$  S) is the driving source.
  41. No source identified; flow position refers to H<sub>2</sub> knot 4-10 A; source presumably to the NNW of 4-10.
  42. Source: faint, extended K'-band source, no optical counterpart, position refers to this source; IRAS: associated with faint point source IRAS 05329-0614 (PSC gives detection only at 60  $\mu\text{m}$ ), but possibly also detected as faint 12/25  $\mu\text{m}$  source.  $\alpha_{\text{IR}} \sim 3 \Rightarrow$  Class I.
  43. Suspected source: opt./IR star V 1296 Ori; IRAS: point source IRAS 05334-0611. Saturated on K'-band images  $\Rightarrow \alpha_{\text{IR}}$  poorly constrained, presumably slightly smaller than 0  $\Rightarrow$  Class II (flat spectrum source).



44. No source identified; source presumably to the NW of 5-3; flow position refers to H<sub>2</sub> knot 5-3 A; no IRAS point source or HIRES source found NW of 5-3.
45. Suspected source: IR star at given position associated with faint opt./IR RN; IRAS: no point source associated, possibly very weak 25/60 μm source in HIRES maps. Presumably IR Class I ( $\alpha_{\text{IR}} \sim 1$ ,  $\lambda = 2.1 \dots 25 \mu\text{m}$ ).
46. Source: HH 304 IRS: IR star associated with bipolar opt./IR RN; IRAS: no point source associated, no source found on HIRES maps. Tentatively classified as Class I ( $\alpha_{\text{IR}} < 1$ , not well constrained, but very red at opt./IR).
47. No source identified; flow position refers to H<sub>2</sub> knot 5-6 B; source presumably to the NNW of 5-6; IRAS: no point source or HIRES source in that direction.
48. No source identified; flow position refers H<sub>2</sub> knot to 5-9 D; source possibly to the SW of 5-9 B between 5-9 and 5-19; IRAS: no point source or HIRES source in that direction
49. Source in L 1641-N cluster, source identification ambiguous; suspected source: diffuse K'-band nebula at given position, no optical counterpart detected; detected as 10 μm source (0.7 Jy) with TIMMI; IRAS: point source IRAS 05338–0624 associated, but confusion with other sources in cluster likely; submm/mm emission detected at  $\lambda = 350 \mu\text{m}$  to 1.3 mm (Zavagno et al. 1997, Dent et al. 1998), which however probably originates mainly from other sources in the cluster (in particular Chen et al. (1993b) source N1; see # 53).  $\alpha_{\text{IR}} \sim 3 \Rightarrow$  (very early) Class I.
50. No source identified; suspected source position between 5-15 A/B and 5-15 C/D; at this position no IRAS point source or HIRES source is found (confusion with IRAS 05338–0624 at 60/100 μm; see # 49); no 1.3 mm source found.
51. Source: mm-peak at given position (3); located between 5-16 A and B at apex of V-shaped K'-band RN; IRAS: no point source associated, weak 12/25 μm source resolved on HIRES maps, at 60/100 μm confusion with IRAS 05338–0624 (see # 49). Tentatively classified as (early) Class I ( $\alpha_{\text{IR}} \gtrsim 3$ ).
52. No source identified; source presumably somewhere in L 1641-N cluster; flow position refers to center of cluster.
53. Source identification unclear; suspected source: Chen et al. (1993b) source N1 (a few arcseconds SW of 5-14 C); not detected at 10 μm with TIMMI (fluxlimit 0.2 Jy); IRAS: point source IRAS 05338–0624 associated, but presumably confusion with other sources in cluster (in particular # 49); submm/mm emission detected from cluster region at  $\lambda = 350 \mu\text{m}$  to 1.3 mm (Zavagno et al. 1997; Dent et al. 1998), which probably originates mainly from this source as is indicated by interferometric 2 mm measurements (Chen et al. 1996); submm/mm fluxes measured for the region will be attributed to this source, but confusion with other sources in cluster is likely (see also # 49, 50, 51, 54); submm/mm fluxes taken from Zavagno et al. (1997). Conservatively classified as Class I ( $\alpha_{\text{IR}} \gtrsim 3.5$ ), but NIR SED not well defined; possibly Class 0 ( $L_{\text{bol}}/L_{\text{submm}} \sim 80$ ); confusion!
54. Suspected source: red star associated with bipolar opt./IR RN resembling star+edge-on disk/flattened envelope; IRAS: no point source associated, no source found in HIRES maps, confusion with other sources in L 1641-N possible (see also # 49, 50, 51, 53); not detected on 1.3 mm map (3).  $\alpha_{\text{IR}} < 0 \Rightarrow$  Class II
55. Source: HH 34 IRS; opt./IR star associated with opt./IR RN; detected at 10 μm with TIMMI (0.35 Jy); IRAS: point source IRAS 05329–0628 60'' W, peak position at 25 μm coincident with position of HH 34 IRS on HIRES maps, at 60 μm the peak is shifted a bit to the west, at 100 μm the peak position seems to be at the position of HH 34 IRS again; detected at submm/mm wavelengths (Reipurth et al. 1993a; Dent et al. 1998).  $\alpha_{\text{IR}} \sim 1.7 \Rightarrow$  Class I
56. Source identification unclear; there is a faint star at the northern as well as at the southern end of the jet; position refers to middle of the jet; IRAS: no point source associated, no source found on HIRES maps; no 1.3 mm source associated.
57. Suspected source: opt./IR star BE Ori (not certain) associated with small optical RN; IRAS: point source IRAS 05345–0635.  $\alpha_{\text{IR}} \sim -0.55 \Rightarrow$  Class II.
58. Source: star associated with small fan-shaped IR RN; no optical counterpart detected; IRAS: no point source associated, no HIRES source found. Tentatively classified as Class I because of very red opt.-K-band SED; spectral index derived from K-band photometry and IRAS 12/25 μm upper limits consistent with Class I.

59. Source: V 380 Ori NE MMS located on jet axis (own 1.3 mm map); not detected at opt./NIR wavelengths; IRAS: confusion with extended E–W ridge of MIR/FIR emission, point sources IRAS 05342–0639 and IRAS 05339–0641 associated with E–W ridge, at 100  $\mu\text{m}$  the peak of emission seems to be very close to the position of the 1.3 mm source on the HIRES maps with a flux of order 50–100 Jy; detected at  $\lambda = 450 \mu\text{m}$ –1.3 mm (Zavagno et al. 1997).  $L_{\text{bol}}/L_{\text{submm}} < 30 \Rightarrow$  Class 0.
60. Source identification unclear; possibly V 380 Ori or some unknown nearby source; flow position refers to NE H<sub>2</sub> knot of 6-7
61. Source: weak, possibly slightly extended K'-band source coincident with H<sub>2</sub> knot 6-13; no optical counterpart detected; IRAS: point source IRAS 05338–0647 17'' south probably associated with outflow source, but confusion with other sources in V 380 Ori/HH 1/2 region likely, peak of 25  $\mu\text{m}$  emission on HIRES maps seems to be at position of the K'-band source, at 60/100  $\mu\text{m}$  confusion; detected as mm source as HH 1/2 MMS2 (Chini et al. 1997a) at  $\lambda = 450 \mu\text{m}$ –1.3 mm (Zavagno et al. 1997; Dent et al. 1998). H<sub>2</sub>O maser, HH 1/2 VLA3 (Pravdo et al. 1985).  $\alpha_{\text{IR}} \sim 3 \Rightarrow$  (very early) Class I.
62. Jet and source both very uncertain; suggested source: opt./IR quasi-continuum source at tip of HH 1 (probably an emission line object bright enough to appear bright even in the continuum filter, possibly with some high excitation lines located in the continuum filter).
63. Suspected source: opt./IR star N<sup>3</sup>SK50 (HH 147 IRS; Corcoran & Ray 1995), associated with faint extended optical RN; IRAS: point source IRAS 05339–0646, at 60/100  $\mu\text{m}$  confusion with other sources in V 380 Ori/HH 1/2 region; detected as HH 147 MMS (Chini et al. 1997a) at  $\lambda = 350 \mu\text{m}$  . . . 1.3 mm (Zavagno et al. 1997; Dent et al. 1998).  $\alpha_{\text{IR}} \sim -0.1 \Rightarrow$  (very early) Class II (flat spectrum source).
64. Source: HH 1/2 VLA1 (Pravdo et al. 1985); source itself not detected at opt./NIR wavelengths, but opt./K'-band RN a few arcseconds to the NW; not detected at 10  $\mu\text{m}$  with TIMMI (fluxlimit 0.15 Jy); IRAS: confusion with other sources in V 380 Ori/HH 1/2 region, no point source directly associated, weak ( $\sim 1.5$  Jy) source resolved on HIRES maps, at 60/100  $\mu\text{m}$  confusion with other sources in V 380 Ori/HH 1/2 region; detected at  $\lambda = 450 \mu\text{m}$  . . . 1.3 mm (Dent et al. 1998; Reipurth et al. 1993a; Chini et al. 1997a); probably confusion with HH 1/2 VLA2 (see #65).  $L_{\text{bol}}/L_{\text{submm}} \sim 50 \Rightarrow$  Class 0; associated with NIR/opt RN  $\Rightarrow$  may also be extreme Class I source.
65. Suspected source: HH 1/2 VLA2; not detected at opt./NIR wavelengths; not detected at 10  $\mu\text{m}$  with TIMMI (fluxlimit 0.15 Jy); IRAS: no point source directly associated, confusion with other sources in V 380 Ori/HH 1/2 region at all 4 IRAS bands; submm/mm: confusion with HH 1/2 VLA1 (see #64).
66. No source identified (and flow identification very uncertain); there are several NIR/IRAS/mm sources on or close to suspected jet axis; flow position refers to H<sub>2</sub> knot 7-2 A
67. Source: HH 43 MMS1; no opt./NIR counterpart found; IRAS: no point source in PSC, but HIRES maps resolve 60/100  $\mu\text{m}$  source (IRAS 05355–0709C, Cohen 1990); source detected at 1.3 mm (Stanke et al. 2000), compact but possibly slightly extended.  $L_{\text{bol}}/L_{\text{submm}} \sim 11 \Rightarrow$  Class 0.
68. Source: HH 43 IRS1, IR star associated with bipolar IR RN (Moneti & Reipurth 1995); star not detected at optical wavelengths, RN very faintly visible, presumably star+disk/flattened envelope seen edge on; IRAS: point source IRAS 05357–0710 detected in all IRAS bands (no flux given for 100  $\mu\text{m}$  band in PSC, but detected in HIRES maps; Cohen 1990); detected at 1.3 mm (Reipurth et al. 1993a) and at 450/800  $\mu\text{m}$  (Dent et al. 1998).  $\alpha_{\text{IR}} \sim 0.3 \Rightarrow$  Class I.
69. Suspected source: IR star associated with fan-shaped IR RN; IRAS: possibly associated with point source IRAS 05367–0712 54'' to the W, possibly weak 12/25  $\mu\text{m}$  emission from NIR source, but confusion with IRAS 05367–0712; possibly weak 1.3 mm source (3); there may be 2 young stars (one the NIR source, the second the IRAS point source), driving two flows (7-13 from the NIR source, 7-12 from the IRAS point source). Classified as Class I, since it seems to be extremely red ( $I-K' > 6$ ) and possibly detected at IRAS 12/25  $\mu\text{m}$ .
70. Source: opt./IR star HBC 491 associated with opt./IR RN (Strom et al. 1986); IRAS: point source IRAS 05363–0714; not detected on 1.3 mm map (3).  $\alpha_{\text{IR}} \sim 0.15 \Rightarrow$  Class I (flat spectrum source).
71. Source: nebulous K'-band source between H<sub>2</sub> knots; IRAS: no point source associated, possibly very faint 25  $\mu\text{m}$  source seen on HIRES maps; not detected on 1.3 mm map (3). Tentatively classified as Class I based on spectral index as derived from the K'-band measurement and possible IRAS 25  $\mu\text{m}$  detection.

72. Suspected source: Haro 4-255 FIR (Evans et al. 1986); faint opt. nebulosity, bright NIR nebulosity, position refers to K'-band peak; IRAS: point source IRAS 05369–0728 associated (but confusion with Haro 4-255; see # 73), on the HIRES maps, the peak at 25/60/100  $\mu\text{m}$  seems to be at the position of the FIR source rather than Haro 4-255, the flux at these wavelengths is thus attributed to the FIR source; detected on 1.3 mm map (3).  $\alpha_{\text{IR}} \sim 1 \Rightarrow$  Class I.
73. Suspected source: opt./IR star Haro 4-255 associated with opt. RN; IRAS: point source IRAS 05369–0728 associated, but flux at 25/60/100  $\mu\text{m}$  seems to be at the position of Haro 4-255 FIR rather than Haro 4-255; only flux at 12  $\mu\text{m}$  is attributed to Haro 4-255 (see #72); weak 1.3 mm emission associated (3).  $\alpha_{\text{IR}} \sim -0.6 \Rightarrow$  Class II.
74. Suspected source: very faint K'-band source between H<sub>2</sub> knots; optical counterpart at detection limit; IRAS: no point source associated, no source visible on HIRES maps; not on 1.3 mm map. Conservatively classified as Class II (optical emission seen), but possibly very low luminosity Class I object.
75. No source identified; flow position refers to middle between 9-3 A and B; there are two K'-band sources which may be associated with the H<sub>2</sub> emission; IRAS: no nearby point source, no source found on HIRES maps; area directly around H<sub>2</sub> features not on 1.3 mm map.
76. Source: L 1641-S3 MMS1; slightly extended K'-band source associated (see also Chen & Tokunaga 1994), not detected at optical wavelengths; IRAS: point source IRAS 05375–0731 associated; position refers to peak position on 1.3 mm map; millimetre source detected at  $\lambda = 350 \mu\text{m}$ . . . 1.3 mm (Zavagno et al. 1997; Dent et al. 1998; Stanke et al. 2000).  $L_{\text{bol}}/L_{\text{submm}} \sim 80-90 \Rightarrow$  Class 0; detection in short IRAS bands and association with K' nebulosity suggests that this source may be approaching the Class I stage already.

## C.3 Spectral energy distributions

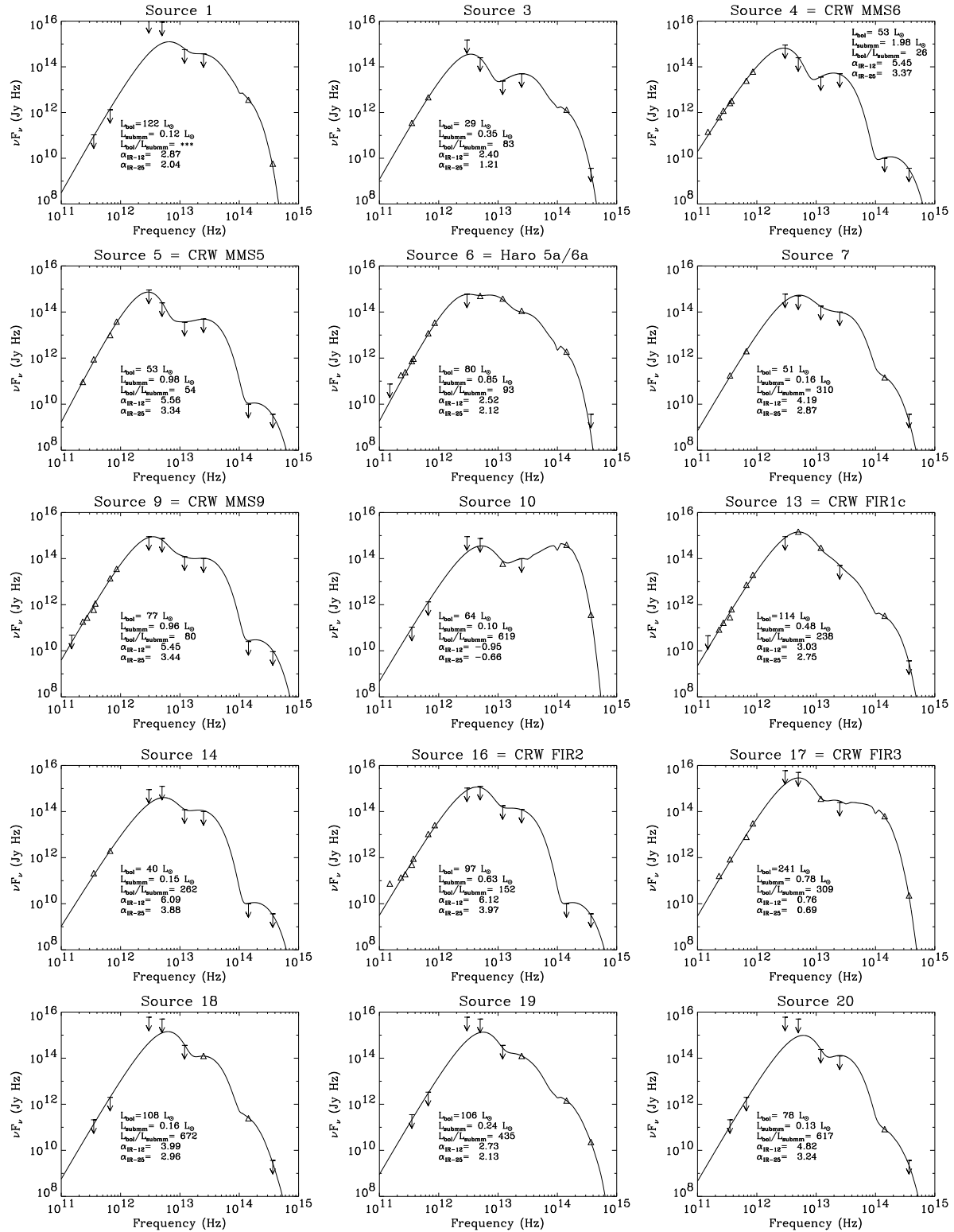


Figure 66: Spectral energy distributions of candidate outflow driving sources.

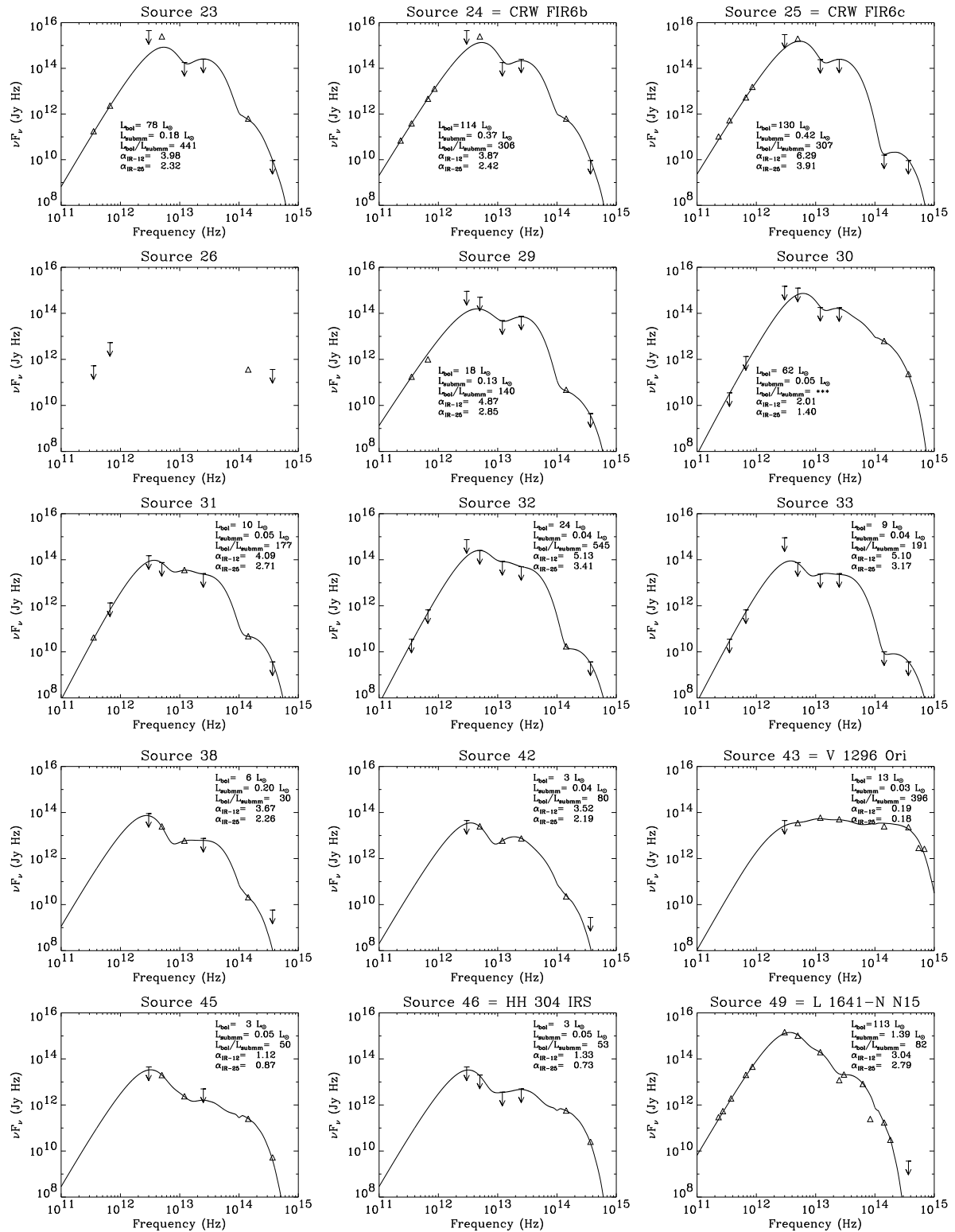


Figure 67: Continued: Spectral energy distributions of candidate outflow driving sources.

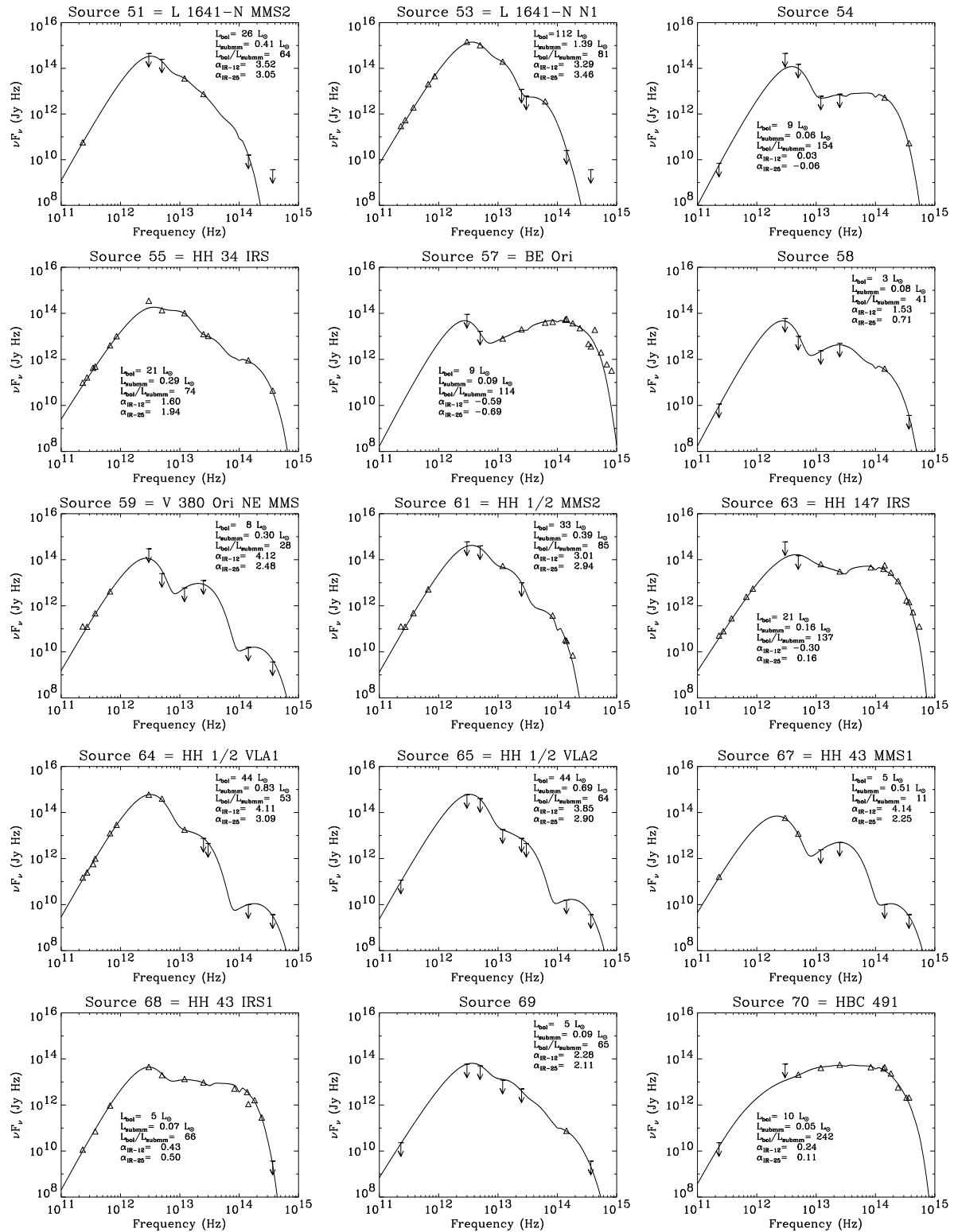


Figure 68: Continued: Spectral energy distributions of candidate outflow driving sources.

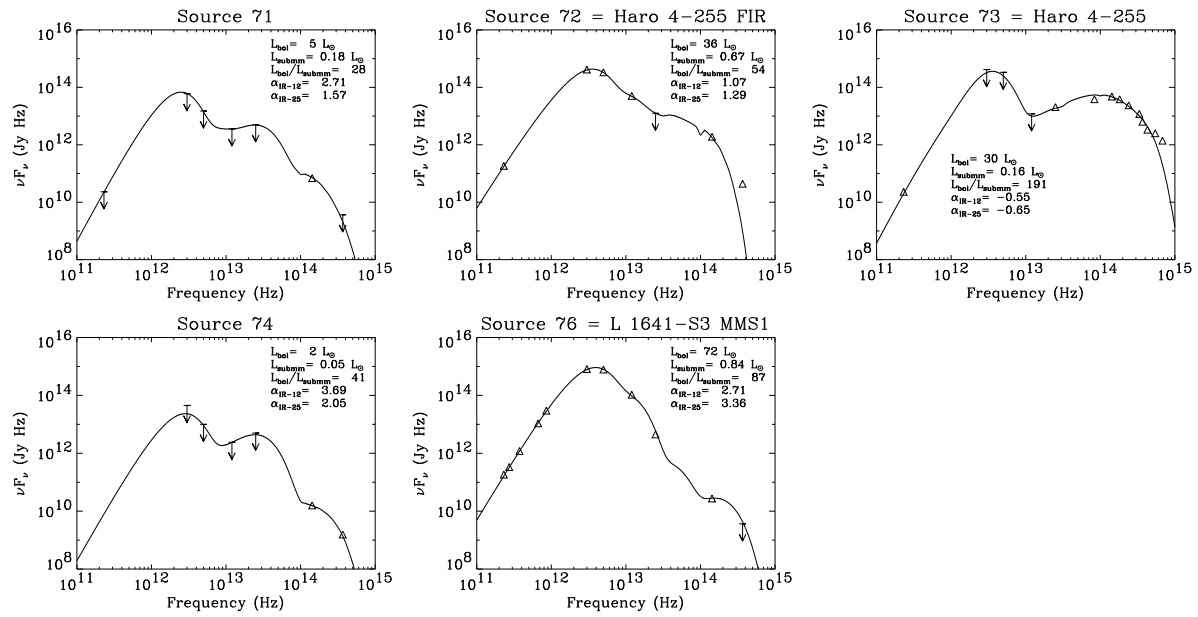


Figure 69: Continued: Spectral energy distributions of candidate outflow driving sources.

## D H<sub>2</sub> jets and molecular (CO) outflows: Details

A number of molecular (CO) outflows are known in the survey area. Here I will compare the H<sub>2</sub> data to existing maps of molecular outflows in Orion (usually taken in the <sup>12</sup>CO  $J=1-0$  line). As noted in Section 2.2 the term “molecular outflow” will be reserved for the CO outflows, in which the bulk of the material is seen in CO, rather than for the H<sub>2</sub> jets, in which only shock heated molecular gas is seen.

**The OMC-1 outflow** (Kwan & Scoville 1976; Zuckerman et al. 1976; Solomon et al. 1981; Erickson et al. 1982) is well known to be associated with H<sub>2</sub> emission (Gautier et al. 1976; Beckwith et al. 1978a). The H<sub>2</sub> emission in this case is found in a system of clumps and fingerlike jets suggestive of an almost spherically symmetric outflow (Taylor et al. 1984; Allen & Burton 1993; McCaughrean & MacLow 1997; Schultz et al. 1999). This feature is seen in the upper part of Fig. 71.

**OMC-2/3.** Besides the extremely energetic OMC-1 outflow, some other molecular outflows are known in the northern part of the survey area. Evidence for high velocity molecular gas in the OMC-2/3 region has been reported by Fischer et al. (1985), Castets & Langer (1995), Chini et al. (1997b), Aso et al. (2000), and Yu (2000). The clustered environment in this area makes it difficult to disentangle the outflows: Yu et al. (1997) report the presence of about a dozen collimated H<sub>2</sub> flows in the area. In Fig. 70 the contours indicating high velocity molecular gas (adopted from Chini et al. 1997b) are superposed on the H<sub>2</sub> mosaic of the OMC-2/3 area. Starting to the north, an irregular distribution of blueshifted gas with some blobs of redshifted gas scattered in is seen in the area of the H<sub>2</sub> flows #2, #3, #4, and #5. The multitude of H<sub>2</sub> flows and the absence of redshifted molecular gas make it difficult to associate H<sub>2</sub> flows with the features seen in CO. A maximum in CO emission is seen very close to the flow #2, possibly suggesting an association of these two features. The general east-west orientation of the blueshifted CO emission makes flow #3 a likely H<sub>2</sub> counterpart to the CO flow. On the other hand, the brightest part of the CO emission extends from the area of H<sub>2</sub> flow #5 to the north-east towards the group of H<sub>2</sub> features SMZ 1-3 (which is assigned to flow #3). At the eastern end of H<sub>2</sub> flow #5, an elliptical H<sub>2</sub> knot points in a north-eastern direction, and H<sub>2</sub> feature SMZ 1-3A might be interpreted as a bow shock in a flow coming from south-west: possibly there is yet another flow in this area, in addition to those listed in Appendix B. Further south, a small blueshifted and a brighter redshifted blob are found to the west of the bipolar reflection nebula Haro 5a/6a. They might well be part of H<sub>2</sub> flow #6, which extends in an east-west direction and is driven by the illuminating source of Haro 5a/6a. Perhaps the most remarkable feature in the high-velocity CO maps is a well developed, bipolar flow located between Haro 5a/6a and the bright H<sub>2</sub> flow #9. Chini et al. suggested MMS 8 right in the middle between both lobes as driving source. No H<sub>2</sub> emission is found in the blueshifted lobe. Yu (2000) also present high velocity CO maps of the OMC-2/3 area. He notes that there seems to be a shift in coordinates between his data and the map by Chini et al. In the maps presented by Yu (2000), the CO outflow is located  $\sim 30''$  further south, including at its southern edge the well developed western lobe of the H<sub>2</sub> flow #9. Feature SMZ 1-16 appears to be associated with the peak of the redshifted lobe. The suggested H<sub>2</sub> flow #8 might be the H<sub>2</sub> counterpart to the redshifted lobe of the CO flow. However, another lobe of blueshifted emission is found to the south-west of the redshifted lobe, possibly forming an alternative bipolar flow at a position angle of  $\sim 60^\circ$ . It might originate in the area around MMS 10 or the bright infrared source seen in the blue lobe. The suggested H<sub>2</sub> flow #10 may be an H<sub>2</sub> counterpart to this alternative CO flow. But again, the region is very confused and complicated. To the south of H<sub>2</sub> flow #9, another blob of blueshifted emission is found. It might be associated with H<sub>2</sub> flow #7, #11, or #13. To the south of this blueshifted blob, another redshifted blob is found. It might be associated with H<sub>2</sub> flow #15. Bright blue- and redshifted emission is seen superposed on the H<sub>2</sub> flow #17 and the general surroundings of the OMC-2 cluster. This is the known OMC-2 outflow (Fischer et al. 1985). Finally, the northern end of H<sub>2</sub> flow #25 might be associated with some blueshifted molecular gas.



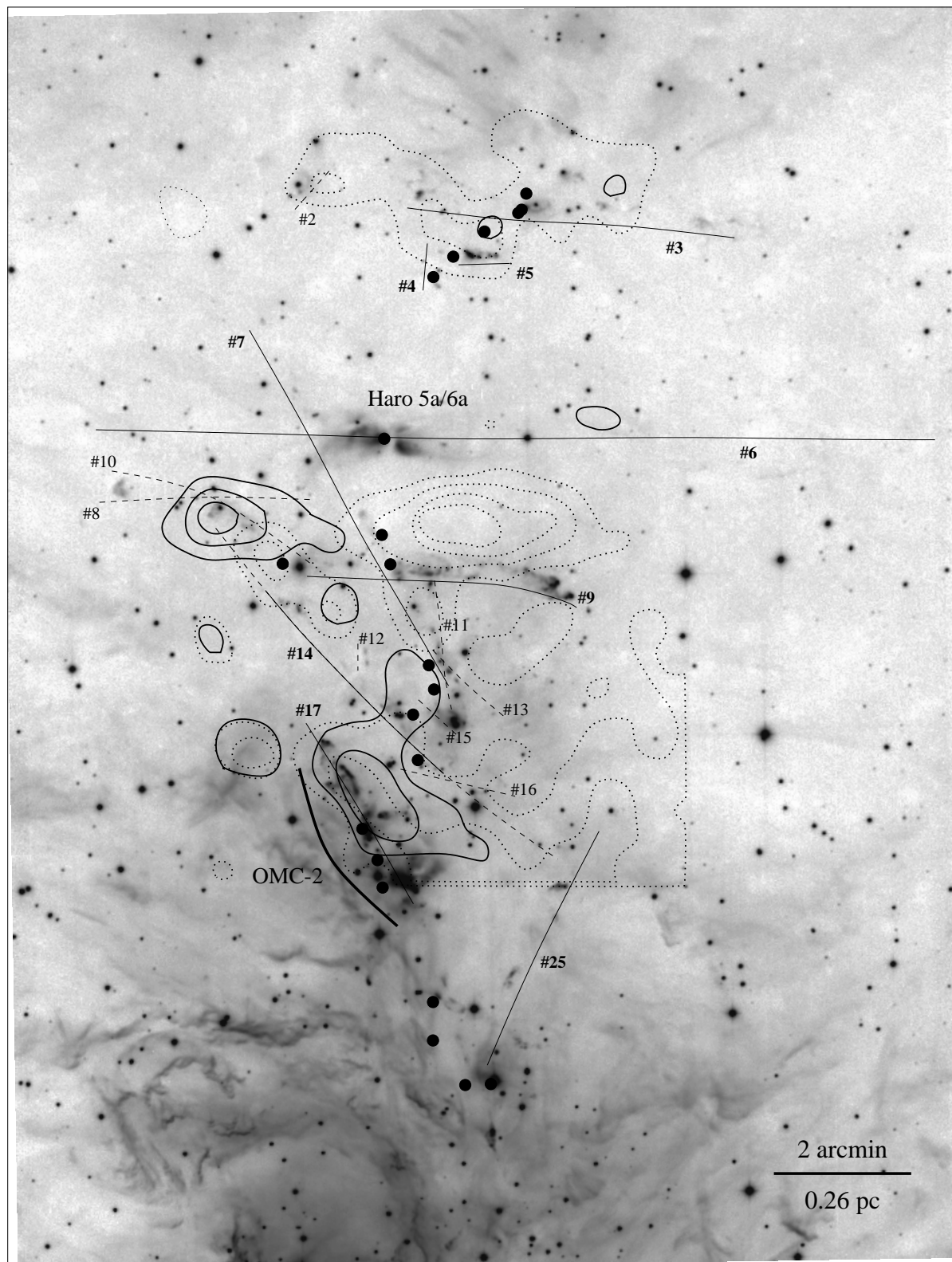


Figure 70: Distribution of high velocity molecular gas (adopted from Chini et al. 1997b) superposed on the  $2.12\mu\text{m}$  mosaic of survey field 1. Blueshifted gas is marked by the dotted contours, redshifted gas by the solid contours. The black dots mark the positions of the 1.3 mm continuum sources found by Mezger et al. (1990) and Chini et al. (1997b).

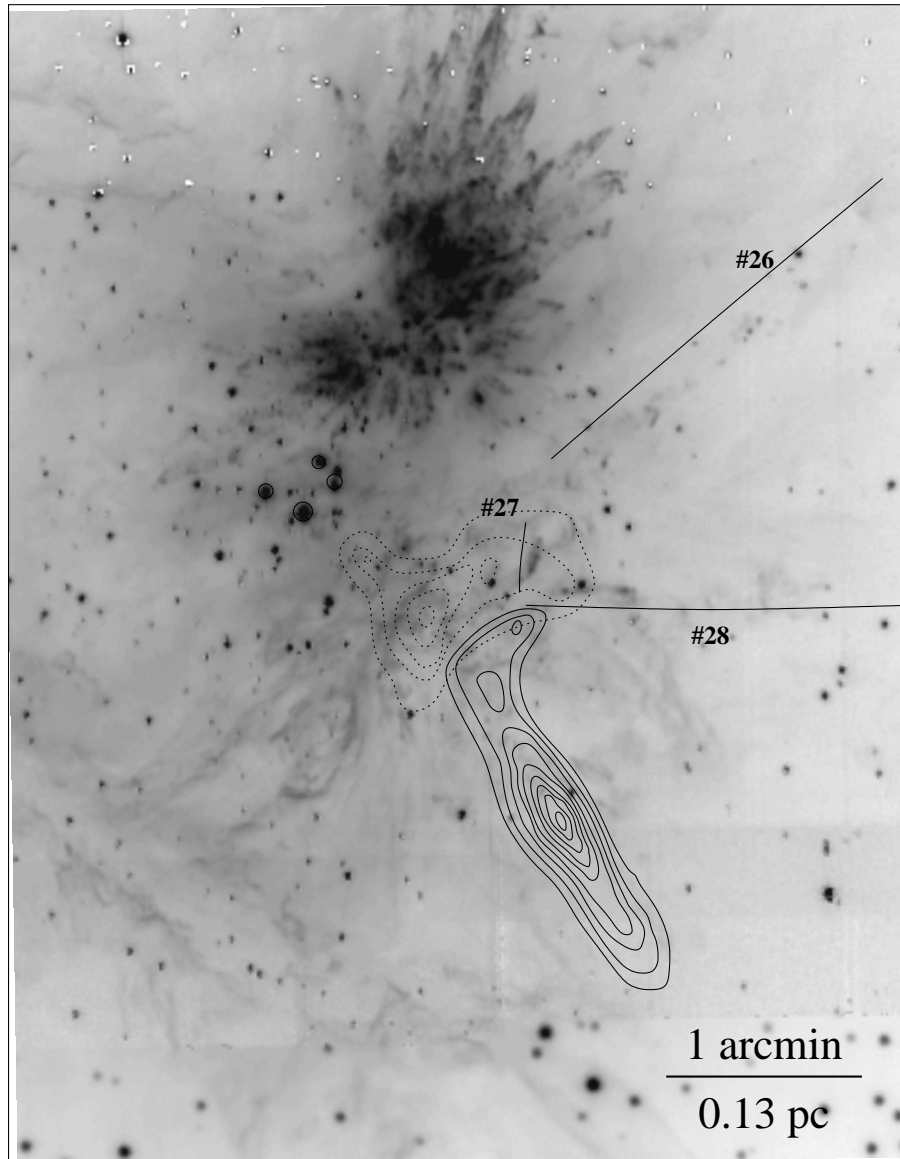


Figure 71: Distribution of high velocity molecular gas (adopted from Schmid-Burgk et al. 1990) superposed on a  $2.12\mu\text{m}$  image of the Orion Nebula/OMC-1 area (the continuum subtracted H<sub>2</sub> image is from new data taken recently). Blueshifted gas is marked by the dotted contours, redshifted gas by the solid contours.

**OMC-1S.** Some more evidence for outflow activity is found in OMC-1 besides the outflow from the BN-KL area. Wilson & Mauersberger (1991) report evidence for a high velocity CO emission source two arcminutes north of BN-KL, which is however located in a very confused region in the outskirts of the BN-KL H<sub>2</sub> finger system. Another molecular outflow is found about 2 arcminutes south of BN-KL (OMC-1S; see Ziurys & Friberg 1987; Ziurys et al. 1990; Schmid-Burgk et al. 1990). Fig. 71 shows the high-velocity CO contours superposed on a continuum subtracted  $2.12\mu\text{m}$  image of the OMC-1 area, including the BN-KL area and its outflow and the centre of the Orion Nebula around the Trapezium stars. No H<sub>2</sub> features are found in the well collimated redshifted lobe of the CO jet. Rather fluffy, filamentary H<sub>2</sub> emission is found in the area of the blueshifted counterlobe, but this is more likely to be fluorescent emission from gas exposed to the intense UV radiation of the Trapezium stars. The absence of H<sub>2</sub> emission from the jetlike redshifted CO lobe may be due to extinction, as the receding jet lobe protrudes deep into the dense cloud in this area. The blue CO lobe shows a somewhat fainter extension towards the west, and a similar extension is also seen in the redshifted lobe. These features suggest the presence of additional CO outflows in the area. The H<sub>2</sub> flows #27 and #28 seem to be the counterparts to this additional CO flow(s).

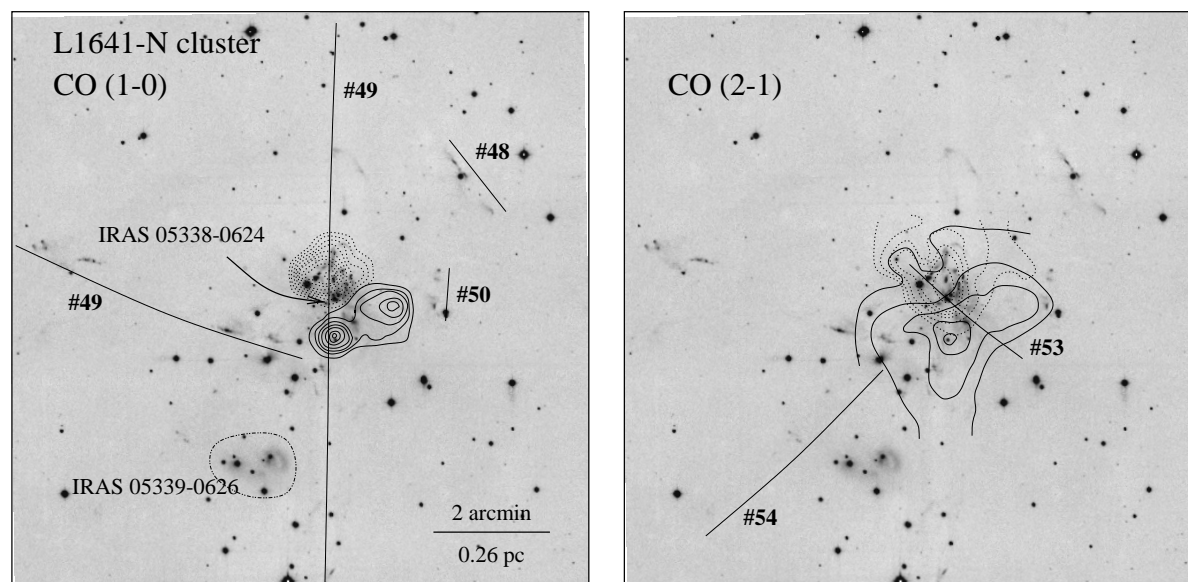


Figure 72: Distribution of high velocity molecular gas in the area of the L1641-N embedded infrared cluster (left panel: CO (1–0) contours adopted from Fukui et al. 1988; right panel: CO (2–1) contours adopted from Wilking et al. 1990b) superposed on a 2.12  $\mu\text{m}$  image of the L1641-N cluster (see also Davis & Eisloffel 1995 for a similar figure). Blueshifted gas is marked by the dotted contours, redshifted gas by the solid contours.

The L1641-N bipolar molecular CO outflow was discovered by Fukui and coworkers in their unbiased search for CO outflows in various molecular clouds (Fukui et al. 1986; 1988; Fukui 1988, 1989). It is centred on IRAS 05338–0624, which is associated with a dense embedded cluster seen at near infrared wavelengths (Strom et al. 1989a; Chen et al. 1993b; Hodapp & Deane 1993). The map of high velocity molecular gas presented by Fukui et al. (1986; 1988) is superposed on a 2.12  $\mu\text{m}$  image of the L1641-N cluster in Fig. 72 (left panel; see also Davis & Eisloffel 1995). The right panel of Fig. 72 shows an overlay of the map presented by Wilking et al. (1990b), which covers a somewhat larger area. The structure seen in both maps is similar. The redshifted lobe has a maximum south of the cluster, and a secondary peak west of the cluster. The blueshifted lobe is more compact, but shows signs of substructure, too. The Wilking et al. map suggests a main component extending roughly north-south, plus a secondary component extending from the cluster centre towards the north-east. The redshifted lobe appears to continue to the south of the area mapped by Wilking et al.; this is confirmed on a more recent map presented by Reipurth et al. (1998) which covers a much larger area (see Fig. 73). High velocity CO emission was also detected at the position of IRAS 05338–0624 (i.e., the L1641-N cluster) and IRAS 05339–0626 (the nebulous group of infrared sources south of the L1641-N cluster) by Morgan & Bally (1991). Morgan et al. (1991) pointed out that the predominantly redshifted emission in IRAS 05339–0626 might be the continuation of the redshifted lobe of the L1641-N outflow. Thus there seems to be a dominant north-south molecular outflow from the L1641-N cluster, plus some additional high velocity gas, possibly indicating another flow running from south-west to north-east. The dominant north-south outflow can be identified with the  $\text{H}_2$  flow #49, which extends over more than 4 pc to the south of the cluster, and is presumably driven by a nebulous near-infrared and 10  $\mu\text{m}$  source (Stanke et al. 1998, 2000). The northern lobe is seen as a chain of Herbig-Haro objects extending over 6.3 pc (Reipurth et al. 1998; Mader et al. 1999).

The possible second outflow might be associated with the  $\text{H}_2$  flow #53. It is presumably driven by the dominant millimetre and radio continuum source in the L1641-N cluster (L1641-N VLA, L1641-N MMS1; Wilking et al. 1989; McMullin et al. 1994; Chen et al. 1995, 1996). Evidence for an outflow at a position angle of  $\sim 45^\circ$  has also been reported by McMullin et al. (1994): they observe SiO emission (a shock tracer) to the north-east and south-west of the millimetre continuum source, as well as red-shifted CS emission to the south-west and blue-shifted CS emission to the north-east of the millimetre continuum source. The north-eastern blueshifted CS peak is almost coincident with the  $\text{H}_2$  feature SMZ 5-14A1, which resembles a bright bow shock heading due north-east. The position angle of this system of  $\sim 45^\circ$  makes a connection with the large scale north-south oriented L1641-N giant flow unlikely. There seem to be two molecular outflows with sources at the heart of the L1641-N cluster, one associated with the L1641-N giant flow ( $\text{H}_2$  flow #49), and a second one associated with

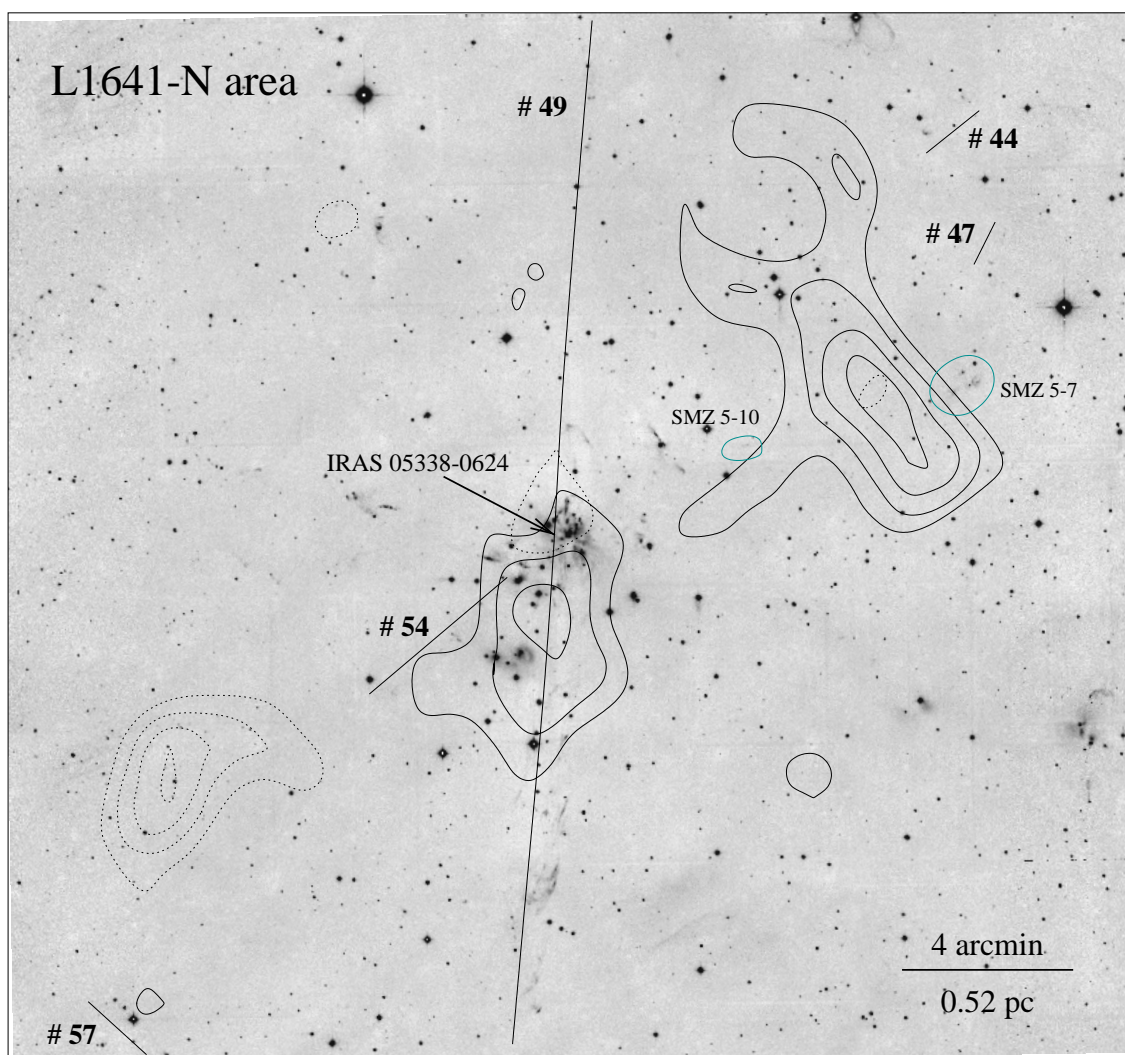


Figure 73: Distribution of high velocity molecular gas (adopted from Reipurth et al. 1998) superposed on a large scale 2.12  $\mu\text{m}$  image of the L1641-N area. Blueshifted gas is marked by the dotted contours, redshifted gas by the solid contours.

the shorter H<sub>2</sub> flow #53. Note that even more Herbig-Haro and H<sub>2</sub> flows seem to have their origin in or near the cluster (Reipurth et al. 1998; Mader et al. 1999; H<sub>2</sub> flows #51, #52).

The wide field map of high velocity CO presented by Reipurth et al. (1998) shows two additional large features: a redshifted lobe is found to the north-west of the cluster, and a blueshifted one southeast of the cluster (see Fig. 73). These two lobes are interpreted as another giant molecular outflow from the L1641-N cluster by Reipurth et al., but no associated Herbig-Haro objects were so far identified. There are some H<sub>2</sub> features which might be related to these outflow lobes. SMZ 5-7 is located at the north-eastern boundary of the redshifted CO lobe, and feature SMZ 5-10 might be associated with the protrusion of the red lobe extending back towards the L1641-N cluster. The small faint H<sub>2</sub> flows #44 and #47, both located to the north-west of the red lobe, both point in a direction towards the big red lobe. Finally, the H<sub>2</sub> flow #54, originating in a bipolar nebulous source located in the outskirts of the L1641-N cluster, points towards the blueshifted lobe (without however reaching it). Thus the driving source of H<sub>2</sub> flow #54 might have created the blue (and possibly red) lobe of this huge bipolar CO configuration in an earlier outflow phase. Finally, a small blob of redshifted emission seen in the lower left corner of Fig. 73 might be associated with H<sub>2</sub> flow #57.

**HH 34.** Figure 74 shows the contours of high velocity CO in the HH 34 region (adopted from Chernin & Masson 1995). The HH 34 system is one of the best examples of a highly collimated, optical Herbig-Haro jet (Reipurth et al. 1986; Mundt et al. 1987). More recently, the HH 34 jet and bow-shock were found to be only the

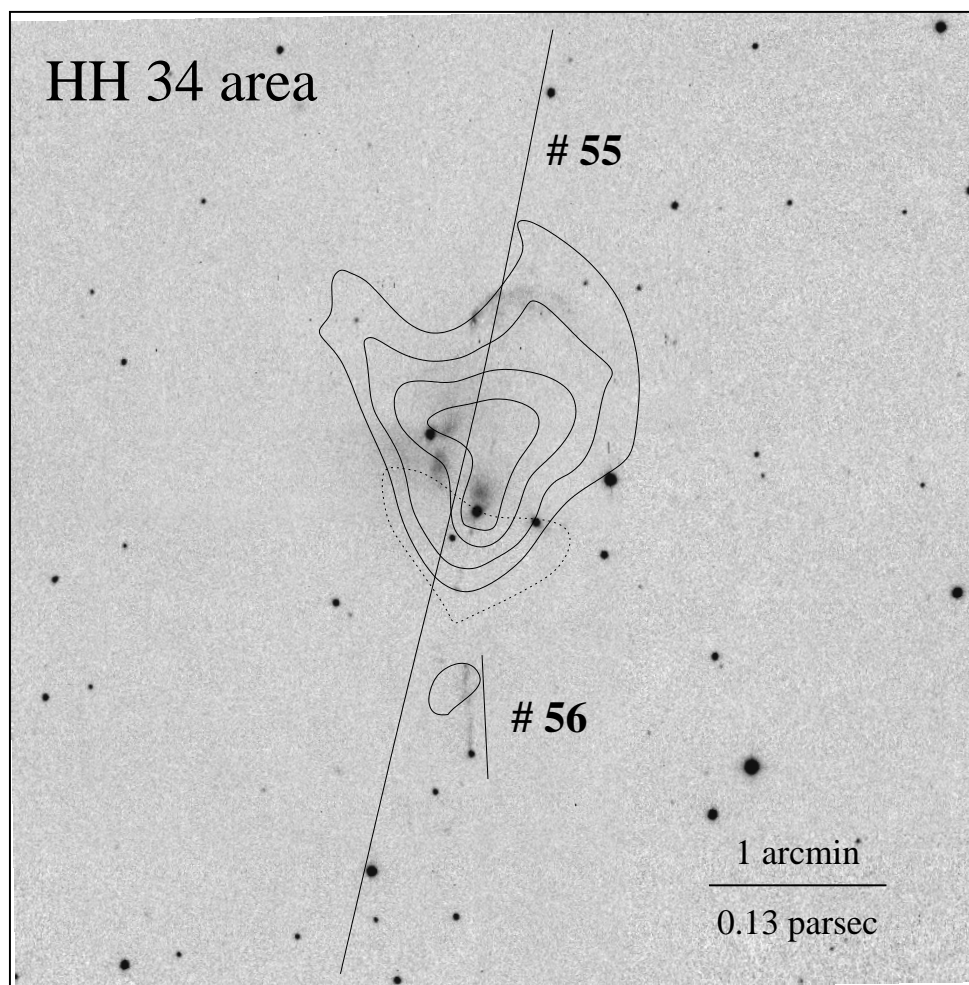


Figure 74: Distribution of high velocity molecular gas (adopted from Chernin & Masson 1995) superposed on a  $2.12\ \mu\text{m}$  image of the HH 34 area. Blueshifted gas is marked by the dotted contours, redshifted gas by the solid contours.

innermost part of a much longer Herbig-Haro jet, the prototypical HH 34 giant flow (Bally & Devine 1994; Devine et al. 1997; Eislöffel & Mundt 1997;  $\text{H}_2$  flow #55). Although it is such a nice example of a well developed jet, Reipurth et al. (1986) did not find evidence for an associated molecular outflow. Only the higher resolution, higher sensitivity data taken by Chernin & Masson (1995) showed a very weak molecular outflow within the bounds of the harbouring cloud core. It was one of the weakest molecular outflows known at that time. The comparison of the  $\text{H}_2$  image with the CO outflow map does not reveal many new features. Maybe the only noteworthy thing is that the diffuse bow SMZ 5-21A seems to be located just at the northern boundary of the redshifted CO lobe, and might represent an entraining bow-shock.

**V 380 Ori/HH 1/2.** The distribution of high velocity gas in the area around V 380 Ori, the illuminating star of NGC 1999, is shown in Fig. 75 (contour map adopted from Morgan et al. 1991). The high velocity CO in the area has been mapped by Edwards & Snell (1984), Levreault (1988a), and Morgan et al. (1991), and was also detected in the unbiased survey by Fukui et al. (1986). The maps all showed that the high velocity CO in the region is mostly redshifted, with one main lobe centred roughly on V 380 Ori, and another roughly north-south elongated lobe extending south of HH 2. These features were generally attributed to V 380 Ori, but the situation in this area is difficult: in contrast to this north-south oriented configuration, Corcoran & Ray (1995) suggested an east-west oriented outflow from V 380 Ori.

The new  $\text{H}_2$  data presented here do not help to pick out a definitive solution. A number of  $\text{H}_2$  features are located within the area of the redshifted CO emission around V 380 Ori (SMZ 6-3, 6-7, and 6-8) or at its edge (SMZ 6-4).  $\text{H}_2$  feature SMZ 6-16 is found at the southern end of the southern CO lobe. The features around

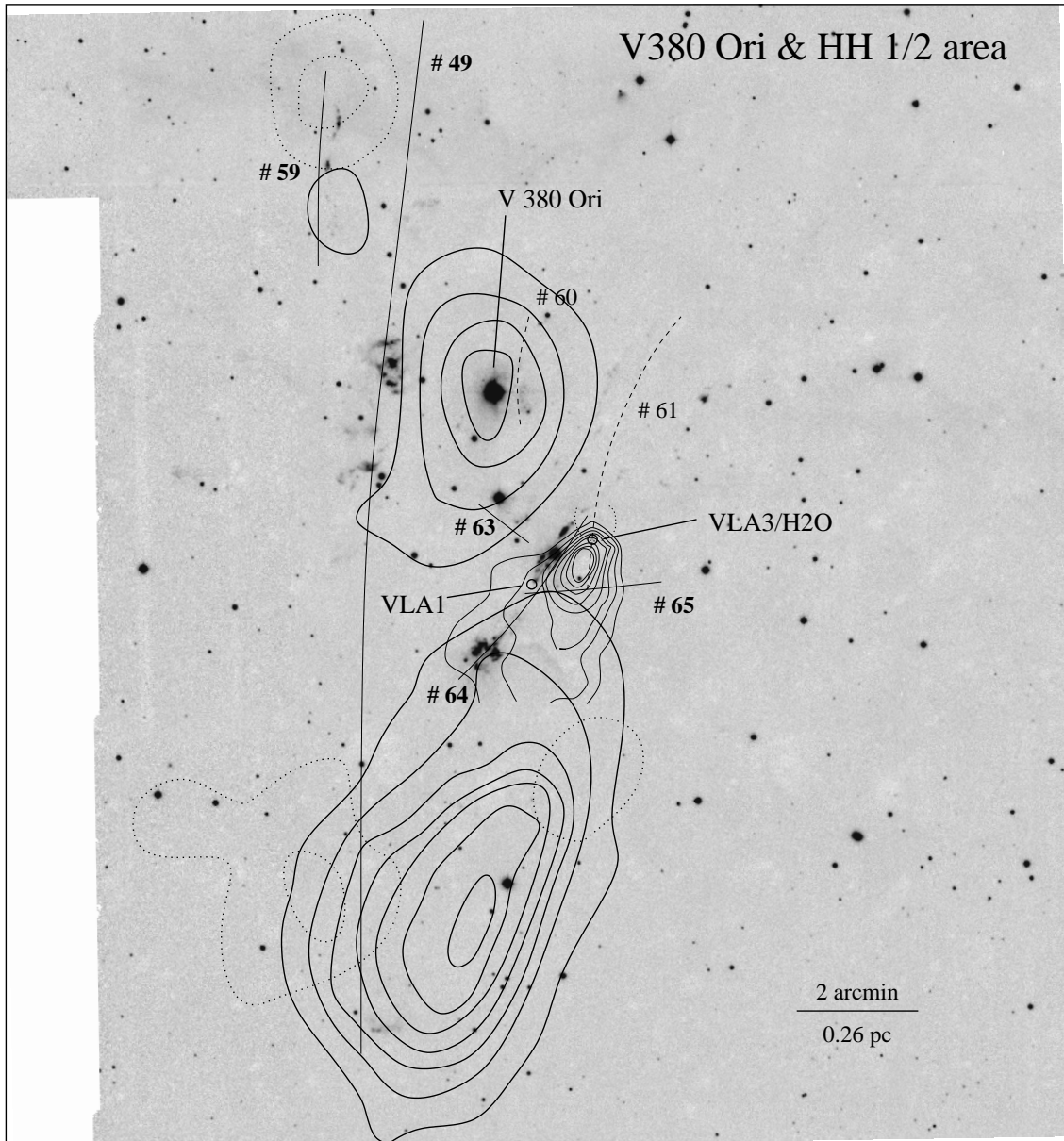


Figure 75: Distribution of high velocity molecular gas (adopted from Morgan et al. (1991; thick contours) and Chernin & Masson (1995; thin contours)) superposed on a large scale  $2.12\mu\text{m}$  image of the HH 1/2 area. Blueshifted gas is marked by the dotted contours, redshifted gas by the solid contours. The circles mark the positions of HH 1/2 VLA1 and HH 1/2 VLA3, which is associated with a water maser (Pravdo et al. 1985).

V 380 Ori may be associated with a flow driven by V 380 Ori (or a source in its vicinity). The H<sub>2</sub> features SMZ 6-4 and SMZ 6-16 are suggested to belong to a giant flow originating in the L1641-N cluster further north. Their location close to or within the redshifted lobes around and to the south of V 380 Ori may imply that part of these lobes are driven not by objects in the surroundings of V 380 Ori, but by the L1641-N giant flow.

**V 380 Ori NE.** The maps presented by Levreault (1988a) and Morgan et al. (1991) revealed an additional bipolar CO structure to the north-east of V 380 Ori, termed the V 380 Ori NE outflow. This feature clearly has an H<sub>2</sub> counterpart in H<sub>2</sub> flow #59. The CO outflow has recently been mapped by Davis et al. (2000b) at higher resolution in the CO  $J=4-3$  transition. The CO outflow appears to be very well collimated and has a S-shaped symmetry which is also evident in the H<sub>2</sub> images. As noted by Davis et al., the bright H<sub>2</sub> features SMZ 5-28A and B have peaks in the CO emission as counterparts, which is taken as evidence for bow-shock entrainment. The faint H<sub>2</sub> knots SMZ 6-1 trace the southern, redshifted CO lobe. The southernmost of these knots coincide with

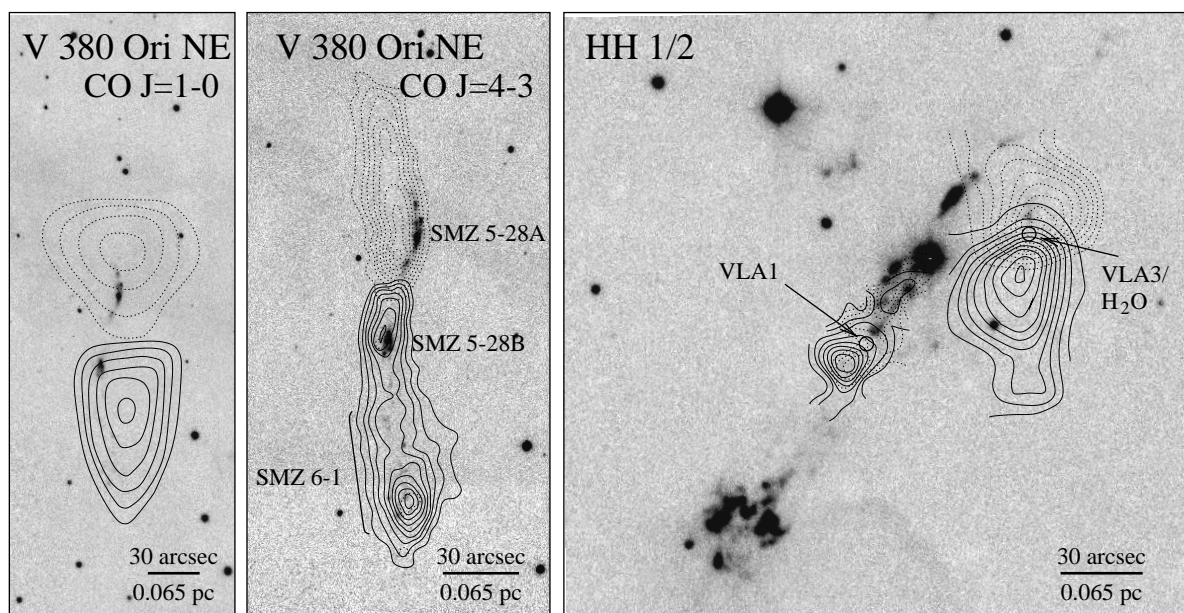


Figure 76: Distribution of high velocity molecular gas in the V 380 Ori NE outflow (left panel: CO  $J=1-0$ ; adopted from Morgan et al. 1991; see also Levreault 1988a; mid panel: CO  $J=4-3$ ; adopted from Davis et al. 2000b) and around HH 1/2 (right panel; adopted from Correia et al. 1997; see also Moro-Martín et al. 1999) superposed on  $2.12\ \mu\text{m}$  images of the respective regions. Blueshifted gas is marked by the dotted contours, redshifted gas by the solid contours.

the southern CO peak in the redshifted lobe (denoted  $R_2$  by Davis et al.) and might correspond to an outer bow shock currently entraining the CO associated with peak  $R_2$ .

**HH 1/2 VLA3.** Further outflow searches towards the HH 1/2 optical jet system (Chernin & Masson 1995; Correia et al. 1997) revealed another bipolar outflow from the VLA 3 source north-west of HH 1/2 VLA1 (the driving source of HH 1/2; see Pravdo et al. 1985). This molecular outflow might have an  $\text{H}_2$  counterpart in flow #61, or might be the origin of some other  $\text{H}_2$  features in the area (SMZ 6-11, SMZ 6-6). It is also tempting to speculate whether this outflow might be seen at larger scales as the redshifted CO lobe south of HH 2. This is suggested by the combination of the large scale CO map by Morgan et al. (1991) and the smaller scale, higher resolution map by Chernin & Masson (1995) as shown in Fig. 75. The  $\text{H}_2$  feature SMZ 6-16 may then represent the terminating working surface of this flow, which would then also be one of the parsec scale flows. Finally, repeated attempts with increasing resolution and sensitivity led to the discovery of high velocity molecular gas associated with the HH 1/2 Herbig-Haro flow (see Fig. 76, right panel; Correia et al. 1997; Moro-Martín et al. 1999;  $\text{H}_2$  flow #64).

**Haro 4-255.** In Fig. 77 the distribution of high-velocity CO around Haro 4-255 is shown superposed on a  $2.12\ \mu\text{m}$  image of the region (see also Davis & Eislöffel 1995). The molecular outflow has been discovered and mapped by Levreault (1988a) and subsequently been mapped at higher resolution by Morgan et al. (1991). It was also detected in the unbiased survey for CO outflows by Fukui et al. (1986). The dominating outflow is not driven by the pre-main-sequence star Haro 4-255, but by a more deeply embedded source to its north-west (Haro 4-255 FIR: Evans et al. 1986). Davis & Eislöffel (1995) suggested the molecular outflow to be actually a superposition of two outflows. More recently, Aspin & Reipurth (2000) found a Herbig-Haro jet and bow-shock (HH 470) originating from Haro 4-255 itself. They also interpret the CO map as being due to two outflows, one driven by the Herbig-Haro flow from Haro 4-255, the other one by the more deeply embedded FIR source. The new  $\text{H}_2$  images presented here resemble those of Davis & Eislöffel (1995), but cover a larger area. The conclusions from the new images largely remain the same. There are at least two active jets in the area. One is the Herbig-Haro jet from Haro 4-255, of which however only the bow shock HH 470A is visible as faint  $\text{H}_2$  feature (SMZ 8-6;  $\text{H}_2$  flow #73).  $\text{H}_2$  feature SMZ 8-3 might be located in the counterlobe of this flow. The second flow is the  $\text{H}_2$  jet from the FIR source also seen by Davis & Eislöffel ( $\text{H}_2$  flow #72). The  $\text{H}_2$  features SMZ 8-2 and SMZ 8-7 might also belong to this flow, making it much larger than previously assumed. It should be kept in mind that a number of knots found in the nebulosity around the embedded FIR source do not have a really satisfying explanation;

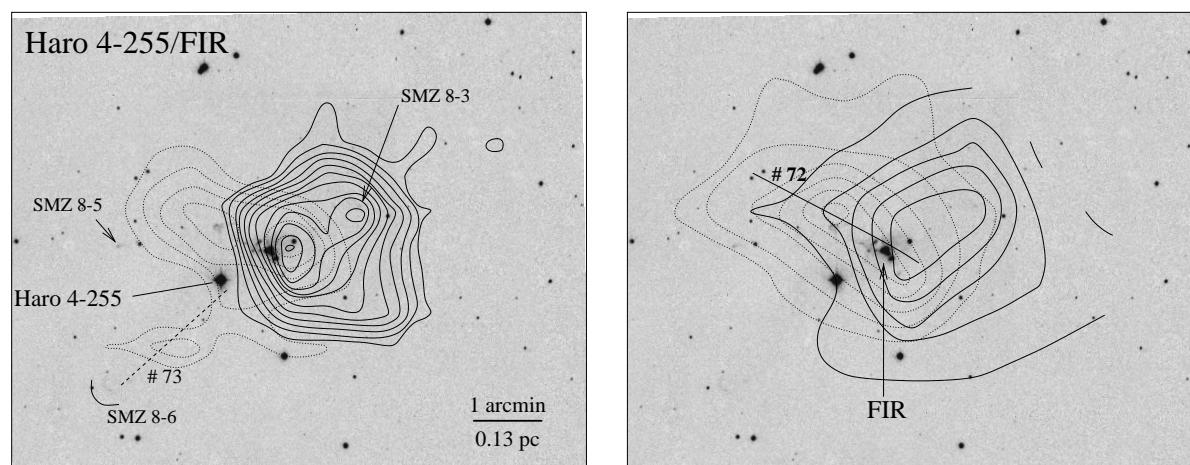


Figure 77: Distribution of high velocity molecular gas in the area around Haro 4-255 (left panel: adopted from Morgan et al. 1991; right panel: adopted from Leveault 1988a), superposed on 2.12  $\mu\text{m}$  images of the respective regions (see also Davis & Eisloffel 1995). Blueshifted gas is marked by the dotted contours, redshifted gas by the solid contours.

possibly even more flows are present. Finally I would like to note that recent 450  $\mu\text{m}$  maps (not shown here) taken with SCUBA at the JCMT have revealed the FIR source to be a double source with an angular separation of order  $10''$ . I will only regard the H<sub>2</sub> flow #72 as certainly associated with high-velocity CO.

**Re 50/L1641-S/L1641-S3.** In Figure 78 the distribution of high velocity CO in the area around the luminous infrared source Re 50 N (= IRAS 05380–0728; Reipurth 1985a; Reipurth & Bally 1986) is shown. An apparently bipolar CO outflow was found centred on this source by Reipurth & Bally (1986) and Fukui et al. (1986) and termed the L1641-S outflow by the latter authors. The outflow was later on mapped by Morgan et al. (1991; their flow MB 40: see also Morgan & Bally 1991).  $3'$  to the south and  $7'9$  to the west the IRAS source IRAS 05375–0731 was found to drive the L1641-S3 outflow (Fukui et al. 1989). It was later on mapped by Morgan et al. (1991; flow MB 41) and Wilking et al. (1990b). The contours in Fig. 78 are adopted from Morgan et al. (1991), and comprise the bipolar outflows MB 40 and MB 41 (Morgan & Bally 1991). The distribution of high velocity gas in the area was interpreted as two independent bipolar outflows. The L1641-S outflow was suggested to be driven by the source embedded in the Re 50 N nebulosity (and its associated radio jet, see Anglada 1995). The L1641-S3 outflow was thought to be driven by the associated IRAS source. Based on the new 2.12  $\mu\text{m}$  images, a different picture of the region is suggested: the redshifted lobes of the L1641-S and L1641-S3 outflows form one single, huge outflow lobe, which is traced by the H<sub>2</sub> emission features SMZ 9-4, 9-5, and 9-6. The outflow is driven by L1641-S3 IRS/IRAS/MMS (see Chen & Tokunaga (1994) for near infrared images of the driving source region, and Stanke et al. (2000) for the identification of the MMS and a more detailed discussion of this flow). The beginning of the blueshifted lobe of this large scale flow is traced by the blueshifted lobe of the L1641-S3 outflow and by a number of H<sub>2</sub> features. Together with the features in the redshifted lobe, they constitute the H<sub>2</sub> flow #76.

Finally, to complete this compilation, one more molecular outflow (the L1641-C outflow) in the survey area has been claimed by Fukui (1988), but no map exists in the literature. Morgan et al. (1991) attempted to map the source, but concluded that no high velocity CO due to outflow could be identified. The outflow, if it exists, would be located just to the south and west of the H<sub>2</sub> features SMZ 7-1/7-2/7-3 in the L1641-C cluster (Strom et al. 1993). It might be associated with H<sub>2</sub> flow #66. Further evidence for an additional outflow in OMC-1 has been reported by Wilson & Mauersberger (1991)  $2'$  north of the BN-KL area; in fact, there are some H<sub>2</sub> features in this area which seem not to fit into the pattern of the OMC-1 H<sub>2</sub> fingers. These H<sub>2</sub> features may belong to the outflow noted by Wilson & Mauersberger, but the region is much too confused to say anything more about this outflow.

The following H<sub>2</sub> flows will be regarded as probably associated with high velocity CO emission: #3, #6, #17, #49, #53, #55, #59, #61, #64, #72, and #76. More uncertain CO associations are found for the H<sub>2</sub> flows #2, #25 (and a number of other suggested flows in the OMC-2/3 area), #27, #28, #54, and #73.



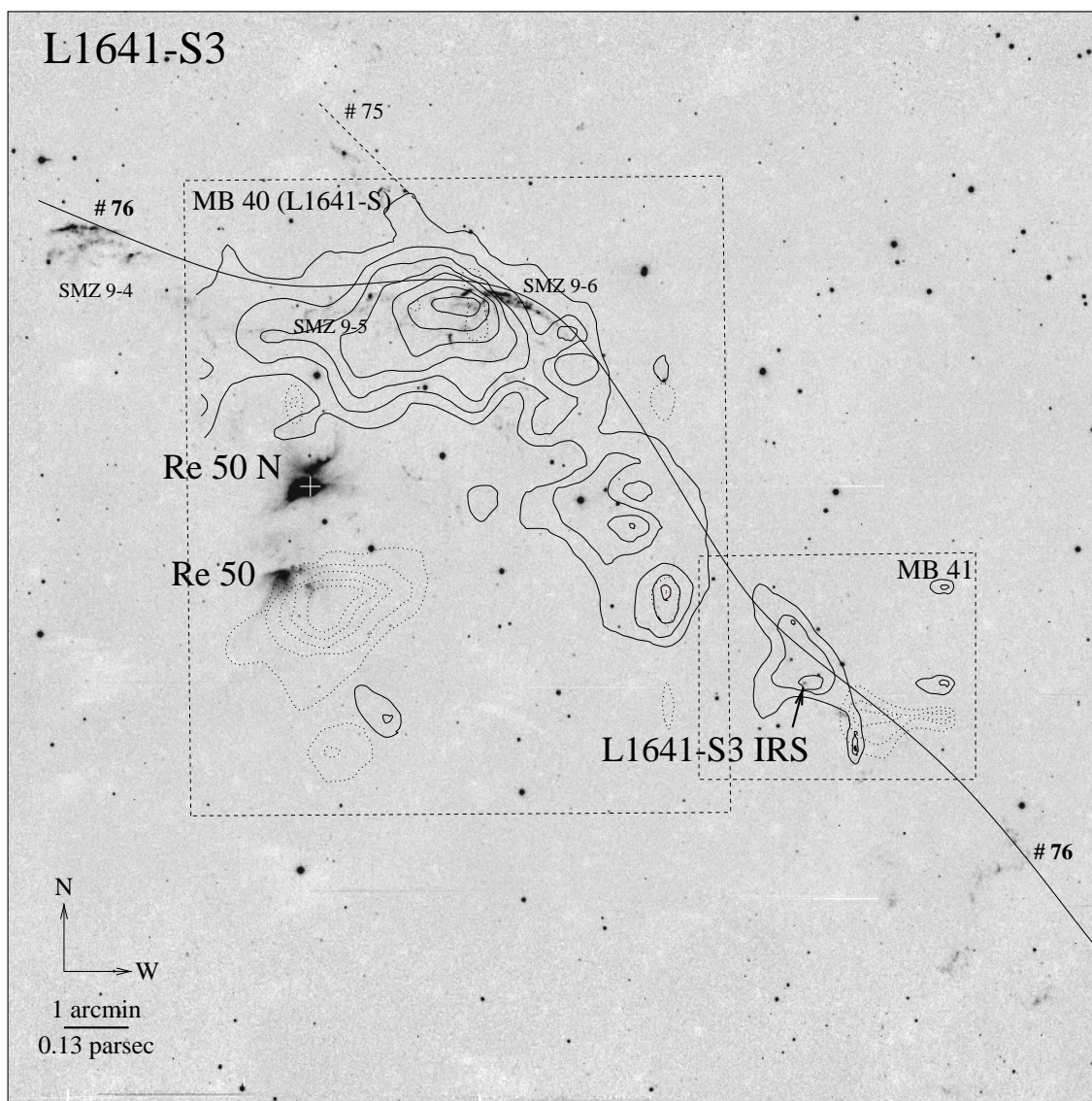


Figure 78: Distribution of high-velocity molecular gas in the L1641-S/L1641-S3 area (adopted from Morgan et al. 1991). Blueshifted gas is marked by the dotted contours, redshifted gas by the solid contours.



## Acknowledgements/Danksagung

An dieser Stelle möchte ich allen danken, ohne deren Hilfe und Inspiration diese Arbeit nicht möglich gewesen wäre:

Zuallererst möchte ich dem Initiator dieses Projektes, Dr. Hans Zinnecker, danken für die Themenstellung und den überaus großen Freiraum bei der Entwicklung und Gestaltung der Arbeit. Es ist immer interessant mit ihm zusammenzuarbeiten, wenn er gerade mal da ist.

Mark McCaughrean sei gedankt für viele Diskussionen über Jets, Datenauswertung und das “schöne Bilder daraus machen”, für den Versuch einer Einweisung an Teleskop und Kamera (“if you can’t see the Trapezium any more, then there must be *lots* of ice on the camera...”) und für weitere wichtige Tips (was man alles am Calar Alto machen kann, wenn das Wetter schlecht ist).

Mike Smith für viele Diskussionen über Jets und über sein “unification scheme”, das er mir als Programm zur Verfügung gestellt hat, und für seine stets aufmunternden Kommentare (“... it struck me this morning that our work really is important ...”).

All denen, die einen Teil ihrer Zeit darauf verwendet haben, diese Arbeit zumindest teilweise korrekturlesen: Rainer Köhler (und natürlich Friedrich), Mike Smith, Wolfgang Brandner, Alison Peck, und Mark McCaughrean.

Dem AIP und all seinen Insassen für eine sehr schöne, kollegiale Arbeitsatmosphäre, für die vielen Möglichkeiten, viele Blicke über verschiedenste Tellerränder werfen zu können, und für die Möglichkeit, mich auch als Kanufahrer profilieren zu können. Robert Schmidt und Ingo Lehmann sei nochmals gedankt für viele Späßchen während der letzten Jahre und für die kleinen, aber wichtigen Hilfestellungen jetzt am Schluß. Und Robert (bzw. Elke) nochmal für die Einführung des Gummibärchenglases!

Karl Menten und meinen neuen Kollegen am MPIfR dafür, daß sie mich diese Arbeit in aller Ruhe zuende haben bringen lassen, obwohl es doch um einiges länger gedauert hat als ich versprochen hatte. Besonderer Dank für erste Hilfe bei den Millimeter Beobachtungen am Pico Veleta und der dazugehörigen Datenreduktion geht dabei an Frank Bertoldi, Ernst Kreysa, Frédérique Motte, Bernd Weferling und Robert Zylka.

Ken’ichi Tatematsu und Doug Johnstone haben mir FITS-files ihrer Daten zur Verfügung gestellt, die sehr hilfreich waren.

Hermann sei gedankt für die stets fachkundige Unterstützung und für seine Geduld, wenn ich mal was nicht gleich verstanden habe, Kasimir für seine tatkräftige Unterstützung bei verschiedensten Beobachtungsaufenthalten, und natürlich dem ganzen Rest dafür, daß es bei uns zuhause nie langweilig wird.

Last, but not least, geht ein besonderer Dank für viel Geduld auch an meine Familie und vor allem an Katrin, die immer noch weiß wie ich aussehe, obwohl sie mich eigentlich die letzten Monate kaum noch zu Gesicht bekommen hat.

- This research was supported by the *Deutsche Forschungsgemeinschaft, DFG*, project number Zi 242/9-1 and Zi 242/9-2.
- This research is based largely on observations made at the Calar Alto 3.5 m telescope. It would have been impossible without the support of the observatory staff there (but much easier with better weather. . .). I have been a Visiting Astronomer, German-Spanish Astronomical Centre, Calar Alto, operated by the Max-Planck-Institute for Astronomy, Heidelberg, jointly with the Spanish National Commission for Astronomy.
- Based in part on observations collected at the European Southern Observatory, Chile, proposal numbers 60.C-0728 and 62.I-0848.
- Based in part on observations collected with the IRAM 30 m telescope located on Pico Veleta/Spain.
- The HIRES processed IRAS data were provided by Infrared Processing and Analysis Center (IPAC), operated by the California Institute of Technology, Jet Propulsion Laboratory under contract to the National Aeronautics and Space Administration (NASA).
- The data reduction and analysis has been performed on the Dec-Alpha cluster of the AIP using the ESO-MIDAS data reduction package. Spectral energy distributions and the “unification scheme” have been calculated using IDL.
- This research has made use of CDS’s Astronomical Database SIMBAD.
- This research has made use of NASA’s Astrophysics Data System Abstract Service.
- This research has made use of the HST guide star catalog.

The Guide Star Catalog was produced at the Space Telescope Science Institute under U.S. Government grant. These data are based on photographic data obtained using the Oschin Schmidt Telescope on Palomar Mountain and the UK Schmidt Telescope.

The Oschin Schmidt Telescope is operated by the California Institute of Technology and Palomar Observatory.

The UK Schmidt Telescope was operated by the Royal Observatory Edinburgh, with funding from the UK Science and Engineering Research Council (later the UK Particle Physics and Astronomy Research Council), until 1988 June, and thereafter by the Anglo-Australian Observatory. The blue plates of the southern Sky Atlas and its Equatorial Extension (together known as the SERC-J), as well as the Equatorial Red (ER) were all taken with the UK Schmidt.

- I acknowledge the use of NASA’s *SkyView* facility (<http://skyview.gsfc.nasa.gov>) located at NASA Goddard Space Flight Center.

Thomas Stanke  
Max-Planck-Institut für Radioastronomie  
Auf dem Hügel 69  
53121 Bonn  
e-mail: tstanke@mpifr-bonn.mpg.de  
Tel: 0228 525 214  
Fax: 0228 525 229

Bonn, 28. Juni 2001

## **Erklärung**

Hiermit erkläre ich, daß ich die eingereichte Dissertation mit dem Titel  
“An unbiased infrared H<sub>2</sub> search for embedded flows from young stars in Orion A”  
selbständig verfaßt, keine anderen als die angegebenen Hilfsmittel verwendet und die Arbeit an keiner  
anderen Hochschule bzw. Universität veröffentlicht habe.

(Thomas Stanke)